Université Paris Cité

École doctorale EDITE - ED130
Institut Pasteur, Machine Learning for Integrative Genomics (ML4IG)
ENS ULM, Department of Applied Mathematics, Centre Science des Données (CSD)

Transformers on single-cell RNA-sequencing data as large cell models

Par Jérémie KALFON

Thèse de doctorat d'Intelligence Artificielle

Dirigée par Laura CANTINI
Et par Gabriel Peyré

Présentée et soutenue publiquement le 15 Décembre 2025

Devant un jury composé de :

Prénom NOM, HDR	Université de Ville	Rapportrice
Valentina Boeva, DR	Université de Y	Examinateur
Eran Segal, Pr	Université Paris Cité	Examinatrice
Thomas Walter, Pr	INSERM	Membre du comité de suivi
Laurent Jacob, DR	CNRS	Membre du comité de suivi
Laura CANTINI, DR	CNRS	Directrice de thèse
Gabriel Peyré, Pr	CNRS	Directeur de thèse

Résumé

Titre : Modèles d'Intelligence Artificielle sur la génétique à cellule unique comme modèle de la cellule.

Mots clefs : scRNA-seq ; Foundation-model ; Interprétation ; Intégration de données ;

Abstract

Title : Single Cell Foundation Models as Large Cell Models.

Keywords : sc-RNA-seq ; Foundation-model ; Transformers ; Virtual Cell ; Network Inference ; AI ;

Abstract : Lorem ipsum dolor sit amet, consectetuer adipiscing elit. Ut purus elit, vestibulum ut, placerat ac, adipiscing vitae, felis. Curabitur dictum gravida mauris. Nam arcu libero, nonummy eget, consectetuer id, vulputate a, magna. Donec vehicula augue eu neque. Pellentesque habitant morbi tristique senectus et netus et malesuada fames ac turpis egestas. Mauris ut leo. Cras viverra metus rhoncus sem. Nulla et lectus vestibulum urna fringilla ultrices. Phasellus eu tellus sit amet tortor gravida placerat. Integer sapien est, iaculis in, pretium quis, viverra ac, nunc. Praesent eget sem vel leo ultrices bibendum. Aenean faucibus. Morbi dolor nulla, malesuada eu, pulvinar at, mollis ac, nulla. Curabitur auctor semper nulla. Donec varius orci eget risus. Duis nibh mi, congue eu, accumsan eleifend, sagittis quis, diam. Duis eget orci sit amet orci dignissim rutrum.

Nam dui ligula, fringilla a, euismod sodales, sollicitudin vel, wisi. Morbi auctor lorem non justo. Nam lacus libero, pretium at, lobortis vitae, ultricies et, tellus. Donec aliquet, tortor sed accumsan bibendum, erat ligula aliquet magna, vitae ornare odio metus a mi. Morbi ac orci et nisl hendrerit mollis. Suspendisse ut massa. Cras nec ante. Pellentesque a nulla. Cum sociis natoque penatibus et magnis dis parturient montes, nascetur ridiculus mus. Aliquam tincidunt urna. Nulla ullamcorper vestibulum turpis. Pellentesque cursus luctus mauris.

Nulla malesuada porttitor diam. Donec felis erat, congue non, volutpat at, tincidunt tristique, libero. Vivamus viverra fermentum felis. Donec nonummy pellentesque ante. Phasellus adipiscing semper elit. Proin fermentum massa ac quam. Sed diam turpis, molestie vitae, placerat a, molestie nec, leo. Maecenas lacinia. Nam ipsum ligula, eleifend at, accumsan nec, suscipit a, ipsum. Morbi blandit ligula feugiat magna. Nunc eleifend consequat lorem. Sed lacinia nulla vitae enim. Pellentesque tincidunt purus vel magna. Integer non enim. Praesent euismod nunc eu purus. Donec bibendum quam in tellus. Nullam cursus pulvinar lectus. Donec et mi. Nam vulputate metus eu enim. Vestibulum pellentesque felis eu massa.

Quisque ullamcorper placerat ipsum. Cras nibh. Morbi vel justo vitae lacus tincidunt ultrices. Lorem ipsum dolor sit amet, consectetuer adipiscing elit. In hac habitasse platea dictumst. Integer tempus convallis augue. Etiam facilisis. Nunc elementum fermentum wisi. Aenean placerat. Ut imperdiet, enim sed gravida sollicitudin, felis odio placerat quam, ac pulvinar elit purus eget enim. Nunc vitae tortor. Proin tempus nibh sit amet nisl. Vivamus quis tortor vitae risus porta vehicula.

Fusce mauris. Vestibulum luctus nibh at lectus. Sed bibendum, nulla a faucibus semper, leo velit ultricies tellus, ac venenatis arcu wisi vel nisl. Vestibulum diam. Aliquam pellentesque, augue quis sagittis posuere, turpis lacus congue quam, in hendrerit risus eros eget felis. Maecenas eget erat in sapien mattis porttitor. Vestibulum porttitor. Nulla facilisi. Sed a turpis eu lacus commodo facilisis. Morbi fringilla, wisi in dignissim interdum, justo lectus sagittis dui, et vehicula libero dui cursus dui. Mauris tempor ligula sed lacus. Duis cursus enim ut augue. Cras ac magna. Cras nulla. Nulla egestas. Curabitur a leo. Quisque egestas wisi eget nunc. Nam feugiat lacus vel est. Curabitur consectetuer.

Essentially, all models are wrong,
but some are useful

George E. P. Box - 1976

A Ph.D. is not a scprint,
it is a marathon

Someone

Remerciements

Je tiens à remercier chaleureusement mes collègues du laboratoire ML4IG de l'institut Pasteur ainsi que ceux du centre de science des données de l'ENS et tout particulièrement Jules Samaran, Remi Trimbour et Geert Huizing, pour leur accueil et leur aide durant cette thèse.

Je veux aussi bien sûr remercier Laura Cantini et Gabriel Peyré, mes co-encadrants, pour leur acceuil, leur soutien et leur disponibilité durant ces années. Leur expertise, leurs conseils et leur rigueur scientifique m'ont été d'une aide précieuse dans la réalisation de ce travail. Je suis entêté, je ne suis pas toujours clair, mais ils ont toujours su m'orienter et me guider dans la bonne direction.

Je remercie ma compagne, Juliette Hirsch, pour avoir toujours été à mes côtés ainsi que pour ses conseils, ses questions et son écoute constante. Malgré le stress qui n'a pas toujours fait ressortir le meilleur chez moi, elle a su être le soleil dans mes journées et la patience dans mes doutes.

Je remercie Patrice, Johanna, Marie-Astrid et Emmanuel Kalfon, sans qui je n'en serais pas ici aujourd'hui et qui m'ont conduit, par leur confiance, à faire ce travail. Je remercie Genevieve et Henri Spanjersberg ayant respectivement fait de la recherche en biologie et la même école que moi 50 ans auparavant ont su m'apporter l'intéret pour la science et l'ingérnierie. Je remercie Lucien Kalfon pour m'avoir montré qu'on pouvait rêver à de grandes choses. Finalement, Je tiens à remercier tout particulièrement Monique Obineau, pour son soutien indéfectible, sa bienveillance et son amour inconditionnel, je n'en serais pas là sans elle, son écoute et ses mots.

Je remercie Alex Wolf, Sergei Ribakov, Brice Rafestin et beaucoup d'autres pour leur aide dans le développement informatique des méthodes que je présente ici.

Je remercie les membres de l'institut Pasteur, du département de biologie computationnelle, le hub de bio-informatique, du département de Mathématiques appliquées de l'ENS, ainsi que ceux du supercalculateur Jean Zay sans qui ces méthodes n'auraient pu être entraînées.

Je remercie mes amis, Baptiste Tesson, Oscar Simon, Pier Michele Kaubari, Emile D'allens, Louis Cauquelin, Suzanne Lazarus, Anne-lise Aupetit, Quentin Van Straaten, sans qui je savais d'avance que je n'aurais été capable d'accomplir ce travail.

Je remercie aussi les membres de Nucleate, Whitelab Genomics, Blossom, dot Omics, Biographica et d'autres pour leur intérêt et soutien durant cette thèse.

Table des matières

Liste des figures

Liste des tableaux

Liste des abréviations

AI Artificial Intelligence. The simulation of human intelligence processes by machines, especially computer systems. xvii, 14, 52

AIVC Artificial Intelligence for a Virtual Cell. xvii

AP-MS Affinity Purification Mass Spectrometry. xvii, 29

ARI Adjusted Rand Index. A measure of the similarity between two data clusterings. xvii

ASO Antisense Oligonucleotide. xvii

ASW Average Silhouette Width. A measure of how similar an object is to its own cluster (cohesion) compared to other clusters (separation). xvii

ATAC-seq Assay for Transposase-Accessible Chromatin using sequencing. A technique used in molecular biology to assess genome-wide chromatin accessibility. xvii, 9

AUPRC Area Under the Precision-Recall Curve. A performance metric for binary classification problems. xvii, 26, 39–41, 43, 95, 113, 142

BERT Bidirectional Encoder Representations from Transformers. A transformer-based machine learning technique for natural language processing pre-training. xvii, 19, 34

BPH Benign Prostatic Hyperplasia. xvii, 26, 33, 34, 47–52

BS-seq Bisulfite Sequencing. The use of bisulfite treatment of DNA before routine sequencing to determine the pattern of methylation. xvii, 9, 13

CAF Cancer-Associated Fibroblast. A cell type within the tumor microenvironment that promotes tumorigenic features. xvii, 49

CCE Categorical Cross Entropy. A loss function used in multi-class classification tasks. xvii

cFM Cell Foundation Model. A foundation model trained on cellular data. xvii, 26, 77, 79, 81, 82, 84, 86

CGT Cell Graph Transformer. xvii

ChIP-seq Chromatin Immunoprecipitation Sequencing. A method used to analyze protein interactions with DNA. xvii, 9, 26, 42–44, 53

CNRS Centre National de la Recherche Scientifique. The French National Centre for Scientific Research. xvii, 30

CRISPR Clustered Regularly Interspaced Short Palindromic Repeats. A family of DNA sequences found in the genomes of prokaryotic organisms such as bacteria and archaea, used in gene editing. xvii, 10, 11

CxG CellxGene. xvii, 25, 28, 33–37, 45, 46

DNA Deoxyribonucleic Acid. Molecule that carries genetic information for the development and functioning of an organism. xvii, 2, 5–9, 13, 26, 31, 37, 53, 78, 80, 86

ECM Extracellular Matrix. xvii, 26, 29, 34, 51, 52

ENCODE Encyclopedia of DNA Elements. A public research project which aims to identify all functional elements in the human genome sequence. xvii, 26, 39–42

EPR Early Precision Ratio. xvii, 26, 27, 39–41, 43, 84, 85

ESM Evolutionary Scale Modeling. Protein language models trained on evolutionary data. xvii, 25, 27, 28, 36–38, 40, 78, 82, 83, 85–87

FFPE Formalin-Fixed Paraffin-Embedded. xvii

FM Foundation Model. A large machine learning model trained on a vast amount of data at scale that can be adapted to a wide range of downstream tasks. xvii

FSQ Finite Scalar Quantization. A quantization method for latent representations. xvii, 80, 89

FSQ-VAE Finite Scalar Quantization Variational Autoencoder. xvii, 89

GELU Gaussian Error Linear Unit. xvii

GEO Gene Expression Omnibus. A public functional genomics data repository supporting MIAME-compliant data submissions. xvii, 28

GN Gene Network. xv, xvii, 7, 33–35, 39, 44, 51–53

GNN Graph Neural Network. A class of artificial neural networks for processing data that can be represented as graphs. xvii, 22–24, 28, 120

GPT Generative Pre-trained Transformer. A type of large language model (LLM) and a prominent framework for generative artificial intelligence. xvii, 19

GPU Graphics Processing Unit. A specialized electronic circuit designed to manipulate and alter memory to accelerate the creation of images in a frame buffer intended for output to a display device. xvii, 16, 35, 52, 88, 96, 107

GRN Gene Regulatory Network. A collection of molecular regulators that interact with each other and with other substances in the cell to govern the gene expression levels of mRNA and proteins. xvii, 7, 21–25, 30, 33, 34, 38, 40, 41

GSEA Gene Set Enrichment Analysis. A computational method that determines whether an a priori defined set of genes shows statistically significant, concordant differences between two biological states. xvii, 39

gwps Genome-wide Perturb-seq. xvii, 29, 44

IB Information Bottleneck. A method for extracting relevant information from an input variable. xvii, 88, 89

iLISI Integration Local Inverse Simpson's Index. A metric to quantify the degree of mixing of datasets in an integrated embedding. xvii

ipTM interface predicted Template Modeling score. xvii

kBET k-nearest-neighbor Batch Effect Test. A metric to quantify batch effects in single-cell RNA-seq data. xvii

KNN K-Nearest Neighbors. A non-parametric method used for classification and regression. xvii

KO Knockout. A genetic technique in which one of an organism's genes is made inoperative. xvii

latex Is a mark up language specially suited for scientific documents. xvii

LLM Large Language Model. A language model notable for its ability to achieve general-purpose language generation and understanding. xvii, 14, 18, 78

lncRNA Long Non-Coding RNA. A type of RNA, defined as being transcripts with lengths exceeding 200 nucleotides that are not translated into protein. xvii, 6

log1p Logarithm of (1 + x). xvii

LoRA Low-Rank Adaptation. A technique for fine-tuning large language models. xvii, 81, 88

LR Learning Rate. A hyperparameter that controls how much to change the model in response to the estimated error each time the model weights are updated. xvii

LSE Log-Sum-Exp. xvii

mFM Molecular Foundation Model. A foundation model trained on molecular data. xvii, 26, 78, 79, 81

MHC Major Histocompatibility Complex. A set of cell surface proteins essential for the acquired immune system to recognize foreign molecules. xvii, 29

miRNA MicroRNA. A small single-stranded non-coding RNA molecule (containing about 22 nucleotides) found in plants, animals and some viruses, that functions in RNA silencing and post-transcriptional regulation of gene expression. xvii, 6

ML Machine Learning. A field of inquiry devoted to understanding and building methods that 'learn', that is, methods that leverage data to improve performance on some set of tasks. xvii, 14, 16, 30

MLP Multi-Layer Perceptron. A class of feedforward artificial neural network. xvii, 25, 27, 37, 81, 83, 85, 88, 118, 123, 124, 129, 132

MMD Maximum Mean Discrepancy. A kernel-based statistical test used to determine whether two given samples are drawn from the same distribution. xvii, 136, 148

mRNA Messenger RNA. A single-stranded RNA molecule that corresponds to the genetic sequence of a gene, and is read by a ribosome in the process of synthesizing a protein. xvii, 6, 9

MSA Multiple Sequence Alignment. The alignment of three or more biological sequences (protein or nucleic acid) of similar length. xvii, 86

MSE Mean Squared Error. A measure of the average of the squares of the errors—that is, the average squared difference between the estimated values and the actual value. xvii, 28, 99, 118, 124, 125

MVC Model-View-Controller. xvii

nFM Nucleotide Foundation Model. A foundation model trained on nucleotide sequences. xvii, 26, 78, 79, 81, 83, 86

NGS Next-Generation Sequencing. A high-throughput method used to determine the sequence of nucleotides in DNA or RNA samples. xvii, 8

NLP Natural Language Processing. A subfield of linguistics, computer science, and artificial intelligence concerned with the interactions between computers and human language. xvii, 80

NMI Normalized Mutual Information. A normalization of the Mutual Information (MI) score to scale the results between 0 (no mutual information) and 1 (perfect correlation). xvii

NN Neural Network. A method in artificial intelligence that teaches computers to process data in a way that is inspired by the human brain. xvii, 12, 14, 17

NNZ Number of Non-Zeros. xvii, 28

ODE Ordinary Differential Equation. xvii, 38, 53

OR Odds Ratio. xvii

OT Optimal Transport. A mathematical theory that deals with the problem of finding the most efficient way to move objects from one location to another. xvii, 13

PCA Principal Component Analysis. A statistical procedure that uses an orthogonal transformation to convert a set of observations of possibly correlated variables into a set of values of linearly uncorrelated variables called principal components. xvii, 108, 120, 146

PE Positional Encoding. A mechanism in Transformers to inject information about the relative or absolute position of the tokens in the sequence. xvii

PEFT Parameter-Efficient Fine-Tuning. Approaches to fine-tune large models with a small number of parameters. xvii

pLM Protein Language Model. A language model trained on protein sequences. xvii, 80

PPI Protein-Protein Interaction. The physical contact between two or more protein molecules as a result of biochemical events. xvii, 29, 53

QKV Query, Key, Value. The three matrices used in the attention mechanism of transformers. xvii, 81

RBP RNA Binding Protein. xvii

RNA RiboNucléique Acide. Polymeric molecule essential in various biological roles in coding, decoding, regulation and expression of genes. xvii, 5, 6, 9, 13, 26, 33, 34, 53, 78, 79, 86, 87

RNA-seq RNA Sequencing. A technique used to analyze the transcriptome of gene expression patterns. xvii, 9, 12, 19, 31, 37, 79, 81, 93

rRNA Ribosomal RNA. A type of non-coding RNA which is the primary component of ribosomes, essential to all cells. xvii, 6

scATAC-seq Single-cell ATAC-seq. A method to map chromatin accessibility at the single-cell level. xvii, 13, 33

scFM Single-cell Foundation Model. A foundation model specifically designed for single-cell biology tasks. xvii, 24, 27, 28, 93–99, 101–103, 107, 111, 114, 115, 125, 126, 130

scGEN Single-cell Generative. A tool for predicting single-cell perturbation responses. xvii, 47

scGPT Single-cell Generative Pretrained Transformer. A foundation model for single-cell biology based on the GPT architecture. xvii, 25–27, 30, 34, 37–41, 43–45, 47, 81, 85

scIB Single-cell Integration Benchmark. A benchmark for single-cell RNA-seq integration methods. xvii, 26–28, 47, 84, 87, 95, 99, 106, 108, 110, 138, 142, 143

scPRINT Single-cell PRe-trained INference Transformer. The model developed in this thesis. xi, xv–xvii, 25–30, 33–52, 81, 83–87, 93–113, 115, 117, 119, 121, 123, 125, 127, 129–135, 137, 139, 141–143, 145, 147, 149, 151

scRNA-seq Single-Cell RNA-Sequencing : Method to measure the RNA content of a cell. xvii, 9, 10, 18, 21–23, 33, 37, 38, 42, 45–48, 50, 52, 53, 105, 125, 139, 146, 149

scVI Single-cell Variational Inference. A probabilistic framework for analyzing single-cell RNA sequencing data. xvii, 47, 80

SEM Structural Equation Modeling. xvii, 25, 38, 39, 41, 43, 44

SGD Stochastic Gradient Descent. An iterative method for optimizing an objective function with suitable smoothness properties. xvii, 17

siRNA Small Interfering RNA. A class of double-stranded RNA non-coding RNA molecules, typically 20-24 base pairs in length, similar to miRNA, and operating within the RNA interference (RNAi) pathway. xvii, 6

SMILES Simplified Molecular Input Line Entry System. A specification in the form of a line notation for describing the structure of chemical species using short ASCII strings. xvii, 78

SOTA State of the Art. xvii, 19, 26, 33–35, 38, 44–47, 80, 81

TF Transcription Factor. A protein that controls the rate of transcription of genetic information from DNA to messenger RNA, by binding to a specific DNA sequence. xvii, 6, 23, 26, 33, 38–44, 130

tFM Tissue Foundation Model. A foundation model trained on tissue data. xvii, 26, 79, 81

TME Tumor Microenvironment. The environment around a tumor, including the surrounding blood vessels, immune cells, fibroblasts, signaling molecules and the extracellular matrix. xvii, 26, 34, 49, 52

tRNA Transfer RNA. An RNA molecule that helps decode a messenger RNA (mRNA) sequence into a protein. xvii, 6

UCE Universal Cell Embedding. A foundation model for single-cell biology. xvii, 37

UMAP Uniform Manifold Approximation and Projection. A dimension reduction technique that can be used for visualization similarly to t-SNE, but also for general non-linear dimension reduction. xvii, 96, 105, 108, 110, 148

VAE Variational Autoencoder. A type of artificial neural network used to learn efficient data codings in an unsupervised manner. xvii, 12, 13, 28, 80, 84, 89, 108, 109, 124, 130, 132, 133, 136

VQ-VAE Vector Quantized Variational Autoencoder. A generative model that learns discrete latent representations. xvii, 89

W2 Wasserstein-2 Distance. xvii

XPEFT XPressor-based Parameter-Efficient Fine-Tuning. xvii, 28, 29

ZINB Zero-Inflated Negative Binomial. A distribution used to model count data that has an excess of zero counts. xvii, 28, 95, 99, 105, 117, 124, 125, 132, 133

Preamble

This Ph.D. started relatively late in my career. I'd like to spend some of the introduction mentioning the reasons that pushed me to do a Ph.D. now.

0.1 My background for this thesis

PiPle

Many of the opportunities I had coming out of school have been very exciting. Initially, I decided to create a company called PiPle with a friend, Paul Best, who is now a Post-doctoral Researcher at the University of Vienna in Machine Learning for bio-acoustics.

Funily enough, it was completely unrelated to biology. We worked on creating novel means of communication. We had—and still have—big ideas about how to improve utterly inadequate messaging apps, emails, and similar tools using machine learning and innovative designs. Doing this, we learnt a lot about managing complex projects, selling ideas, building large codebases, teamwork, and designing interfaces.

However, we did not gain enough traction from this, and we felt that after a year of hard work, the road ahead was paved with too many sacrifices.

the Broad Institute

This is when I passed on Ph.D. opportunities a second time to work at the Broad Institute instead. Having visited the labs, Boston, and Kendall Square, I knew that this was the kind of experience I wanted to have, and Ph.D.s seemed long and cumbersome. At Broad, I worked on many very-high-impact research projects, and I felt I was part of something bigger than myself. I published as the first author and even started my own research projects, which would inform the thesis I am presenting here.

While I still understood that a Ph.D. was the best place to undergo such projects, I was uncertain about the specifics. I also understood the length, harshness, and sometimes arbitrary nature of U.S. Ph.D. programs. I also wanted to continue working on team-based projects and wanted to experience the start-up environment.

whitelab genomics

Figure 1 – Whitelab Genomics.

Along with some other personal decisions, it led me to return to France and work as the team lead of the computational biology group at Whitelab Genomics in Paris.

In Whitelab, I learned how to build a team and how to manage people. I learned a lot about what it means to grow companies from 10 to 50 people. I also learned about the biotech industry and how to build and sell such products.

Whitelab had a good mix of expertise in computational biology, machine learning, structural biology, and business development. While starting the first project there, I significantly enhanced the potential of foundation models for the biotech industry.

From DNA language models to cell foundation models and knowledge-graph-based models, it became clear that they would be the path forward to aggregate the sparse and disparate information across many fields of biology and medicine.

a Ph.D.

I was not looking for any other positions and intended to stay at least a few years to assess how we had grown during that time.

However, I was already in contact with Laura Cantini, with whom I had previously discussed Ph.D. projects. At some point, Laura came back to me with this Ph.D. proposal. I spent the good part of a month in a challenging position. Thinking about which decision would not become a regret in the future.

There was no perfect time to do this, but it felt like it was now or never. I was also very impressed by the level of various Ph.D. students in the labs of Laura and Gabriel. Seeing people 4 years younger than me, already having such a high level of expertise and knowledge, was very humbling. Finally, the Ph.D. topic and group were really on point with what I

wanted to do. But mostly, my work/life environment was welcoming, surrounded by family, friends, and activities. I knew what I wanted to work on and what I wanted to learn.

Therefore, I decided to start this Ph.D. journey.

0.2 Introduction

In this Thesis, we will focus on models of the Cell.

In the mid-17th century, Robert Hooke made a groundbreaking discovery while observing a piece of cork through his microscope. He observed structures that he named "cells" and, as a result, marked the beginning of cellular biology[1]. Cells have since been identified as life's fundamental structural and functional units, and biologists have endeavored to map the diverse cell types that comprise multicellular organisms. Additionally, they have sought to understand the transient cell states that occur during development, disease progression, and tissue regeneration[2].

The objectives of cellular biologists are to understand and control, with the dream of engineering life from plants to animals and even generating entirely new synthetic life[3]. But what for ?

0.2.1 The promises of cellular biology

drug design

Before developing a drug for a disease, one must understand the disease and identify a potential target gene or set of target genes. It refers to the genes in specific cell types that need to be reactivated, deactivated, or modified to address the disease's underlying mechanism.

But drugs don't have to be small molecules. CAR-T cell therapies have revolutionized blood cancer treatment by modifying a patient's own immune cells to fight the cancer. Similar approaches could be developed for many other conditions[4]. Here, the drug becomes a cell.

Helping creating these cellular drugs as well as more classic ones is one of the key applications of the work we will present in this thesis.

other applications

But diseases are not the only nails one could hit with such a mighty hammer. Indeed, life is everywhere, and engineering has already helped us make better crops, create synthetic meat, and design fungi that remove pollution. When people talk about nanorobots, I urge you to think about engineered cells[3].

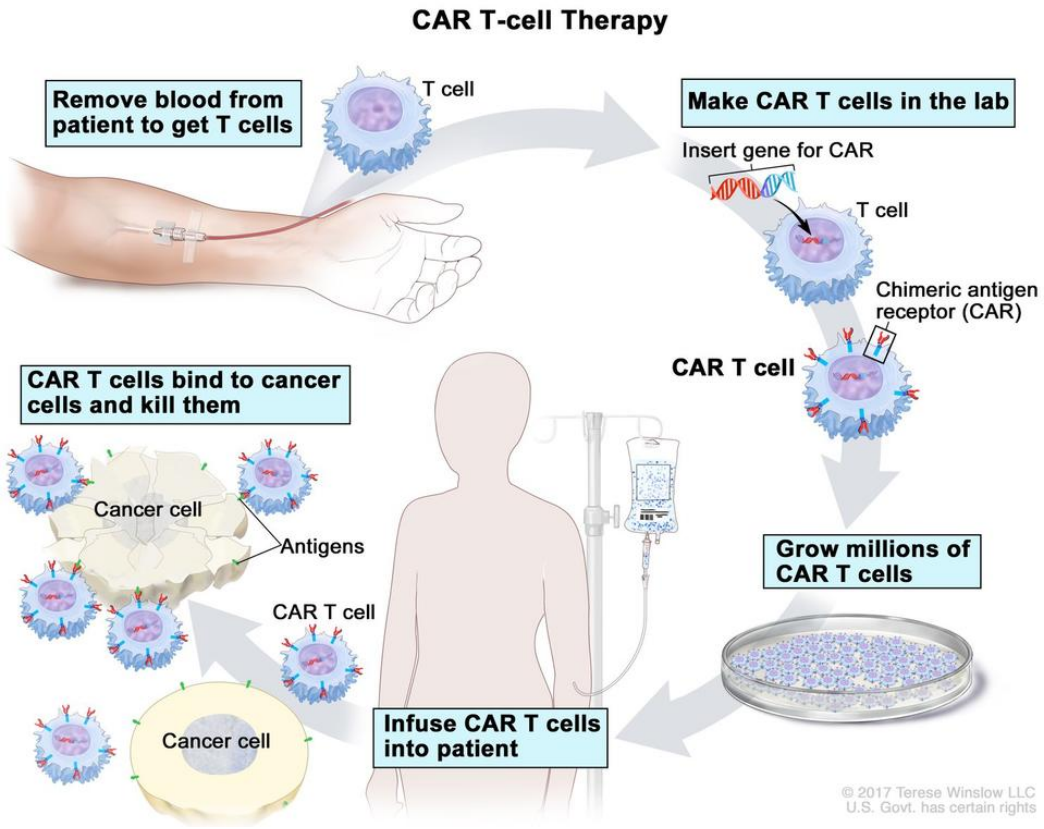

Figure 2 – Illustration of the CAR-T cell therapy.

Richard Feynman famously said, "What I cannot create, I do not understand." Therefore, the Modeling of the cell stands as a key milestone in cellular biology, and indeed, one cannot succeed in the aforementioned promises without a correct cellular blueprint.

virtual cells

Therefore, hundreds of companies, from tech to bio, and dozens of institutes are pursuing efforts to create such virtual cellular models [5]. Achieving even limited predictive accuracy would have significant impacts on cellular biology.

In this thesis we look into virtual cell modelling using modern machine learning methods but interogating them using the classic biological concepts.

We will investigate the primary data modality used to create cell models and how we can train them using modern machine learning methods based on neural networks. We will explore how these models can be useful today and how we might make them better in the future. For that, we will need to understand some essential facts about the cell and how biologists think about it.

0.2.2 GRN and the cell

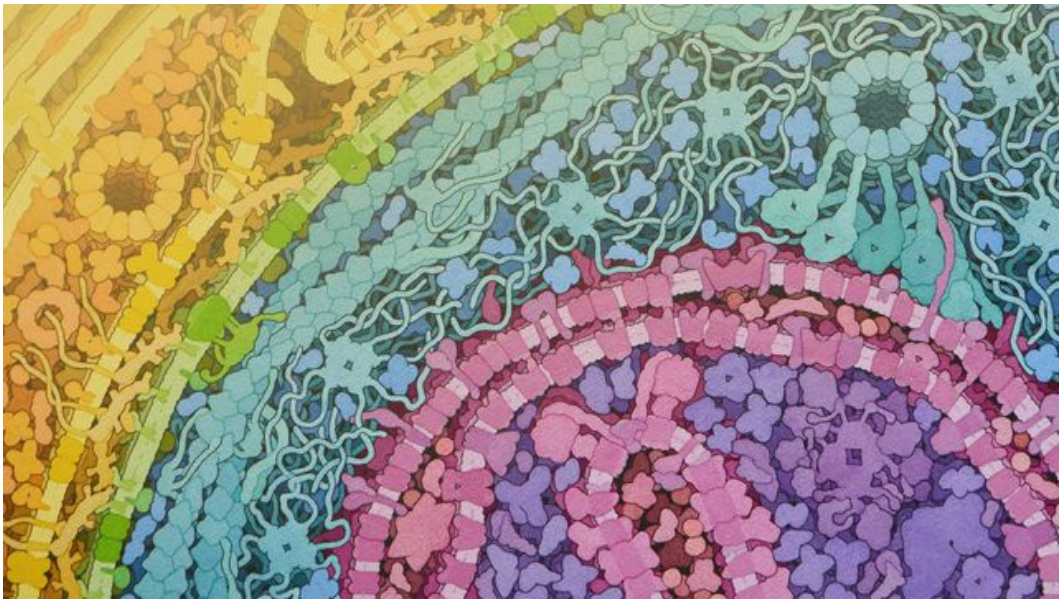

Figure 3 – Graphical view of a small part of the cell.

Let's first look at the cell. The cell is the fundamental unit of life and is composed of various components, including proteins, nucleic acids, lipids, and carbohydrates. Each of these components plays a crucial role in the cell's structure and function. Proteins are responsible for most cellular processes, while nucleic acids (DNA and RNA) carry genetic information. Lipids form cell membranes, and carbohydrates serve as energy sources and structural components.

It is at the Institut Pasteur in the 1950s that André Lwoff, Jacques Monod and his wife Agnes Ullmann made significant discoveries in the role of messenger RNA, gene regulations, and genetic programs to the function of the cell. Together with François Jacob, yet another Pasteur Institute scientist, they proposed the operon model of gene regulation in prokaryotes, which explained how genes are turned on and off in response to environmental signals. For their discoveries, François, André and Jacques were awarded the Nobel Prize in Physiology or Medicine in 1965[6]. This is again at Institut Pasteur, near the Monod's and Jacob's buildings that this Ph.D. was undertaken, trying to understand further mRNA's role and the cell's regulation through AI models.

RNA

Indeed, RNA biology is a critical aspect of cellular function, encompassing processes such as transcription, translation, and regulation. Transcription is the process by which DNA is copied into RNA, which then serves as a template for protein synthesis during translation. Regulation of these processes is essential for maintaining cellular homeostasis and responding to environmental changes. This regulation can occur at multiple levels, including transcriptional control, RNA processing, and post-translational modifications[2].

Figure 4 – Lwoff, Jacob, Monod.

The RNA hypothesis posits that RNA molecules were the first self-replicating entities, leading to the evolution of life as we know it. This hypothesis suggests that early life forms relied on RNA for both genetic information storage and catalytic functions, paving the way for the development of DNA and proteins, showing how RNA might be one of the most central components of the cell[7].

Many different types of RNA exist, each with distinct functions. Messenger RNA (mRNA) carries genetic information from DNA to ribosomes for protein synthesis, while transfer RNA (tRNA) and ribosomal RNA (rRNA) allow translation of mRNAs into proteins. Other types of RNA, such as small interfering RNA (siRNA) and microRNA (miRNA), are involved in gene regulation and silencing. Long-non-coding RNAs (lncRNAs) also play crucial roles in regulating gene expression and chromatin structure[8]. Unfortunately, many of these RNA types are still poorly understood, and their functions are an active area of research. In eukaryotic cells, like our own, RNAs are produced through genetic expression and are actively regulated by the cell.

gene expression

Gene expression is the process by which information from a gene is used to synthesize a functional gene product, typically a protein. This process involves several key steps, including transcription, where DNA is transcribed into mRNA, and translation, where mRNA is translated into a protein. Transcription factors (TFs) are proteins that bind to specific DNA sequences to regulate the transcription of genes. They play a crucial role in determining which genes are expressed in a cell at any given time, influencing cellular function and identity[2].

They also interact with other proteins, such as cohesin, which helps maintain chromatin and the specific 3D structure of the DNA. Chromatin is the complex of DNA and proteins that forms chromosomes within the nucleus of eukaryotic cells. The organization of chromatin is essential for regulating gene expression, as it determines the accessibility of DNA to transcription machinery.

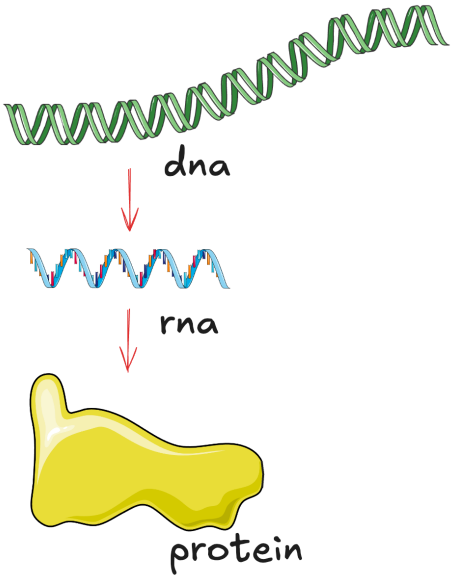

Figure 5 – The central dogma of biology.

regulation

In this context, biologists have relied on the concept of gene regulatory networks (GRNs) to simplify the complex interactions within the cell [9]. GRNs are networks of molecular interactions that govern gene expression levels in a cell. They consist of genes, transcription factors, and other regulatory elements that interact to control the timing and level of gene expression. Although very coarse and likely wrong in many ways, these modeled interactions allow researchers to gain insights into how cells might respond to various stimuli, differentiate into specific cell types, and maintain homeostasis.

Gene networks (Gene Network (GN)s) are a more general concept that encompasses not only gene regulatory networks but also other types of interactions, such as protein-protein interactions and metabolic pathways. While GRNs focus specifically on the regulation of gene expression, GNs provide a broader view of the cellular processes and interactions that contribute to the overall function of the cell.

In this thesis it is using gene expression measurement that we will train models of the cell, and we will often refer to gene regulatory networks as a way to understand how these models work and what they have learned about the cell. We will now focus further on the measurement mechanisms underpinning the gene expression data we will use in this thesis.

0.2.3 Single-cell genomics

sequencing

These measurements started within the field of genomics. Genomics is the study of an organism's complete set of DNA, including all of its genes. It involves sequencing and

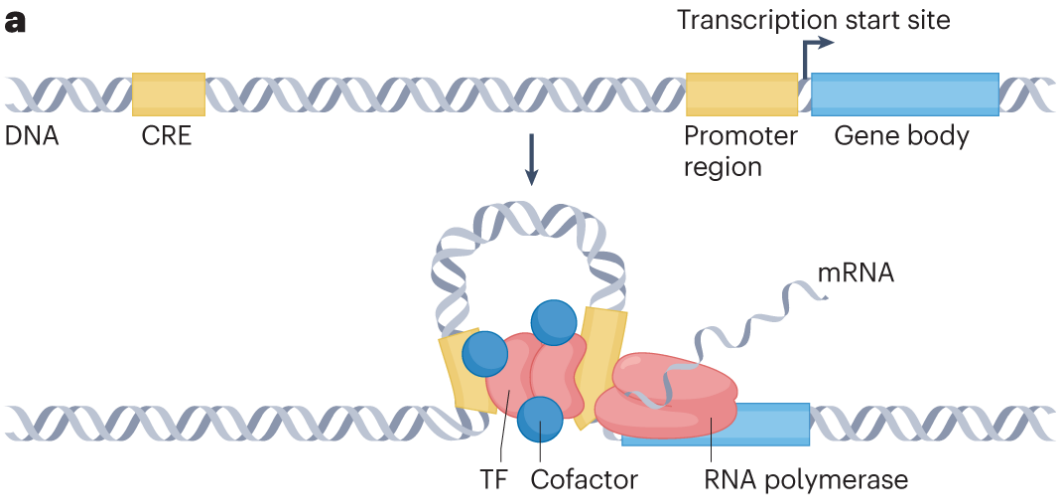

FIGURE 6 – the classic view of the gene expression and regulation

analyzing the entire genome to understand its structure, function, and evolution. Then, the development of high-throughput sequencing technologies revolutionized genomics, allowing researchers to sequence entire genomes quickly and cost-effectively.

Initially, DNA sequencing was performed using Sanger sequencing, the first method developed for this purpose. It involves selectively incorporating chain-terminating dideoxynucleotides during DNA replication, allowing researchers to determine the sequence of nucleotides in a DNA molecule. This method was labor-intensive and time-consuming, but it laid the foundation for modern sequencing techniques[10].

next-generation sequencing

Nowadays, we use next-generation high throughput sequencing (NGS) technologies, which allow for massively parallel sequencing of millions of DNA fragments—also called reads, simultaneously. This has significantly reduced the time and cost required for genome sequencing, enabling large-scale genomic studies and personalized medicine approaches[11].

Reads, small chunks of DNA, often likened to tiny puzzle pieces, are multiplied and sequenced in parallel. The resulting sequences are then aligned (or mapped) to a reference genome, which serves as a template for assembling the reads into a complete genome sequence. The average number of overlapping reads that cover a specific region of the genome is referred to as sequencing depth or coverage. Higher sequencing depth generally leads to more accurate and reliable results, as it reduces the likelihood of errors and increases the confidence in variant detection.

In the last decade, large-scale sequencing efforts such as the 1 million genomes project, the Human Genome Project, and the 1000 Genomes Project have provided valuable insights into human genetic variation and disease susceptibility[12, 13]. Genetic sequencing now allows us to define the genetic basis of many diseases, identify which drug might work for specific patients, and establish follow-ups for high-risk patients. It is driving more and more

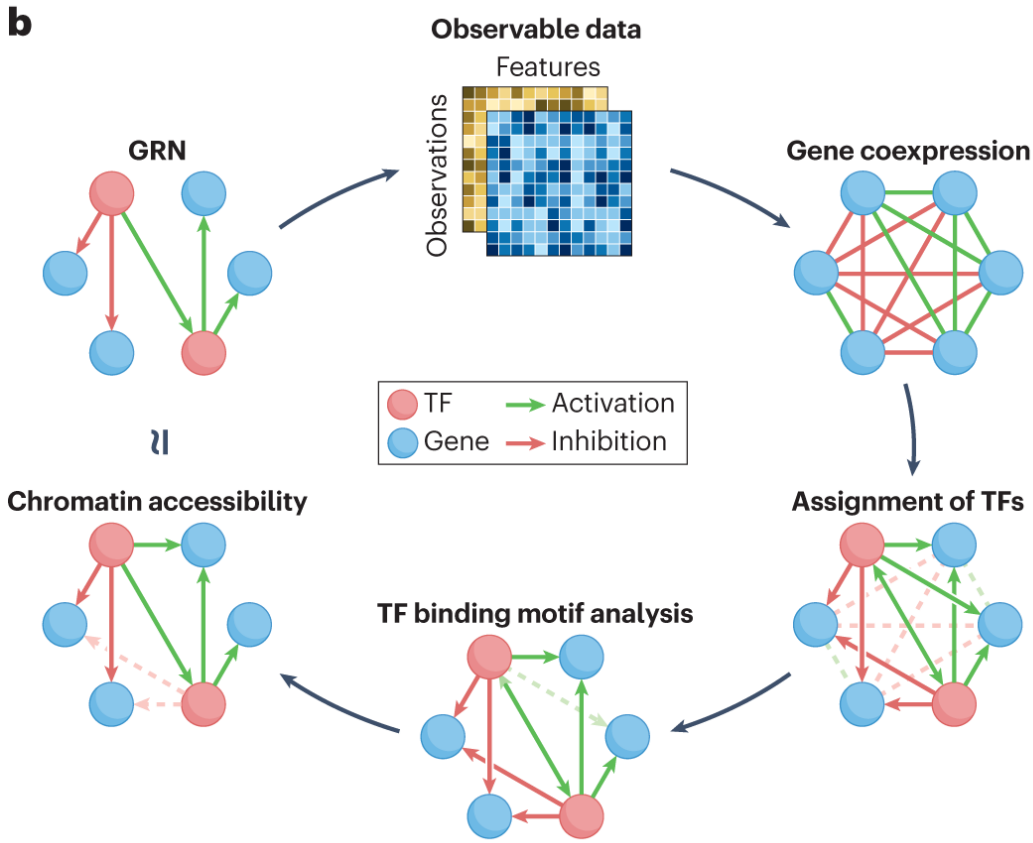

Figure 7 – infering gene networks with single cell data

clinical decisions and is becoming a standard part of patient care.

new modalities in sequencing

But sequencing also allowed many new applications, such as the study of gene expression using sequencing. Here we are using sequencer to read the mRNAs present within specific tissues, a process known as RNA sequencing (RNA-seq)[14]. Other examples abound, such as the sequencing of DNA states such as methylation (BS-seq), open chromatin (ATAC-seq), and chromatin immunoprecipitation (ChIP-seq) provides a view of how the genome is being read at a point in time. From DNA and its mutations to its state in different contexts and how these lead to changes in RNA's expression and state, we have begung to develop a holistic view of various cellular mechanisms[15].

However, these methods only provided a view of the average of sequences across the cells of a tissue, not of the individual cells. In 2014, the first single-cell RNA sequencing (scRNA-seq) methods were developed, allowing researchers to analyze gene expression at the single-cell level[16]. This was a breakthrough in genomics, as it enabled the study of cellular heterogeneity and the identification of rare cell populations that was previously missed from bulk analyses.

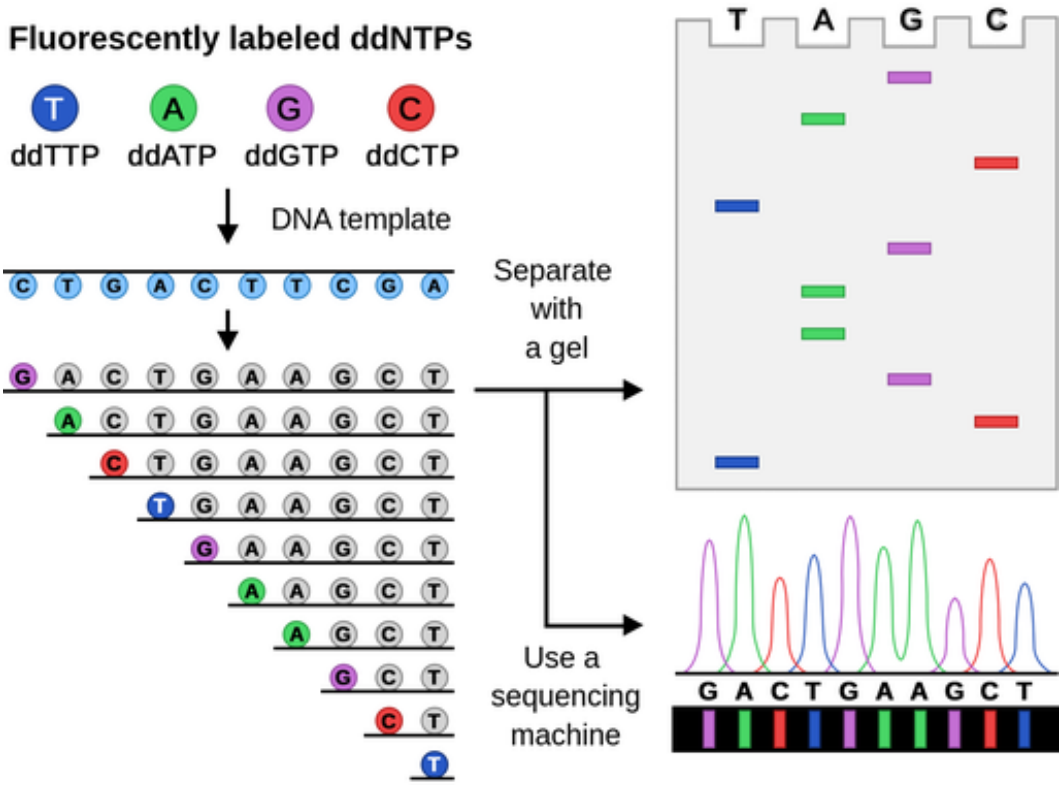

FIGURE 8 – main method for sequencing DNA

Since then, single-cell sequencing technologies have rapidly advanced, with new methods being developed to sequence the other omics modalities at the single-cell level. Studies conducted on tens of thousands of cells in the 2010s are now done on millions of cells[17], generating what has been called cell atlases.

In our work, we are gathering all the publicly available scRNA-seq datasets and atlases across tissues, diseases and species, to train foundation models.

future...

Recently, the development of spatial transcriptomics and imaging techniques has allowed researchers to study the spatial organization of gene expression within tissues, providing a more comprehensive view of cellular function in its native context, along with cell imaging[18]. Protein measurements are also being developed, unlocking an additional layer of information[19].

Current applications have been primarily focused on the understanding of diseases and drug effects within tissues. The technique allowed the identification of hundreds of new cell types and states, and improved the study of cellular development and differentiation. It had a substantial impact on cancer, neurological diseases, and immunology[20, 21].

Together with the development of perturbation techniques such as CRISPR-cas9 [22, 23], we can now go beyond observations and start to understand the causal relationships between

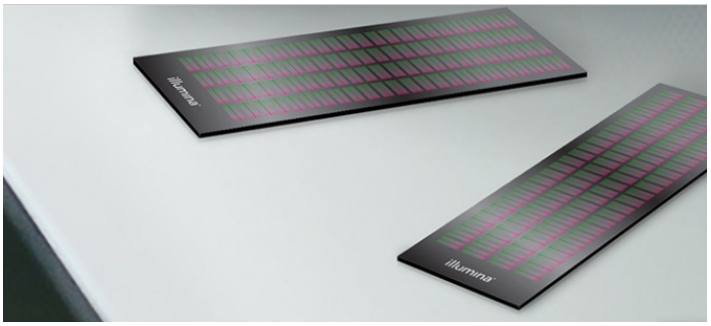

Figure 9 – illumina next-generation sequencing chip

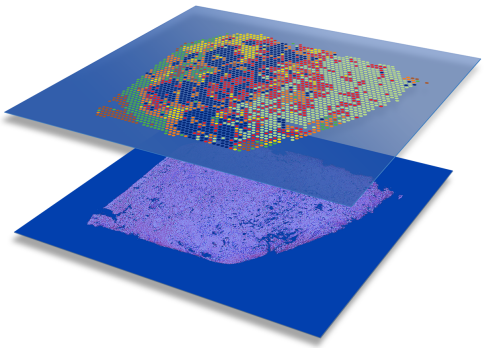

Figure 10 – spatial transcriptomics data example

genes and their functions. Indeed, these CRISPR screens allow researchers to systematically deactivate genes in individual cells and observe the resulting changes in gene expression, providing further insights into gene function and regulatory networks.

...and challenges

However, single-cell sequencing also comes with its own set of challenges. One of the main issues is the sparsity and noise underlying most of the current single-cell sequencing methods. Secondly, some strong ”batch-effect” biases in the data generation process can make it challenging to perform analysis across datasets.

Worse, the dataset themselves have issues. We currently miss many tissues and cell types that are rare and hard to sequence. We have yet to perform such analysis on species other than humans and mice, and specific cell states related to aging, fetal growth, disease, and treatment are missing. It is hoped that machine learning and artificial intelligence might allow us to solve these issues and infer the missing data computationally.

0.2.4 Current single cell tasks

While these models could be very performant, reliable, and reproducible, benchmarks that align with real use-cases from the user’s perspective remain scarce. Fortunately, the field

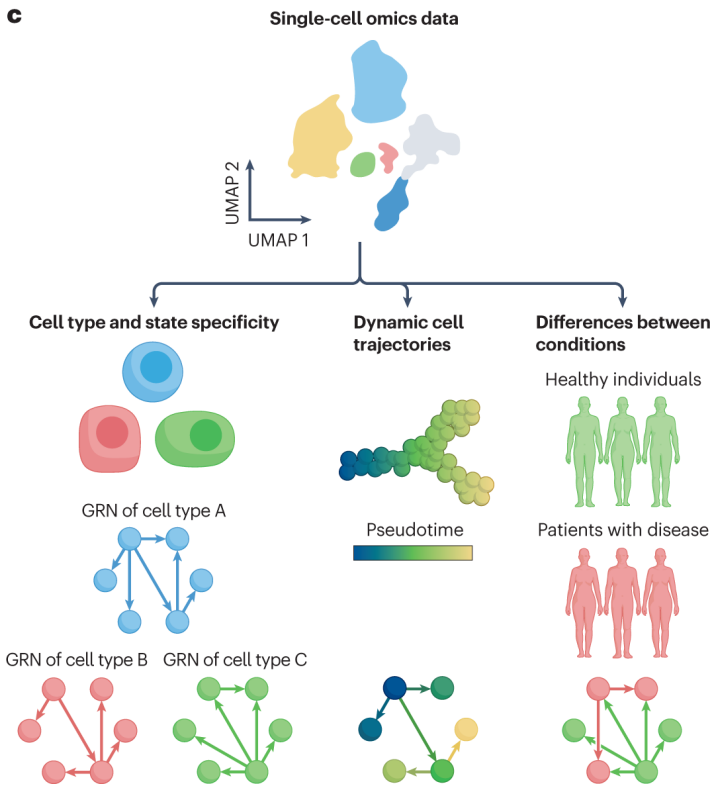

FIGURE 11 – single cell data analysis pipeline and relationship to gene networks

has matured sufficiently for the creation of standardized tasks and pipelines to understand, assess and analyse the data.

In single-cell RNA-seq data, a typical pipeline is as follows and contains several possible steps :

1. **Alignment.** It all starts with preprocessing the raw sequencing data : detecting/imputing the cell index, aligning the sequencing reads with a reference genome's gene locations, detecting low-quality cells, reads, doublet events, cell death events, and more[24]. These choices will impact the output dataset as biases.
2. **Normalization and clustering.** The data might be normalized to correct for sequencing depth and other gene-level biases, and clusters of cells would be defined based on their expression profile similarity. Finally, differential-expression analysis is performed, whereby clusters of cells are compared to identify genes that are differentially expressed between them. This might also be done after the other steps[25].
3. **Batch correction / atlas alignment.** The dataset might be aligned to a reference atlas in cases where this exists. This is done by using batch-correction methods, often built around nearest-neighbor mapping, matrix factorization, or neural networks (NN) called variational auto-encoders (VAEs), which are the current state of the art in the domain [26].
4. **Annotation and labeling.** Cluster-level and dataset-level labels might be inferred, such as cell type, tissue, disease, and age. These often come from prior knowledge, manual annotation based on differential expression features, automated tools, or

alignment with other prelabeled datasets. Thanks to these correlations between gene expression, labels might be defined and guide further research. Clustering tools and dimensionality reduction techniques used for visualizing high-dimensional datasets as point clouds on 2D surfaces often employ nearest-neighbor-based methods[27].

5. **Denoising / imputation.** In cases where specific clusters contain a low number of cells, denoising or zero-imputation methods can be used [28], but they haven't shown consistent usefulness in practice since they rely on cluster-level information, which is itself used for most other tasks. Nearest-neighbors-based smoothing was the previous state of the art[29].
6. **Multimodal integration.** If users have access to datasets of the same tissue from other modalities (scATAC-seq, BS-seq, protein measurements, imaging, etc.), multimodal alignment methods can be applied, often reusing prior knowledge and paired datasets where modalities are measured in the same cells. Such alignments help bridge genotype (DNA/mutations) and phenotype (expression, protein levels, pathology). State-of-the-art tools combine VAEs and heuristics.
7. **Trajectory inference.** If the dataset was measured in a non-static context, one can infer "cellular trajectories", i.e., how cells transition from one state to another based on many single-cell snapshots, such as during differentiation or perturbations. Many tools exist for trajectory inference ; state-of-the-art methods often employ techniques like optimal transport (OT) [30].
8. **Spatial analysis and cell-cell interactions.** If the dataset contains spatial information—how cells are positioned in a tissue—one can infer cell-cell interactions, meaning how cells influence each other based on proximity and expression profiles. This often requires specialized imaging techniques, where cell morphology is also assessed. Spatial interaction analysis is still nascent ; methods frequently use foundation models and heuristics based on cell type and proximity[31].
9. **Perturbation response prediction.** If the dataset includes perturbation experiments, one can predict how cells respond to specific perturbations, such as drug treatments or genetic modifications. This helps identify key regulatory pathways and potential therapeutic targets[32].

These analysis and tools are available in a set of packages called scverse, which our work relies heavily on and has contributed to.

Now that we understood more about the biology underpinning this Ph.D.'s work, let's understand the specific method we are trying to develop. A method where we are bringing artificial intelligence to the modeling of the cell.

0.3 The AI virtual cell

A virtual cell model has been the dream of computational and systems biologists for decades. Initially, these models were based on simplified representations of cellular processes, often focusing on specific pathways or interactions. The models examined chemical reaction parameters involving proteins, RNAs, and DNA. However, in addition to computational

challenges, these models were not able to generate realistic predictions of cellular behavior.

Nowadays, an idea has emerged that artificial intelligence techniques, would allow us to solve some of these problems. But first, what is AI, and what is the difference between machine learning (ML), data science, and informatics ?

0.3.1 AI and neural networks

definitions

Data Science encompasses the gathering, management, and analysis of data in information systems. Machine Learning happens when one uses statistical methods to generate predictions from data. But these methods can be more complex, and while they can be seen in the framework of statistics, they also have an underpinning in other domains, like neuroscience (with neural networks) and applied mathematics with Algebra, Topology, Analysis, and most importantly, Optimization. These methods often allow powerful modeling of the data statistics.

Artificial Intelligence (AI) is a broad term that has had multiple meanings in society and culture. For many, it mainly refers to applications of machine learning methods to human and animal-related tasks, such as understanding images, videos, speech, and text, as well as robot manipulation. For the field, it has often been a much broader term encompassing even knowledge bases and many statistical methods. This creates many bridges and links between data science, machine learning, statistics, informatics, and AI.

Recently, Machine Learning (ML) has made great strides in many areas, primarily due to a significant increase in data generation, along with improvements in optimization methods and neural networks.

intuition

Most of the potent machine learning tools today are part of the representation learning category. These tools convert concepts and objects into high-dimensional vectors, called embeddings. In Neural Networks (NN) these embedding vectors are then processed through layers of mathematical operations, often involving matrix multiplications and non-linear functions[33]. The layers are designed to learn hierarchical representations of the input data, capturing increasingly complex features as the data passes through the network.

Such tools have also been heavily applied in the study of single-cell data, with many methods relying on representation learning and NNs to denoise, align, and analyze the data[26].

Recently, specific neural network architectures with powerfull scaling properties and trained on a large swath of the internet, also named Large Language Models (LLMs), have become ubiquitous. Researchers have started to extend their abilities to novel data modalities in what has been termed **world models**[34]. These models, trained on physics simulations,

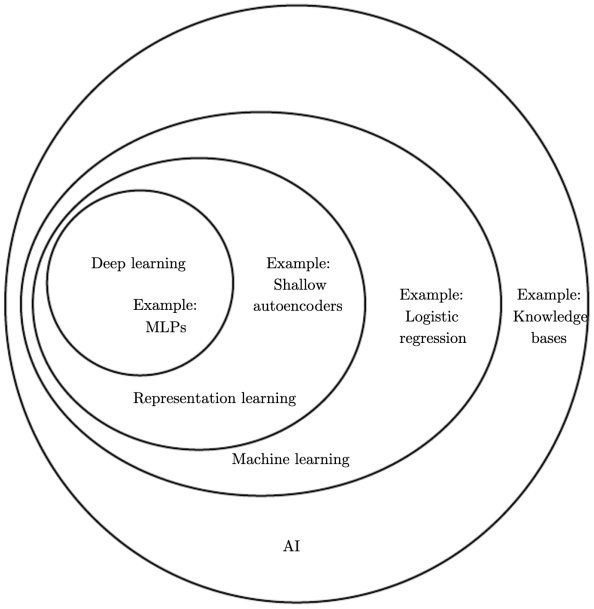

Figure 12 – placing terms in their context. From Deep Learning Book.

videos or more, aim to predict the next state of complex physical phenomena, such as what happens when someone throws a ball or how water flows down a river.

World models have already shown promise in powering, for example, humanoid robots. In different domain, Google DeepMind recently released a model for predicting the weather better and faster than the best ”physics-based” models[35]. But why and how are these models so powerful ? While this remains an active area of research, essential theories have been presented.

why does it work ?

Contrary to the previously accepted machine learning dogma, deep learning researchers showed, in the 2010s, that increasing the number of parameters did not necessarily lead to overfitting, i.e., the model learning by heart to reproduce its training data. Instead, thanks to some light regularization methods the models were able to learn more complex patterns in the data. There methods such as dropout and weight decay, involve randomly removing some neurons during training and penalizing large weights.

To make deep models a final element called skip connections was introduced. Skip connections prevented a previous known issue called vanishing gradients. This innovation led to architectures like ResNet and VGG, which significantly improved performance on various tasks[36, 37].

Finally, transformer architectures, introduced in 2017, generalized neural networks further by working on matrices instead of vectors and using invariances in the model architecture itself. This allowed the models to scale even further and learn more complex patterns in the data[38].

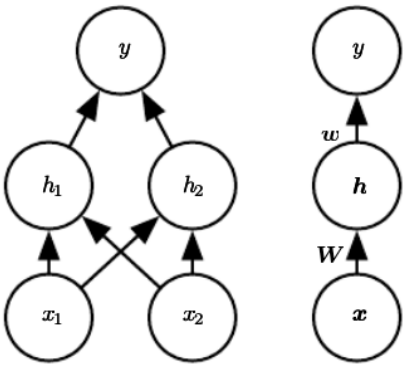

FIGURE 13 – example of a feed-forward neural network architecture, drawn in 2 different styles. From Deep Learning Book.

Another enabler to achieve large models was the advent of Graphical Processing Units (GPU)s, which allowed large and very efficient parallel matrix operations. Furthermore, thanks to interconnects, hundreds of GPUs can be linked to form nodes and pods of compute clusters.

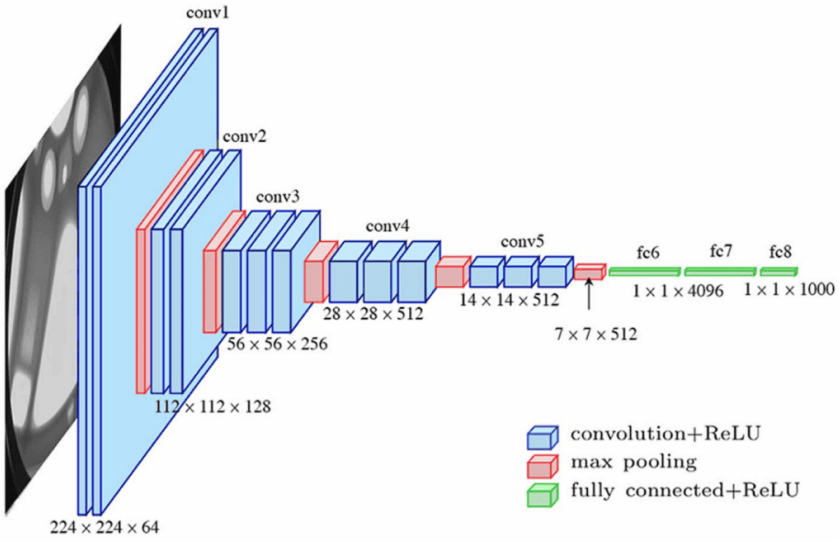

FIGURE 14 – Example of the VGG architecture, which allowed training deeper neural networks thanks to skip connections.

Now, the final piece of the puzzle is in how we train such models.

optimization and loss landscapes

Interestingly, whether small or large, neural network or else amost all ML methods are trained using variants of gradient descent optimization methods. These methods aim to minimize a loss function, which quantifies the difference between the model's predictions

and the actual data. By iteratively adjusting the model's parameters in the direction that reduces the loss, these optimization algorithms help the model learn from the data.

But this is through *stochastic* gradient descent (SGD) methods like Adam that we succeffully train NNs. Indeed, using only a small subset of the data at each training step is not only much faster to minimize the loss function but it also helps escape local minima and saddle points[39].

To understand this, we need to understand the loss landscape. Imagine a 3D landscape where the height represents the loss value, and the two other "surface" dimensions are the model's parameters. The goal of the model is to find the lowest point in this landscape, which corresponds to the best set of parameters to fit the data. However, this landscape is very complex, with many local minima and saddle which would prevent the model from reaching a nice minima. The model wanders blindly and can only sense its immediate surroundings.

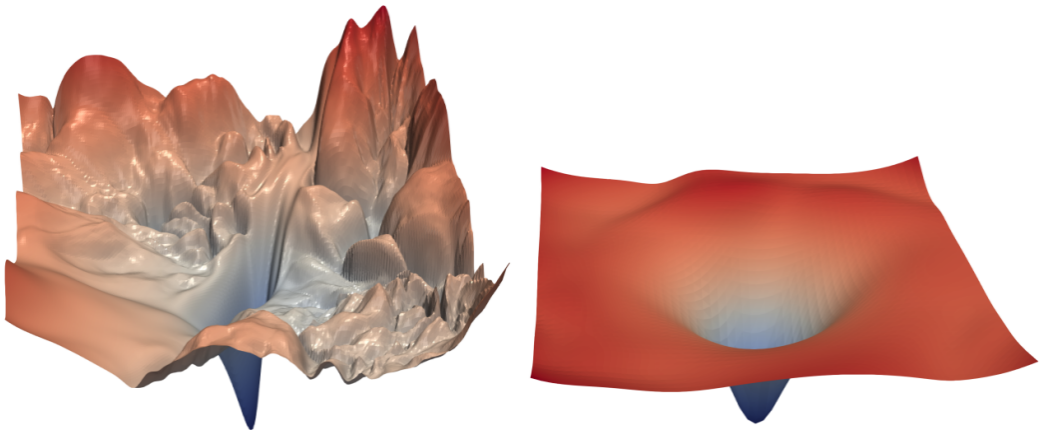

(a) without skip connections (b) with skip connections

Figure 15 – visualization of a loss landscape with and without skip connections

In very high dimensions, however, when the model has millions of parameters and SGD, by being stochastic, alters the loss landscape each time, thus letting the model easily find a possible escape direction.

Behind this unexpected behavior is the unsettling theory of emergence. Or how small objects can combine and interact in ways that would be unexpected and difficult to predict based on their individual properties. This theory tries to explain phenomena in dunes, snowflakes, ant colonies, and life itself, which might explain how large neural networks achieve such complex behaviors[40].

0.3.2 Bio-Foundation models

large language models

For text, images, videos, and audio, LLMs are everywhere now. In other domains, we often call similar models, trained on all the available data in some modalities, foundation models.

Foundation models epitomize a switch from small, simple neural architectures trained per dataset to larger, more powerful transformers models, trained across the entirety of the available datasets. The stated goal is for them to generalize better to unseen dataset and novel tasks. To do this however they will need to be fine-tuned.

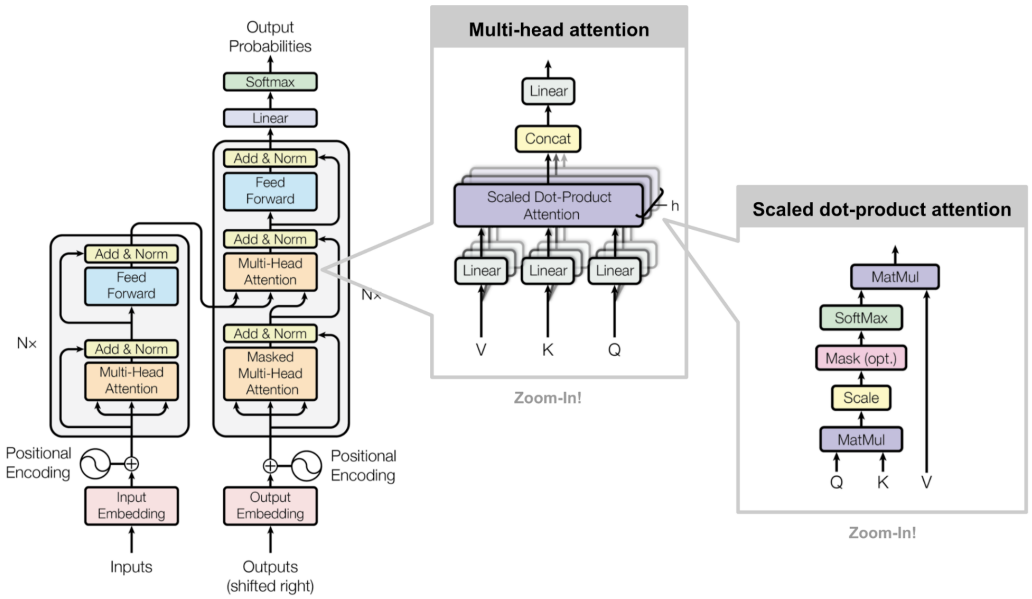

FIGURE 16 – Transformer architecture overview. From Attention is all you need.

fine-tuning

After this initial training phase using a very generic unsupervised task, often referred to as pre-training, foundation models can be further fine-tuned to specific downstream objectives. Fine-tuning involves training the model on a smaller dataset with a goal specific to the task we want it to learn. In other domains, this has allowed the model to adapt its learned representations, enabling it to quickly gain higher accuracy than would be achieved without pre-training. For example, going from predicting the next word in a sentence to classifying the sentiment of a text, or to becoming a chatbot. For this reason, essential innovations in fine-tuning methods involve creating losses that best align the model with the task[41, 42].

This is such foundation models, pre-trained on scRNA-seq data that we want to understand in this thesis. In many domains outside of text or images, they are still in their infancy

and we have important research questions to ask : Do they work ? Can they be useful to current research ? and how can we improve their training, architecture ?

initial single-cell foundation models

The first practical example of a single-cell (RNA-seq) foundation model could have been scBERT, released in 2021. However, it was only used and benchmarked for cell type classification and pre-trained on 1 million single cells[43]. The first real foundational model, Geneformer, was released a year later [44]. There, the author displayed the model's ability to perform various single-cell tasks, such as cell type classification, gene regulatory network inference, and perturbation prediction. Geneformer was trained on a much larger dataset of 33 million single-cells.

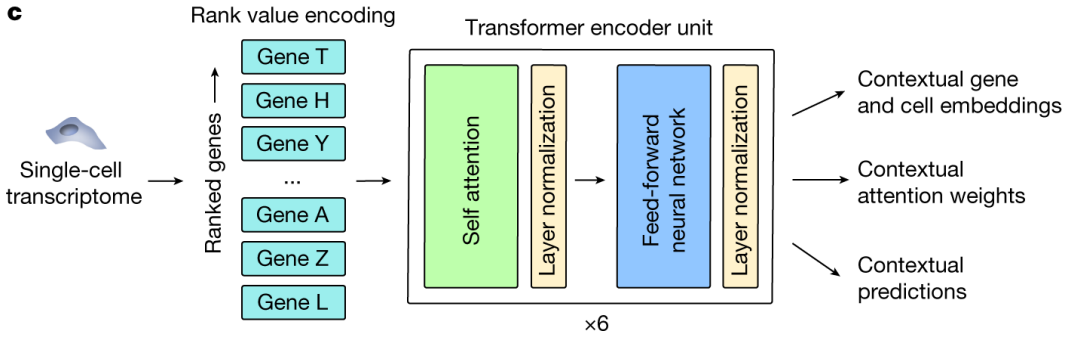

Figure 17 – the geneformer model, where genes are represented as words and cells as sentences where the genes are ordered by their expression level. From Geneformer.

However, Geneformer, like scBERT, was really an LLM, here BERT, applied to single-cell data. In this context, words are gene names and they are listed in order of expression level in the cell, to make up a sentence.

current single-cell foundation models

In 2023, a year after Geneformer, a few additional foundation models were released from scGPT [45], showcasing a take on the GPT architecture and presenting various losses for fine-tuning the model. It was the first example of fine-tuning in a single cell and a more in-depth benchmark of the model across four different abilities : cell type prediction, gene network inference, perturbation prediction, and batch correction. However, it did not outperform state-of-the-art (State of the Art (SOTA)) methods[46, 47].

At the same time, Universal Cell Embedding [48] demonstrated how one could train these models across multiple species to achieve state-of-the-art cross-species cell embeddings —vectors that represent the cell according to the model. It also showed a new kind of loss function to generate embeddings of the cells.

Finally, scFoundation [49], despite being closed-source, showcased a truly novel architecture specifically built for single-cell data and a novel training method based on the

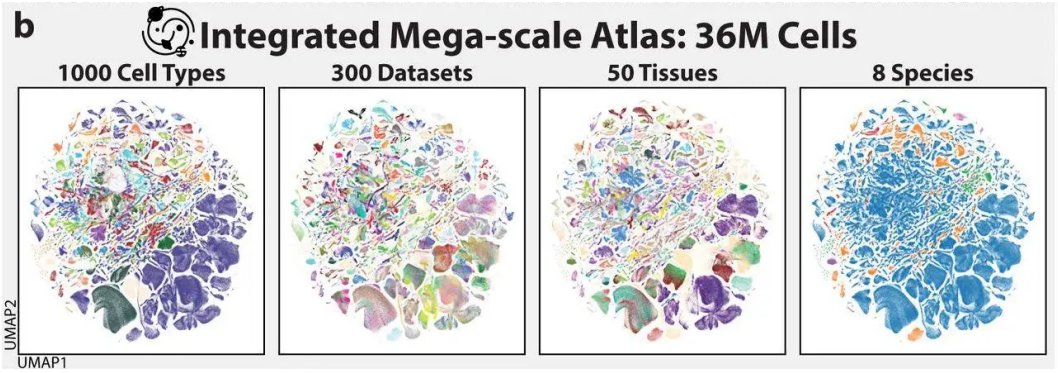

Figure 18 – low dimensional visualization of universal cell embeddings across species. Each point is a cell where its position is position is near similar cells according to this Foundation Models. From Universal Cell Embeddings.

noise-to-sequencing-depth relationship of single-cell data.

This is right after the release of scGPT and UCE that this Ph.D. started. The field of single-cell foundation models had just began. In the next chapter, we will present the specific scientific questions and objectives of these thesis and how we decided to tackle them.

Thesis Objectives

At the start of the project, two things were certain : I wanted to understand how single-cell foundation models worked and whether they indeed worked. I also wanted to see if I could improve gene regulatory network (GRN) inference from single-cell RNA sequencing (scRNA-seq) data. Knowing that I might see a possible interplay between the two.

To start, it is important to reflect on what I wanted to achieve initially, without knowing what I know now.

In the second part I will introduce the different chapters of the thesis and how they relate to my Ph.D. objectives. This being a Thesis by Articles, each of the three chapters relates to a specific publication.

0.4 At the start : Personal Objectives during the thesis

This is copied from my initial objectives written in my research proposal at the start of the Ph.D.

I had the chance to see many friends doing their Ph.D.s before starting mine. A main mistake I saw during one's Ph.D. is to not see the time passing by. My goal for this Ph.D. was to be as product-first as I was at Whitelab genomics. Delivering results quickly & improving until it is publishable. This mistake, thinking "Well, I have 3 years..." is in part at least responsible for the stress, the crash and the unpreparedness for what happens after the Ph.D. that some students might experience. Thus, I plan to give myself a short timeline, knowing I will likely go over. And I will prepare everything around this idea. I will also start to prepare for what is next from the get-go.

To do that best, one needs to take the opportunity of the Ph.D. to make connections with other labs (industry or academic). Moreover, a good advice I have been given is to *know what you want to do and what you don't want to do.* Know what you are here for. Learn to say no. And I learned to say no in the last 4 years. My goal is to work on large models & large datasets, mostly in transcriptomics, and always to go back to first principles and biology. I also know I want to make something useful, create something that can be a stepping stone for others. Something that has an impact on the community. I know that to do that, you have to go the extra mile in terms of development and be honest with yourself about any shortcomings.

Finally, I have been fortunate to become often addicted to my work. I like working hard and I like challenges. But for this to happen, I need to keep enjoying what I am doing. I also wish to have no regrets about this decision. Thus, my final goal is to enjoy it as much as I can.

Figure 19 – A view of the Pasteur Institute in Paris, where I did my Ph.D.

0.5 Initial Ph.D. objectives

This Ph.D. aimed to develop new approaches using deep learning, possibly by using innovative graph neural network architectures on large scRNA-seq datasets, to assess their predictability in high-quality benchmarks and package them as an open-source Python library. Our principle idea was to use Graph Neural Networks (GNN)s. GNNs are a class of deep learning layers designed to operate on graph-structured data. They are specifically tailored to handle modalities where edges connect the different input elements (nodes or vertices)[50, 51].

Traditional neural networks are primarily designed for processing grid-like data, like images, or sequential data, such as text. However, GNNs extend this capability to graph-structured data by incorporating a pooling operations across connected nodes.

Objectives. We wished to improve GRN predictions from scRNA-seq data. Our approach was :

1. To use larger neural network models that scale linearly with the dataset size, taking advantage of the tens of millions of data points now becoming available.
2. To use novel GNN layers that could reduce the "search space" of the model by constraining the set of possible topologies it is learning.
3. To improve the pretraining and fine-tuning of these models to the predictive task they have to perform, and the constraints of the system they are predicting.
4. To formulate better layers that correspond to the sparse interactions between genes and our current knowledge about their functions.
5. To create formal and rational benchmarks that best capture the ability of a GRN methodology.
6. To assess predictions and any usefulness or lack of it by having biologists test hypotheses using the model.

0.6 potential impacts

Impact of the project. This Ph.D. project would thereby contribute to methodological breakthroughs by providing new tools and methods to use neural networks on unstructured data, like scRNA-seq. To improve the state of the art in GRNs prediction from scRNA-seq.

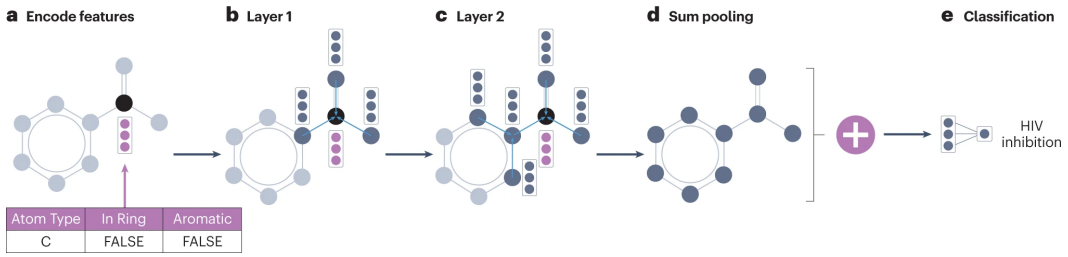

FIGURE 20 – illustration of the graph neural network mechanism, update and pooling (e.g. summing) across multiple connected nodes represented as vectors

The proposed methodologies will impact computational (bioinformatics, machine learning) and biomedical fields. These new GNN layers could solve challenges faced by fields similar to those utilizing scRNA-seq profiles, including environmental research, industrial biotechnology, and biofuel studies[52, 53, 54].

The initial objectives were separated into three possible work packages :

1. Review of current tools and creation of a set of benchmarks
2. GNN model/layers to better predict TF-gene relationships
3. Collaboration to test the model's prediction on novel data

0.7 Revised objectives

The first objective was thus to review existing methods for inferring GRNs from multi-omics data, as well as the existing foundation models and benchmarks used to evaluate the performance of these methods.

What I quickly learnt is that GNNs were not the best approach for this problem. Indeed, we do not have good ground truths for GRNs, so we cannot start from a known graph. Moreover, GNNs tend not to scale well, and benchmarks show them as almost invariably performing worse than transformer-based models[55, 56]

0.7.1 transformers

Thus, we quickly decided to stick with transformers, which can be seen as GNN working on fully-connected graphs[57, 58, 59, 60]. The main issue with transformers is their quadratic complexity in relation to the number of input tokens. Thus, we worked on making them scale sub-quadratically with the number of input genes and cells. This is one of our contributions in this thesis.

Transformer-based models can be seen as GNNs, and examples had already been presented of using single cell foundation models (scFM)s to generate putative GRNs directly from their non-graph input data[45, 44]. This was a feat that regular GNNs cannot achieve.

0.7.2 building our own models and benchmarks

Moreover, as we aimed to benchmark these methods, which had made claims about their ability, we realized there were many shortcomings, from usability to ease of use, reproducibility of pretraining. We also found that they were not very usable in standalone mode and had made many arguable decisions. This led us to create our own model. Improving scFMs to generate better representations of cells, genes, and their networks thus became one of the main objective of this Ph.D.

We also sought to create a new benchmark, better suited to the single-cell genomics field and especially to GRN inference. The goal of the benchmarks were to be more driven by real life applicability. Indeed the current methods often tended to use artificial data and groundtruths that are not representative of the real biological systems. The tasks and scores were more reminiscent of classical machine learning benchmarks than of biological relevance. The known single-cell standardized benchmarks were also almost never used by the first generations of scFMs papers.

0.7.3 collaborations

Finally, while we managed to get some collaborations going, this is something that we did not manage to achieve successfully. I think it would surprise no-one to say that we are in a challenging environment for cross-discipline collaborations. I still realize the need for these foundation models to be made more accessible, which also became one of the objectives and contributions in this thesis. It is represented not only in the effort to release easy-to-use open source models but also in various side contributions and outreach efforts.

0.8 Chapters overview & main contributions

This thesis is structured around three main publications, each presented as a chapter. Below, we provide detailed summaries of our contributions and results for each chapter.

0.8.1 Chapter 1 : scPRINT : pre-training on 50 million cells allows robust gene network predictions

In this chapter, we present scPRINT (single-cell PRe-trained Inference of Networks with Transformers), a large cell model designed for cell-specific gene network inference at genome scale. This work addresses a fundamental challenge in cellular biology : inferring the network of molecular interactions that governs cell behavior.

Model architecture and training innovations. We trained scPRINT on more than 50 million cells from the CellxGene (CxG) database, representing approximately 80 billion tokens across multiple species, diseases, and ethnicities. Our model introduces several architectural innovations : (1) a protein-based gene encoding using ESM2 embeddings, which reduces parameters while enabling cross-species generalization ; (2) a learned expression tokenization via MLP rather than hand-crafted binning ; and (3) positional encoding of genomic location to capture co-regulation patterns. We designed three complementary pretraining tasks : a denoising task (transcript upsampling), a bottleneck learning task (embedding compression and reconstruction), and a label prediction task with hierarchical classification for disentangled cell embeddings representing different phenotypic facets.

Gene network inference methodology. A critical contribution is our method for extracting cell-specific gene networks from the transformer's attention matrices, inspired by similar approaches in ESM2 for protein contact prediction. We made this approach scalable to compute genome-wide networks for thousands of cells on commodity hardware. We also introduced an attention head selection mechanism, where a subset of heads can be selected based on correlation with known ground truth networks, significantly improving network quality in larger models.

Comprehensive benchmarking framework. We created BenGRN and GRnnData, novel benchmarking suites for GRN inference that address the lack of standardized evaluation in the field. We benchmarked scPRINT against scGPT, Geneformer v2, DeepStructural

Equation Modeling (SEM), and GENIE3 using multiple ground truth types : literature-based networks (Omnipath), cell-type-specific ChIP-seq/perturb-seq intersections (MCalla et al.), and genome-wide perturb-seq data. Our results demonstrate that scPRINT outperforms all other methods on most benchmarks. On the Omnipath benchmark across 26 cell types, scPRINT recovered 67% more connections than GENIE3 and showed superior enrichment for TFs and their ENCODE-validated targets (20% of TFs with significant enrichment, compared to 0% for scGPT). On the MCalla et al. cell-type-specific ground truth, scPRINT consistently outperformed all methods on both AUPRC and Early Precision Ratio (EPR) metrics.

Zero-shot capabilities on orthogonal tasks. Beyond gene network inference, we demonstrated that scPRINT's learned cell model enables competitive zero-shot performance on denoising, cell type prediction, and batch effect correction—without fine-tuning. For denoising, scPRINT matches SOTA methods (MAGIC, KNNsmoothing2) on bulk populations and outperforms them on rare cell types where neighborhood-based methods fail. For cell type classification, scPRINT achieves 62% accuracy as a zero-shot predictor across 200+ cell types, outperforming marker-based methods like CellTypist. For batch effect correction, scPRINT achieves competitive scIB scores without using batch labels, outperforming all methods that similarly do not require batch annotation.

Biological application and discovery. We applied scPRINT to an atlas of 83,000 cells from normal and Benign Prostatic Hyperplasia (BPH) prostate tissues. In rare switched memory B-cells, we identified early TME markers including BAG5, a known B-cell-associated prostate cancer marker. In fibroblasts, our gene networks revealed differential hub genes between normal and BPH-associated cells, recovering known biology around PAGE4 and uncovering interconnected pathways linking ion exchange, Extracellular Matrix (ECM) remodeling, oxidative stress, and chronic inflammation—hallmarks of premalignant states.

0.8.2 Chapter 2 : Xpressor : Towards foundation models that learn across biological scales

In this chapter, we present Xpressor, a framework and architecture enabling cross-scale learning between biological foundation models. This work addresses a fundamental challenge : while foundation models exist at multiple biological scales (molecules, sequences, cells, tissues), they operate in isolation, unable to leverage the rich interconnections between scales.

Motivation and conceptual framework. We begin with a comprehensive review of foundation models across four biological scales : mFMs for atomistic molecular representations, nFMs for nucleotide and amino acid sequences (DNA, RNA, proteins), cFMs for cellular abundance profiles, and tFMs for tissue-level spatial organization. We argue that information flows between scales : lower-scale models (e.g., protein sequences) can improve input representations for higher-scale models (e.g., cells), while relationships learned at higher scales can inform lower-scale representations. Each scale's vocabulary can be seen as built from the compressed representations of the scale below—amino acids from atoms, genes from proteins, cells from genes, tissues from cells.

The Xpressor architecture. Our first contribution is a cross-attention-based compression mechanism called Xpressor that transforms high-dimensional gene-level representations into lower-dimensional cell-state vectors. The architecture introduces additional transformer blocks that perform cross-attention between the output embeddings of a foundation model and a set of learned latent tokens. This creates a bottleneck that compresses m gene tokens of dimension d_c into n cell tokens of dimension d_t, where $n \ll m$ and $d_t < d_c$. Critically, the same transformer can then decompress these cell representations back to gene-level predictions using cross-attention with gene ID tokens. This compression/decompression framework is grounded in the information bottleneck theory of Tishby et al., where the goal is to retain maximal information about relevant variables while achieving compression. We further regularize the latent space using contrastive losses between embedding dimensions and dimension-specific classifiers, ensuring each cell embedding dimension captures distinct biological information.

Multi-scale fine-tuning approach. Our second contribution is a method for fine-tuning lower-scale models using upper-scale tasks via adapter layers. We demonstrate this using ESM2 (a protein language model) as the lower-scale model and scPRINT as the upper-scale model. Rather than simply using frozen ESM2 embeddings as gene tokens, we add a trainable MLP adapter that transforms each protein embedding during scPRINT's pretraining. We provide a formal proof that such an MLP has sufficient capacity to learn any arbitrary mapping—including acting as a lookup table that assigns each of D proteins to a unique learned output. This allows the adapter to enrich ESM2's representations (which encode protein sequence, evolutionary constraints, and structure) with co-expression information learned from millions of single-cell profiles.

Empirical results on the scPRINT benchmark gymnasium. We evaluate both contributions on three tasks from the scPRINT benchmark : cell-type prediction, embedding quality (scIB score for batch correction and biological consistency), and gene network inference (EPR on genome-wide perturb-seq and Omnipath ground truths). For the Xpressor architecture versus standard class-pooling (as used in scGPT), we observe substantial improvements : cell-type prediction accuracy increases from 0.60 to 0.72 (+20%), and embedding quality improves from 0.48 to 0.52 (+8%), while gene network inference remains comparable. For multi-scale fine-tuning, comparing frozen ESM2 embeddings versus fine-tuned ones, we see cell-type prediction improve from 0.60 to 0.70 (+17%), embedding quality from 0.48 to 0.49, and gene network inference improve on the Omnipath benchmark from 2.0 to 2.4 EPR (+20%). Notably, fine-tuned ESM2 embeddings outperform both frozen ESM2 and randomly initialized embeddings across nearly all metrics.

0.8.3 Chapter ?? : scPRINT-2 : Towards the next-generation of cell foundation models and benchmarks

In this chapter, we present scPRINT-2, a next-generation single-cell foundation model whose design decisions were systematically validated through an unprecedented additive benchmarking framework. This work addresses the critical gap in the field : while many scFMs have been proposed, the relative importance of their architectural choices, training strategies, and data modalities has never been rigorously assessed in isolation.

The additive benchmark : a systematic evaluation framework. We designed a comprehensive benchmark to evaluate 42 different configurations of scFM components, including pre-training databases, architectures, and training tasks. Each model variant was trained 6 times across multiple seeds to generate statistical error bounds, and evaluated on a gymnasium of tasks : cell-type classification, batch correction (scIB scores), expression denoising, and gene network inference. Our benchmark revealed several key findings : (1) denoising is superior to masking as a pre-training task for classification and embedding quality ; (2) un-normalized expression outperforms normalized input ; (3) ESM-based gene tokens significantly outperform learned embeddings from scratch ; (4) genomic location encoding improves model convergence ; (5) MSE loss outperforms ZINB on average, but a hybrid ZINB+MSE loss provides the best balance between accuracy and expressivity ; and (6) model size correlates with improved gene network inference and cell-type prediction.

The scPRINT-2 corpus : the largest single-cell database to date. We assembled a pre-training database of over 350 million cells from 16 eukaryotic organisms spanning more than one billion years of evolution. This corpus integrates data from CxG, the Tahoe-100M dataset, and the scBasecount database (20,000 reprocessed GEO datasets), totaling 25 TB of unique data with approximately 400,000 distinct genes and 4,764 different cell labels across 140,000 cell groups. We demonstrated that cell-state diversity and data quality are more important than sheer cell count—reducing to 200 human datasets caused only minimal performance decrease, while using low-diversity datasets alone caused performance to plummet. We introduced cluster-weighted sampling and Number of Non-Zeros (NNZ)-weighted sampling to address dataset imbalances, enabling effective training on this heterogeneous corpus.

Architectural innovations. scPRINT-2 incorporates 12 distinct contributions validated through our benchmark. Key innovations include : (1) the XPressor architecture, a cross-attention-based compression mechanism that transforms gene-level representations into cell-level tokens and back, enabling the model to be generative ; (2) a GNN-based expression encoder that leverages neighborhood information from similar cells or spatial neighbors ; (3) criss-cross attention, a sub-quadratic attention mechanism inspired by Recurrent Interface Networks that dramatically improves training speed while retaining model capabilities ; (4) VAE-based compression with dissimilarity losses between cell tokens, improving batch correction ; and (5) an updated hierarchical classification loss that penalizes predictions based on ontological distance rather than binary correctness.

State-of-the-art performance across benchmarks. On the Open Problems benchmark (November 2025), scPRINT-2 achieved 75% zero-shot cell-type classification accuracy, outperforming scPRINT-1 (47%) and all other zero-shot scFMs (40-60%). With our XPressor-based Parameter-Efficient Fine-Tuning (XPEFT), scPRINT-2 surpassed every existing supervised and unsupervised method on the platform. For expression denoising, scPRINT-2 became state-of-the-art, outperforming MAGIC across all tested contexts, with particularly strong improvements on low- and mid-quality datasets where the GNN encoder can leverage neighbor information. For batch integration, scPRINT-2's zero-shot performance exceeded all other methods, and fine-tuned performance achieved the best overall scIB scores.

Generalization to unseen modalities and organisms. We demonstrated scPRINT-2's ability to generalize beyond its training distribution. On Xenium spatial transcriptomics data (a modality absent from training), scPRINT-2 successfully denoised expression, imputed 5,000

unseen genes with correlation scores matching denoised genes, and produced biologically meaningful cell-type and disease predictions. On cat and tiger lung tissues (organisms not seen during training), scPRINT-2 achieved 42% cell-type classification accuracy across 500 possible labels, with differential expression analysis confirming that scPRINT-2 sometimes corrected expert annotations. With cluster-based logits averaging and XPEFT fine-tuning, accuracy improved to 95%.

Counterfactual reasoning and generative capabilities. The XPressor architecture enables scPRINT-2 to perform counterfactual generation. We demonstrated this by replacing organism-specific cell embeddings from mouse cells with human embeddings to generate "humanized" mouse expression profiles. The Wasserstein-2 distance between these counterfactual profiles and real human cells decreased significantly, and over-representation analysis showed 58% enrichment in correctly predicted differentially expressed genes. Pathway analysis revealed biologically meaningful differences in immune function, membrane-ECM interactions, and tissue elasticity.

Gene embeddings and network inference. We showed that the XPressor architecture produces output gene embeddings with meaningful biological clustering (enriched for known pathways), whereas standard transformers without XPressor produce embeddings that merely encode expression values. For gene network inference, we introduced a computationally intensive extraction method biased toward co-expressed genes. Benchmarking against six ground-truth networks (including the cellmap Affinity Purification Mass Spectrometry (AP-MS) data, human interactome, and Genome-wide Perturb-seq (gwps)), scPRINT-2 showed improved performance on odds-ratio metrics. We demonstrated cross-species gene network analysis in macrophages, identifying conserved hub genes involved in feroptosis, pathogen phagocytosis, and MHC pathways. We also showed how scPRINT-2's predictions can cross-validate PPI ground truths, identifying connections (HLA-DRA/CD74, B2M/B2M) that RoseTTAFold2-PPI missed but AlphaFold-Multimer confirmed.

Full open-source release. All components are released under the GPL-v3 license : scPRINT-2 model weights, the 350-million-cell corpus with an interactive visualization of 1% of cells aligned into an atlas, pre-training code and datasets, all 42 additive benchmark model weights and training traces, and the scDataLoader package enabling efficient weighted random sampling over billions of elements.

0.8.4 Other contributions

This thesis presented other contributions not in the form of publications :

— The first ones are six open source Python packages named :

scPRINT : where the model is made available, together with training scripts and notebooks to use the model, functions to download and preprocess data, and more. https://github.com/cantinilab/scPRINT

scPRINT-2 : where the second model is made available, together with training scripts and notebooks to use the model, functions to download and preprocess data,

and more. https://github.com/cantinilab/scPRINT-2

scDataloader : a package to load efficiently thousands of large single-cell datasets, with preprocessing, filtering, and loading options. It also allows a first-of-its-kind efficient weighted random sampling over billions of elements. https://github.com/jkobject/scDataLoader

Bengrn : a package to benchmark GRN inference methods on single-cell data, using multiple types of metrics and ground truth networks. https://github.com/jkobject/Bengrn

GRNNdata : a package to work with gene regulatory networks and single-cell data jointly, using the Anndata format. https://github.com/cantinilab/GRNNdata

Xpressor : a package to reproduce the second paper's experiments and create an Xpressor model from scratch. https://github.com/cantinilab/XPressor

Simpler Flash : Initially a package to facilitate the use of flash attention before it became part of the pytorch implementation itself. It now includes multiple types of efficient attention mechanisms, such as softpick-flash and our flash criss-cross attention mechanism. https://github.com/jkobject/simpler_flash

Hierarchical Classifier : a package to implement hierarchical classification for single-cell data. https://gist.github.com/jkobject/5b36bc4807edb440b86644952a49781e

— Another contribution, as previously mentioned, is around accessibility. Not only did I release model weights and inference code, but I also provided easy-to-use inference tools, pre-training methods and datasets, training traces, and documentation. Moreover, tutorials were implemented in Google Colab, and versions of the models got released on the Chan–Zuckerberg model hub (https://virtualcellmodels.cziscience.com/) and Superb.io's platform (https://superbio.ai).
— Finally, I made a Docker implementation of scPRINT, scGPT, and Geneformer for their benchmarking on the open problems platform and participated in the improvement and creation of two benchmarks on the platform.
— In addition to publication, I wrote a blog post with Lamin.ai on training on large datasets. I also wrote with multiple x-plainers on X, LinkedIn, Bluesky, and Threads, as well as my personal website, to share some of our findings with a possibly wider audience. Similarly, I wrote vulgarisation articles for the Pasteur Institute's and CNRS's websites and created one of the most viewed videos on the Pasteur Institute's YouTube and Instagram accounts, presenting my work. I also got highlighted on Whitelab's blog posts and released four YouTube videos of diverse presentations of my work.
— Other outreach efforts were done through conference presentations and invited talks with :

  A participation in three international ML conferences

  Over 25 invited talks and five poster presentations.
— Finally, I also contributed to the European ecosystem of start-ups, translating works from Academia to Industry. I became part of a worldwide organization called Nucleate

to help Master students, PhDs, and Post-docs translate their research into start-ups. I also worked as a consultant for four start-ups : Whitelab Genomics, Biographica, Blossom, and dot-omics, assisting them in developing strategies for foundation models in single-cell RNA-seq and DNA sequencing.

scPRINT : pre-training on 50 million cells allows robust gene network predictions

1.1 Summary

A cell is governed by the interaction of myriads of macromolecules. Inferring such a network of interactions has remained an elusive milestone in cellular biology. Building on recent advances in large foundation models and their ability to learn without supervision, we present scPRINT, a large cell model for the inference of gene networks pre-trained on more than 50 million cells from the CxG database. Using innovative pretraining tasks and model architecture, scPRINT pushes large transformer models towards more interpretability and usability when uncovering the complex biology of the cell. Based on our atlas-level benchmarks, scPRINT demonstrates superior performance in gene network inference to the SOTA, as well as competitive zero-shot abilities in denoising, batch effect correction, and cell label prediction. On an atlas of BPH, scPRINT highlights the profound connections between ion exchange, senescence, and chronic inflammation.

1.2 Introduction

Understanding the cellular mechanism is considered a milestone in biology, allowing us to predict cell behavior and the impact of drugs and gene knock-outs[61, 62, 63, 64, 65]. A cell is regulated by a complex interplay of myriads of macromolecules that define its state. We can simplify these interactions via a GN[9] (GN). Many approaches have been developed to infer these networks, focusing on TF-to-gene links using single-cell omics data modalities like scRNA-seq and scATAC-seq[66, 67, 68, 69, 54, 70, 56, 71, 72, 73, 74, 75]. This gene network subset regulating the cell gene expression levels is often called a GRN. However, many other gene products than TFs impact RNA abundances in the cell, like RNA-RNA and protein-TF interactions[76, 77, 78, 79, 80]. Most GRN inference methods do not scale to the number of

genes and cells present in single-cell RNA datasets, and they need many cells, thus impairing their ability to reconstruct cell-state-specific networks. Other methods consider datasets where differentiating cells can be ordered temporally to predict more causal GRNs. While this approach is interesting, temporal ordering is often hard to predict[71, 81].

Benchmarks like BeeLine[82] and MCalla et al.[83] have shown that despite the existence of many methods, GN inference remains a challenging problem. Indeed, it is underconstrained and has limited prior knowledge. New foundational models trained on tens of millions of measurements could help solve these difficulties. Transformers like BERT[38, 84] have gained traction in computational biology and have held promise to learn a model of the cell that would translate across many tasks of cellular biology, such as cell type annotation, batch-effect correction, perturbation prediction, and gene network inference[44]. Among them, scGPT[45] got much attention, proposing a novel encoding of genes and their expression, a new pretraining methodology similar to autoregressive pretraining in language models, and the possibility of extracting GRN from its model (see 1.5. methods).

Inspired by these efforts, we propose scPRINT (single-cell PRe-trained Inference of Networks with Transformers), a foundation model designed for gene network inference. scPRINT brings inductive biases and pretraining strategies better suited to GN inference while answering issues in current models (see Supplementary Table 6.1.1). scPRINT outputs cell type-specific genome-wide gene networks but also generates predictions on many related tasks, such as cell annotations, batch effect correction, and denoising, without fine-tuning.

We extensively benchmark scPRINT on challenging gene network inference tasks, from literature-based networks to cell type-specific ones generated via orthogonal sequencing methods. We show that scPRINT outperforms the SOTA on most of these atlas-level benchmarks. In addition, our model focused on GN inference, is also competitive on a compendium of tasks like denoising, cell type prediction, and embedding with batch effect correction. This suggests that by learning a cell model, scPRINT gains zero-shot abilities in many tasks of cellular biology. We use scPRINT to analyze an atlas of normal and senescent prostate tissues where we identify rare cell populations with early markers of the TME in B-cells. In fibroblasts, we study gene networks and recover known hubs such as PAGE4, linking the senescence of fibroblasts to changes in the ECM and downstream inflammation. We find key interconnected pathways of the oxidative stress response and extracellular matrix building via metal and ion exchange in the gene network of BPH-associated fibroblasts. We also show that healthy and disease-related cells exhibit different network patterns, demonstrating that scPRINT can help identify novel pathways and targets while considering them in their specific cellular and molecular contexts.

scPRINT[85] (https://github.com/cantinilab/scPRINT) is a fast and open-source tool that can be readily integrated into the bioinformatics pipeline. We make public the code and model weights, but also the pretraining strategies, datasets, and our own dataloader for use with vast training sets like the CxG databas[86]. We also release a Gene Network benchmarking suite : *BenGRN*[87] and *GrnnData*[88].

1.3 Results

1.3.1 scPRINT : a scRNAseq foundation model for gene network inference

We propose scPRINT (Figure 1.1A), a SOTA bidirectional transformer designed for cell-specific gene network inference at the scale of the genome. scPRINT is trained with a custom weighted-random-sampling method[89] over 50 million cells from the CxG[86] database from multiple species, diseases, and ethnicities, representing around 80 billion tokens (see 1.5. Methods). We train scPRINT at various scales (from 2M to 100M parameters) and very efficiently by using flashattention2[90], e.g., only requiring an A40 GPU for 48 hours to train our medium model, significantly reducing the barrier to entry for any computational biology lab (see Supplementary Table 6.1.2).

To push scPRINT to learn meaningful GNs and their underlying cell model, we design a unique set of pretraining tasks, as well as expression encoding and decoding schemes (Figure 1.1B).

scPRINT's pretraining is composed of three tasks which loss are added and optimized together : a denoising task, a bottleneck learning task, and a label prediction task. The objective is to let scPRINT learn to represent meaningful gene connections while also endowing it with a breadth of zero-shot prediction abilities.

Indeed, similarly to ADImpute[91, 28], we expect a good gene network to help denoise an expression profile by leveraging a sparse and reliable set of known gene-gene interactions.

We implement this denoising task as the upsampling of transcript counts per cell (see 1.5. Methods). While most other methods have been using masking as a pretraining task, our method is related to the downsampling and masking task of scFoundation[49]. We show that this strategy performs better than masked language modeling and gives scPRINT the ability to upsample any expression profile.

In addition, we expect that a cell model tasked to compress expression profiles into embeddings can learn the regularities of modules and communities of gene networks. Therefore, the bottleneck learning task drives scPRINT to generate an embedding and a cell expression profile from its embedding only. The embedding is generated by scPRINT and is used again, this time without the cell expression values, to regenerate the true profile (see 1.5. Methods).

Finally, the cell's gene network should represent the cell state and its different phenotypic facets. Effectively, scPRINT generates not just one embedding per cell but multiple. A hierarchical classifier is then applied to each distinct cell embedding to predict its associated class, such as cell type, disease, sex, organism, ethnicity, and sequencing platform. The embeddings thus become disentangled, each representing a specific facet of the cell state[92]. This last training task pushes the large cell model and its gene network to represent the cell state.

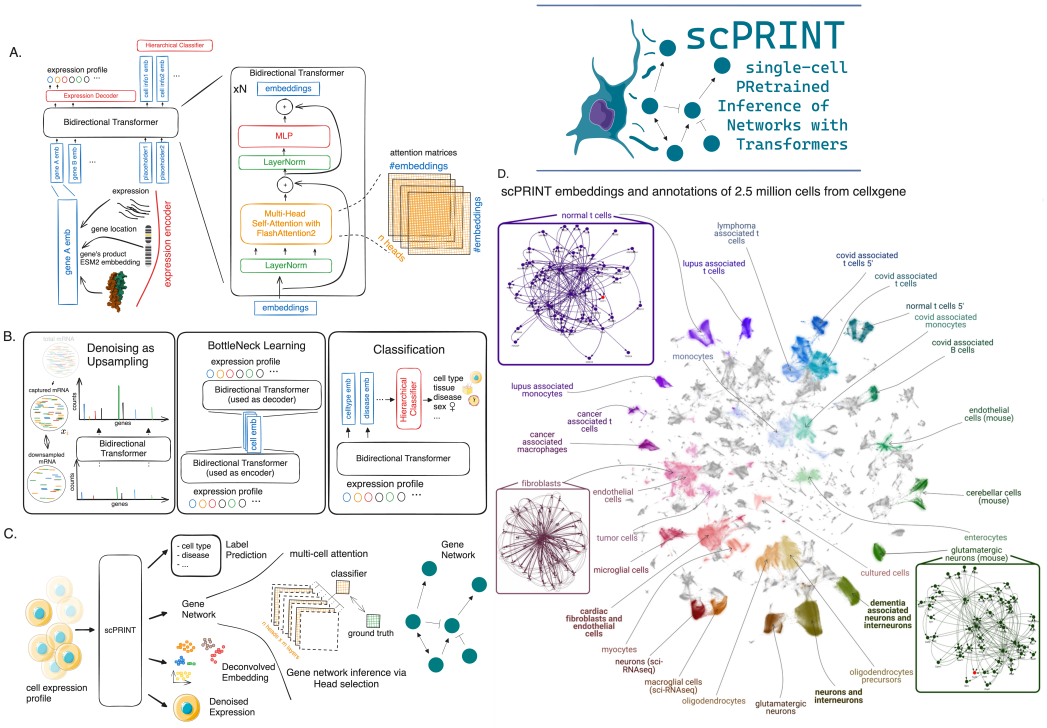

Figure 1.1 – (a) Schematic representation of scPRINT with its bidirectional encoder, gene expression embedding encoding via gene location, matched protein ESM2 embedding, and gene expression. (b) scPRINT pre-training tasks : Denoising task whose goal is to recover the known transcriptomic profile from a purposefully downsampled expression profile. Bottleneck learning reconstructs the expression of requested genes using only their cell embedding. The same model is used for both The encoding and decoding steps. Hierarchical classification is achieved by applying a hierarchical classifier to each disentangled embedding. This pushes the first embedding to contain cell type info, the second embedding to contain disease info, and so on (see 1.5. methods). (c) The different outputs in scPRINT. scPRINT generates label predictions of cell type, tissue, disease, sex, sequencer, ethnicity, and organism. scPRINT generates multiple embeddings (which we call disentangled embedding), a general one, as well as a specific embedding for each class. scPRINT also generates a reconstructed expression profile at any requested sequencing depth (i.e., total transcript count) (denoising). scPRINT also generates a Gene Network by selecting and combining various attention heads into a gene x gene matrix. (d) Example of a scPRINT output from a random subset of 2.5 million cells from the CxG database. Embeddings and labels are generated by scPRINT, together with the example cell type-specific gene networks. We show only subparts of the networks extracted from a central node, represented in red.

Thanks to the CxG database requirement for complete annotations and our innovative hierarchical classifier, we have added label prediction as part of the pretraining of scPRINT. While the assumption is that in other modalities, the scarcity and noisiness of such labels make it infeasible, we show that this approach is a net positive in our case (see Supplementary Table 6.1.3 ; 1.5. Methods). Indeed, it helps us disentangle the various cell embeddings and

performs zero-shot predictions on unseen datasets. These disentangled embeddings are opening a future possibility to perform counterfactual generation : mixing embeddings representing different facets of cell states, e.g., fibroblast + cancer + pancreas tissue + female, to generate novel unseen expression profiles.

scPRINT converts the gene expression of a cell to an embedding by summing three representations or tokens : its id, expression, and genomic location (Figure 1.1A, see 1.5. Methods). scPRINT encodes the gene IDs using protein embeddings. This gene representation is made using the ESM2[93] amino-acid embedding of its most common protein product (see Supplementary Figure 6.2.1). First proposed in UCE[48], the model learns to leverage representations that can potentially apply to unseen genes and species, using the structural and evolutionary conservation of the sequence encoded by ESM2. While drastically reducing the number of weights used in the model compared to scGPT and Geneformer (see 1.5. Methods), this representation also contains some priors needed to infer protein-protein[94] interactions (Figure 1.1A).

The gene's expression is tokenized via a MLP using log-normalized counts. This MLP lets the model learn a metric behind gene expression, whereas scGPT and Geneformer apply a specific prior for the encoding of their gene expression (see 1.5. Methods).

Finally, we help the model know that genes with similar locations tend to be regulated by identical DNA regions, using the positional encoding of their location in the genome (see 1.5. Methods).

These three embeddings are summed and then concatenated across all the genes expressed in a cell together with additional placeholder cell embeddings to form the transformer model's input.

scPRINT is pretrained using 2,200 randomly selected expressed genes in a cell profile. If a cell doesn't have enough expressed genes, the list is padded with randomly selected unexpressed genes. A context of 2200 genes, while not genome-wide, captures all the expressed genes in more than 80% of the cell profiles in the CxG database. We also show that scPRINT can make predictions on much larger sequences of genes at inference time without using attention approximation methods[95].

Using unexpressed genes, combined with the denoising task, let scPRINT discriminate the true zeros from dropouts in scRNA-seq47. The expression decoder of scPRINT further helps model this statistic of the data. It is a zero-inflated negative binomial graphical model inspired by previous literature in single-cell RNA-seq modeling48. Here, the loss (also used for bottleneck learning) is thus the log-likelihood of the gene expression given the distribution parameters.

As shown in Figure 1.1C, at inference time, scPRINT can generate multiple outputs across any scRNA-seq-like cellular profile of various mammalian species without fine-tuning. Figure 1.1D shows scPRINT's prediction at the scale of an atlas of 2M randomly sampled cells from CxG. From its pre-training, scPRINT performs denoising, label prediction, and cell embedding without fine-tuning. However, a critical emergent output of scPRINT is its cell-specific gene networks. Following a similar approach to ESM2, we generate cell-level gene networks via the bidirectional transformer's input-wise weighted matrices, called

attention matrices -or heads-. They represent general gene-gene connections and can be subsetted to TF-gene connections (i.e., GRNs). Remarkably, we made this approach scalable enough to compute attention heads-based gene networks for 1 to 10,000 cells, at the genome scale, with commodity hardware and in a few minutes. These networks both showcase the ability of scPRINT to model cellular biology and help make it a more explainable tool for the community, showing the network assumptions made during inference. The attention heads are either all aggregated by averaging or can be selected to better reflect connections of interest (Figure 1.1C). This is done using the average of the heads most correlated with literature or perturbation-based ground truth networks. Finally, while we do not assess scPRINT's ability to model inhibition due to the scarcity of such annotations, we leave open the possibility of using our head selection technique for such a task.

Similarly to what has already been done in ESM2 and the Large Language Model literature[96, 97, 98], we deeply investigate the meaning of attention matrices in the context of cellular biology, an aspect under-studied in the literature of foundation models applied to genomics.

In the following sections, we benchmark scPRINT on gene network inference against scGPT, DeepSEM[75], GENIE3[99], and Geneformer v2[100], the updated version of Geneformer. scGPT and Geneformer v2 are highly cited and published transformer models for single-cell scRNA-seq, mentioning the inference of gene interactions[45]. DeepSEM is an autoencoder model jointly learning its weights and a gene network matrix. GENIE3 generates networks via regression by finding the set of genes that best predict another gene's expression. It is one of the top-performing and most used methods for GRN inference (see 1.5. Methods). However, it suffers from very long run times and high memory requirements (see Supplementary Table 6.1.4).

1.3.2 scPRINT recovers biological features in its gene networks

We benchmark scPRINT against the SOTA based on whether their recovered networks contain meaningful biological knowledge. We consider two main benchmarking methodologies, one using a simulated expression profile from a well-established biological network. Because simulated data does represent real cell expression data (see 1.5. Methods), our second and main approach focuses on biological features of a network inferred from real cell expression profiles. Indeed, we assume that a meaningful gene network should have some of its hub nodes being TFs. TFs should be more connected to their known target, on average. We should recover known gene-gene connections and expect enrichment of cell type-specific marker genes in the network.

We compare each gene network inference method's ability to recover a known network from 1000 simulated single-cell scRNA-seq expression profiles generated by the Sergio Ordinary Differential Equation (ODE) model[101] from the ground truth network Regnetwork[102] (see 1.5. Methods). Only scPRINT was able to recover meaningful connections (see Supplementary Table 6.1.5). One explanation is that through its training, scPRINT has learned the common gene connections that also exist in the RegNetwork ground truth.

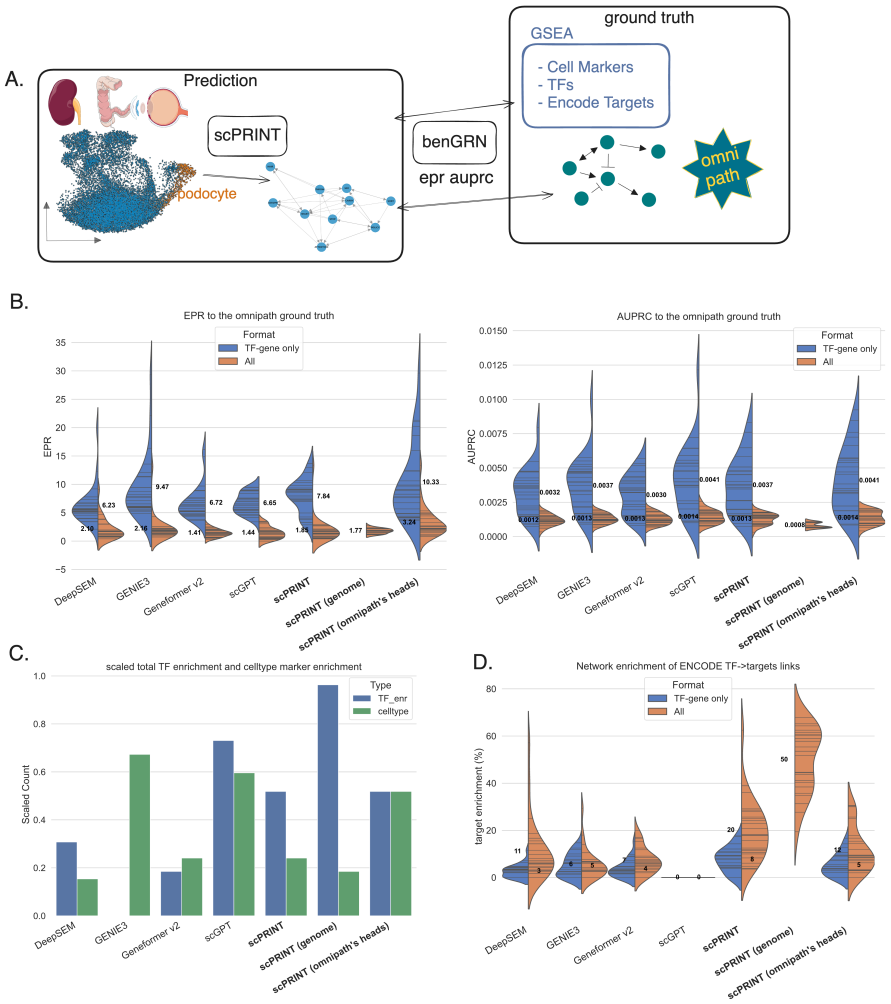

FIGURE 1.2 – (a) We extract cell type-specific gene networks for each cell type in the dataset (n=26 cell types across 3 datasets). We perform Gene Set Enrichment Analysis (GSEA)[103] on the network's nodes (n=4000 genes). We compute the ability of the edges to recover the Omnipath ground truth's connections. (b) Violin plot of the ten different AUPRC and EPR values obtained when comparing the inferred cell type-specific networks with the Omnipath network for scPRINT : average of all attention heads, scPRINT (genome) : same scPRINT version but computing a genome-wide gene network, scPRINT (omnipath's heads) : same scPRINT version but with attention heads selected using a subset of omnipath, scGPT, DeepSEM, Geneformer v2, and GENIE3, when considering only TF-gene connection or all gene-gene connections. (c) Violin plot of the average number of TF with enrichment for their ENCODE target in each cell-type-specific network. (d) Number of GNs with a significant enrichment of TFs and of their cell type's marker genes.

On gene network inference from real expression data, we noticed that depending on cell type and datasets, the different tools could vary greatly in the similarity of their GNs to the Omnipath[104] ground truth. Because of this, we focused our benchmark on three randomly selected test datasets of kidney, retina, and colon tissues comprising 26 cell types[105, 106,

21] (see 1.5. Methods, per dataset results in Supplementary Figure 6.2.2). Of note is that we could not determine if these datasets were used during the training of scGPT or Geneformer.

We build one network per cell type, using the same 1024 cells and their 5000 most differentially expressed genes for all benchmarked methods. We evaluate the quality of the networks based on their overlap with Omnipath. We also compute the network enrichment for cell type markers, TFs, and ENCODE TF targets using the prerank[103] algorithm (Figure 1.2A).

Although the scGPT code mentions GRN inference only using perturb-seq data, we reapply the same method without the perturbation-baseline comparison. This is to make it comparable with other benchmarked methods and because most of our datasets are not perturbation-based. Similar to what is presented in its paper, we use the mean of the attention matrices across cells and the four attention heads of the last layer of the human pre-trained model. We retain this method across our benchmarks for scGPT (see 1.5. Methods). We apply a similar strategy for Geneformer (see 1.5. Methods).

For scPRINT, we generate three network versions : one simply called scPRINT, based on the average of all heads in the model. scPRINT (omnipath's heads), based on the average of heads selected with our abovementioned head selection method inspired by ESM2, and scPRINT (genome), which is like the scPRINT network but uses our method to generate genome-wide networks (see 1.5. Methods) instead of using the 5000 most differentially expressed genes. Indeed, in transformer models, the choice of attention heads is important. Although transformers can learn the causal structure of their input, it has been shown that some attention heads, especially in larger networks, can become unused, containing predominantly random connections[107]. Some work has been done at pruning these heads[108] or forcing a head selection mechanism during inference and training[109]. For scPRINT (omnipath's heads), we select heads based on a linear classifier's prediction of the best set of heads to predict a subset of Omnipath (see 1.5. Methods). Similarly to the scPRINT network, these heads are then averaged to generate the scPRINT (omnipath's heads) gene network. To perform this selection, we split the omnipath dataset into train/test and select heads, using 50% of the ground truth and only the first cell type of each dataset. We then use the same combination of heads across all other cell types. This shows that our selection process builds consistent networks across cell types and parts of the ground truth. This innovative approach contrasts with previous ones like scGPT's and GENIE3 by using part of an available ground truth to select heads.

First, we look at how much information from Omnipath is contained in the inferred networks. Omnipath contains around 90,000 curated gene-gene connections, mainly from the literature. These connections are cell type agnostic, and most are TF - gene. On this benchmark, we evaluate the networks based on AUPRC and EPR, two metrics often used in GRN benchmarks[82] (see 1.5. Methods), where we define our task as a binary classification of connections on all gene-gene pairs. Due to the row-wise normalization of networks generated by all methods, and because Omnipath has many sources with only a few targets (see Supplementary Figure 6.2.3), we here use the transpose of our inferred networks when making comparisons with Omnipath (see 1.5. Methods). In Figure 1.2B, we can see that scPRINT (omnipath's heads) outperforms all methods on average across all cell types. While scPRINT (omnipath's heads) uses some ground truth information to select its head, we see

that scPRINT still outperforms scGPT and Geneformer v2 on the EPR metric, showing that its top predicted edges more closely match the ground truth.

AUPRC results are very low overall because we do not expect most Omnipath connections to be present in the cell type's gene network, as many connections in Omnipath might only be true in some cellular contexts. Moreover, we do not expect most connections in our generated network to exist in Omnipath as it only contains a small fraction of all real gene-gene connections. Although overall AUPRC values are small, we can see that both scGPT and scPRINT outperform the other methods in the number of connections recovered. Indeed, on average, scGPT and scPRINT respectively recover 42% and 67% more connections than GENIE3.

However, GENIE3 is often used by biasing the method to only predict TF-gene connections (see 1.5. Methods). This type of network, usually called a GRN, is most often used, given the importance of TFs in regulating gene expression. To compare the other methods to this GRN version of GENIE3, we also use a GRN version of their networks by subsetting them to TF-gene connections only. In this context, all the methods significantly improve their predictions without altering their relative performances (Figure 1.2B). This is unsurprising, considering that Omnipath is strongly biased towards TF-gene interactions.

Interestingly, we have seen that smaller scPRINT models containing fewer heads perform better when taking the average of their heads. In contrast, head selection is often more advantageous in larger models with more heads (see Supplementary Table 6.1.7). As presented at the beginning of the results section, it might be that as models become larger and less regularized, some heads tend to become unused and contain mostly noise. As a consequence, a head selection is advantageous in larger models.

We also expect biologically meaningful gene networks to have their central nodes enriched for TFs. In addition, because these networks are cell type-specific, we expect their central nodes to be enriched for some marker genes of their associated cell types (see 1.5. Methods). In this regard, both scGPT and scPRINT achieve very similar and strong network enrichment for TFs compared to GENIE3, DeepSEM, and Geneformer v2, whose networks are not enriched for TFs (Figure 1.2C).

Moreover, amongst the 178 cell types we have marker gene sets for in pangaloDB[110], all methods find some enrichment, especially GENIE3 and scGPT (see 1.5. Methods). We notice that selecting heads based on Omnipath significantly improves scPRINT's network enrichment for cell-type markers. Of note, our goal is not to annotate cell types from the gene network but mainly to showcase the network's cell type specificity.

Finally, we also examine how much the connections of each TF are enriched for that TF's target. Here, scPRINT overperforms all other methods (Figure 1.2D). In the scPRINT networks, 20% of the Transcription Factors for which we have data on ENCODE have connections significantly enriched for their ENCODE-validated gene targets[111]. Interestingly, only our large cell model achieved a great performance, and scGPT did not display any enrichment across the 26 cell types assessed. While we acknowledge that ENCODE is used in the Omnipath database, we cannot expect Omnipath to represent the ENCODE targets. Indeed, it combines and processes 57 additional data sources to build its consensus network.

scPRINT (genome) has been added despite its performance not being comparable to other methods. Indeed, comparing its overlap with Omnipath is unfair as it includes many more genes and connections, many of which will have almost no data on this ground truth. While scPRINT (genome) showcases our ability to generate genome-wide networks, it also shows strong performances in TF enrichment and ENCODE TF-target enrichments. This highlights that even at such a large scale, networks generated by scPRINT are enriched in biological knowledge gained solely from its pre-training tasks.

Overall, we have shown that scPRINT generates, in one forward pass, cell type-specific gene networks that are biologically meaningful. We will now examine them using cell type-specific ground truths extracted from orthogonal experiments.

1.3.3 scPRINT outperforms the state of the art on cell type-specific ground truths

Although we have shown that our networks represent meaningful biology, the Omnipath ground truth is literature-based and not cell type-specific. Here, we use two different modalities, perturb-seq[22], and ChIP-seq[112], as ground truths to compare predicted gene networks against.

In the MCalla et al.[83] ground truth, ChIP-sequencing and perturb-seq are intersected to get at the small subset of possibly direct connections between TFs and genes for both human and mouse embryonic stem cells (ESC) (Figure 1.3A, see 1.5. Methods). We have seen that these ground truth networks show a different pattern than literature-based networks (see Supplementary Figure 6.2.3). Some TFs regulate only a few genes, whereas others are highly connected.

To generate our networks, we use as input one human and two mouse ESC scRNA-seq datasets from MCalla et al. with the addition of another human dataset from Yan et al.[113] Networks are generated over the same 1024 cells, and the 5000 most variable genes for all methods. For scPRINT, three networks have been generated : one averaging all the attention heads (scPRINT), one averaging heads selected based on how well they predicted Omnipath ground truth data : scPRINT (omnipath's heads), and one averaging heads selected from one of the MCalla ground truths : scPRINT (Han et al.'s heads). For more details, see the results section 2 : scPRINT recovers biological features in its gene networks. Of note, due to the small amount of genes assessed in the ground truth, we do not add the genome-wide network version here. Moreover, only the TF version of GENIE3 and the TF-gene subsets of the other method's networks are used since the ground truth only contains TF-gene connections.

Contrary to Omnipath, some elements in these biological networks are highly connected, whereas many others display no connections. This imbalance means that a method predicting only the highly connected TFs will perform well on the MCalla et al. benchmark. As a consequence, we are not transposing the attention matrix as done in the previous section.

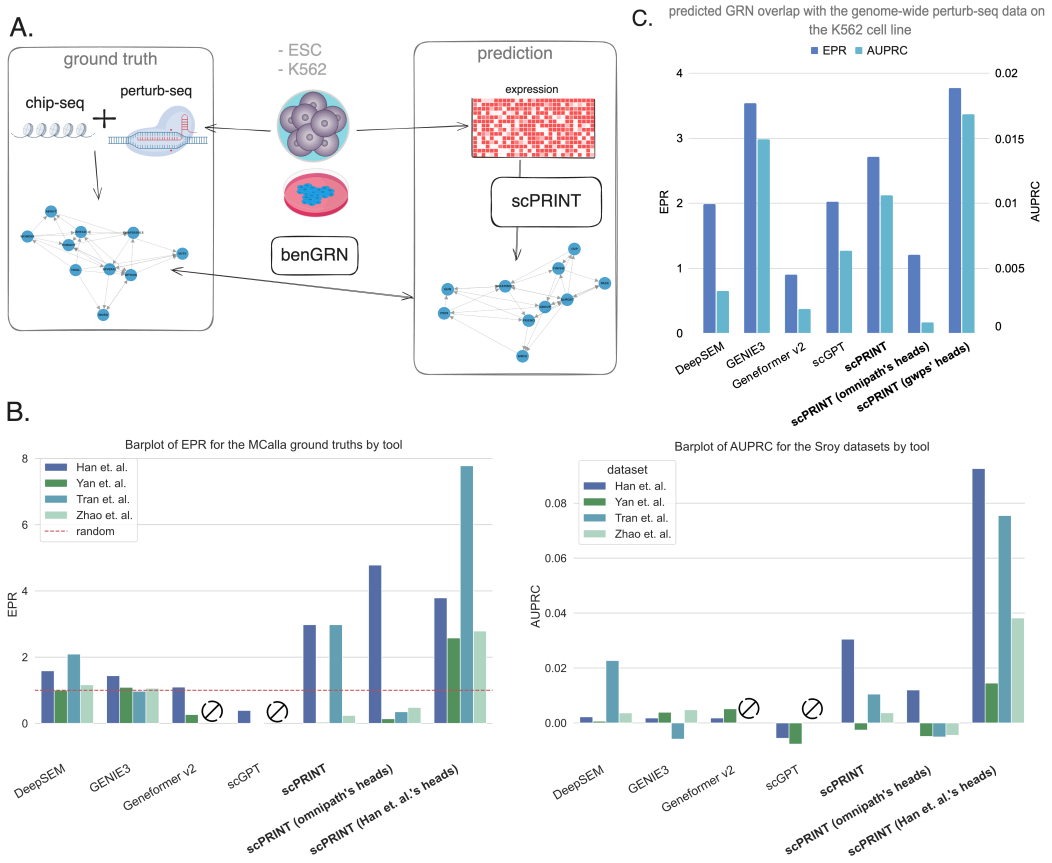

FIGURE 1.3 – (a) The ground truths are generated via orthogonal sequencing assays on the same cell type. ChIP-seq and perturb-seq are intersected for the MCalla et al. dataset on human (hESCs) and mouse (mESCs) Embryonic Stem Cells, whereas perturb-seq on the K562 cell line is only used for the genome-wide perturb-seq ground truth. (b) Performance of scPRINT, scPRINT (omnipath's heads) : same scPRINT version but with attention heads selected using a subset of omnipath, scPRINT (Han et al.'s heads) : same scPRINT version but with attention heads selected using a subset of the Han et al.'s ground truth dataset, compared to GENIE3, DeepSEM, Geneformer v2, and scGPT on the MCalla et al. ground truth using the AUPRC and EPR on two human and two mouse ESC datasets. (c) Same as (b) but on the genome-wide perturb-seq dataset with scPRINT (Han et. al.'s heads) replaced with scPRINT (gwps' heads) : same scPRINT version but with attention heads selected using a subset of the genome-wide perturb-seq ground truth. EPR and AUPRC are provided here in one barplot, left to right.

Based on both AUPRC and EPR, scPRINT outperforms all other methods on this benchmark (Figure 1.3B). This means, for example, that when training GENIE3 to only predict a gene's expression based on TF expressions, it is not selecting the right TFs amongst the set of a few dozen assessed in MCalla et al.

scGPT, Geneformer v2—and, in a few cases, scPRINT—can have values worse than random guessing. Thus, their predictions are often specific to some TFs but not necessarily the right ones (Figure 1.3B).

It also appeared that selecting heads based on Omnipath, although helping slightly in one instance, is not a net benefit for this dataset (see Supplementary Table 6.1.9). This makes sense since MCalla et al. itself does not overlap much with Omnipath (see Supplementary Table 6.1.7). However, selecting heads based on the ground truth itself, only using 50% of the connections available, shows substantial improvement. These same heads also show reliable behavior when using them on the second dataset of the same species.

This shows that scPRINT can better decipher direct from indirect TF-gene connections than scGPT, DeepSEM, Geneformer v2, and GENIE3, although more tests would likely be needed.

However, the results also highlight that the high imbalance (i.e., TFs being not connected or highly connected) combined with the dataset size (i.e., only a few dozen TFs assessed) and the low number of cells make the results in MCalla et al. very variable. Some of this might be true biology or explained by ChIP-seq, which can be very noisy depending on the quality of its antibodies[114].

To answer this issue, we selected another dataset : genome-wide perturb-seq (gwps)[115]. Here, we measured the effect on transcription of knocking out all expressed genes in the K562 cell line. We transformed it into a network using a cutoff of 0.05 on the significance level of each gene's differential expression before and after the KO of each other gene. Although this does not tell us which connections are direct or indirect, we now have a much broader set of connections over thousands of genes and better statistics to assess our gene network inference methods.

GENIE3 performs best, directly followed by scPRINT. Interestingly, Geneformer v2 shows poor performance (Figure 1.3C). Perturbation experiments are known to correlate somewhat to expression correlation, and this might explain GENIE3's strong performance. However, when using our head selection mechanism, scPRINT (gwps' heads) outperforms GENIE3. Again in this dataset, selecting heads based on Omnipath does not help ; the small overlap between the gwps network and the Omnipath ground truth network seems likely to be the culprit (see Supplementary Table 6.1.7). These overlaps show that the three ground truth networks are very different and that a different set of heads predicts each type of ground truth. We also assess the networks on the TF-gene only subset of the gwps ground truth. Here, we see a large drop in performances for most methods, except GENIE3 (see Supplementary Figure 6.2.4).

Finally, we have seen that on both MCalla and gwps, scPRINT also predicts networks that agree with the Omnipath ground truth and are again enriched for cell type markers and TFs (see Supplementary Tables 6.1.8 and 6.1.9).

Since GNs can be seen as approximations of a cell model, we expect that when a tool has good internal cell models, it should generate meaningful results on tasks such as denoising, cell type prediction, embedding and batch effect correction, perturbation prediction, trajectory inference, and more. We will now focus on three tasks orthogonal to GN inference to compare the ability of scPRINT to the SOTA.

1.3.4 scPRINT is competitive on tasks orthogonal to GN inference

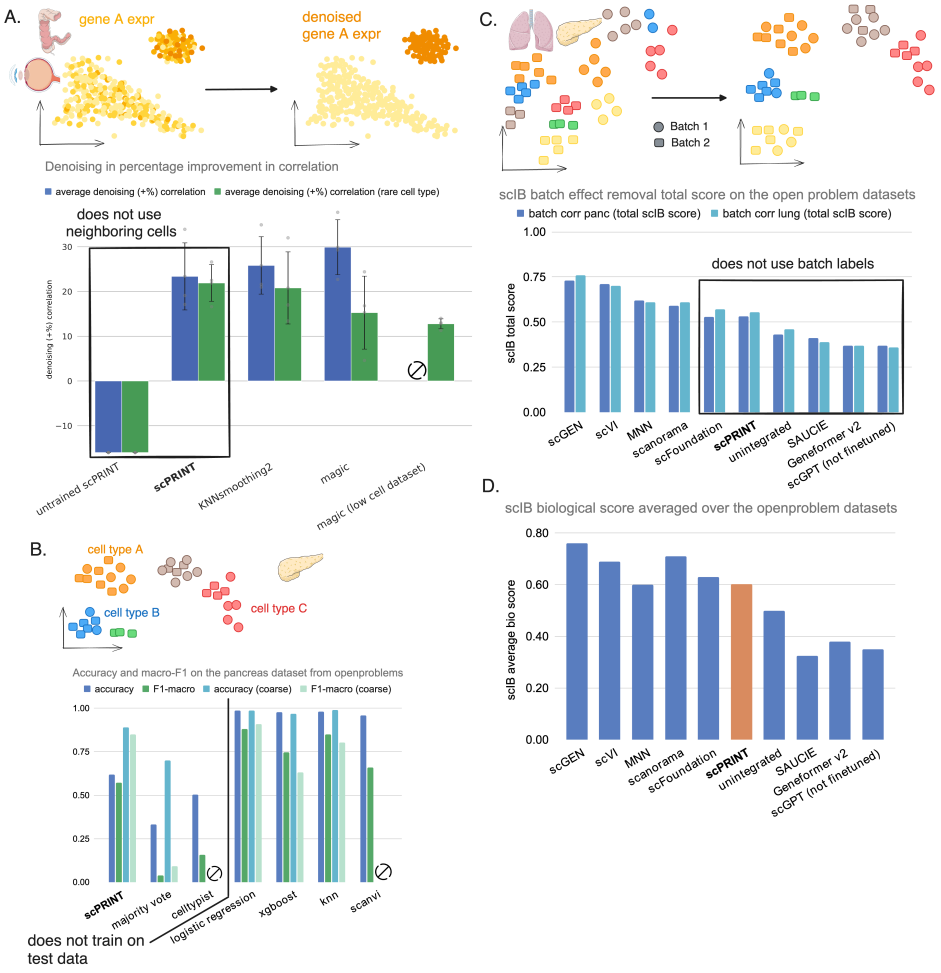

FIGURE 1.4 – (a) Performance for a denoising task compared to SOTA methods MAGIC and knnsmooth2 on 3 datasets (ciliary body, colon, and retina tissues) from CxG. Here, we generate a noisy profile by downsampling 70% of the cell transcripts and computing the Spearman correlation increase of the correlation between the denoised and the true profile compared to the one between the noisy and the true profile. (b) Performance on cell-type label prediction compared to SOTA methods as well as CellTypist. Showing accuracy, F1 and macro-F1 scores for the open-problems human pancreas dataset. (c) The performance of scPRINT as well as scGPT and Geneformer v2 on batch effect correction on the human pancreas and lung datasets from the openproblems challenge showing the scIB aggregated score. They are compared to SOTA methods which results were extracted from the openproblems benchmark. Unintegrated means only PCA was applied. (d) The scIB avgBIO score on both datasets.

To test the quality of the cell model learned by scPRINT, we now consider denoising, cell type prediction, and batch effect correction as a representative set of classic scRNA-seq

and cellular biology benchmarks.

Similarly to our pretraining task, we simulate lower transcript count profiles and then ask scPRINT and two other SOTA methods, MAGIC[29] and KNNsmoothing2[116], to recreate the true expression profile. We use Spearman correlation to the original gene expression profile as our metric. In Figure 1.4A, we show the increase in correlation after denoising the downsampled profile on 3 test set datasets, composed of ciliary body, colon, and retina tissues[106, 117, 118], randomly selected from CxG (see 1.5. Methods).

ScPRINT is competitive with both SOTA methods, while contrary to MAGIC and KNNSmoothing2, it operates independently over each cell in the test set (see 1.5. Methods). We have also seen a 10% variability in denoising ability across the different datasets used (see Supplementary Table 6.1.10). This was similar across all tools and possibly related to the number of genes expressed in each dataset.

However, these test cases mostly contain very similar cell states, whereas denoising is helpful in cases with rare cell types or transitory cell states that have low cell counts by default. We show that since scPRINT does not aggregate profiles over neighboring cells, it outperforms MAGIC and KNNsmoothing2 in rare cell states subsets of the datasets (respectively : pericytes microfold cells of epithelium of small intestine and microglial cells) with around 10 to 200 cells (Figure 1.4A, Supplementary Figure 6.2.5). Computing MAGIC and KNNsmoothing2 over only this rare cell population gives even lower performances for MAGIC and creates an error for KNNsmoothing2 (see Supplementary Table 6.1.10). These results suggest that a good cell model reliably using learned gene-gene interactions can help denoise an expression profile.

For cell type classification, we expect scPRINT to be able to find sets of genes that can predict a cell type across multiple batches and under the high dropout rate of single-cell scRNA-seq. To evaluate cell type classification, we use the multi-batch benchmark pancreas dataset of openproblems, its metrics, preprocessing, and hyperparameter choices (see 1.5. Methods)[119, 120].

scPRINT is a zero-shot predictor of cell labels. Indeed, it does not need to train on the dataset itself to make its predictions, unlike other methods that often need to use more than 70% of the test dataset for training. scPRINT also makes predictions over more than 200 cell type labels, while other methods often only predict a few cell types. Conversely, the other classifier methods, like Logistic Regression or XGBoost, and previous foundation models are trained or fine-tuned on the test dataset, thus giving a strong advantage over scPRINT. We, therefore, also compare scPRINT to the marker-based classifier CellTypist[121] and its pancreas marker database (see 1.5. Methods). A method that also does not use the labels of the test dataset.

scPRINT reaches 62% classification accuracy, largely outperforming CellTypist (Figure 1.4B, Supplementary Figure 6.2.6). Interestingly, with the macro F1 score, which considers each cell type group equally regardless of its size, scPRINT achieves similar results to the SOTA[120] methods : Logistic Regression and XGBoost. This is probably because scPRINT is not influenced by the number of cells in each category.

In addition, we have noticed that scPRINT is challenged by some specific pancreatic cell

types in this dataset. Indeed, scPRINT often switches the assignment of A, B, D, and E cells. Thus, when using the coarser "endocrine pancreatic cell" label to define these cell types, we see a big improvement in the accuracy and macro-F1 score of scPRINT, even outperforming SOTA methods.

Here, we have shown the accuracy of scPRINT independently of cell neighborhood. However, like gene marker-based methods, scPRINT can annotate cell types in novel datasets. In this context, its predictions could be smoothed and improved using majority voting over predefined cell clusters.

Finally, scPRINT predictions are given as probability vector overall cell type labels. They can be used to display the top K labels and learn about the model's uncertainty.

Thanks to its disentangled embeddings, scPRINT can generate cell representations that partially remove batch effects from cell profiles. On the human pancreas and lung datasets of open problems[122], we see that, based on the scIB metrics, scPRINT shows convincing batch effects removal ability, while not on par with the SOTA methods scGEN and scVI (Figure 1.4C, Supplementary Figure 6.2.7). Concerning foundation models, scPRINT and scFoundation show strong zero-shot performances compared to Geneformer v2 and scGPT. Except for Geneformer v2, scGPT, and scFoundation, we did not rerun previous algorithms for this benchmark and show their performances from the openproblems portal (open-problems-v2.3.6, march 2024). However, we also ran the Geneformer v2 and scGPT foundation models on the openproblems benchmark and showed that without fine tuning on this specific dataset, they are not able to meaningfully correct for batch effect (see 1.5. Methods).

Moreover, scPRINT is one of the few methods that do not train on the test dataset and do not use already annotated batch labels. When only looking at methods that do not use batch labels as prior information, e.g., SAUCIE[123], LIGER[124], scPRINT is the top performer. We have also noticed that the scPRINT cell embeddings preserve biological information competitively to SOTA methods (Figure 1.4D, Supplementary Figure 6.2.8). This also exemplifies that a reliable cell model can perform well at disentangling the different facets of a cell expression profile and its underlying batch effect.

Overall, we have seen that scPRINT can achieve zero-shot performances on par with many famous single-cell scRNA-seq tools on multiple important tasks of single-cell biology, showing that our architecture and foundational pre-training tasks are a powerful new foundation for large cell models.

1.3.5 scPRINT highlights the role of ion exchange and fibrosis in the ECM of Benign Prostatic Hyperplasia

To showcase the ability of scPRINT, we focus on premalignant neoplasms from an atlas of two studies of human prostate tissues[20]. The data contains both normals and pre-cancerous lesions, also called BPH, across sequencers and age groups. Starting from post-alignment raw counts, scPRINT generates a consistent and batch-corrected embedding of the datasets (Figure 1.5A, Supplementary Figure 6.2.9). scPRINT also annotates the cell

type, sequencer, sex, ethnicity, and disease type of each cell with an accuracy of 0.71, 0.99, 0.99, 0.95, and 0.85, respectively.

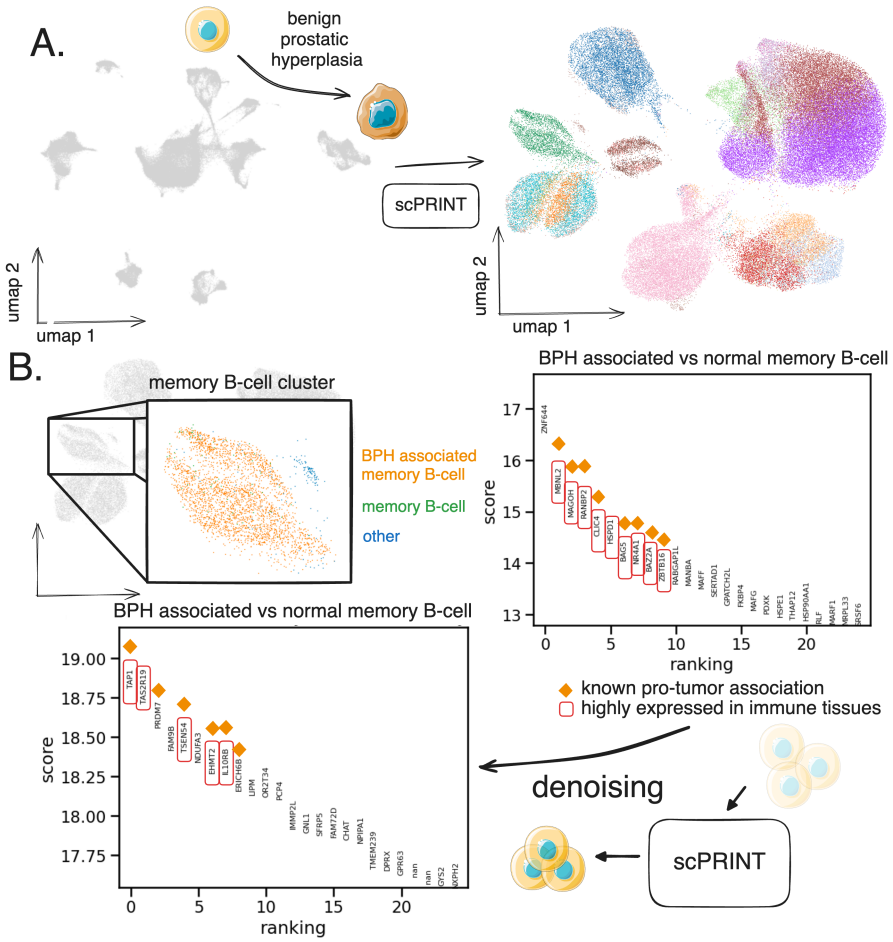

Figure 1.5 – (a) Single-cell scRNA-seq atlas of BPH and normal prostate tissues of 83,000 cells given to scPRINT. scPRINT generates a set of embeddings and label predictions for each cell. To clean our predictions, we drop cell types with less than 400 cells and diseases with less than 1000 cells, replacing them with the “other” label (see Supplementary Figure 6.2.9). (b) Zooming in on one cluster, we see annotations of a switched memory B-cell cluster, some labeled ”benign hyperplasia” and others ”normal”. Differential expression analysis on the two groups of B-cells showing enrichment of B-cell & cancer markers when assessing its top 10 genes. We performed upsampling of the transcript count before performing a new differential expression analysis where we now see new genes amongst the top 10 differentially expressed ones some of them also associated with cancer and immune tissues.

We then focus on a switched memory B-cell cluster composed of a group of cells labeled as benign prostatic hyperplasia and another as normal (Figure 1.5A). B-cells are known to be dominant in prostate cancer and are often switched memory B-cells[125]. First, we show that they differentially express many known B-cell markers (see Supplementary Figure 6.2.10). In addition, when comparing the BPH to the normals B-cells, we recover that the top 10

BPH B-cells differentially expressed genes contain many known cancer markers, B cell markers, and a specific B-cell associated prostate cancer markers : BAG5[126] (highlighted in Figure 1.5B, Supplementary Table 6.1.11). Moreover, many other genes have evidence in other cancers, like CLIC4, known to be involved in the maintenance of the TME in breast cancer[127].

However, the number of healthy cells, especially normal memory B-cells, in this dataset is small : only 26. By performing denoising, we can recover genes that might have been missed during differential expression analysis of such a low cell count. Increasing the counts of all the genes by a factor of ten and re-doing differential expression analysis highlights some new genes whose differential expression scores are even higher than those previously cited.

Interestingly, amongst them, TSEN54, EHMT2, and IL10RB are known to impact the function of B-cells in malignancies (see Supplementary Table 6.1.11). Other genes have evidence in immunity and cancer, like TAP1, which is known to be highly expressed in immune organs and is an immunomodulation gene known to play many roles in various cancers[128], while some genes have, of yet unknown significance, like LIP, whose paralog LIPA is a known cancer target[129] (Figure 1.5B).

This demonstrates how scPRINT can embed, align, and annotate diverse datasets in a meaningful way so that one can then analyze specific and rare cell clusters to recover both known and new biology.

Finally, for the second part of the analysis, we move to another cell type of interest : fibroblasts. Fibroblasts are known to be involved in cancer[130], also called cancer-associated fibroblasts (CAFs), of which many subtypes exist, with different roles in tumor progression and invasion[131]. In our dataset, we can see a large cluster of cells labeled as “fibroblast of connective tissue of glandular part of prostate”, of which 500 are coming from normal tissues, and 600 are coming from hyperplasia and are possible precursors of CAFs (Figure 1.6A). Interestingly, 40% of the cells annotated as BPH-associated fibroblasts are coming from healthy tissue, according to the authors of the dataset. However, it is known that more than 50% of adult males over the age of 50 will have BPH[132]. Thus, one possibility is that some of the fibroblasts of these healthy tissues already present patterns of gene activation similar to those of pre-cancerous ones.

We generate a gene network of the BPH and normal fibroblasts using the 4000 most variable genes and taking the average over all heads in the network (Figure 1.6A). Looking at the top 15 hubs, using degree centrality, we can see S100A6 as the top element in normal fibroblasts. This gene is known to be a fibroblast and epithelial cell marker that regulates, among other things, cell cycle and differentiation[133, 134]. We also see MIF, IGFBP7, and other genes involved in immune signaling and growth[135, 136, 137].

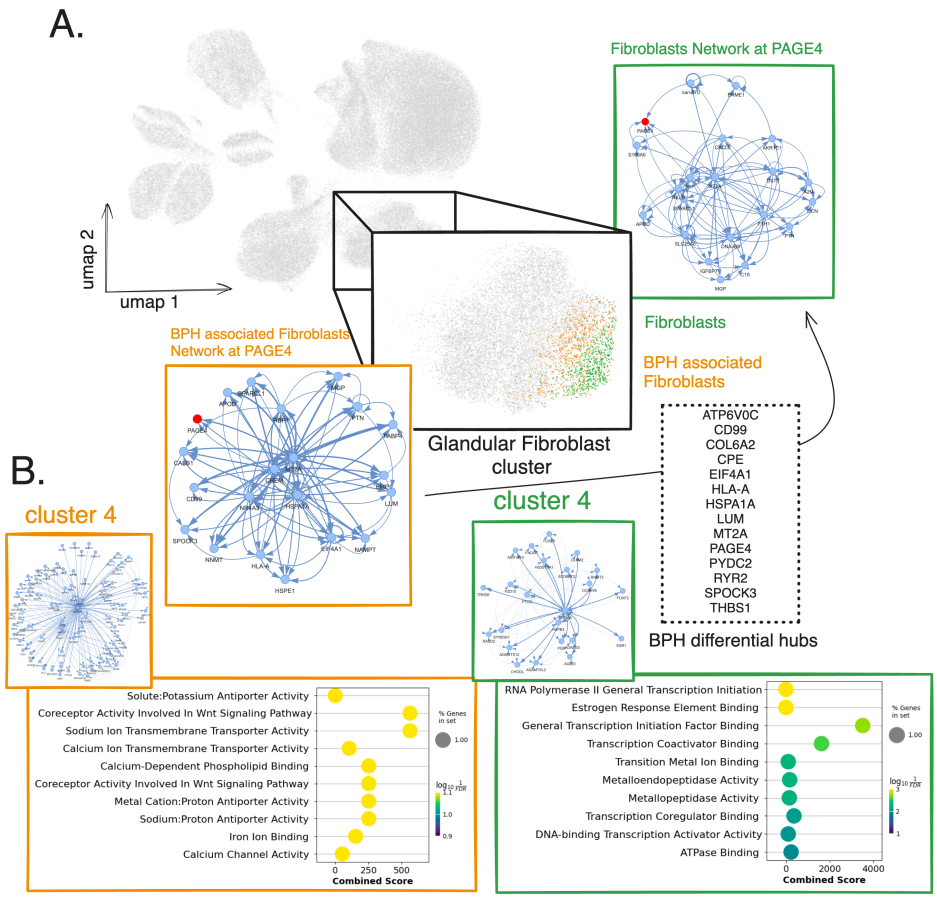

Figure 1.6 – Continuing on the single-cell scRNA-seq atlas of BPH and normal prostate tissues of 83,000 cells given to scPRINT (a) Zooming in on another cluster from scPRINT's cell embeddings and annotations, we see a group labeled as "fibroblast of connective tissue of glandular part of prostate", some labeled as "benign prostatic hyperplasia", and others "normal". We generate gene networks from each and highlight a sub-network of the PAGE4 differential hub gene in BPH, showing different connection strengths and patterns between normal and BPH-associated fibroblasts. (b) Left to right : gene-set enrichment analysis, using Enrichr, of the gene community 4 found by the Louvain algorithm in the BPH-associated fibroblast gene network, same but on the normal fibroblast gene network. It shows the top 10 most strongly enriched gene sets from GO_MF_2023 according to q-value (i.e. adjusted p-value).

However, some of these genes are not in common with the BPH fibroblasts ones. Over the set of 2881 common nodes between the two networks, the genes HSPA1A, MT2A, SPOCK3, ATP6V0C, DEFA1, EIF4A1, and CD99 are considered differential hubs (i.e., more central) in the BPH fibroblasts compared to normal ones (see Figure 1.6A, Supplementary Table 6.1.12).

Another definition of centrality, eigenvector centrality, recovers 55% of the genes already identified as hubs, plus some new ones. As an example, Prostate Associated Gene 4 (PAGE4), which is part of the GAGE family of genes, is expressed in a variety of tumors and

reproductive tissues, especially BPH, where it is related to oxidative stress response and fixation (i.e., anti-invasion)[138, 20, 139]. Interestingly, although the networks share 75% of their genes, they only share 50% of their edges when considering the top 20 edges per gene. It shows that over the same set of genes, scPRINT discovers distinct gene networks across biological contexts. Taking as an example the differential hub PAGE4 (Figure 1.6A), we see that it is connected to many of the top 15 hub nodes in the BPH network, such as MT2A, HSPA1A, SPOCK3, and CD99. This shows a master node sub-network linking metal and ion exchange, oxidative stress response, and inflammation[140, 141, 142, 143]. Some genes are also part of the IL24 signaling inflammatory pathway (EIF4A1 ;COL6A2 ;HLA-C ;HSPE1), and the secretory senescence phenotype (H2AZ1 ;UBE2S ;UBE2C ;IGFBP7)[144], hallmarks of fibrosis and malignancies[145, 146]. The PAGE4 network in normal fibroblasts, while having some elements in common, like metal transport, is much less connected (seen by the strength of the edges in Figure 1.6A). It also contains a different set of genes, which are less related to senescence, inflammation, and ion exchange (see Supplementary Figure 6.2.11).

Furthermore, we can use these networks, defined over only a few cells, to perform community detection. Taking community 4, containing 92 genes and defined with the Louvain algorithm on the BPH-associated fibroblasts GN, we see two hub nodes : SPOCK3 and HERC3 (Figure 1.6B). Interestingly, not much is known about those genes except that HERC3 has been linked to inflammation and the ECM via metallopeptidase and the NCOA1 gene[147]. SPOCK3, moreover, is known to be related to prostate malignancies and collagen in the ECM[141]. Gene set enrichment tells us that the genes in this subnetwork are primarily related to calcium, sodium, iron, and metal transport, validating the evidence around HERC3 and SPOCK3 (Figure 1.6B). In normal fibroblast, however, taking the community most associated with metal transport (community 4, see details in Supplementary Figure 6.2.12 and Methods) shows RNASEK, SELENOM, and an unknown ubiquitin ligase, paralog of ITCH. While RNASEK is related to RNA degradation, its expression has been linked to a lower risk of prostate cancer[148]. SELENOM is of unknown function, but some SEL proteins have been related to cell adhesion[149] .

Through its networks, scPRINT highlighted the role of ion exchange and fibrosis in the ECM in BPH. While some of the same genes would have been found from differential expression analysis, these results show us how gene networks can be used to describe the intersection of genes and their molecular functions. Putting genes into the context of their connections, one can validate known functions or relate them to new ones. From such contextualization, a picture starts to emerge, whereby through specific genes, glandular fibroblasts in senescence enter a wound-healing state. This fibrosis is caused by the export of more metal and ions to generate ECM and change its acidity levels. This might cause a loss in tissue flexibility and potentially create oxidative stress[150]. In our networks, these pathways seem connected to inflammation. Chronic inflammation and wound healing states are hallmarks of BPH and a predisposition to future malignancies[151, 152].

1.4 Discussion

We can simplify the complex macromolecular interactions governing a cell through what is often referred to as a gene network. However, creating such a network in a meaningful way remains a challenging task.

We have created and benchmarked scPRINT, a novel single-cell scRNA-seq foundational model trained on more than 50 million single-cell profiles across tissues, diseases, and species contexts. scPRINT uses three foundational pre-training tasks, as well as new encoding and decoding mechanisms specifically designed for gene expression data. Although it has not been directly trained for it, scPRINT generates gene networks. These networks can be used to better understand the model predictions and help make more informed decisions about the significance and role of a potential target. Finally, we present a mechanism to best select heads containing the known biology of these networks. This approach also helps users fine-tune the type of network they are interested in. Given the discrepancy amongst ground truth networks, we advise users to consider using all-head averaging and to only revert to head selection when some high-confidence interactions are available. Indeed, general collections like Omnipath did not improve performance in most of our tests.

We show that we outperform other foundation models on most of our benchmarks while using a similar model size. We believe that our inductive biases and training procedures helped scPRINT achieve such a performance. Moreover, while GENIE3 is still a competitive tool, we outperformed it on many of our benchmarks, showing that pushing training to millions of cells and large parameter sizes will be an essential direction for further work on gene network inference.

In addition, contrary to any other method assessed, our large cell model can also achieve zero-shot performances on par with many famous single-cell scRNA-seq tools on multiple important tasks. While some specialized tools might be better suited to some use cases, scPRINT's versatility and speed make it a worthwhile alternative in many instances. Indeed, users can directly use scPRINT in their bioinformatics workflows with commodity hardware (1 CPU, 1 GPU with 10GB of memory and 16GB of memory).

Finally, we put scPRINT to the test on a challenging atlas of normal and senescent prostate tissues showing BPH. We identify rare cell populations with early markers of TME in B-cells. In fibroblasts, we study gene networks and recover known hubs such as PAGE4, thereby linking the senescence of fibroblasts to changes in the ECM and downstream inflammation. We find key interconnected pathways of the oxidative stress response and extracellular matrix building via metal and ion exchange in the gene network of BPH-associated fibroblasts. We also show that healthy and disease-related cells exhibit different network patterns, demonstrating that scPRINT can help identify novel pathways and targets while considering them in their specific cellular and molecular contexts.

An assumption in natural language processing is that fewer inductive biases make for better models. Our work shows that adding good inductive biases and rethinking architectures will likely be important directions for AI models in biology.

A challenging aspect of GN inference is that no perfect ground truths exist, and many

GN methods are, unfortunately, benchmarked on ODE-generated mock-up expression data. In contrast, ChIP-seq, perturb-seq, and literature-based ground truths remain scarce and ambiguous. With BenGRN and GRnnData, our suite of tools for benchmarking Gene Networks inferred from single-cell scRNA-seq, we present an extensive set of real-world ground truths representative of the diversity of networks we can assess. However, improvement in performance and benchmarking will need to come from innovative experimental approaches that can produce causal, genome-wide, and cell-type-specific networks containing the many different types of connections and regulations that exist, from PPI, RNA-DNA, RNA-protein, to inhibition, activation, cooperation, and more.

We acknowledge that work remains to be done, from the transformer's ability to generate graphs to their explainability and the breadth of tasks they can undertake. Questions still remain regarding the pre-training tasks and how to integrate additional data modalities into foundational models.

Transcription is much more complex than what gene networks currently represent. In the future, we expect such large cell models to work in tandem with new sequencing techniques measuring information such as time, space, protein amounts, DNA configuration, and non-coding RNA species to solve the gap in our understanding and our ability to model cell biology.

1.5 Methods

we propose scPRINT, a foundation model designed for gene network inference. ScPRINT brings novel inductive biases and pretraining strategies better suited to GN inference while answering issues in current models. scPrint outputs cell type-specific genome-wide gene networks but also generates predictions on many related tasks, such as cell annotations, batch effect correction, and denoising, without fine-tuning.

1.5.1 Architecture

The model architecture is composed of :

- An encoder that takes the raw data and embeds it in a high-dimensional space used by the transformer.
- A bidirectional multi-head transformer
- A decoder to transform the expression embeddings into expression values
- A decoder that transforms the cell embeddings into cell-specific label prediction over a range of classes.

Expression encoder

In scPRINT, each gene in a cell is converted to an embedding : It corresponds to the sum of 3 different elements :

1. An embedding representing the gene itself (see Supplementary Tables for scPRINT. Supplementary Table S2 for model embedding size). ESM2 embedding of each gene's most common protein product was used to represent that gene. While imperfect in some ways, this inductive bias allows the model to learn representations that potentially apply to even unseen genes from unseen species or integrate specific genetic mutations into its representation. First implemented in UCE, this provides the model information related to the gene product's structure, ontology, and similarity to other genes. This also speeds up the training greatly, particularly for small models. We show that this is a great gene representation, but that model performance can be increased by refining gene embeddings further during training. However, we elect not to do so to maintain the model's versatility in working on unseen genes.

We encode the genes' embeddings using ESM2. The mapping process happens the following way :

— A gene name is mapped to its canonical protein name using Ensembl.
— We recover the protein sequence of the protein using Ensembl
— We use the protein sequence to generate an embedding using ESM2 by averaging all the amino-acid output embeddings, as done in the ESM2 paper.

With the embedding function provided in our code, one can easily do this with any species in Ensembl.

scPRINT can effectively be retrained with any set of gene embeddings, which can be frozen during training or used only for initialization (tried, for example, in our ablation studies, Table S3).

2. An embedding of the gene location in the genome. This has also been proposed in UCE and helps the model understand that genes with similar locations tend to be regulated by similar regulatory regions, a relationship well-known in cellular biology.

We encode the genes' locations using positional encoding. Every gene less than 10,000 bp from the next is said to be in the same location ; otherwise, we increment location by 1. We do this for all genes in the Ensembl database per species.

We then embed these locations by applying the Positional Encoding (PE) algorithm of Vaswani et al. .

3. An embedding of the gene expression in the cell. For this, we embed the gene's expression using an MLP. While GeneFormer devised a ranking strategy based on a gene expression compared to a baseline expression, scGPT instead used binning of log normalized counts. On our end, we haven't found that this approach was the simplest, nor was it performing better than only using the log-transformed counts. We thus directly take the log-transformed counts

$$\mathrm{e_{i,j}} = MLP(log_2(x_{i,j} + 1)),\ x_{i,j} \in \mathbb{R},\ \mathrm{e_{i,j}} \in \mathbb{R}^d \tag{1.1}$$

where $\exp r_{i,j}$ is the embedding of the expression, $x_{i,j}$ is the expression value of the gene j in the cell i, and the MLP is a two-layer neural network, where each layer is composed of

$$Dropout(ReLU(LayerNorm(Linear(\mathrm{e_{i,j}})))) \tag{1.2}$$

where the Dropout rate is fixed at 0.1, and the dimensions are specified as $1 \longrightarrow d$ for the first layer of the MLP and $d \longrightarrow d$ for the second layer, with d representing the model dimension.

Of Note : Geneformer used positional encoding to encode gene expression, a function often used to encode the position of words in a text. Similarly to gene name token, scGPT learned an embedding for different ranges of expression values, binning them to remove sampling noise.

Both approaches apply a specific prior for the metric that defines expression. Geneformer defines expression amount as ranking based on how each gene is expressed in the cell compared to its average across all cells. Unregarding the batch effect issues, this is an assumption that expression values are not meaningful and only the ranking of the relative abundance is meaningful information. Meanwhile, scGPT has the bias that an expression of 1, 2, or 3 are the same and that an expression 1, and 5 are different by some amount learned by the model.

By using an MLP with two layers, we effectively let the model learn the metric of transcription expression. Moreover, again, we decrease the number of parameters used compared to scGPT while being able to make predictions on count values unseen during training, such as those of bulk or pseudo-bulk RNAseq.

Finally, when encoding a cell expression profile, only a subset of 2200 genes is used during pretraining. If less than 2200 genes are expressed, we randomly choose 2200 expressed genes and pad them with randomly sampled unexpressed genes (meaning with an expression value of 0). This approach allows the model to see different patches of the same cell profile during training. We chose 2200 genes as 2/3rds of the cells in cellxgene had less than this number of genes expressed, striking a balance between computation and gene usage.

We decided to add unexpressed genes because, combined with our denoising methodology, this lets the model figure out that some genes are true 0s during training. In contrast, others are only caused by dropout and a function of the transcript counts. This causes scPRINT to model dropout as a function of read depth (i.e., total transcript count).

Moreover, this completes the minibatch by token matrix without padding and fully utilizes the GPU during the attention computation.

Of note, some models have been able to reach context lengths of 20,000 genes using the performer architecture. Performer is an often-cited method and part of the literature on attention approximation. However, most state-of-the-art transformer models do not use attention approximation as they are known to lead to worse performance.

Moreover, in cellxgene, more than 80% of the cells have less than 2200 genes being measured. This means that most of the memory and compute power is likely lost on tokens that are almost always zeros due to dropout.

The full set of embeddings of cell i sent to the transformer is the matrix X_i where

$$X_i = [\mathrm{g}_0 + \mathrm{e}_{\mathrm{i},0} + \mathrm{l}_0, \mathrm{g}_1 + \mathrm{e}_{\mathrm{i},1} + \mathrm{l}_1, ..., \mathrm{e}_{\mathrm{i,t}}, \mathrm{p}_{\mathrm{default}}, \mathrm{p}_{\mathrm{celltype}}, \mathrm{p}_{\mathrm{disease}}, ...] \tag{1.3}$$

where g_j is the gene j encoding, $\mathrm{e}_{\mathrm{i,j}}$ is the encoding of the expression of gene j in cell i, l_j is the gene j location encoding, and p_A is a learnt embedding for the class A.

The total count information is stored separately and encoded similarly to the expression,

$$\mathrm{e}_{\mathrm{t,i}} = MLP(log_2(1 + t_i)), \text{ where } t_i = \sum_j x_{i,j} \tag{1.4}$$

with $x_{i,j}$ the expression value of gene j in cell i, and the MLP is a two-layer neural network similar to the previous one.

The full cell total count (t) lets scPRINT model its denoising based on this required total count parameter.

The placeholder tokens (total count, default cell embedding, cell type, disease, sex, ethnicity, assay, organism) are learned embeddings that stay the same across all inputs. They only act as placeholders for the model to fill in during the forward process. At the transformer's output, they will have been modified to contain the embeddings requested. At least two are used, one containing the default cell embedding and another the profile's total depth. More tokens can be used, one for each predicted cell label.

Model

The model is a bidirectional autoencoder similar to BERT with n layers, h attention heads, and a dimension of d. It uses the flashattention2 methodology implemented in Triton to compute its attention matrix. It uses the pre-normalization technique, with a sped-up layer norm implemented in Triton's tutorial. It uses a stochastic depth with increasing dropout probability.

It has a 2-layer MLP with a 4x width increase in its hidden layer and a GELU activation function.

Expression decoder

scPRINT uses a novel expression decoder for foundation models, which outputs the parameters of a zero-inflated negative binomial (*ZiNB*) function for each gene i in cell j. The *ZiNB* distribution is defined as

$$X \sim ZiNB(\mu, \theta, \pi) \tag{1.5}$$

where the parameters $\mu,\ \theta,\ \pi$ are obtained from a multi-layer perceptron (MLP) applied to the expression embeddings outputted by the transformer model at its last layer (e), which are the :

$$\mu, \theta, \pi = MLP(\mathrm{e}) \tag{1.6}$$

The MLP is a two-layer neural network with dimensions [*d, d*, 3]

Based on the work of Jiang et al., zero inflation is the best distribution when considering a broad range of transcriptomic measurements, where some have enough dropouts, and a zero inflation term is needed to model it. In our case, and similarly to scVI, we define our *ZiNB* as

$$ZiNB(x|\mu, \theta, \pi) = \pi\delta_0(x) + (1 - \pi)NB(x|\mu, \theta) \tag{1.7}$$

where $\delta_0(x)$ is a point mass at zero, and $NB(x \mid \mu, \theta)$ is the negative binomial distribution with mean μ and dispersion θ.

With these parameters, the negative binomial distribution is represented in the following way

$$NB(x|\mu, \theta) = \frac{\Gamma(x + \theta)}{x!\Gamma(\theta)} \left(\frac{\mu}{\mu + \theta}\right)^x \left(\frac{\theta}{\mu + \theta}\right)^\theta \tag{1.8}$$

where μ is the mean and θ the overdispersion parameter, representing the inverse of the dispersion. From Hibe et al., we know that this is a parameter change from the most used probability mass function (PMF) given by

$$P(X = x) = \binom{x + r - 1}{x}(1 - p)^r p^x \tag{1.9}$$

where r is the number of successes, p is the probability of success, and k is the number of failures.

One can interpret such a negative binomial distribution as a Poisson distribution with an additional overdispersion term that makes the variance not tied to the mean. In scPRINT, we use the zero-inflated Poisson for count downsampling as we can't easily infer the gene overdispersion parameter from each cell profile. By removing this zero-inflated Poisson from the gene expression profile, we keep the potential overdispersion in the profile (see the Negative Binomial to Poisson relationship section in Methods).

Compared to scVI, where the overdispersion parameter θ is learned for each gene, we make scPRINT output it together with $\mu,\ \pi$ (see Supplementary Tables for scPRINT. Supplementary Figure S13)

Effectively, the model learns that the dispersion might change depending on the gene, the sequencer, the cell type, and the sequencing depth.

Class decoder

scPRINT also outputs a variety of class embeddings, such as default cell embedding, cell type embedding, disease embedding, etc., by filling the different placeholder tokens given as input (see the Expression encoder section in the Methods).

Effectively, for each class, we have the model learn to produce a new disentangled embedding (e.g., cell type, disease, tissue, age). This means the model uses an MLP to transform each token where A is a class. For each, we jointly train a classifier :

$$\widehat{\mathrm{c_A}} = \sigma(MLP_A(\widehat{\mathrm{e}_A})) \tag{1.10}$$

where :

- $\widehat{\mathrm{c}_A}$ represents the logits for a class A of a dimension d_A whose size corresponds to the number of labels.
- σ denotes the Sigmoid activation function.
- MLP_A stands for the Multi-Layer Perceptron trained to predict the logits of the class A.
- $\widehat{\mathrm{e}}_A$ is the output embedding for the class A of dimension d.

However, some classes, like cell type, have up to 800 labels. Fortunately, cellxgene classes follow an ontology, a robust structure that defines relationships among the labels. We reduce the size of the output labels by training the model only on the leaf labels in the ontology hierarchy (i.e., the most precise available). For cell types, this represents around 400 different labels (see Supplementary Tables for scPRINT. Supplementary Table S13).

Thus, when a label is not very specific for a cell type (e.g., neuron), the model will predict the best leaf label (e.g., dopaminergic neuron). This way, we can generate meaningful training signals from even very coarse labels (see The classification task section in methods for more information and definition of the loss). We only apply this hierarchical classifier to the cell type, disease, and assay labels.

In the following section, we show how we train such classifiers. During the classifiers' training, we sum up their loss without applying any scaling between the different classes.

1.5.2 Ablation study

We perform an ablation study of multiple of our additions in scPRINT for its medium size version. Removing positional encoding, replacing log-normalization with a total-normalization, replacing denoising with masking, using the cell-gene product method of scGPT vs our own encoder-decoder approach to learn a cell embedding, using 2 vs 4 heads

per attention blocks, not using weighted random sampling, not freezing the gene ID embeddings, and using mean-squared-error instead of the ZINB loss. For each, we re-train scPRINT entirely on the same dataset and validate its test performance with our automated benchmark platform. We provide the results in Table S3.

1.5.3 Pretraining

The three tasks of the multi-task pretraining are the denoising task, the classification task, and the bottleneck learning task. While the denoising loss enhances the model's ability to find meaningful gene-gene connections, the other two try to make the model and its underlying networks more robust and cell-type-specific. All three losses are summed without rescaling.

Optimization method

The optimization is done with fused ADAMW, with a weight decay of 0.01. We noticed a total inability to learn when using base ADAM, which has a similar weight decay. This can be explained by a known inequivalence issue in ADAM.

We use the stochastic weight averaging method during training with a learning rate of 0.03.

During pre-training, the hyperparameters are set to dropout of 0.1, a learning rate (LR) of 1e-4, the precision is set to 16-mixed with residuals in fp32. We clip gradients to 100 and train in many sub-epochs of 7000 training batches and 2000 validation batches with a warmup duration of 500 steps.

Across epochs, we use a linear LR decrease of 0.6 with a patience of 1 and stop training after three consecutive increases in validation loss (patience : 3). In the final layer of the class decoders, we initialize values to a normal distribution around 1 for weights, 0 for biases, and -0.12 for biases.

Our batch size is 64, and we use a pre-norm strategy for the transformer with a linearly increasing stochastic depth dropout rate of 0.02 per layer. We use a noise parameter of 60%. We split the cells in the datasets into 98% train and 2% validation and reserve at minimum 2% of separated datasets for testing.

Finally, we use weighted random sampling on our training data based on the different class values we have to predict. We use a factor of 50, meaning the rarest elements will, on average, be sampled only 50 times less than the most common ones. The sampling factor used for each group is then $\frac{50}{count+50}$, instead of $\frac{1}{count}$ where count is the number of cells in each group.

The classification task

We perform label prediction during pretraining for different classes, currently : cell type, disease, sequencer, ethnicity, sex, and organism. Due to issues in the ontologies, we have omitted tissue type and age classes.

Due to the hierarchical structure of the prediction, we also created a hierarchical loss. Here, we compute the loss regularly when the label is a leaf label. Otherwise, we replace all associated leaf labels to the given label by the log-sum-exp, such that for a cell label, the loss is :

$$Loss_{classification} = CE(\sigma(\overline{\mathrm{c}}, \mathrm{c})) \tag{1.11}$$

with :

$$\overline{\mathrm{c}} = \begin{cases} \widehat{\mathrm{c}} & \text{if } \{i | c_i = 1\} \subseteq T \\ LSE\,(\widehat{\mathrm{c}}_d)\,||\widehat{\mathrm{c}}_{\sim d} & \text{else} \end{cases} \tag{1.12}$$

where :

- $\widehat{\mathrm{c}}$ is the predicted vector with dimension equal to the number of leaf labels
- T being the set of label indices marking the labels that are leaf labels.
- $\widehat{\mathrm{c}}_d = \{\widehat{c_i}, \forall\, i \in T\}$ all the values in vector $\widehat{\mathrm{c}}$ whose indices are in T. Same for c.
- $\widehat{\mathrm{c}}_{\sim d} = \{\widehat{c_i}, \forall\, i \notin T\}$ all the values in vector $\widehat{\mathrm{c}}$ whose indices are not in T. Same for c.
- LSE is the log-sum-exp operation

The CE (cross-entropy) is defined as :

$$CE(\mathrm{p}, \mathrm{q}) = -\sum_u q_u \log(p_u) \tag{1.13}$$

And the LSE (log-sum-exp) is defined as

$$LSE(X) = \log\left(\sum_{p \in X} e^p\right) \tag{1.14}$$

This loss allows the classifier to learn even in cases where the labels can be of varying coarseness without the coarseness of some labels impacting the ability of the model to predict the true fine-grained labels (see Supplementary Tables for scPRINT. Supplementary Figure S14)

The loss is hierarchical for the classes : cell type, disease, sequencer, ethnicity ; the labels follow a hierarchy defined by (Cell Ontology, MONDO, EFO, HANCESTRO), respectively.

We do not compute the loss for cells where a class has an unknown label. We perform these classification tasks in one pass, using the embeddings generated directly from the downsampled expression profile.

The denoising task

Similarly to ADImpute, we expect a good gene network to help denoise an expression profile by leveraging a sparse and reliable set of known gene-gene interactions. In addition, we expect a good cell model to help embed and reconstruct an expression profile by leveraging the regularities of modules and communities within its network.

We view denoising similarly to upsampling, and inversely, we view adding noise as downsampling a cell profile.

Noise is similar to downsampling because of the distribution we are working with. Note that contrary to vision tasks (e.g. diffusion models), where additive Gaussian noise is added, in the context of expression data, where the distribution is often seen as a Poisson, NB, or ZINB, the data is already noisy, and the more counts are sampled, the less noise. No information is similar to not sampling data.

We downsample an expression profile using a zero-inflated Poisson model of the data. With this formulation, on average, half of the counts to be dropped are dropped by randomly removing a number of reads per gene, given by sampling from a Poisson whose lambda parameter is proportional to the number of counts in that gene. The remaining half of the counts to be dropped are dropped by randomly setting some genes to 0, i.e. a complete dropout of that gene. It is to be noted that with this definition of downsampling, the exact average amount of counts dropped for both parts depends slightly on the dropout *r*. During our pretraining, *r* is set to 0.6, meaning, on average, 60% of the transcript counts are dropped per cell.

Let $\mathrm{x_i}$ be the gene expression vector of cell i with dimensions n_{genes} ; we create a downsampled *version* by doing

$$\widehat{\mathrm{x}}_\mathrm{i} = \max((\mathrm{x_i} - \mathrm{p_i}) \cdot \pi_\mathrm{i}, 0) \tag{1.15}$$

with :

- $\mathrm{p_i} \sim Poisson(\mathrm{x_i} \times r \times 0.55)$ a vector of size n_{genes} where the poisson is samples for each element $\mathrm{x_i}$ of x
- $\pi_\mathrm{i} = I(u \geq r \times 0.55)$ a vector of size n_{genes} , the binary mask vector indicating non-dropout genes.
- $\mathrm{u_i} \sim Uniform(0, 1)$, a vector of size n_{genes}. of random values drawn from a uniform distribution.
- $\cdot$ denotes the element-wise multiplication.
- *r* being the dropout amount. We scale it by a tuning hyperparameter of 0.55 instead of 0.5 for numerical reasons.

The goal of the model is then using $\widehat{x_i}$ as an input to output the parameters μ_i , θ_i , π_i of a *ZINB* distribution of the true profile x_i , all vectors of size n_{genes}. The contribution of cell i to the loss is then computed as the negative log-likelihood of the count data given the distribution parameters being generated by the model

$$Loss_{denoising} = Loss_{ZINB} = -\frac{1}{n_{gene}m}\sum_{i=0,j=0}^{n_{gene},m}\log(L(x_{i,j}|\mu_{i,j},\theta_{i,j},\pi_{i,j})) \tag{1.16}$$

where n_{gene} is the size of the expression profile x_i , m is the size of the minibatch and

$$L\left(x|\mu,\theta,\pi\right) = \begin{cases} \frac{\pi}{\pi-\theta\cdot(\log(\theta)-\log(\theta+\mu))} & \text{if } x=0 \\ \frac{\left(\frac{\mu}{\theta+\mu}\right)^{x}\cdot\Gamma(x+\theta)\cdot\sigma(-\pi)}{\exp(\pi)\cdot\left(\frac{\mu}{\theta+\mu}\right)^{\theta}\cdot\Gamma(\theta)\cdot\Gamma(x+1)} & \text{if } x>0 \end{cases} \tag{1.17}$$

with σ the sigmoid function.

We show that models trained with such a framework perform better than regular MSE-trained models (see Supplementary Tables for scPRINT. Supplementary Table S3), for which one only outputs one value instead of three, directly representing the data's log-transformed count. In this case, the loss is the mean squared error between the predicted and true count values.

scPRINT effectively lets the user choose between the three formulations : *ZINB* with a *ZINB* loss, NB with an NB loss, and direct log-transformed count reconstruction with an *MSE* loss.

However, we have noted that the *NB* and *ZINB* loss still have some notable issues. They can easily overflow, especially when working with lower precision systems (like fp16, bf16, etc). These losses are also proportional to the total expression count, meaning cells with higher expression will have a higher loss on average. It also appears that the log-likelihood cannot go below ~1.1 loss on average and plateaus quickly. This makes evaluation of the loss less practical when comparing models. Finally, this minimal loss also depends on the total number of zeros in the true expression dataset, as the zero-inflation part of the loss converges smoothly to 0.

The bottleneck learning task

Bottleneck learning is a method that drives the model to generate a cell expression profile only from its embedding. Cell-embedding which can be passed again to that same model without the gene expression information, such that from the cell-embedding only, scPRINT can re-generate the cell's expression profile. The model thus finds the best compression of the cell's expression according to the information-theoretic theorem by Tishbi et al. .

While many transformer models and Geneformer directly use the average of gene embeddings to generate a cell embedding, this will likely squash the expression information.

scGPT used another methodology (called MVC) to generate an embedding vector such that

$$x_{i,j} = \mathrm{e_i} \odot \mathrm{g_j} \tag{1.18}$$

where $x_{i,j}$ is the expression of gene j in cell i, and $\odot$ is the dot product. For each gene embedding $\mathrm{g_j}$, the embedding only contains information about the gene name, not gene expression. Regular MSE on each $x_{i,j}$ is then used as the training loss.

This pushes the cell embedding $\mathrm{e_i}$ to contain all the expression information of the cell i.

This is less computationally intensive to train than our bottleneck learning method. However, we have noticed poorer reconstruction through this methodology than ours (see Supplementary Tables for scPRINT. Supplementary Table S3).

In our case, we consider that our model scPRINT can act as two parts of an autoencoder. The encoding part is when we give scPRINT the expression profile of a cell and retrieve a set of disentangled cell embeddings (see the Class decoder section of the methods). The decoder part is when we provide scPRINT only the gene labels without their corresponding expression values and the disentangled cell embedding in place of the empty placeholder embeddings (see Supplementary Tables for scPRINT. SupplementaryFigure S15).

This means the encoder is considered as

$$\mathrm{e_{A,i}} = scPRINT([\mathrm{g_O} + \mathrm{e_{0,i}} + \mathrm{l_0}, \mathrm{g_1} + \mathrm{e_{1,i}} + \mathrm{l_1}, ..., \mathrm{p_A}]) \tag{1.19}$$

where $\mathrm{e}_{A,i}$ is the output embedding of the placeholder embedding token A for the cell i (in our case, we use multiple (default, totalcount, cell_type, disease, sex, organism, ethnicity, sequencer). Then the decoder is defined as

$$\mu_\mathrm{i}, \theta_\mathrm{i}, \pi_\mathrm{i} = scPRINT([\mathrm{g_O} + \mathrm{l_0}, \mathrm{g_1} + \mathrm{l_1}, ...], \mathrm{e_{0,i}}, \mathrm{e_{1,i}}, ..., \mathrm{e_{t,i}}) \tag{1.20}$$

With μ_i , θ_i , π_i vectors of size n_{genes}. Finally, the loss is given by the ZINB loss :

$$Loss_{bottleneck} = \sum_{i=0}^{m} Loss_{ZINB}(\mathrm{x_i}|\mu_\mathrm{i}, \theta_\mathrm{i}, \pi_\mathrm{i}) \tag{1.21}$$

where $\mathrm{x_i}$ is the cell i expression profile and m the minibatch size.

Implementing a set of disentangled embeddings is not straightforward. In our case, we push the embeddings to be as different from one another as possible with a contrastive loss defined as

$$Loss_{contrastive} = \frac{1}{m^2} \sum_{i=1}^{m} \sum_{i'}^{m} 1 - \cos(\mathrm{e_i}, \mathrm{e_{i'}}) \tag{1.22}$$

where e_i and $e_{i'}$ are the cell embeddings, m is the minibatch size, and cos denotes the cosine similarity. This pushes each embedding to represent the correct information using the classifiers. However, more is needed to remove all the batch effects or entirely prevent information leakage across embeddings.

Finally, we have also used the classifier output logits as cell embeddings. This works particularly well for cell type, disease, or sequencer classes containing many labels. It has been shown that classifier logit outputs behave similarly to embeddings and, in our case, offer an even better removal of the batch effects (see Supplementary Tables for scPRINT. SupplementaryFigure S7).

For the bottleneck loss, we directly reconstruct expression using the cell embeddings generated from the noisy, downsampled expression profile of the denoising process, doing the entire process in one single pass. We sum all the losses without scaling them :

$$Loss = Loss_{contrastive} + Loss_{bottleneck} + Loss_{denoising} + Loss_{class} \tag{1.23}$$

1.5.4 scDataloader

Parallel to this work, we worked with Lamin.ai to develop a dataloader for large cell atlases, described and benchmarked in Rybakov et al.. One key advantage of this dataloader is its ability to perform weighted random sampling on hundreds of millions of cells without being a bottleneck during pretraining. scDataloader samples cells amongst the 800+ datasets of cellxgene's mid-2023 release, using the cell labels to inform how rare the specific combination of labels is.

From this, the dataloader produces a cell sampling weight, rescaled with a hyperparameter. The dataloader will sample, with replacement, more consistently rare cell types than more common ones.

We have produced an additional wrapper package around the laminDB "mapped-dataset" called scDataloader. scDataloader works with lamin.ai but can also interface with scVI and AnnData formats to enable downloading, preprocessing, and QC of large single-cell databases and datasets. It is very flexible and can represent expression data in the formats used by scPRINT, scGPT, and Geneformer. It also implements a lightning datamodule scheme and command line interfaces for quick setup (see Supplementary Tables for scPRINT. SupplementaryFigure S16).

Overall, we preprocess each of the 1200 datasets in cellxgene by only keeping primary cells from either humans or mice and dropping all the spatial omics datasets. Spatial omics are not true single-cell assays, and we decided for now not to include them. We also drop any cells with less than 200 expressed genes. Finally, we drop any resulting dataset smaller than 100 cells, with less than 10,000 genes, or from which more than 95% of the cells have been removed. This results in a new database of 54,084,961 cells and 548 datasets.

We believe that the weighted random sampling strategy allowed our pre-training to be much faster by creating more diverse minibatches.

1.5.5 Extracting meta-cell gene networks from attention matrices in scPRINT

Transformers compute multiple attention matrices per layer, called attention heads. This is done by splitting the generated $\boldsymbol{K}$, $\boldsymbol{Q}$, and $\boldsymbol{V}$ embedding into m sub-embeddings, thus defining m attention heads. Each attention head computes the attention matrix via the equation :

$$\text{softmax}\left(\frac{\text{QK}^T}{\sqrt{d_k}}\right) \tag{1.24}$$

However, we would want to aggregate those over multiple cells from a similar cell state to increase the signal obtained from only one cell. We are doing so by averaging the Keys and Queries embeddings over the set of cells U passed to the model :

$$\text{softmax}\left(\frac{mean_U(\text{Q}) \cdot mean_U(\text{K})^T}{\sqrt{d_k}}\right) \tag{1.25}$$

By doing this, the attention matrix behaves as if each query vector for cell i was "looking" across the key vectors of all the cells in U.

The resulting object is a row-wise normalized n^*n matrix, where n is the size of the input context (i.e. the number of genes passed to the model). However, we also include the possibility to generate large matrices and gene networks, referred to as genome-wide gene networks. We take the average over different sets of expressed genes for each cell in the set U. This allows us to compute a genome-wide attention matrix while only doing forward passes on smaller subsets of the genome per cell.

1.5.6 Heads selection

With scPRINT, we present a method to select heads based on some available ground truth data. This is inspired by the ESM2 paper and uses a somewhat similar method. Using all the available attention matrices from all of the model's heads, we use a linear classifier RidgeClassifier from scikit-learn (with an L2 penalty set to 1, a positivity constraint on the coefficients, and without an intercept) to classify the ground truth's edges based on a combination of each head. The classifier converts the target values into {-1, 1} equals to {no connections, connections} and then treats the problem as a regression task with mean squared error.

Instead of taking the classifier's output, we use the average of the subset of heads associated with a non-zero coefficient in the classifier, without weighting them. Thus, the classifier only serves as a means to select the heads with relevant information in predicting a ground truth of interest and decreases the possibility of overfitting (see Figure 1C).

1.5.7 Normalization and network interpretation

In scPRINT and scGPT, the attention matrix is normalized via the softmax function over the query (i.e., row) dimensions. This means that all row elements sum up to 1 or that the same mass flows from each network component. This rescaling is essential as it corrects that some row element scales can be much higher than others in the attention matrix. Similarly, in regularized models like GENIE3, only a small set of genes are connected for each gene in the matrix, meaning all genes have directed edges toward a small subset of genes. Thus, our interpretation is that the row elements are the targets in our network, each connected to a small subset of genes. The column elements are thus the regulators and can regulate many / most genes in the network.

For biological ground truths like MCalla et al. and gwps, which fit this assumption of highly connected regulators and sparsely regulated targets, we directly compare them to the inferred network. Tables S12 and S13 show that this performs better than taking the opposite view by transposing the inferred networks.

This assumption is challenged for Omnipath, which has most of its elements connected to a sparse set of other elements (see Supplementary Tables for scPRINT. SupplementaryFigure S3). Due to the sparsity of connections for regulators (i.e., sources) in the ground truth network and the large number of regulators (8000+), the methods are challenged and perform much better when taking the transpose of their network and matching the regulators to the sources and sources to regulators.

1.5.8 Simulated datasets, BoolODE and Sergio

BoolODE is a method to generate count data via a stochastic differential equation applied over a user-defined Boolean network. It was used and developed as part of the BEELINE benchmark algorithm, which was created as an improvement over the GeneNetWeaver algorithm. However, this model is still very simple compared to cell biology. Due to its computational complexity, it can only model up to a couple hundred gene relationships over a few dozen genes.

Sergio, a slightly more recent ODE model marks an improvement over BoolODE on the size of the networks it can simulate (up to a thousand genes) and its similarity to scRNAseq data.

Indeed, Sergio's simulated data is not similar to real expression data. This means that the biases that Transformer models learn should not help them predict Sergio's data. Correlation and regression-based methods do not have biases. They are therefore expected and have traditionally shown better performance on these benchmarks.

We generated the Sergio ground truth network and simulated single cell expression by using the notebook : https://github.com/g-torr/SERGIO/blob/v2/minimal_example.ipynb from the repository : https://github.com/g-torr/SERGIO which present some debugs and improvements to the initial repository : https://github.com/PayamDiba/SERGIO. Indeed only this fork of the initial Sergio repository led us to successfully generate

a network.

We used RegNetwork as input and simulated 1000 cells from its 3546 connections over 813 genes with default parameters from the notebook.

1.5.9 BenGRN and gene network metrics

We use the packages benGRN and GRnnData released with this manuscript to work With Gene networks and perform our benchmarks.

Our three main metrics are EPR, AUPRC, and enrichment. They all take advantage of the fact that the predictions are generated as scores over edges between nodes :

- We have computed the Early Precision Ratio (EPR) as the diagnostic odds ratio : (TP x TN) / (FP x FN) at the cutoff of the scores giving K positive predictions, where K is the number of positive elements in the ground truth.
  In this context, 1 is a random prediction, and inf is a perfect prediction ; values below one mean that inverting the predictor would provide better results.
- Area Under the Precision-Recall Curve (AUPRC) is the area (computed with the composite trapezoidal rule) under the curve defined by the precision ($PR = TP / (TP + FP)$) and recall ($RE = TP / (TP + FN)$) where TP is the number of true positives, FP is the number of false positives, and FN is the number of false negatives. This curve is obtained through a range of cutoffs going from 0 predicted positives to all predicted positives. Here, we compute a version of the AUPRC where the floor of the area is not given by the Precision=0 line but by the line of the prevalence of the positive class. Moreover, we do not interpolate the curve between the last recall value and the perfect recall : 1. We do this to properly compare AUPRC values across benchmarks and models. Random precision values are given in the supplementary data.
- Enrichment is computed using the prerank methodology, where, given an ordered set of genes, it is computed by :
  - 1. Summing all scores of edges of the matrix row-wise. (Target - Hub) Or
  - 2. Summing all scores of edges of the matrix column-wise. (Regulators - Hub) Or
  - 3. Computing the eigenvector centrality of nodes in the graph using NetworkX's implementation. Prerank's background comprises all the genes in the set (centrality).

Of note, we did not design an automated method for cell-type enrichment. Instead, the assessment of whether or not a network is enriched for the correct cell type is done manually, identifying cell type names in the top 10 cell types listed in the enrichment results of the network.

1.5.10 Other evaluation metrics

All evaluation metrics from the section "scPRINT is competitive on tasks orthogonal to GN inference" of the results come from the openproblems benchmark and are standards in the field.

scIB's batch correction score is an average of the avgBatch score and the avgBio score, which are themselves averaged over many scores. Details of each value are available in our package's notebooks.

- scIB avgBio is a combination of label-based and label-free metrics using for example : the Adjusted Rand Index (ARI) and the Normalized Mutual Information (NMI) on clusters computed from the K-Nearest Neighbor graph. Other scores are used, some using the conservation of trajectories and of the cell cycle variance, and some on the rare cell population conservation, overlap of highly variable genes (see scIB), and more.
- scIB avgBatch is a similar combination of label-based and label-free metrics, using, for example, the average connectivity across clusters of different batches : ASW, the graph integration local inverse Simpson's Index : graph iLISI, the k-nearest-neighbor Batch Effect Test (kBET), and more.

Finally, we also use two metrics in our classification task :

- Macro-F1 : also called macro-average, is the average of the F1 score across each class in a multi-class task. Where the F1 score is : $2 \times \frac{PR*RE}{PR+RE}$.
- Accuracy : the accuracy is computed as $\frac{TP + TN}{TP+TN +FN+FP}$

1.5.11 Denoising Benchmarks

To validate the denoising ability of scPRINT, MAGIC, and KNNsmoothing2, our test function, available in the scPRINT package, uses a representative subset of 10,000 cells of each dataset to generate the denoised expression over the 5000 most variable genes in this dataset.

Before that, counts are removed from the dataset following the same procedure as done for scPRINT's pretraining (see The denoising task section of the methods).

For each cell, we compare the denoised and un-denoised profiles to the true profile (e.g. before denoising). We compute the Spearman's correlation over the genes initially expressed in the cell, taking the average across all cells. We do not use the unexpressed genes as we are working with a dataset with high dropout and expect that a good denoiser will set genes that are 0 in the profile with some value. We notice that this improves the score of all denoising methods and makes more sense given the data.

For the rare cell population test, we keep everything similar but compute only the Spearman correlation over a rare cell population in the dataset.

We run KNNsmoothing2 with default parameters and a K of 10. We run MAGIC using the Scanpy implementation with default parameters and the approximate solver for computational speed. When computing KNNsmoothing2 or MAGIC over a small set of cells we use a K of 5 for the nearest neighbors.

1.5.12 Fine-tuning

Contrary to most other foundation models for scRNAseq, we do not finetune scPRINT at any moment in our benchmark and all results are provided for the pre-trained model only.

While we haven't assessed fine-tuning we believe this is an important feature of foundation models and release various scPRINT models so that they can be re-trained, fine-tuned, and modified by the community for novel tasks or to improve its performance on the tasks we have presented.

1.5.13 State-of-the-art methods used in benchmarking

All methods presented here generate networks from their input data. Given gene-level expression data, they will generate gene-networks. Without additional information, no method can distinguish the type of molecular interactions that underpin their predicted network edges.

Gene network inference with an ensemble of trees (GENIE3)

Developed originally for bulk transcriptional data, *GENIE3* computes the regulatory network for each gene independently. It uses a random forest, a weak learner ensemble method, to predict the expression profile of each target gene from profiles of all the other genes. The weight of an interaction comes from the feature importance value of an input gene in the predictor for a target gene's expression pattern. Aggregating these weighted interactions over all the genes yields the regulatory network. This method was the top performer in the DREAM4 in silico network challenge (multifactorial subchallenge).

GENIE3 can be seen as a generalization of correlation-based methods for inferring gene networks. Instead of looking at genes that correlate most with another gene, GENIE3 finds how to combine a set of correlated genes to get an even better correlation. We run GENIE3 on raw counts as it is said from both the BEELINE benchmark and the R package vignette that GENIE3 can be run on either log normalized or raw count data and that while it will change the results, there are no preferred methods. This is something we have also noted in our trials.

We use all default parameters and choose 100 trees for computational feasibility reasons. We compute the networks on the same set of cells and genes as the other methods.

We also use a TF-gene only version of the method where the regression is performed

only using the expressed transcription factors instead of all expressed genes as input. This is the most used version of *GENIE3* and is much faster.

DeepSEM

DeepSEM is an autoencoder model made for gene network inference. It learns to decompose a set of cells as a set of embedding and an adjacency matrix (i.e., a gene network). The formula of the VAE then becomes : $X = f_1((I - W^\top)^{-1}Z)$, for the decoder and $Z = (I - W^\top)^{-1} f_2(X)$ for the encoder, where X is the expression data, Z is the embedding dimension, W is the adjacency matrix, I the identity, and f_1, f_2 are MLPs.

We preprocess the anndata by normalizing gene expression to 10,000 genes, applying a logp1 transformation, and then computing the z-score per gene, as explained in the associated research paper.
We use DeepSEM with default parameters and on the same set of cells and genes as the other methods. We use the DeepSEM-provided functions for loading and parsing Anndatas.

Single-cell generative pretraining transformer (scGPT)

scGPT is a transformer-based model of roughly 100M parameters, pre-trained with a generative process similar to Language models. scGPT proposes to build similarity networks based on the output gene embeddings of the model but also based on its attention matrices. It computes networks as the difference between the rank-normalized version of the average attention matrix in a baseline expression profile vs a perturbed one in perturb-seq data. The attention matrix is the average of attention matrices over the heads of the last layer and over the cells given to the model.

We run scGPT following the examples given in their "Tutorial_Attention_GRN.ipynb" notebook.

We use the "scGPT_human/best_model.pt" from the list of available models with default parameters. All runs are in our fork : "https://github.com/jkobject/scGPT" in the "mytests/" folder. Similarly, we take the mean over cells and over the heads of the last layer. We compute softmax similarly to the attention computation but without applying the rescaling factor $\sqrt{d_k}$. We finally drop the first element corresponding to the cell embedding token.

We extract cell embeddings from scGPT by directly using the cell embedding token of the model without fine-tuning it on a batch correction task. This is done in order to compare it to scPRINT which is itself not fine-tuned. We compute the networks on the same set of cells and genes as the other methods.

Geneformer

Geneformer is a BERT model. Gene expression data is transformed into a sentence or genes ordered by their scaled expression. It is trained with mask language modeling and

contains somewhere around 80M parameters. We use the new versions of 2024 Geneformer models trained on 100M cells (2x more than scPRINT). We follow the preprocessing and inference scripts used in the geneformer huggingface repository and notebooks : https://huggingface.co/ctheodoris/Geneformer/tree/main. Our inference script updates to extract gene networks from Geneformer are available in our scPRINT repository : https://github.com/cantinilab/scPRINT/tree/dev/tools.

We extract gene networks from Geneformer using the mean of all attention heads per cell. Since Geneformer only uses expressed genes in a cell, we have to map the attention matrices back to the full network size before computing its average over cells, taking into account the NaN values. We compute the networks on the same set of cells and genes as the other methods.

We extract a cell embedding from Geneformer using the cell embedding from the "gf-12L-95M-i4096_MTLCellClassifier_CELLxGENE_240522" model that has been fine-tuned on predicting the cell labels of cellxgene datasets.

scFoundation

scFoundation is a foundation model for single-cell RNAseq based on the xtrimogene architecture. It was built by the Biomap company. It is able to work on the full genome sequence of transcripts for each cell by considering the high number of zeros and embedding them separately. The tool is aimed at performing a range of tasks, such as denoising, embedding, and predicting perturbation response. It has been trained with a mixed masking and denoising pre-training. However, we could not compare scFoundation to scPRINT and MAGIC on the denoising benchmark, as scFoundation's denoising only happens at the level of the cell embedding at inference time.

We could not validate scFoundation on our Gene network inference benchmark as extracting a network from the attention matrices was much more complex due to the xtrimogene architecture. scFoundation mentions the generation of gene modules using clustering of its output gene embeddings. It also mentions the interference of gene networks. However, it is achieved using RcisTarget, a prior gene network based on motif analysis. This approach is not comparable to the gene networks generated by scPrint, Geneformer, and scGPT. Indeed, RcisTarget could be applied to every model we have benchmarked and would prevent us from doing an unbiased benchmark. Neither our approach nor Hao et al.'s could extract gene networks directly from scFoundation. It is being left to further investigations.

For batch effect correction, we use scFoundation with default parameters and follow the steps for cell embedding in the "model/README.md" file in their GitHub repository : https://github.com/biomap-research/scFoundation. However, we give scFoundation single cell profiles of the 5000 most variable genes in each dataset. This is because we could not run scFoundation on genome-wide expression profiles with our GPU. We then apply a PCA to the output embedding to reduce the dimensionality from 3224 to 512. This is because the initial dimension was too high for scIB to compute a score from on our machine (40CPU Intel Xeon, 32GB RAM + 64GB SWAP, GPU NVIDIA A4500 with 20GB of memory).

Marker-based cell type prediction with CellTypist

To showcase the novel ability of scPRINT to perform zero-shot prediction of cell type labels, we use the CellTypist method, which similarly performs de-novo prediction of cell type labels given its precomputed databases of cell type markers.

CellTypist works by mapping cell gene expression to genes known to be specifically expressed in combination in a cell type. Thus, it predicts cell type from these marker genes.

We use it with default parameters on the normalized and log-transformed counts over the full set of genes in the dataset. We use the 'Adult_Human_PancreaticIslet' database, which contains markers for 14 cell types and overlaps with only four of the cell types in the dataset.

We decided to still use it as is to showcase the marker-based method's inability to recover the full set of cells and the tradeoff between the number of cell types and accuracy.

Fortunately, these four cell types (A, B, D, PP) represent 70% of the dataset. With its current database, CellTypist can only reach a maximum accuracy of 70%. Even when taking this into account, CellTypist only overperforms scPRINT on the accuracy metric and by roughly 9 points.

Classification benchmark and associated methods

Our classification benchmark is run using following the openproblems benchmark. It uses the same input, output data, and metric. It also similarly splits the train-test by batch and preprocesses the expression matrix to what is presented in the open problem benchmarks.

For this task, methods can access the full set of genes by default. scPRINT will use its random sampling of genes approach with a context of 4000 genes. Classifiers like logistic regression and xgboost were run according to the openproblem process, using the 25 principal components of the count normalized, logp1 transformed expression data. CellTypist was run on the normalized and logp1-transformed cell expression profile.

1.5.14 Ground truth preparation

McCalla et al.

For the MCalla et al. dataset, we downloaded the data from the supplementary datasets of their paper . After undoing the logp1 transform, we re-generate the true count expression matrix from the normalized one by dividing the expression of each cell by the smallest value in its expression profile. This fully recovered the true counts, all values being integers. For the additional human dataset we used, we downloaded it from the gene expression atlas database.

We used the intersection (gold standard) ground truth dataset for both human and mouse,

converting this list of sources to target genes into a directed binary network.

Omnipath

We generate the Omnipath network using all the interactions from the Omnipath Python package, excluding small molecules, lncRNAs, and any element without a unique HGNC symbol. We then transform it into a directed binary network of source to target. These interactions are extracted from the literature and represent mainly TF to gene connections as well as many protein-protein interaction connections and a small number of other connections known from the literature like RNA-RNA interactions, protein-RNA interactions, and more. All interactions are mapped back to their gene IDs, generating a gene-gene network encompassing the various interactions the genes and their molecular products can have.

Gene networks from genome-wide perturb-seq

We created a gene network from the genome-wide perturb-seq dataset using the supplementary matrix containing the results of differential expression in the dataset. This matrix represents the multiple hypothesis testing corrected p-values of a differential expression test of cells with KO of gene A compared to the baseline cell expression. This is available for all 8000+ expressed genes in the K562 cell line. We used a cutoff of 0.05 on these values to define the directed binary connection between genes.

This effectively gives a gene x gene-directed binary graph that tells if a statistically significant connection exists from the source $gene_A$ to the target $gene_B$ according to genome-wide perturb-seq.

For all ground truths, download, preprocessing, and extraction of the network and expression data are available in the BenGRN package.

1.5.15 Details on the Benign Prostatic Hyperplasia analysis

We download our dataset from cellxgene under the reference : *574e9f9e-f8b4-41ef-bf19-89a9964fd9c7*.

We preprocess the dataset using scDataloader's preprocessing function. We generate embedding and classification using 3000 expressed genes in each cell. Similarly to pretraining, we take 3000 randomly expressed genes ; if less than 3000 are expressed, we complete with randomly selected unexpressed genes. We display embeddings generated using the cell type classifier logits (see section The classification task in methods)

We use the Scanpy toolkit to generate our Umap plots directly from the embeddings, as well as our differential expression results and our clusters. We define the clusters using the Louvain algorithm with 10 k-nearest-neighbors and a resolution of 1. We perform denoising on 5000 genes per cell selected similarly to the embedding and classification part. We use

the 4000 most variable genes in each cell type to generate our gene networks in the BPH and normal fibroblasts.

On the gene networks, we perform gene set enrichment with the Enrichr method on the GO_MF_2023 gene sets. For community detection, we use the Louvain algorithm with parameter 1.5. We perform analysis only on the communities with between 200 and 20 genes. (4 and 5 in the BPH-associated fibroblasts, 3 and 4 in the normal fibroblasts)

All analysis and results are available in the *cancer_usecase_1* and *cancer_usecase_2* notebooks.

1.5.16 Negative Binomial to Poisson relationship

As explained in The denoising task and Expression decoder section of the methods, in our model, we have used the ZINB as our loss, an extension of the NB distribution to zero-inflated data.

Moreover, we have also used the zero-inflated Poisson mechanism to downsample the cell expression profiles. These are consistent because we can view the Poisson distribution as a NB without overdispersion. The relationship between *NB* and *Poisson* is given by making the dispersion term go to 0 and the inverse dispersion term $\theta \longrightarrow \infty$. Doing so, the term $\frac{\theta}{\theta+\mu}$ approaches 1. Thus, the PMF simplifies to :

$$P(X = x) \approx \frac{\Gamma(x+\theta)}{x!\Gamma(\theta)} 1^{\theta} \left(\frac{\mu}{\theta+\mu}\right)^{x} \tag{1.26}$$

For large θ, we use Stirling's approximation of the Gamma function : $\Gamma(\theta) \approx \sqrt{2\pi\theta}(\frac{\theta}{e})^{\theta}$

we get :

$$\Gamma(x+\theta) \approx \sqrt{2\pi(x+\theta)} \left(\frac{x+\theta}{e}\right)^{x+\theta} \tag{1.27}$$

$$\Gamma(\theta) \approx \sqrt{2\pi\theta} \left(\frac{\theta}{e}\right)^{\theta} \tag{1.28}$$

Simplifying the ratio of the Gamma functions :

$$\frac{\sqrt{2\pi(x+\theta)} \left(\frac{x+\theta}{e}\right)^{x+\theta}}{\sqrt{2\pi\theta} \left(\frac{\theta}{e}\right)^{\theta}} = \sqrt{\frac{x+\theta}{\theta}} \left(\frac{x+\theta}{\theta}\right)^{\theta} \left(\frac{x+\theta}{e}\right)^{x} \tag{1.29}$$

For large θ, $\frac{x+\theta}{\theta} \sim 1$, so : $\sqrt{\frac{x+\theta}{\theta}} \approx 1$

$$(\frac{x\ +\ \theta}{\theta})^{\ \theta}\ \approx\ 1$$

Thus, the expression simplifies to :

$$P(X = x) \approx \frac{1}{x!}\left(\frac{\mu}{\theta + \mu}\right)^{x}\left(\frac{\theta + x}{\theta}\right)^{x} \tag{1.30}$$

Finally, $(\frac{x\ +\ \theta}{\theta\ +\ \mu})^{x}\ \approx\ 1$ for large θ, so :

$$\lim_{\theta\to\infty} P(X = x) = \frac{\mu^{x}}{x!}e^{-\mu} \tag{1.31}$$

This is the PMF of the Poisson distribution with mean μ.

1.5.17 Data availability

The model weights are publicly available on Hugging Face. Pre-training logs to assess the model's training are available on Weights and Biases. The full pre-training dataset is publicly available on CellxGene under its census data release version : LTS 2023-12-15, accessible at https://cellxgene.cziscience.com/. All other datasets used in this work can be downloaded through their respective public databases via the helper scripts on the scPRINT, BenGRN, GRnnData, and scDataLoader packages. Source data are provided to re-generate the figures. Code to generate the large UMAP of Figure 1 is available as a notebook on GitHub at https://github.com/cantinilab/scPRINT/blob/1.6.4/figures/nice_umap.ipynb. Code to re-generate the source data is available as notebooks on our Github.

1.5.18 Code availability

The code and notebooks used to develop the model, perform the analyses, and generate results in this study are publicly available and have been deposited in cantinilab/scPRINT at https://github.com/cantinilab/scPRINT under MIT license. The specific version of the code associated with this publication is archived in the same repository under the tag 1.6.4 and is accessible via https://github.com/cantinilab/scPRINT/tree/1.6.4/ and DOI :10.5281/zenodo.14749466.

Additional developed packages for this analysis are defined in the pyproject file and project submodules. They are available on GitHub :

- **GrnnData** : https://github.com/cantinilab/GRnnData, DOI :10.5281/zenodo.10573141
- **BenGRN** : https://github.com/jkobject/benGRN, DOI :10.5281/zenodo.10573209
- **scDataLoader** : https://github.com/jkobject/scDataLoader, DOI :10.5281/zenodo.10573143

– **scGPT and notebooks to reproduce the results** : https://github.com/jkobject/scGPT/tree/main/mytests

Xpressor : Towards foundation models that learn across biological scales

2.1 Summary

We have reached a point where many bio foundation models exist across 4 different scales, from molecules to molecular chains, cells, and tissues. However, while related in many ways, these models do not yet bridge these scales. We present a framework and architecture called Xpressor that enables cross-scale learning by (1) using a novel cross-attention mechanism to compress high-dimensional gene representations into lower-dimensional cell-state vectors, and (2) implementing a multi-scale fine-tuning approach that allows cell models to leverage and adapt protein-level representations. Using a cFM as an example, we demonstrate that our architecture improves model performance across multiple tasks, including cell-type prediction (+12%) and embedding quality (+8%). Together, these advances represent first steps toward models that can understand and bridge different scales of biological organization.

2.2 Introduction

Biology processes information across different scales, from individual molecules to entire tissues. Recent advances in artificial intelligence have led to the development of foundation models that excel at representing biological data at specific scales, such as protein structures [153] or cell states [154, 45]. However, these models typically operate in isolation, unable to leverage the rich interconnections between different biological scales. Having models that can learn across biological scales will be crucial to capture the complexity of the biological phenomena.

The main premise of our work is that by using information gained from a lower scale (e.g., molecules), we might improve the input representations of an higher scale phenomena (e.g., cells) [5, 155]. Reciprocally, using relationships learned at the higher scale, we might

improve the lower-scale models too. Finally, we would want to use joint representations of molecules, DNA, proteins, cells, and tissues, which are all the elements of the organisms we want to study.

While it is likely infeasible to learn across all scales at once, we might be able to use foundation models that have been trained at specific scales, which we call uniscale models, using only fine-tuning and some architectural changes (see Figure 2.1). We first review the existing uniscale foundation models in depth for each of the four main biological modalities [156].

2.2.1 Foundation models across scales

mFMs try to model with atomistic precision the complex quantum physics-based rules that govern molecules and their interactions [157]. They generate embeddings of molecules by encoding their chemical representation, often using SMILES notation. These embeddings should contain information to predict molecular measurements such as binding to a target, potency, solubility, and more [158, 159]. The models are often built with invariances concerning the symmetries of molecules (relative positions and angles) [52]. These models can also be paired with ones that learn to predict the structure and dynamics of these molecules. Training data in this context is mostly limited by compute since molecular dynamics simulations can be generated at will [160]. The first use cases of such models are in material generation and drug discovery.

However, computing binding affinities and force-fields similar to the most precise molecular dynamics methods remains a frontier [161, 162].

nFMs are a category of models designed to analyze sequences of nucleotides or amino acids, which are encoded in triplets of nucleotides, primarily using data derived from sequencing across various life forms. Although new architectures have been introduced to handle large context sizes [163], most models generally rely on traditional transformer models with small context sizes and are trained with masking. These models are based on the transformer architecture and language model techniques (LLM) [38] to produce representations of the lengthy and repetitive molecular structures found in DNA and RNA, sometimes termed dnaLM and rnaLM [164, 165, 166, 167].

While protein language models like ESM2 [153] have shown real-world usage in helping generate 3D models of proteins, dnaLM mainly focused on the task of understanding regulatory mechanisms, such as binding interactions and chemical modifications on DNA. It has been shown however, that representations learned by dnaLM can also contain information about the secondary structures of proteins and even protein-protein interactions [167, 168].

For these reasons, we fold protein language models into the nFM category, proposing that their distinctions will blur in the future.

Numerous challenges still exist in accurately predicting the diverse conformations of RNA, DNA, and proteins, as well as in modeling their intricate interactions [157]. Indeed, it is still hard to measure complexes with the same accuracy as individual proteins. A goal would be to generate nFMs that learn across the very related lexicons, which are DNA, RNA,

and proteins, by introducing architectures and training modalities that go beyond what exists today [169]. Indeed, there we could use the framework of "learning across scales" by using the representations of molecules, learned and compressed by mFMs, as the very tokens of nFMs, allowing them to talk about ribonucleotides, deoxyribonucleotides, amino acids, and their potential modifications.

Currently, the main applications of nFMs have been in drug, and target discovery, as well as many other fields of biology.

cFMs are a class of models trained on a matrix of abundances of the different chemical elements (proteins, RNAs) present in cells. [5, 154, 44, 45, 49, 48]. Their architecture is often based on bidirectional encoder-based transformers trained on single-cell RNA-sequencing data. While diverse training strategies have been presented, the model's architectures have, for now, remained fairly classical. The goal of these cFMs is to generate an accurate model of the cell that would allow predictions of cell evolution and response to perturbations [170].

However, immense challenges remain. Current promises have not stood up to experimental validations [171, 46]. While many reasons can be formulated, issues exist around data quality, diversity, and coverage. Indeed, single-cell data is very noisy, only measures a tiny fraction of the molecular composition of cells, and has been mostly produced on human and model animals [86]. While data will remain an important challenge, an area of improvement would be to, again, distill the rules of molecular interactions from sequence learned at the sequence level onto cFMs. This allows them to better learn the complex regulatory mechanisms of the cell.

tFMs strive to understand the interactions between cells that form tissues, mostly in higher-order organisms. Often based on imaging techniques, they consider the 2D structural relationship of cells or group of cells in a tissue slice. The stained microscopy slides allow the prediction of tissue type, organs, and even some protein expression levels. These models are often versions of the famous vision transformer architecture and framework (Dino V2), applied to medical images [172, 173]. They thus learn on image patches where each pixel has some channels of information (often from 2 to 30 different chemical elements are represented within these channels) [174, 175]. The number of channels can go up to tens of thousands in spatial transcriptomics image modalities, where each channel represent a transcripts location at a subcellular level(e.g., xenium) or at a cell-group-level (e.g., visium).

Overall, even more challenges arise in tissue foundation models. Most of the data exists behind institutional barriers, the resolution of high channel count modalities is really poor, while the channel amount of high-resolution modalities is really small, making it hard to predict even the cell state. Slices are often of tiny subparts of tissues. Most of the available data is in 2D slides, and 3D modalities are still burgeoning [176]. We lack good measurements of what cells are communicating, but we know that they do, from sequences to molecules and even entire organelles [177]. tFMs' vocabulary can be seen as made of cells. Their tokens are cell representations and could be be the rich representations learned by cFMs. The goal of a tFM is then to predict the presence of cells given other cells in spatial context.

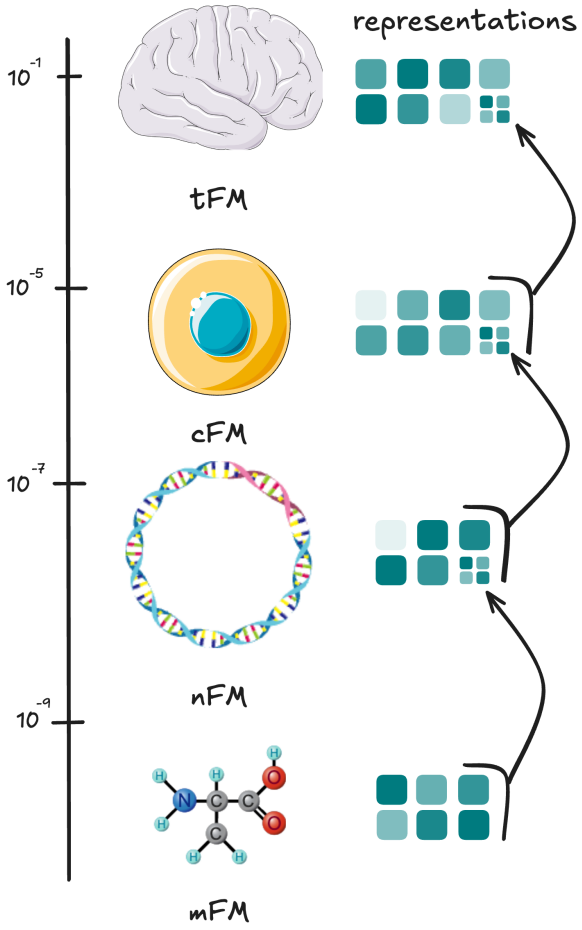

Figure 2.1 – we show how the representation of different foundation models could feed the upper scales and their learning could inform the lower scales' representations.

2.2.2 Architectural modifications : compressed representations

For biological representations, previous methods have leveraged many different methods from matrix factorization, nearest neighbors, and neural networks [178, 179]. Popular approaches are VAE such as scVI and scArches [26, 180]. In the domain of protein embedding, the HourGlass embedding method [181] introduced FSQ [182] as a framework to encode both amino acid sequences and 3D structural information from a pLM into a quantized latent space. Meanwhile, DNA sequence model embeddings have been mostly restricted to metagenomics, with the exception of DNA-BERT-S [183].

Finally, it has been shown not only in biology but also in the NLP community that for transformer models, embeddings based on average,max,sum-pooling of last-layer tokens are very restrictive and do not perform well [184, 185, 186]. Indeed, current SOTA methods use more complex approaches such as cross-attention mechanism and additional pre-training or fine-tuning tasks.

In the following, we will show that we can use a similar cross-attention mechanisms to compress the output embeddings of a foundation model into a set of lower-dimensional vectors.

2.2.3 Training modifications : fine-tuning

An extensive literature exists on fine-tuning. The simplest and most powerful approach remains to continue training on a small set of epochs and with a lower learning rate [187]. Common tools include low-rank approximations of the MLP and QKV matrices using LoRA, QLORA, and COLA [188, 189, 190, 191], which allow cheap fine-tuning of large foundation models. Other common approaches also mostly revolve around reducing the memory footprint of fine-tuning by only back-propagating the loss across a specific subset of parameters, from updating only specific layers of the model, only the MLPs, the QKV matrices, or only the biases of the MLPs [192, 193]. Finally, adapter layers have also been used for their versatility. They often consist of an additional MLP on top of the large model's output representations [194].

In the following, we will show that the adapter layer is a sensible approach to perform multi-scale fine-tuning.

2.2.4 Contributions

Following up on these recent advances, we propose :

— A cross-attention "compressor" block whose goal is to compress a foundation model's output embeddings into a small set of low-dimensional vectors, called the *Xpressor* (Cross-Attention Compressor transformer). This is learnt using an auto-encoding approach with a reconstruction loss. The Xpressor is modality agnostic and can be used by mFMs, nFMs, cFMs, tFMs, or even other non-biological domains, and can work in addition to other training tasks like masking or denoising (see Figure 2.2A).
— A multi-scale fine-tuning approach using adapter layers. This allows the fine-tuning of models from one level using the upper-scale model's task (see Figure 2.2B).

2.3 Xpressor

2.3.1 Background

scPRINT [154] is a foundation model trained on more than 50 million unique single-cell RNA-seq profiles, representing around 100B tokens. It learns with a multi-task pre-training loss, allowing SOTA zero-shot abilities in denoising and label prediction. scPRINT builds on previous foundation models, like scGPT [45] and scFoundation [49]. It improves upon them on multiple benchmarks and is also easier to use and faster to train than many other similar

models. Additionally, it comes with a gymnasium of benchmarks presented in Kalfon et al. [154]. For these reasons, we chose to use it as our cFM and the starting point for our work.

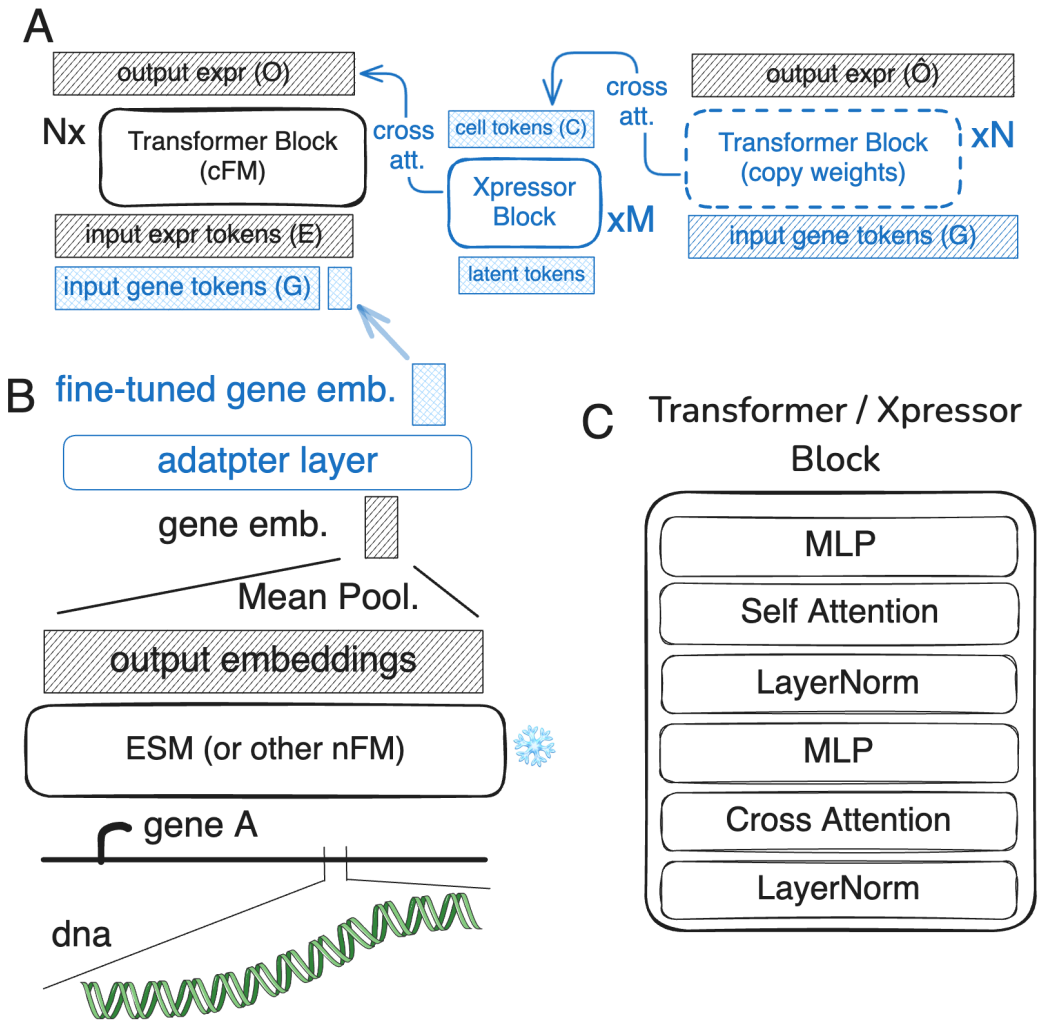

Figure 2.2 – A. The Xpressor architecture, composed of M layers, shows how gene-level representations are compressed into cell-state vectors through cross-attention over the output embeddings of a transformer, composed of N layers. These compressed representations are then decompressed back using the same initial transformer model with cross-attention given the initial gene-level tokens. B. Example of the multi-scale fine-tuning setup illustrating how the adapter layer enables joint training of gene-level representations that are then used by a cFM. C. Detailed structure of the transformer and Xpressor blocks showing the cross-attention and self-attention sub-blocks. Blue blocks are our contributions. Shaded blocks indicate inputs and outputs.

ESM2 [153] is a protein language model that learns embeddings of amino acid sequences. It has been shown to be able to learn the evolutionary constraints of proteins and to be able to predict contact maps. Models like ESMfold [195] have been created to predict a protein's

3D structure directly from its output embeddings. It is also simple to use. For these reasons, we chose to use it as our nFM.

2.3.2 Approach

Our first contribution is the compression of output embeddings of foundation models using a transformer block and a bottleneck-learning training modality (see Supplementary Material 2.4.5) : we call it the Xpressor (see Figure 2.2A). Compression / decompression is a key mechanism to transfer representations across scales (see Supplementary Material 2.2.1), we thus models that can compress and decompress their input into a lower-dimensional space. To do so, we introduce an additional set of transformer blocks called "Xpressor blocks". In the context of scPRINT, these blocks represent cell features.

As inputs scPRINT continues to use a set of summed up gene expression and gene ID tokens. The first ones are generated using an MLP on each expression values of genes in a cell j, the other ones are generated from ESM2's output embeddings of each gene sequenced aggregated with mean-pooling. The newly proposed Xpressor block uses as input a set of learned latent tokens $\boldsymbol{T}$. It then performs cross-attention between the last layer of the gene embeddings and the latent tokens (see Figure 2.2A). The goal is for the Xpressor blocks to be of smaller dimensions and context size than the main blocks, such that we end up with $\boldsymbol{C}_j$ a set of n tokens of dimension d_t generated from the encoded gene expression and ID matrices $\boldsymbol{E}_j$ and $\boldsymbol{G}$. Where $\boldsymbol{G}$ and $\boldsymbol{E}_j$ are sets of m tokens of size d_c representing the IDs of the genes and their corresponding expression in cell j, respectively, where $d_c < d_t$ and $n << m$:

$$\boldsymbol{O}_j = \text{Transformer}(\boldsymbol{E}_j, \boldsymbol{G}) \tag{2.1}$$

$$\boldsymbol{C}_j = \text{Xpressor}(\boldsymbol{O}_j, \boldsymbol{T}) \tag{2.2}$$

for a cell j, with the *Xpressor* being initialized with a learned set of input cell tokens, and $\boldsymbol{C}_j$ being the cell tokens associated with the input $\boldsymbol{E}_j$.

The *Transformer* and *Xpressor* are both transformer with N and M layers, respectively. Indeed, we have designed both blocks to contain a cross-attention architecture (see Figure 2.2C) such that we can also do : $\hat{\boldsymbol{O}}_j = \text{Transformer}(\boldsymbol{C}_j, \boldsymbol{G})$, with $\hat{\boldsymbol{O}}_j$ being the output of the *Transformer* when using the *Xpressor* representation as input. We add an optional MLP after cross-attention to a transformation of the embeddings prior to the self-attention round. In our example, the decompression is done with gene ID tokens as input only ($\boldsymbol{G}$) (see Figure 2.2A). These tokens remain the same for all cells of a given species and thus do not depend on j. In the context of protein language models, for example, this would be replaced by positional tokens.

As can be seen in Figure 2.2A, the *Transformer* blocks are applied twice. The first application act as an encoder, only using self attention, while the *Xpressor* and second application of the *Transformer* blocks act as decoders. We follow these definitions from the original "Attention is All You Need" paper [38]. It has to be noted that in our case

Table 2.1 – Comparison of cell embedding approaches

Model	Cell Label Pred.	Embed. Quality	Gene-Net Infer.
Class-pooling	0.60	0.48	**5.2,2.0**
Xpressor	**0.72**	**0.52**	4.1,2.1

cross-attention is performed first instead of last. Related ideas have also been explored in Lee et al. [185], where the authors propose a cross-attention-based method to update tokens using "latent" embeddings followed by a classical mean-pooling.

The goal of the *Xpressor* and the entire model can be seen as to perform compression of the gene tokens into a set of cell tokens similar to the classical information bottleneck from Tishby, Pereira et Bialek [196] (see Supplementary Material 2.4.5). This is our main training objective to train the *Xpressor* blocks, while the *Transformer* is also trained with masking.

In our case, each embedding represents different cell components. At training time, we present multiple losses to both regularize it and ensure differences across them, similar to what can be done in VAEs (see Supplementary Material 2.4.6).

2.3.3 Results

We show that such an instantiation of the transformer leads to better performance over the gymnasium of tasks available in the scPRINT cFM.

Indeed, we now look at three specific tasks : cell-type prediction, embedding quality, and gene-network inference. The tasks are the same as presented in Kalfon et al. [154].

"Embedding quality" refers to the average scIB [119] score for batch correction and biological consistency of cell embeddings. In this context scIB looks at the quality of the embeddings based on measures of similarity, nearest neighbors, and clustering.

Cell-label predictions are generated using a classifier on top of the cell embeddings generated by each model. We follow the approach of Kalfon et al. [154] here, which was recently presented with a different mechanism in Wang et al. [197]. This classification task allows us to see how one can steer the model's embeddings to represent meaningful biological features.

Finally, we display two different metrics for gene-network inference. The gene network inference benchmark tries to estimate the quality of the self-attention matrices based on similarity to a gene-gene ground-truth matrix. Here we use EPR, an odds-ratio measure where, e.g. a value of N means that the predictions are N-times as likely to be correct as a random guess. One is the EPR score on the genome-wide perturb-seq gene-network from

BenGRN [154], while the second is the average EPR of multiple predicted gene-networks across various cell types compared to the BenGRN's omnipath ground truth gene network [104].

In our comparison, the regular transformer's class-pooling is done similarly to scGPT's [45] approach, where a class token is added to the model's input and an additional loss is placed on it : $argmin_{C_j}(||E_j - \boldsymbol{C}_j\boldsymbol{G}_j^T||_2)$. Both models use the same latent dimensions, architectures, training paradigm, and number of input tokens for both genes and cells.

We see that the Xpressor outperforms the simpler class-pooling approach on embedding quality and cell-label prediction, while the gene-network inference results remain roughly similar.

We will now see how we can further train -or fine-tune- these representations using information from the upper scale. While Xpressor layers with their small set of low-dimensional tokens are best suited for this task, we will focus on commonly available foundation models and architectures, presenting a general approach.

2.4 Multi-scale Fine-tuning

2.4.1 Background

To merge foundation models, we need a way to connect the lower-scale models to the upper one. It had been proposed in Rosen et al. [48] et Kalfon et al. [154] to use protein language model-based representations, like those of ESM2, as input tokens for the models. This decreases the number of parameters the model has to learn ; It allows the model to work on genes unseen at training time ; Moreover, it also lets the model use information that it would not have gained otherwise, such as protein structure, homology, and mutations.

2.4.2 Approach

We propose going beyond simply reusing lower-scale models' representations and fine-tuning them during the pre-training of the upper-scale model using an adapter layer (see Figure 2.2B). With such layer, each output embedding $\boldsymbol{e}$ is transformed with a differentiable function f (here, an MLP) :

$$\boldsymbol{i}_k = f(\boldsymbol{e}_k) \tag{2.3}$$

By using an MLP, the adapter layer not only applies a transformation of its input but also adds information (see Supplementary Material 2.4.4). In our case, we use ESM2 as the lower-scale model and scPRINT as the upper-scale model. The initial ESM2 embedding is known to contain a representation of the protein's sequence, evolutionary similarity, and constraints.

Table 2.2 – Comparison of input-gene embedding approaches

Model	Cell Label Pred.	Embed. Quality	Gene-Net Infer.
Random init.	0.62	0.48	4.5,1.0
ESM2 frozen	0.60	0.48	5.2,2.0
ESM2 fine-tuned	**0.70**	**0.49**	**4.8,2.4**

Indeed, this is what allows this representation to replace the MSA step in ESMfold [195]. We posit that this initial embedding already contains the information necessary to understand some of the rules in gene interactions (homology and similar evolutionary constraints). However, representations from ESM2 are very different from those from single-cell foundation models. Our goal is to enrich these representations with knowledge gained from co-expression information across millions of cells.

2.4.3 Results

We show that a cFM trained using the pooled embeddings of a pretrained nFM performs better in most tasks from the Kalfon et al. [154] gymnasium benchmark than one with learned representations (see Table 2.2). This is possible because we allow the model to start from a very rich representation instead of a random set of vectors, while still giving it the flexibility to incorporate additional knowledge. Each foundation model tested uses the same latent dimensions, architectures, training, and number of input tokens. We report the performance at the best epoch, and the training is stopped after 20 epochs.

We also show the difference in cell embeddings obtained between the regular transformer and the Xpressor (see Figure 2.3). The dataset is a very challenging mix of modalities with various batch effects and amounts of noise. Cell types are also quite similar, making the task more difficult. We can see that the Xpressor embeddings contain more structure and resolve different cell types better than a transformer with class-pooling.

Using ESM2's embeddings allows scPRINT to work on genes and sequences unseen at training time, to learn from an unlimited number of species, and to integrate DNA, RNA, and protein-level information such as mutations and structural variants.

Finally, contrary to other methods, this version does not require an update to the original model and can be added to the new model. Moreover, with this approach, scPRINT still maintains its ability to work on genes and sequences unseen at training time.

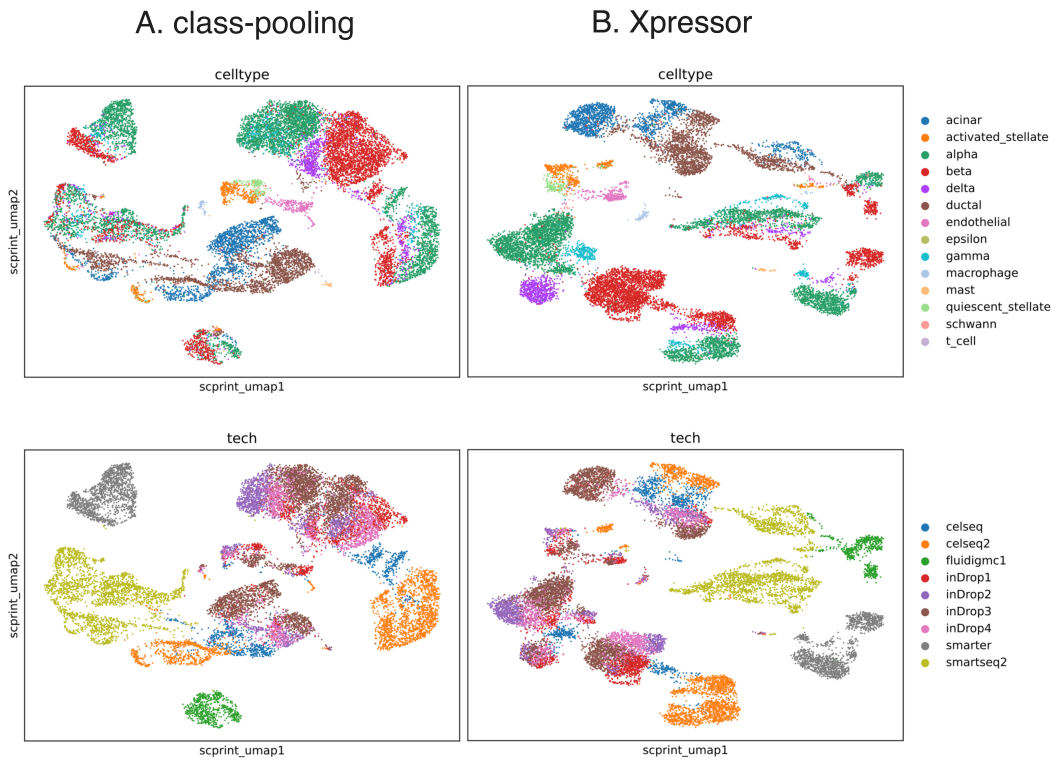

FIGURE 2.3 – between the regular transformer with class-pooling (left), scIB : 0.43, and the Xpressor (right), scIB : 0.48. The Xpressor embeddings contain more structure and resolve different cell types better.

Conclusion

We have proposed a framework towards building compositional hierarchical foundation models for life, from atoms to tissues. We highlighted progress and challenges remaining for each specific scale of biological representations. While data generation efforts focusing on breadth and quality remain paramount to progress, we believe that the composition of foundation models could drive progress forward. Having a vocabulary for biological entities will allow us to better reference them, helping us define the impact of a molecule on a tissue or the interaction between RNA and proteins. Such a model of life should not be seen as one being trained end-to-end but as a set of models distilling the key information that they have learned and that the next one requires.

We have presented one small piece in this approach, where a cell foundation model (scPRINT) uses and fine-tunes a protein sequence foundation model (ESM2). We have also shown how XPressor can compress the output representations of transformers into a small set of lower-dimensional vectors, bridging proteins to cells. Such an approach could be used to bridge molecules to proteins and cells to tissues by using compressed representations that are then fine-tuned. This is a promising back-bone architecture for a general model going from atoms to tissues.

Future work should focus on using Xpressor's representations to power upper scale models or the ability to learn a Xpressor on top of a pre-trained foundation model. The Xpressor approach could also be extended to decoder-based language models. Finally, fine-tuning using and adaptor layer suffers from a main drawback, the non-additivity of MLPs and therefore the limited use of such fine-tuned models in other contexts than for their compressed representations. Implementing intelligent GPU scheduling and using LoRA-type methods to fine-tune only XPressor blocks will allow for more complex fine-tuning in GPU-rich settings. We will need to show that this can be applied to the other scales of biological representations and generate benchmarks that better capture the diversity of real-world biological tasks across these scales.

Supplementary

2.4.4 proof that fine-tuning ESM2 with an adapter layer is at least sufficient to learn to add co-expression information

We show below that an MLP (with at least one hidden layer and a sufficiently large number of neurons) can learn to map each of D input protein embeddings to an arbitrary desired output, even if that output corresponds to a unique lookup for each protein.

1. **Finite Data Interpolation :** Let the set of D protein embeddings be $\mathcal{E} = \{\mathrm{e}_1, \mathrm{e}_2, \ldots, \mathrm{e}_D\} \subset \mathbb{R}^D$, and suppose that for each e_k we want the MLP to output $\mathrm{w}_k \in \mathbb{R}^D$. Because the set $\mathcal{E}$ is finite, it is possible to design a function that exactly maps $\mathrm{e}_k \mapsto \mathrm{w}_k$ for all $k = 1, \ldots, D$.

2. **Constructive Argument Using ReLU Networks :** For a ReLU-based MLP, one can construct "bump" functions that are activated only in a small neighborhood around each e_k. For instance, one may define functions of the form $\mathrm{r}_k(\mathrm{x}) = \sigma(-\|\mathrm{x} - \mathrm{e}_k\| + \delta)$, where $\delta > 0$ is chosen so that $\mathrm{r}_k(\mathrm{e}_k) > 0$ and $\mathrm{r}_k(\mathrm{x})$ is nearly zero for x that are not close to e_k. By associating one or more hidden neurons to each protein embedding e_k, one can form a linear combination $\mathrm{MLP}(\mathrm{x}) = \sum_{k=1}^{D} c_k \, \mathrm{r}_k(\mathrm{x})$, where the coefficients $c_k \in \mathbb{R}^D$ are chosen so that $\mathrm{MLP}(\mathrm{e}_k) = \mathrm{w}_k$ for all k. Because the supports of the functions $\mathrm{r}_k(\mathrm{x})$ can be made nearly disjoint, the MLP can "memorize" the mapping by acting as a lookup table.

3. **Conclusion :** Thus there exists a configuration of weights (and biases) in an MLP that yields $\mathrm{MLP}(\mathrm{e}_k) = \mathrm{w}_k, \quad$ for $k = 1, \ldots, D$. Hence, even though the MLP is simply performing a transformation, its capacity is sufficient to learn any arbitrary mapping for the D proteins. In other words, at worst, it can learn a mapping that is equivalent to a lookup table, thereby ensuring that each of the D proteins is assigned a specific, learned output value.

2.4.5 argument about the Tishby et al. bottleneck learning approach

The IB method seeks a stochastic mapping $p(t|x)$ that compresses the input variable X into a representation T, while preserving as much information as possible about the relevant

variable Y. The trade-off is controlled by the Lagrange multiplier $\beta \geq 0$. The IB objective is to minimize the following Lagrangian :

$$\mathcal{L}_{\text{IB}}[p(t|x)] = I(X;T) - \beta\, I(T;Y), \tag{2.4}$$

where $I(\cdot;\cdot)$ denotes mutual information.

Under the Markov constraint $\mathrm{Y} \leftrightarrow \mathrm{X} \leftrightarrow \mathrm{T}$, the optimization leads to the following self-consistent equations :

$$p(t|x) = \frac{p(t)}{Z(x,\beta)} \exp\left(-\beta\, D_{\text{KL}}\big(p(y|x) \,\|\, p(y|t)\big)\right), \tag{2.5}$$

$$p(t) = \sum_x p(x)\, p(t|x), \tag{2.6}$$

$$p(y|t) = \frac{1}{p(t)} \sum_x p(y|x)\, p(x)\, p(t|x), \tag{2.7}$$

where :

- $D_{\text{KL}}\big(p(y|x) \,\|\, p(y|t)\big)$ is the Kullback-Leibler divergence between the conditional distributions $p(y|x)$ and $p(y|t)$,
- $Z(x,\beta)$ is the normalization factor ensuring that $\sum_t p(t|x) = 1$.

2.4.6 FSQ and other contrastive losses on the cell embeddings

While D_{KL} over a non-informative Gaussian prior is a common formulation for regularizing the embedding space in VAEs, other formulations have been used such as with the VQ-VAE and Finite Scalar Quantization Variational Autoencoder (FSQ-VAE). In these contexts, the D_{KL} is replaced with a discretization objective tailored to the respective quantization schemes.

VQ-VAE. Value Quantized (VQ)-VAE employ a *codebook* of size C, where each codebook entry is a d-dimensional vector. The encoder produces a continuous latent vector, which is then mapped to its nearest entry in the codebook (a hard quantization). A commitment loss term encourages the encoder's outputs to stay close to the chosen codebook vector, making the entire latent representation discrete at the vector level.

FSQ-VAE. By contrast, Finite Scalar Quantization (FSQ)-VAE discretizes each latent dimension *independently*. Specifically, the encoder outputs d values, each constrained to lie within a bounded range (e.g., $[-1, 1]$). Each dimension is then quantized into one of M discrete levels within that range. This dimension-wise quantization can be implemented as either a hard nearest-bin assignment or a differentiable approximation thereof. Because FSQ enforces scalar-level discretization, it provides a simpler and more fine-grained alternative to VQ's vector-level codebook approach, while still offering strong regularization of the latent space.

Contrastive regularization across embedding dimensions. We further encourage each of the d embedding dimensions to encode distinct information by adding a contrastive loss between them. Specifically, we compute pairwise similarities among embedding elements and penalize redundancy, thus pushing each dimension to capture complementary features. A general contrastive loss for this purpose can be written as

$$\mathcal{L}_{\text{contrastive}} = \sum_{i=1}^{d} \sum_{j \neq i} \ell\big(\mathrm{e}_i, \mathrm{e}_j\big), \tag{2.8}$$

where e_i denotes the i-th embedding dimension and ℓ is a contrastive loss function (e.g., InfoNCE [198]) that encourages *dissimilarity* among different embedding components.

Dimension-specific classifiers. To further steer each dimension's content, one can add a separate classifier on top of each dimension to learn about different classes. The classifier for dimension i is trained via a cross-entropy loss

$$\mathcal{L}_{\text{cls}}^{(i)} = -\sum_{c} y_c \log p\big(c \mid \mathrm{e}_i\big), \tag{2.9}$$

where y_c is the ground-truth label and $p\big(c \mid \mathrm{e}_i\big)$ is the predicted probability for class c. Summing these per-dimension losses yields an overall classification objective

$$\mathcal{L}_{\text{cls}} = \sum_{i=1}^{d} \mathcal{L}_{\text{cls}}^{(i)}. \tag{2.10}$$

Together, the contrastive and classification losses ensure each embedding dimension captures unique, discriminative information, resulting in more expressive representations.

Software and Data

The software and data for training scPRINT as well as gymnasium tasks and code to reproduce the results of the manuscript are available at https://github.com/cantinilab/XPressor.

WandB logs, are available in the following link : https://api.wandb.ai/links/ml4ig/h370j6io

Model checkpoints are available in the following link : https://huggingface.co/jkobject/scPRINT/tree/main

Acknowledgments

The project leading to this manuscript has received funding from the Inception program (Investissement d'Avenir grant ANR-16-CONV-0005) L.C. and the European Union (ERC

StG, MULTIview-CELL, 101115618) L.C. We acknowledge the help of the HPC Core Facility of the Institut Pasteur and Déborah Philipps for the administrative support. L.C.

The work of G. Peyré was supported by the French government under management of Agence Nationale de la Recherche as part of the 'Investissements d'avenir' program, reference ANR19-P3IA-0001 (PRAIRIE 3IA Institute). G.P.

Impact Statement

This paper presents work whose goal is to advance the fields of computational biology and machine learning. No ethical issues are raised by the work other than what is typically noted in computational biology and foundation model papers. It might have an impact on building better models for drug discovery, target discovery, and improving our understanding of biological systems. xurl seqsplit

scPRINT-2 : Towards the next-generation of cell foundation models and benchmarks

3.1 Summary

Cell biology has been booming with foundation models trained on large single-cell RNA-seq databases, but benchmarks and capabilities remain unclear. We propose an additive benchmark across a gymnasium of tasks to discover which features improve performance. From these findings, we present scPRINT-2, a single-cell Foundation Model pre-trained across 350 million cells and 16 organisms. Our contributions in pre-training tasks, tokenization, and losses made scPRINT-2 state-of-the-art in expression denoising, cell embedding, and cell type prediction. Furthermore, with our cell-level architecture, scPRINT-2 becomes generative, as demonstrated by our expression imputation and counterfactual reasoning results. Finally, thanks to our pre-training database, we uncover generalization to unseen modalities and organisms. These studies, together with improved abilities in gene embeddings and gene network inference, place scPRINT-2 as a next-generation cell foundation model.

3.2 Introduction

For the last few years, Single-Cell Foundation Models (scFMs), also known as Virtual Cell models, have provided early approaches to modeling the cell using single-cell RNA-seq data as their primary modality[1–4]. The field has been booming with these transformer-based machine learning models trained on large databases of tens of millions of cells. The models themselves contain tens to hundreds of millions of parameters and are trained on unsupervised (or semi-supervised) tasks such as predicting masked gene expression or denoising expression. They can then be used as is to examine their learned representations or fine-

tuned to transfer their knowledge across a range of everyday tasks in that modality. Many examples have now been proposed, such as predicting single-cell perturbation responses, patient drug responses, and disease states ; annotating cells ; correcting for batch effects ; improving noise levels ; imputing unseen gene expression or modality ; generating gene networks ; identifying cell niches ; and more[5,6,6–15].

While many AI Virtual Cell models and scFMs exist, little has been done regarding their comparison[16–20]. A crucial question remains : how to validate the impact of the different proposed methods, regardless of implementation, datasets, or model size. Indeed, reproducing results has been challenging for many, and the literature has yielded discordant conclusions about the performance and capabilities of these models. Showing they often underperform simpler approaches on classification, batch correction, and perturbation prediction[16,17,21–23]. Much work remains to get to feature-rich, easy-to-use scFMs. Models that allow inference in minutes, along with well-crafted reproducible benchmarks that demonstrate how scFMs uniquely solve essential problems in single-cell biology. Open-sourcing not just model weights but their pre-training tasks and datasets.

On this front, scPRINT was released as part of a second batch of scFM, presenting contributions in terms of usability and reproducibility while also showcasing pre-training strategies, data encoding, and decoding[3]. scPRINT was trained on 50 million cells using a multitask pre-training strategy that included expression denoising, autoencoding, and cell-label prediction. It also presented an in-depth benchmark that examined the foundation model's zero-shot performance on these tasks, as well as its internal gene network representation and fidelity compared to multiple ground truths.

Building on these strengths and moving towards the next generation of scFMs, we here use scPRINT (which will be referred to as scPRINT-1) as the reference to showcase an extensive additive benchmark of scFM attributes. We address several key questions about the importance of diverse architectures, datasets, and training modalities. This additive benchmark aims to understand the relative importance of these different features in our task gymnasium, examining the choice of model architecture and pre-training tasks across 42 different scenarios. In these scenarios, we propose a breadth of novel components for scFMs. In addition to those 12 distinct contributions, we also examine various pre-training datasets, compiling a 350-million-cell database—the largest to date—with over 16 organisms.

As a result of the benchmark, we derive a next-generation scFM, extbfscPRINT-2. scPRINT-2 improves upon the previous generation of models by leveraging our database, the scPRINT-2 corpus, and multiple data augmentation approaches. It uses a set of updated pre-training tasks and losses, improving its accuracy in challenging and unseen contexts. Finally, it is equipped with graph-based encoders and the XPressor architecture, enabling unprecedented expression imputation, high-quality zero-shot embeddings, and counterfactual reasoning. We dive into these specific contributions by examining multiple use cases, highlighting behaviors that are often overlooked or under-assessed in classical benchmarks.

scPRINT-2, its dataloader, pre-training datasets, preprocessing, task functions, pre-trained weights, as well as the additive benchmark training traces and all 42 models' weights are fully open-sourced and available under the GPL-v3 License.

3.3 Results

3.3.1 Decoding the impact of a foundation model's architecture through an additive benchmark

Many scFMs have been developed in single-cell genomics. They have mostly been studied in isolation, using their own benchmarks. While most of them maintained relatively similar architectures, the impact of each design's decisions was never thoroughly assessed. For example, scPRINT-1 uses a denoising reconstruction task similar to scFoundation. Still, scFoundation uses the mean-squared-error (**MSE**) for the reconstruction loss, whereas scPRINT-1 uses the zero-inflated negative-binomial loss (**ZINB**) (see Methods). scGPT and Geneformer utilize masking, but scGPT bins expression counts (**binning**), while scPRINT-1 does denoising and employs a continuous embedding with a log transform and a pseudocount of 1 (**logp1**)[1,2]. Other models, like cellPLM, instead use a contrastive learning approach, which encourages embeddings of perturbed and unperturbed cell profiles to be more similar to each other than those of different cell profiles[4]. This method is also known as InfoNCE or Contrastive Cell Embedding (**CCE**) (see Methods)[24].

Additive benchmark

To address the lack of a consistent assessment of these models, we have designed a benchmark to comprehensively evaluate the various components of scFMs, including pre-training databases, architectures, and training tasks. This benchmark is based on a gymnasium of tasks similar to those presented in Kalfon et al.[3] (see Figure 3.1 ; see Table 3.2). The scFM gymnasium assesses each model's ability to predict labels, remove batch effects, denoise, and impute gene expression, as well as discover known gene-gene relationships at different stages of training. For embeddings and cell type classification, we use the scIB and accuracy scores over the same ground-truth test datasets as in Kalfon et al. (see Methods). For denoising, we evaluate the model's ability to recover the noised expression profile of cells from a test dataset, as measured by the improvement in correlation with the ground-truth profile after denoising. For gene-network inference, we examine the Odds Ratio (OR) and AUPRC scores of the model's ability to recover a ground-truth gene network from expression data alone (see Methods).

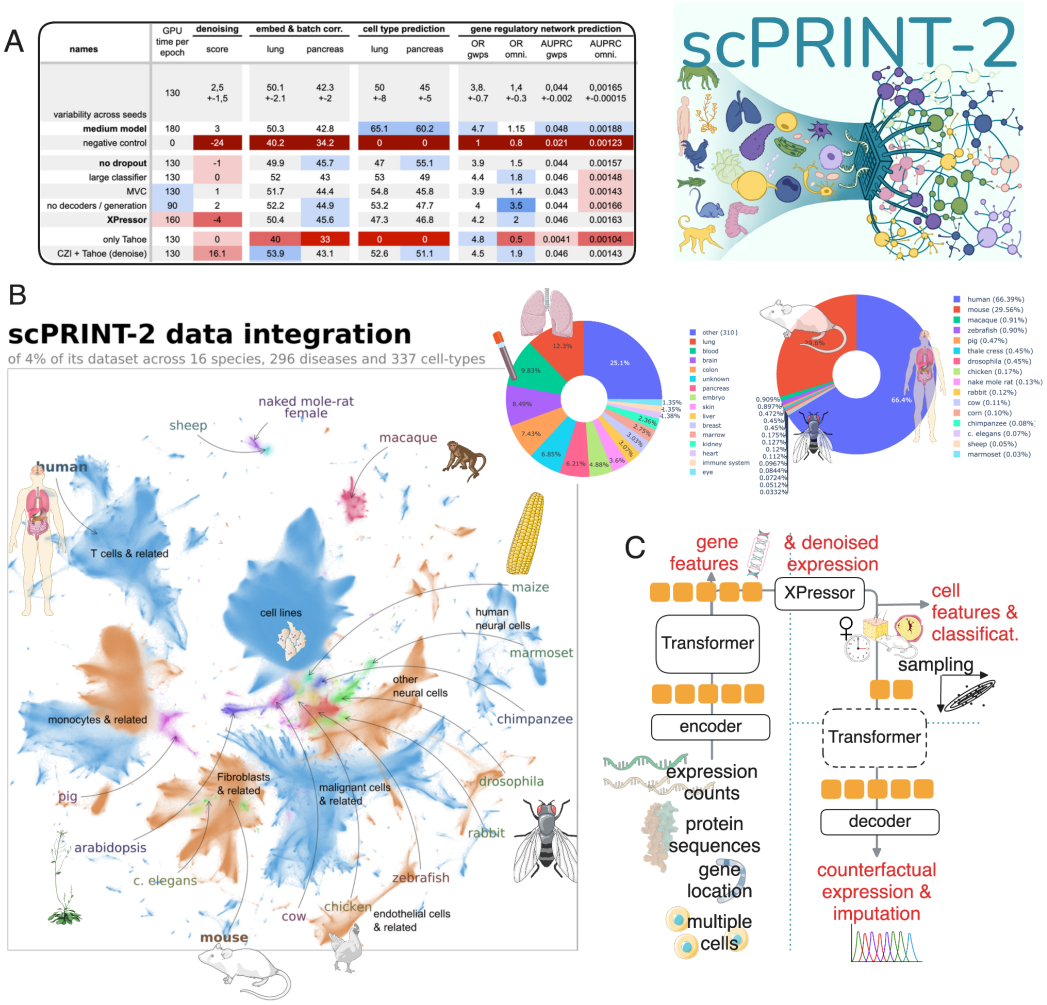

names	GPU time per epoch	denoising score	embed & batch corr. lung	embed & batch corr. pancreas	cell type prediction lung	cell type prediction pancreas	gene regulatory network prediction OR gwps	gene regulatory network prediction OR omni.	gene regulatory network prediction AUPRC gwps	gene regulatory network prediction AUPRC omni.
variability across seeds	130	2,5 +-1,5	50.1 +-2.1	42.3 +-2	50 +-8	45 +-5	3,8 +-0.7	1,4 +-0.3	0,044 +-0.002	0,00165 +-0.00015
medium model	180	3	50.3	42.8	65.1	60.2	4.7	1.15	0.048	0.00188
negative control	0	-24	40.2	34.2	0	0	1	0.8	0.021	0.00123
no dropout	130	-1	49.9	45.7	47	55.1	3.9	1.5	0.044	0.00157
large classifier	130	0	52	43	53	49	4.4	1.8	0.046	0.00148
MVC	130	1	51.7	44.4	54.8	45.8	3.9	1.4	0.043	0.00143
no decoders / generation	90	2	52.2	44.9	53.2	47.7	4	3.5	0.044	0.00166
XPressor	160	-4	50.4	45.6	47.3	46.8	4.2	2	0.046	0.00163
only Tahoe	130	0	40	33	0	0	4.8	0.5	0.0041	0.00104
CZI + Tahoe (denoise)	130	16.1	53.9	43.1	52.6	51.1	4.5	1.9	0.046	0.00143

Figure 3.1 – (a) The additive benchmark example table with its gymnasium scores across the scFM's features. (b) Our scPRINT-2 corpus pre-training dataset, with 16 organisms across 300+ tissues. UMAP of 15 million cells from the corpus integrated using scPRINT-2. Colors represent species. (c) The scPRINT-2 model, its input data, and its different outputs. Source data are provided as a Source Data file.

The base model, on which the additive benchmark is performed (see Figure 3.1, Table 3.2, and Methods), is trained on the CxG database, comprising 500 carefully annotated human and mouse datasets. Its training lasts for a maximum of 20 epochs, each of 20,000 steps, with a minibatch size of 64. We encode the gene expression using the scPRINT-1 approach and decode it with the MSE method. The base model's pre-training task uses a 30% gene expression mask. We pre-train the models 6 times across multiple seeds to generate error bounds. Using Flash-Attention-3, the 20M parameters model trains on 1 H100 GPU for 2 days.

While we will not delve into the details of each feature assessed (see Methods), our benchmark broadly highlights several key points.

Regarding the tasks, we have confirmed what Kalfon et al. and De Waele et al. previously

showed : that denoising is superior to masking as a pre-training task for single-cell data in classification and embedding tasks[3,25]. Similarly, un-normalized expression is better than normalizing it at the input. Classification also serves as a good supplement to the pre-training task, as without it, we observe a slight decrease in performance (see Table 1).

We also present, as part of our study, the **scPRINT-2 corpus**, which comprises more than 350 million single cells (see Figure 3.1). This is the largest dataset ever assembled, consisting of data from the Chan Zuckerberg Institute's Cellxgene (**CxG**), the **Tahoe**-100M dataset, and the scBasecount database, which contains 20,000 reprocessed datasets from the Gene Expression Omnibus[26–28]. The cells themselves are derived from 16 different eukaryotic organisms, spanning more than 1 billion years of evolution. The dataset comprises approximately 400,000 distinct genes, 4,764 different labels, and around 140,000 cell groups, totaling 25 TB of unique data[29]. Our database contains nine main classes : *cell type, disease, age, tissue of origin, assay, ethnicity, sex, cell culture,* and *organism.*

Thanks to this database, we demonstrated the growing importance of data selection in pre-training scFMs. Indeed, when using the Tahoe-100M database solely for pre-training, the model's overall performance plummets, as the sequencing depth and diversity are low despite the large number of cells.

However, including this lower-diversity dataset with the high-diversity CxG database and carefully considering the cell-state imbalances results in only a noticeable decrease in denoising performance. Interestingly, using all available datasets did not change performance across our benchmarks. Reducing the training database to a random subset of only **200 human datasets only,** led to a minimal decrease in denoising and cell type prediction. This shows again that the benchmark fails to highlight abilities on more diverse cell types and organisms[30,31]. But it also indicates diminishing returns in adding more datasets—diversity in cell states and organisms being much more important than cell count.

We thus preprocessed each dataset by removing all duplicates, filtering for low-quality cells, aligning metadata to the CxG ontologies, and computing cell-cell similarity profiles and clusters. It allowed us to introduce multiple data augmentation techniques, such as varying the input context length (**var. context**) during training and randomly creating **meta-cells**, which are averages of similar cell expression profiles across K-nearest neighbors (K-NN) (see Results section 3). Interestingly, we observe that both methods tend to improve the model's performance in most metrics, even though these models do not examine more cells overall. This highlights the importance of effective data augmentation techniques for scFM pre-training[32].

	names	GPU time per epoch	denoising score	embed & batch corr. lung	embed & batch corr. pancreas	cell type prediction lung	cell type prediction pancreas	gene regulatory network prediction OR gwps	OR omni.	AUPRC gwps	AUPRC omni.	run id
Base	ross seeds (masking; ZINB loss; ? + continous expr. emb.; classif. + generative task)	130	2,5 +- 1,5	50.1 +-2.1	42.3 +-2	50 +- 8	45 +- 5	3,8. +-0.7	1,4 +- 0.3	0,044 +-0.002	0.00165 +-0.00015	blooming-dew-714, driven-valley-750, summer-deluge-783, silent-poltergeist-843, unraveling-pumpkin-841
	medium model	180				65.1	60.2	4.7		0.048	0.00188	solar-durian-637
	negative control		-24	40.2	34.2	0	0	1	0.8	0.021	0.00123	
architecture	**no dropout**		-1		45.7		55.1					expert-feather-748
	large classifier		0						1.8		0.00148	chocolate-snowball-718
	MVC	130							1.4		0.00143	celestial-sun-749
	no decoders / generation	90			44.9				3.5			northern-voice-777
	XPressor	160	-4		45.6				2			crimson-wildflower-791
data	CxG (CellxGene's Census)			52.3					2			faithful-dragon-663
	CxG + Tahoe (denoising)		16.1	53.9			51.1		1.9			lurking-cat-846
	only Tahoe		0	40	33	0	0	4.8	0.5	0.0041	0.00104	young-bush-669
	all databases (denoise)	140			39							macabre-apparition-844
	200 human datasets only		0			40.3			1.8			playful-frost-804
	sampling without replacement		0		45	36	34		2.4			autumn-aardvark-702
	cluster-based sampling only			43.3								rosy-firefly-805
attention	softpick								1.8			eldritch-fang-834
	criss-cross (larger context)	80	5.6						x	x	x	uncanny-raven-835
	hyper (denoise, larger context)								0.6	0.04	0.00115	silver-grass-803
loss	contrastive learning (masking + denoising)					39.5					0.00149	northern-frog-797
	elastic cell similarity			52.7			34.9					hopeful-monkey-796
	no embedding ind loss								2.3			devoted-wave-795
	ZINB+MSE (denoising)		25.5		48					0.04		firm-silence-747
	MSE		-4	54	46	62						generous-dawn-666
	VAE compressor	140				38	27					wild-terrain-694
pretraining task	**var. context (larger context)**	170	29.1	53	46		52.2			0.038	0.00146	apricot-snowflake-756
	TF masking								2.3			winter-meadow-772
	denoising		21	52.6	45.1		54.5					efficient-firebrand-753
	no classification				40	0	0				0.00129	copper-frost-625
	adv. classifier (+larger classif)										0.0014	sunny-morning-629
input	sum normalization (denoise)		12.8	45.6	46.5	21.4	22.9	2.4	1	0.029	0.00136	snowy-galaxy-744
	no random level of denoising		19	54.1	45.3				2	0.041		divine-monkey-798
	GNN	150	44	48		38	35				0.00128	balmy-totem-727
	meta-cell			52.8	47.7		51.3			0.04		unique-dawn-806
	binning		0		45.5		52			0.047		twilight-breeze-874
	using only expressed genes											sage-snow-873
	without gene location		3.4	36.2	35	4	5.9	4.8		0.048		youthful-snowflake-792
	learn gene emb (denoising)				45.1					0.041		jumping-night-755
	fine-tuned ESM3										0.00181	not-snowflake-755
Main	small model (V2)	1820	44	53	49					0.041		honest-vortex-815
	medium model (V2)	5600	x	x	x	x	x	x	x	x	x	x
	medium model (V1)	520		52.6	45.6	61.8	57.6		2.2	0.041		bewitched-poltergeist-857
	small model (V1)	160	31.7	52.4	50						0.00138	dry-smoke-852

Figure 3.2 – Table representing the results of the additive benchmark on 42 models, over multiple metrics : batch correction and cell embedding quality, denoising quality, cell type prediction, and gene network inference. Additional information on the different components is available in the methods section. Bold elements are the features that are part of the scPRINT-2 foundation model.

Regarding architecture, we recomputed results from the XPressor manuscript[33], which showed that this architecture improves the embedding quality of scFMs (see Results section 4; see the full table in Supplementary Table 6.3.1). We also demonstrate that using ESM-based gene ID tokens leads to much better performance than learning gene tokens from scratch[34]. Providing each gene's genomic location as additional input information significantly improves model convergence. However, we also noticed that when they do converge, models without gene location information can perform well. We have noticed that model size correlates with higher scores, at least for gene network inference and cell-type prediction. Using a Graph Neural Network (**GNN**) encoder shows significant improvements, with only a slight decrease in the cell-type prediction task (see Results Section 3; see Methods). Additionally, our sub-quadratic attention mechanism, Criss-cross attention, also shows substantial benefits with no reduction in performance (see Results section 4; see Methods).

Moreover, MSE, on average, outperforms ZINB as a loss function while decreasing the model's expressivity (see Methods). A good proposed middle ground is the ZINB+MSE loss (see Results Section 3 ; see Methods).

Some unexpected results showed that omitting the decoder part of scPRINT-1 led to stronger performance ; however, this comes at the cost of generative abilities and decreased cell-embedding fidelity. Indeed, despite its importance for understanding scFMs' behavior and feature importance, we have noted that our benchmark does not yet capture the full breadth of abilities that scFMs do or should have. For example, both scIB and classification scores are very dependent on the dataset' s quality and its labels. Scores presented here show only a facet of the model's ability. We might be interested in the model's performance up-to-convergence instead of stopping them at 20 epochs or looking at unseen species, or assays at training. This is a first attempt to benchmark scFMs, but more extensive efforts will be needed.

scPRINT-2

Overall, we have examined the performance improvements driven by our 12 distinct contributions across 42 training runs. Based on these results and our own considerations, we have elected a set of features to create scPRINT-2, a next-generation cell foundation model (see Supplementary Figure 6.4.1 ; see Methods). We highlight its architecture in Figure 3.1 ; scPRINT-2 is currently available in a small version with only 20M active parameters. Its encoder-compressor-decoder architecture produces cell- and gene-level outputs at multiple levels, working on one or more cells at a time.

Furthermore, to aid in the exploration of this largest-ever cross-organism single-cell dataset, we release all of the 350 million cells in the scPRINT-2 corpus, aligned into an atlas by scPRINT-2, of which 1% are directly accessible through an interactive visualization (see Figure 3.1, see Data availability) along with scPRINT-2 cell label predictions for all classes. This should enable never-before analysis and exploration of single-cell RNA-seq data.

But the additive benchmark leaves some questions unanswered about the effect of combining these features up-to-convergence and the models' abilities on unseen modalities, tasks, and species. In the following sections, we will focus on 1. looking at more diverse and truthful datasets in size, quality, and source domains ; 2. using more scores and ground truth validations ; 3. defining tasks that better reflect the possibilities and real-life use of these models.

3.3.2 A diverse dataset of 350 million cells pushes generalization to unseen organisms

One of the most critical features of foundation models (FMs) is the breadth of their training dataset. From vision to language, AI advancement has been driven by training models on ever-larger datasets[35–39]. Nowadays, most scFMs are trained on 20 to 50 million cells, except the recently released Geneformer-v2 and STATE-SE models, which have been

trained on roughly 300 million cells[40,41].

scPRINT-2 pre-training corpus

In conjunction with our model's architecture, the scPRINT-2 corpus and its 16 organisms enable generalization to organisms unseen during training. This broader cell type diversity, however, comes with additional challenges : annotation quality has decreased due to missing annotations in scBasecount. Additionally, the skew toward low sequencing depth and highly similar cells has increased with the inclusion of spatial transcriptomics datasets and less curated databases such as Tahoe-100M and Arc's scBasecount (see Methods).

Fortunately, a key feature of our dataloader, scDataLoader[3], is its ability to perform weighted random sampling, thereby mitigating the heavy dataset imbalances that currently exist across diverse cell types, sequencing methodologies, and different organisms assessed. We thus present methods to successfully train scPRINT-2 on this large dataset. The first, called cluster-weighted sampling, allows datasets with unclear annotations to benefit from weighted random sampling by defining clusters of high expression similarity (see Methods). This lets us define cell states without requiring any label information and perform sampling that is aware of the different cell states, regardless of the size of each cluster. We address the second issue of uneven cell quality by also skewing sampling toward cells with more non-zero genes (nnz). Both methods were enabled on such a vast database thanks to essential updates to scDataLoader. This re-weighting is performed jointly with weights on cell type, disease, organism, and sequencer labels, thereby addressing the size/diversity issues that plague these larger cell databases[42].

Interestingly, the number of training steps required to achieve convergence increased only 2-fold, indicating that, as in scPRINT-1, the model did not sample as many cells as actually exist in the pre-training dataset before reaching convergence. However, with data augmentation and nearest-neighbor sampling, the model still encountered roughly 2 billion distinct input cell profiles during pre-training, corresponding to 2000 cell profiles per step.

After implementing this feature and training scPRINT-2, its cell-type classification performance on the validation dataset was 76%. For its other predicted labels, its performance was 59% (disease), 96% (ethnicity), 96% (assay), 94% (age), 100% (cell culture), 100% (organism), 93% (sex), and 70% (tissue of origin).

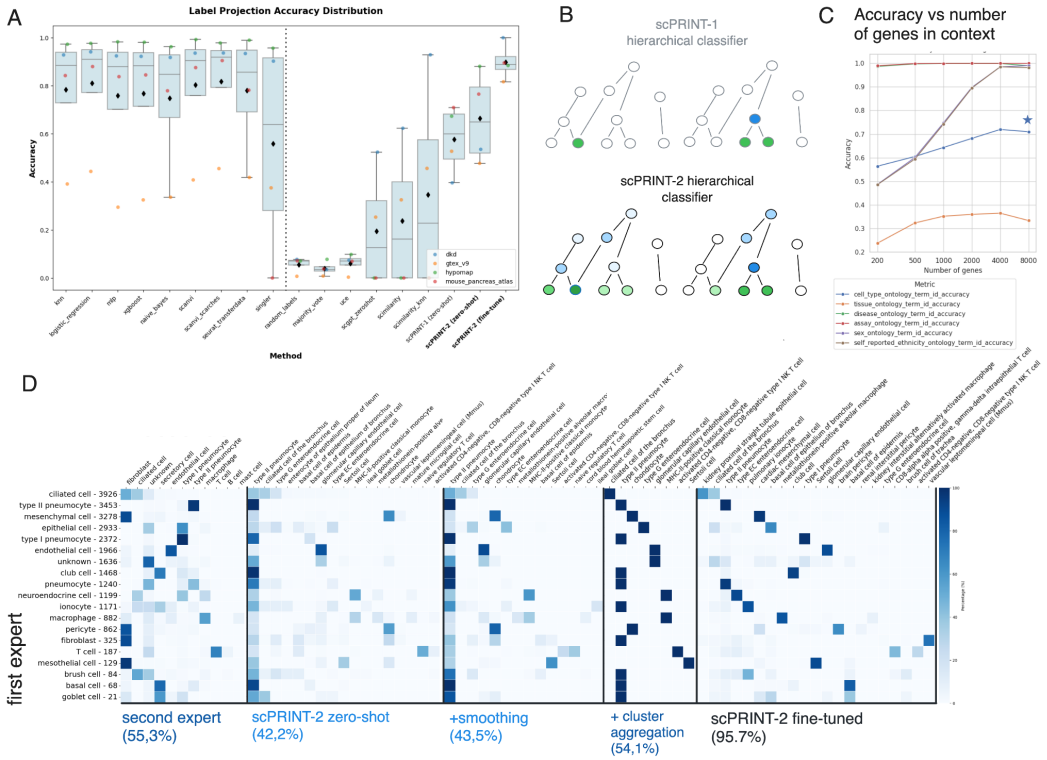

FIGURE 3.3 – (a) Open Problems benchmark results and comparison of scPRINT-1 and zero-shot and fine-tuned scPRINT-2. (b) Illustration of our updated hierarchical classifier loss. (c) Unseen organisms cell type classification for cat and tiger datasets, across two experts and scPRINT-2 zero-shot, after label smoothing, after cluster aggregation, and after fine-tuning. (d) Change in classification accuracy as the number of genes in context increases for high-quality single-cell datasets. The star represents the model's score when label smoothing is used.

On the live benchmark Open Problem from November 2025, it achieved an average zero-shot performance of 75%, putting it above scPRINT-1 (47%) and other zero-shot FMs (40-60%), even above Liger, a supervised technique[43] (see Figure 3.3; see Methods). But scPRINT-2 was the only scFM with UCE that could run on all datasets[44]. Against the two human datasets on which Scimilarity-KNN could be run, it performed slightly better than scPRINT-2. This is most likely due to the smaller capacity of scPRINT-2 (20M parameters) compared to scimilarity (100M parameters), as we also observed in our additive benchmark (see Table 3.2). Another likely reason is that the model likely saw those datasets more often during pre-training, since it is trained only on CxG's human datasets.

We then performed fine-tuning using our XPressor-based Parameter-Efficient Fine-tuning (XPEFT), in which we fine-tune only the XPressor layers of scPRINT-2 (see Methods). In this context, we show that scPRINT-2 fine-tuned outperforms every existing supervised and unsupervised method on the Open-problem (see Part 4; see Methods)[45]. We observed similar trends in the macro-F1 scores (see Supplementary Figure 6.4.2). Of note, neither scGPT nor Geneformer are currently tested in their fine-tuned version on the platform.

These performances are enabled in part by our update to scPRINT-1's hierarchical classification loss (see Figure 3.3). The scPRINT-1 classifier generates predictions for all possible labels in a hierarchical ontology, while producing logits only for the leaf labels. To predict the other labels, it only has to aggregate their leaf logits. In scPRINT-2, we improve on this loss by using the entire ontological graph, meaning that, e.g., given a ground truth of *olfactory neuron,* we will penalize a prediction of *inhibitory neuron* less overall than a non-neuron label, like *fibroblast*. In conjunction with our weighted sampler, this allows the model to learn rich gradients from a low volume of data.

scPRINT-2 generalizes to unseen classification tasks

We have, however, noticed that classification performance does not generalize sufficiently to correctly recover the exact phylogenetic relationships within organisms or, similarly, within ethnicities (see Supplementary Figures 6.4.3, 6.4.4, 6.4.5). This could be biased heavily by tissue representation in rare ethnicities and organisms. However, some relationships were found, such as *Singaporean Indian/Singaporean Chinese, Korean/Japanese/Chinese, American/Latin American,* or *Macaque/Marmoset/Chimpanzee, Drosophila/C. elegans, Human/Mouse, Pig/Cow*, suggesting that with greater diversity and representation, scFMs might learn this relationship classification of gene expression on their own.

We show that this does not prevent scPRINT-2 from generalizing to unseen organisms. Using a randomly selected tomato plant dataset and its corresponding ESM3 gene embeddings, unseen at training time, scPRINT-2 generates an organism label prediction for the two plant organisms it knows about 67% of the time. This is despite the very low prevalence of these organisms in the pre-training dataset (see Figure 3.1). For a horse dataset, scPRINT-2 predicted mammalian organisms 72% of the time.

Unfortunately, these datasets lacked cell-type annotations. Using well-annotated datasets from Zhong et al.[46] of cat and tiger lung tissues, organisms not seen at training time, we generate cell type predictions using scPRINT-2 and achieved a prediction accuracy of 42.2% across the 500 potential cell type leaf labels scPRINT-2 knows about. While this score may seem low compared to supervised approaches, it is worth noting that labels from a secondary source were available in the datasets. Comparing them to the initial ground truth, we found only a 55.3% agreement between the two. Furthermore, we noticed that for some cells, annotations were quite different, such as : *fibroblast* being labelled as *ciliated cell*, *macrophage* as *neuroendocrine cell, and ionocyte* as *secretory cell.*

Given the low correspondence between the two expert annotations, we wanted to determine which was correct between scPRINT-2 zero-shot or the expert ground-truth labels. We conducted a differential expression analysis between cells labeled as *type 2 pneumocyte* by scPRINT-2 (zero-shot) but as *macrophage* by the ground truth (see Supplementary Figure 6.4.6). We saw that the most highly differentially expressed genes were *MAGI1*, *NPNT*, *TEAD1*, and *LMO7*, which are involved in cell-cell junctions, epithelial cells, alveolar cells, and lung tissues. Moreover, the first differentially expressed gene was *SFTPC*, a known "type 2 pneumocyte" marker. This means that, even in this challenging unseen-organism dataset, scPRINT-2 seems to legitimately correct expert annotations. This showcases strong generalization to unseen organisms.

To further improve scPRINT-2's accuracy, we use a method first presented in Hu et al. to aggregate predictions based on **nearest neighbor smoothing** of the model's class logits (see Methods)[47,48]. This approach increased accuracy in most of our use cases but yielded a small 1.3% improvement here. We also provide tools to perform **top-K predictions** and **confidence-based selection**. This means that scPRINT-2 can list multiple putative labels for each cell. When multiple labels have high logits, it can output their shared parental label for that cell instead. When labels disagree, or the logits are low, scPRINT-2 can output an "unknown" label instead. Using both approaches together, we get an additional 3% improvement in accuracy, with 10% of the cells now listed as "unknown".

Additionally, the low accuracy is also related to scPRINT-2 predictions being cell-specific, whereas most ground truth labels are cluster-specific. We propose a **cluster-based logits averaging,** which can be viewed as an extreme case of smoothing (see Methods). With this tool, scPRINT-2 performance increased by 12% (see Figure 3.3). Beyond improved accuracy, these inference-time contributions significantly enhance the usefulness of scFM-based cell annotation for biologists.

Finally, we also demonstrate that with our XPEFT method (presented further in Results section 4), scPRINT-2 can improve its predictions to 95% accuracy in the test subset, while preserving some fine-grained cell-type distinctions not present in the training data (see Figure 3.3).

We then assessed scPRINT-2' s performance as we increased the number of genes in context. We used a Smart-seq-v4 dataset from Jorstad et al., averaging around 6000 nnz genes per cell (see Supplementary Figure 6.4.7)[49]. As shown in Figure 3.3, we observed an overall increase in prediction accuracy across all labels as we increased the context from 200 to 8000 genes, even though scPRINT-2 was pre-trained on only 3200 genes, demonstrating generalization to larger input contexts. Interestingly, classes such as sex and ethnicity reached much better predictive accuracy as we increased the number of genes. When using only the most expressed genes in context, we observed that cell types, which are often defined by highly expressed canonical genes, remained relatively high, even with only 200 genes in context (see Supplementary Figure 6.4.8).

Training scFMs on large dataset sizes does not necessarily improve the model's performance. It is the breadth of cell types, conditions, organisms, and cell quality that produces real generalization abilities. We showcased it here, with scPRINT2 able to label unseen organisms, improving its predictions across various context lengths and rare modalities. We also showed scPRINT-2 reaching state-of-the-art classification accuracy with our fine-tuning.

We will now see how some of our contributions in training loss and data augmentation can similarly improve performance in denoising and imputation in unseen modalities.

3.3.3 A multi-cell denoising auto-encoder task unlocks new modalities and performances

Not all single-cell datasets are at the sequencing depth and quality of Smart-seq-v4. On average, single-cell data has very low depth, preventing scFMs from learning features that

may only be seen in higher-quality cellular profiles.

Meta-cells and graph neural network encoder

In addition to biasing sampling toward cells with more non-zero genes (nnz), scPRINT-2's dataloader now uses neighborhood information, whether defined in expression space or via spatial transcriptomics (see Figure 3.4; see Methods). This allows users to create models that take into account nearest neighbor cells during pre-training. This can be done, for example, by creating **meta-cells**. Meta-cells average the expression over the cell and its neighbors to artificially create a higher-depth cell with less dropout. We demonstrate that this approach achieves improved results across multiple model metrics, but not in denoising (see Table 1). While 17% of cells in the dataset have more than 2600 non-zero values, 11% had at least 3200. With nnz-weighted sampling, we reach 33%. By adding metacells, half of our input expression profiles now have more than 3200 nnz elements—allowing us to extend scPRINT-2's context to 3200 genes.

However, one can go beyond meta-cells and, instead of averaging, use a graph neural network (**GNN**) (see Figure 3.4; see Methods)[50,51]. In this case, the set of neighbors' expressions is encoded in the input token of the transformer. We show that this improves the model's denoising ability. However, we also noticed a decrease in cell embedding and classification (see Table 1). Further experiments showed that this was mitigated with longer training time. As in the variable context case, we variably select 0 to 6 neighbors per minibatch, so the model learns to use a variable number of cell neighbors (see Supplementary Figure 6.4.9, see Methods for details on the choice of neighbors).

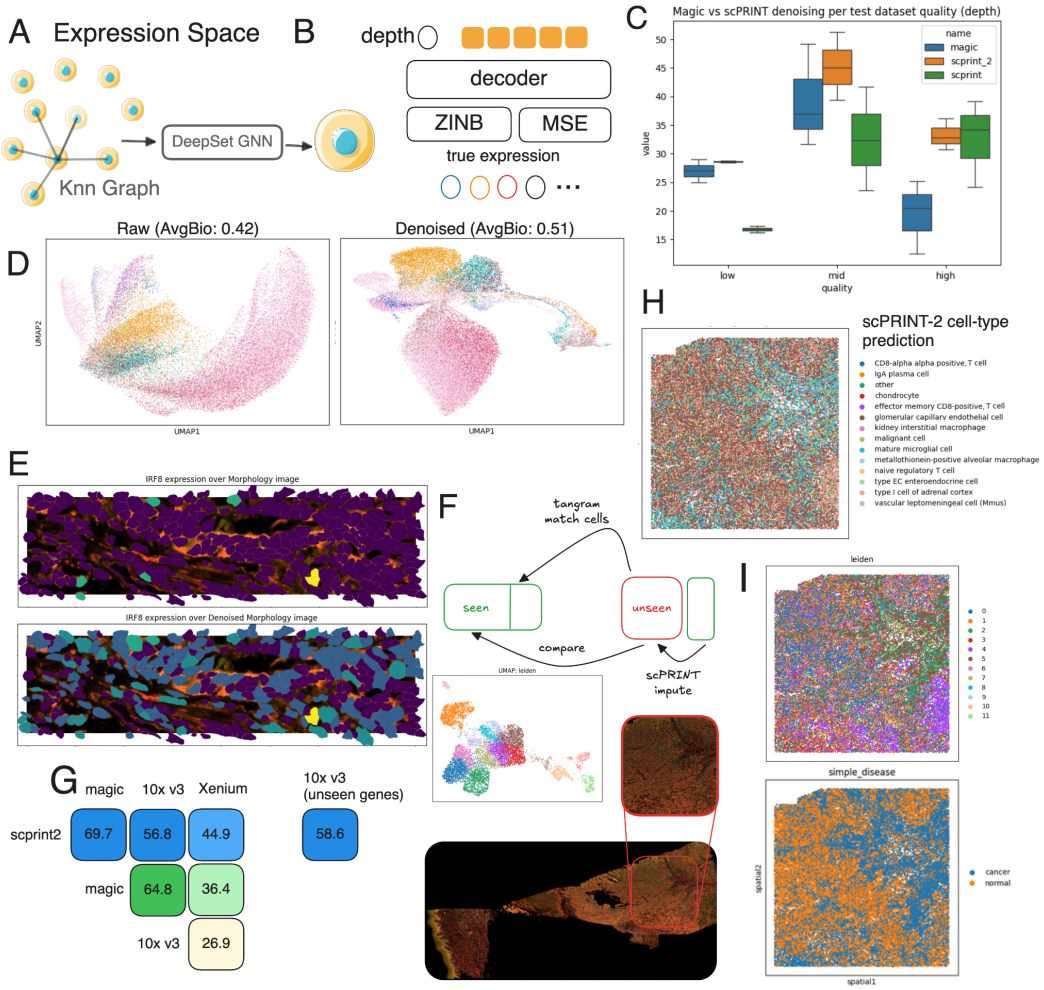

FIGURE 3.4 – (a) Overview of scPRINT-2's multi-cell expression encoder and (b) scPRINT-2's expression decoder loss. Circles represent scalar values, orange blocks represent vectors. (c) Benchmark of scPRINT-2 on expression denoising over nine datasets of varying quality, compared to MAGIC and scPRINT-1. (d) UMAP of the Xenium's patches of cells' expression pre/post denoising with scPRINT-2. (e) Expression denoising of IRF8 with scPRINT-2 over a sub-patch of the Xenium melanoma dataset with cell contour overlaid. (f) Overview of the patch selection in the Xenium dataset, and of the mapping and pseudo-imputation with Tangram using a matched melanoma 10x v3 scRNA-seq dataset. (g) Correlation-based denoising & imputation scores of scPRINT-2 and denoising of MAGIC on the matched dataset. (h) scPRINT-2 cell type prediction over the Xenium melanoma patch. (i) Expression-based clusters and scPRINT-2 disease prediction of cells from the Xenium melanoma patch analyzed. Source data are provided as a Source Data file.

Pushing our analysis further, we realized that a mix of both scores, which we call **ZINB+MSE** (see Figure 3B ; see Methods), yields a better denoising score while retaining the ability to model zero inflation and uncertainty (see Table 3.2). Together, these updates have already made scPRINT-2 better than scPRINT-1 and even better than MAGIC on our denoising benchmarks (see Table 3.2, see Figure 3.4)[52]. While these results are already state-

of-the-art, we wanted to explore the effects of denoising and how to assess our model in unseen contexts.

Looking at denoising scores across technologies, we notice that scPRINT-1 tends to perform much better on datasets with higher nnz genes, i.e., higher-quality datasets (see Figure 3.4, see Methods). However, within each dataset, scPRINT-1 struggles more with low-depth cells than MAGIC & scPRINT-2, which is more consistent overall. We explain this paradox by the fact that, beyond nnz genes, the high-quality dataset often exhibits lower biases in the distribution of nnz genes per cell (see Supplementary Figure 6.4.10). This also explains why MAGIC and scPRINT-2 perform better than scPRINT-1 in these biased datasets. Indeed, they can look at the neighbor's expression and model the expression biases this way. This usage explains the significant improvements in the low- and mid-quality datasets, making scPRINT-2 state-of-the-art across all tested contexts and modalities using its estimate of zero-inflation.

scPRINT-2 generalizes to unseen denoising tasks

Additionally, we decided to look at performance on a Xenium dataset, a modality completely absent from scPRINT-2's training (see Methods)[53]. We elected to use a large, recent skin melanoma dataset with a 5000-gene panel, reaching the upper limit of what is doable with current technology.

A first proof of scPRINT-2's denoising is the scIB biological truthfulness of the Xenium dataset, which improves over the raw expression embedding when using its embeddings (see Figure 3.4 ; see Supplementary Figure 6.4.11 ; see Supplementary Table 6.3.2). To further assess how well scPRINT-2 can denoise this unseen data modality, we leverage the optimal transport-based method Tangram[54]. We used Tangram to map each Xenium cell to another cell in a non-spatial 10X v3 dataset of similar skin melanoma[55] (see Figure 3F). Here, the mapping quality is low due to many differences between the two technologies, e.g., number of cells, number of genes per cell, or biases in cell and gene types (see Supplementary Figure 6.4.12). Still, using the 10X v3 dataset as ground truth, we can see that MAGIC and scPRINT-2 recreate an expression profile that correlates more than 30% better with the 10X dataset than does Xenium (see Figure 3.4). There, MAGIC creates expression profiles closer to the 10X ones, while scPRINT-2 remains closer to the initial Xenium profiles, and both scPRINT-2 and MAGIC tend to agree more with each other than with anything else (see Figure 3.4).

Overall, this suggests that using a tool like scPRINT-2 might be a better alternative for denoising and imputing expression from Xenium than using a secondary non-spatial 10X dataset and aligning it with Tangram.

At the same time, MAGIC can only perform denoising and cannot impute expression for unseen genes. We thus use scPRINT-2 to impute a random subset of 5000 genes present only in the 10X v3 dataset. Interestingly, we noticed that feeding all 5000 (expressed in Xenium) + 5000 (unexpressed in Xenium) genes in context did not lead to good imputation. However, using scPRINT-2's generative architecture, we directly decoded the 5000 10X-only genes from the scPRINT-2's cell tokens generated on the 5000 Xenium genes (see Supplementary

Figure 6.4.13). We show that this imputation scores as high as the denoised Xenium genes (see Figure 3.4).

Finally, we also wanted to examine scPRINT-2's cell-label predictions on this unseen modality. While we did not have access to ground-truth labels in this dataset, we could already spot-check the validity of the predictions. Indeed, many cell types were labeled as *basal* or *epidermis*, with numerous immune cell labels in the cancer-induced lesion in the tissue (see Figure 3.4). This entire lesion region was labeled as *cancer* by scPRINT-2. This was striking as it contained mostly non-cancerous activated immune cells (see Figure 3I; see Supplementary Figure 6.4.14). It likely reflects the biases of the pre-training dataset, where disease labels are often applied at the dataset level rather than the cell level, making scPRINT-2's disease predictions sometimes imprecise. Thankfully, many cells had the cell-type label '*malignant cell*'. These cells were distributed throughout the tissue and showed a strong signal for the five key literature melanoma genes (*BCL2, IGF1, EGFR, FGFR2, SOX10*) (see Supplementary Figures 6.4.15 and 6.4.16).

Overall, we have seen how scPRINT-2 can be used on challenging modalities to augment a given dataset with cell label predictions, expression denoising, and gene imputation. Showing yet again another axis of generalization. We will now focus on how structural changes to scPRINT-2's transformer architecture improve the quality of its embeddings.

3.3.4 An efficient, hierarchical attention architecture makes scPRINT-2 generative

Efficient attention architectures and compression methods

Implementing transformer models on new modalities is a potent way to rethink some of their mechanisms. A common issue with transformer models is their memory and compute requirements, which grow quadratically with their context length (e.g., the number of genes in their input). This is even more pronounced in bidirectional transformers like most scFMs. With the introduction of scPRINT-1, we presented a model that could train in 3 days on a regular A40 GPU and on 50M cells, an order of magnitude faster than most similar scFMs. A first contribution to the scPRINT-2 architecture is the addition of state-of-the-art approaches to reduce the memory footprint and increase training speed. We modified the attention mechanism in multiple ways, using grouped-query attention (GQA) to reduce memory usage. We benchmarked additional attention mechanisms alongside Flash-Attention-3 to assess their performance and their speed.

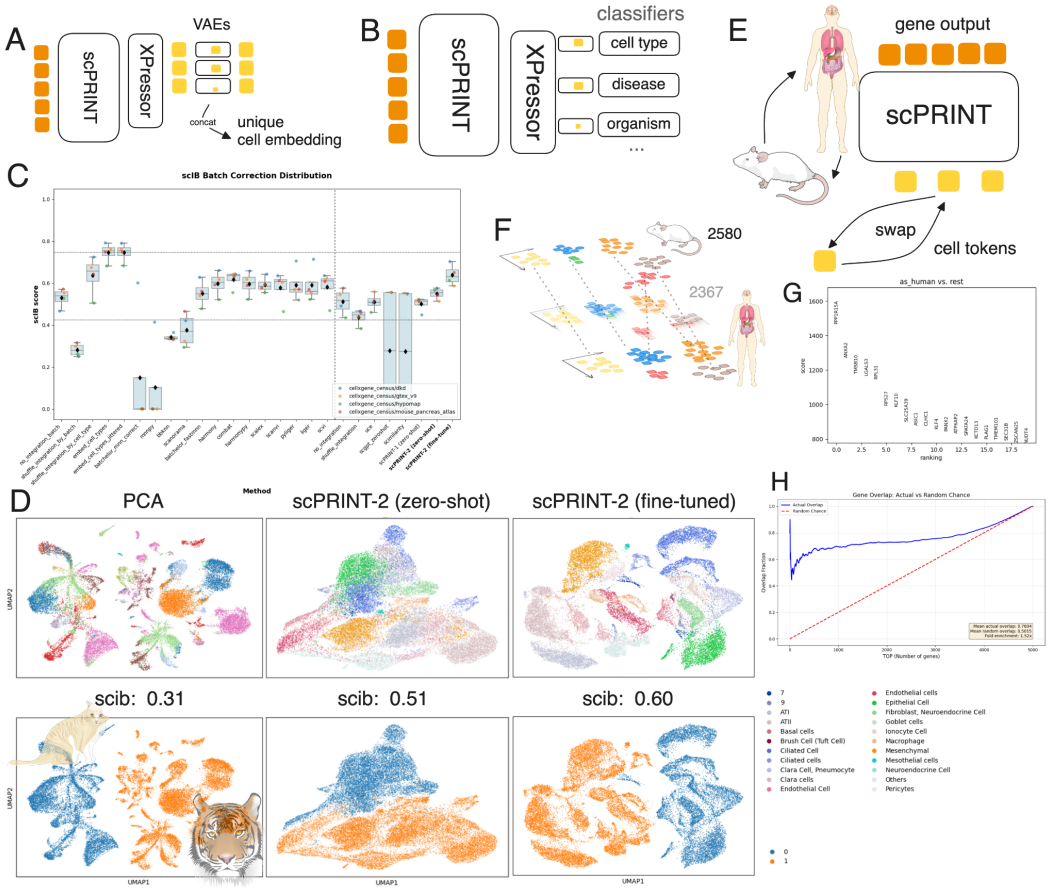

Figure 3.5 – (a) Presentation of the XPressor with VAE-based compression. (b) Schematic representation of going from expression to classification with scPRINT-2, XPressor, and VAE-based compression. (c) Open-Problem scores for scPRINT-2 across all methods. (d) UMAPs of, respectively, PCA embeddings, scPRINT-2 zero-shot cell-type embeddings, and scPRINT-2 fine-tuned cell-type embedding colors by known cell types and batches, with scIB total scores. (e) Schematic representation of the counterfactual generation using scPRINT-2's embedding and replacing them for the organism class from mouse to human. (f) Illustration of the decrease in distance between initially unrelated datasets from applying this counterfactual approach. (g) Differentially expressed genes post vs pre mouse "humanization" with scPRINT-2. (h) Over-representation plot of the top positively differentially expressed genes in both human-like mouse and real human vs. mouse ; the red line indicates random chance. Source data are provided as a Source Data file.

A first one is flash-**hyper attention**, which computes specific attention only on sets of keys and queries known to be similar via locality-sensitive hashing and clustering[56]. A second one is flash-**softpick attention**, a rectified softmax that decreases hyperactivation of specific tokens, often called attention sinks[57]. We also present our own sub-quadratic attention mechanism : **criss-cross attention** (see Methods), inspired by advanced concepts such as the Recurrent Interface Network (RIN) and the Induced Set Attention Block (ISAB)[58,59]. It compresses attention by sketching it in context, using a doubly cross-attention mechanism

with a set of latent tokens that get updated across layers (see Supplementary Figure 6.4.17). We show that only criss-cross attention dramatically improved the model' s speed while retaining all its abilities (see Table 1). However, it is not yet compatible to retrieve gene networks from ; for this reason, our scPRINT-2 architecture, for now, uses flash-attention-3 and XPressor.

On another direction, while single-cell analysis has leveraged VAEs for years to generate meaningful compressed representations of cells, transformers inherently lack this ability[60–62]. We use the **XPressor** architecture presented in Kalfon et al.[33], which compresses output gene embeddings into a set of cell embeddings and decompresses them back into their original gene embeddings (see Figure 3.1, Figure 3.5, and Methods). This innovative architecture draws on ideas that have existed in the transformer literature for several years[59,63–66]. We show in our ablation study that using XPressor results in a slightly better cell representation overall, but does not meet the statistical threshold. This difference might be explained by the limit in the number of epochs and the model's smaller size compared to Kalfon et al. (see Table 3.2, see Supplementary Table 6.3.1). We include an extension to this approach, in which one appends VAEs to each output embedding of XPressor to regularise the different cell embeddings generated by the model (see Figure 3.5). This addition allows us to choose a specific dimension for each cell embedding that is lower than that of XPressor. A second constraint is defined by applying the Kullback-Leibler divergence (KL) loss (see Figure 3.1, see Methods). This creates an information bottleneck for the different cell embeddings, pushing the model to select only the minimum amount of relevant information to represent the label. While our ablation study does not show improvement in cell embeddings with this approach, this is likely because each method was trained for only 20 epochs. Indeed, the VAE-infused model is taking longer to learn to classify cells. However, the batch correction score improved significantly, indicating that the different cell tokens mainly contained information about the class they encoded (see Supplementary Materials). Now that we have highly compressed cell-level embeddings (i.e., tokens), we can apply a **dissimilarity loss** between each for a given cell. This actively pushes them to be as different as possible (see Supplementary Figure 6.4.18 ; see Methods). We demonstrate that this tends to slightly improve the model' s output embedding in our ablation study (see Table 1).

These architectural changes make scPRINT-2 much more efficient at compression and zero-shot batch-correction. Indeed, on the open problem's benchmark, we observe an overall improvement over scPRINT-1, again becoming the state-of-the-art zero-shot method on the platform (see Figure 3.5). This zero-shot performance increase is solely due to the improvement in the batch-correction score from using our VAE method (see Supplementary Figure 6.4.19). We then fine-tune the XPressor architecture alone – our XPEFT approach – to further learn to remove batch effects and predict expert-annotated cell-type labels. We add a Maximum Mean Discrepancy (MMD) loss (see Methods) that penalizes the distance between batch elements[67,68]. Doing so, we observe a jump in scIB scores, especially in biological truthfulness, as measured by the scIB metrics (see Figure 4C ; Supplementary Figure 6.4.20), making scPRINT-2 the best-performing method in the benchmark.

scPRINT-2 generalizes to unseen cell embedding tasks

We then wanted to push our analysis further and test the zero-shot organism-level integration of scPRINT-2 on organisms unseen during training. Again, using our cat and tiger dataset presented in the second result section, we saw that already, scPRINT-2's general cell embedding performs better than doing no correction and keeps lot of biological truthfulness, as shown by the scIB score of 0.44 vs 0.37 for PCA (see Figure 3.5, see Supplementary Figures 6.4.21, 6.4.22, see Supplementary Table 6.3.3). Then, as often, taking the cell-type-specific embedding further increases the biological truthfulness to 0.49, mainly by generating a more faithful biological representation, as reflected in the scIB scores (see Figure 3.5, Supplementary Figures 6.4.22, 6.4.23, Supplementary Table 6.3.3). Again, using XPEFT, we achieve a tremendous 0.60 scIB score, placing us among the top 3 best-performing models in this category, behind SATURN and scGEN (see Figure 3.4, Supplementary Figures 6.4.22, 6.4.24, Supplementary Table 6.3.2). We note that even in this domain, many cell types didn't overlap across organisms. It is a common behavior in this benchmark, and similar cell types now almost overlap in the UMAP, hinting at shared neighbors (see Figure 3.4, see Methods)[69].

Finally, we wanted to examine the model's ability not only to integrate cellular profiles but also to generate entirely new ones at inference time in a zero-shot manner by combining cell tokens (see Figure 3.5). We first approach it using a matched mouse-human multi-organ atlas from Zhong et al.[46]. We then generated cell embeddings for all cells and computed an average "human"-ness cell embedding using the *organism* embeddings of all human cells. We regenerate an expression profile using 1. the human gene embedding and 2. the mouse cell embeddings, replacing the organism cell embedding with the human one (see Figure 3.5 and Methods). We thus generate a set of human-like cell expression profiles from mouse expression profiles. Using the 5000 most variable orthologous genes, we indeed observed a decrease in the Wasserstein-2 (W2) distance on this counterfactual conversion to human (see Figure 3.5, see Methods)[70,71]. Applying a similar approach, but this time to generate females from males in the human dataset, we also notice a similar reduction in expression W2-distance from 1076 to 938.

Looking at how cell expression patterns change after this transition, we found that most of the top differentially expressed genes are the same as those identified in the differential expression analysis of the real human dataset (see Figure 3.5, see Supplementary Figure 6.4.25). Computing an over-representation test, we observe a robust 58% enrichment compared to random, with more than half of the top differentially expressed genes correctly predicted by scPRINT-2 in both over- and under-expressed genes (see Figure 3.5, see Supplementary Figures 6.4.26, 6.4.27). Looking at *Reactome_2022* pathway enrichments, we see multiple pathways related to immune system function, membrane-ECM (Extra-Cellular Matrix) interactions, and tissue elasticity, as well as many other molecular-level pathways (see Supplementary Figure 6.4.28). These align with previous analyses highlighting ECM and immune function differences between human and mouse tissues[72,73].

Overall, we have shown that an entirely novel architecture and a set of learning constraints enable scPRINT-2 to generate high-quality embeddings in a zero-shot manner. Thanks to its multi-organism training, this can be extended to unseen species, while

achieving even stronger results with fine-tuning. We have also demonstrated how one can use the scPRINT-2's cell embeddings to generate counterfactual cellular profiles. This makes it a strong contender for performing atlas-scale analysis across tissues, diseases, and organisms, by learning to disentangle each cell component. We will now see how other parts of the models can be used to extract additional information.

3.3.5 High-quality contextual gene representations from scPRINT-2

scPRINT-2 has rich gene embeddings

scFMs don't just provide cell-level embedding, they have also been used to generate contextual gene-level embeddings given a cell's expression profile or to predict gene-gene connections. The model' s gene embeddings can be used for fine-tuning, such as to predict ATAC-seq activities or gene essentiality[1,2]. We investigate the gene embeddings produced by scPRINT-2 and then delve into how its gene networks can be better extracted and assessed.

A good output gene embedding is also defined by the quality of its input. With scPRINT-2, we introduced a fine-tuning adapter layer on top of ESM3's protein embeddings, jointly trained with the model (see Methods). This approach is one of the few that improve gene network inference without decreasing any other metrics in our additive benchmark (see Table 3.2). It allows us to update gene representations during pre-training while maintaining the ability to work with unseen representations, e.g., from unseen species (see Figure 3.6).

It remains unclear, however, what the right approach is for selecting output gene embeddings, with some heuristics proposing using the last or second-to-last layer. Using our regular transformer model trained with masking, we demonstrate that its output gene embeddings contain only their own expression values (see Figure 3.6). However, when trained with the Xpressor architecture, clusters of genes appear (see Figure 3.6). This is sensible because Xpressor forces gene embeddings to be rich in meaning, as the compression block must query them. We have, however, noticed that for regular models that are not fully trained (only up to 20 epochs), the output gene embedding still contains some input ESM3 features (see Supplementary Figure 6.4.29). The number of enriched pathways in its output gene embedding cluster is still significantly less than for scPRINT-2's XPressor architecture (see Figure 3.6 ; see Methods)

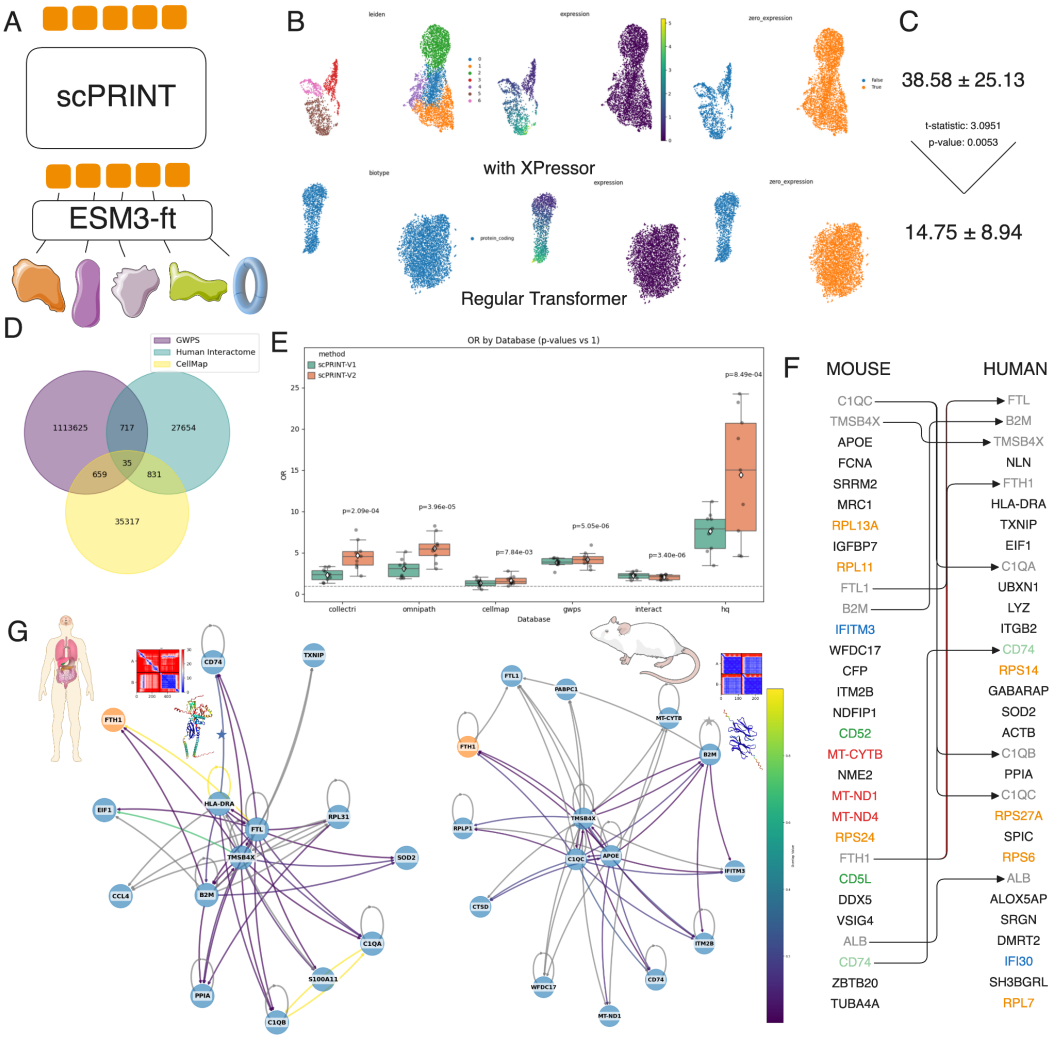

Figure 3.6 – (a) Illustration of fine-tuning of ESM3 while training scPRINT-2 using an adaptor layer. (b) Comparison of gene output-embeddings for a random cell in a model with the XPressor architecture and a model trained without. (c) On the side, the average number of pathways shown to be enriched in the gene output embedding clustering of each method using three main pathway databases. The number below is on the non-fully trained regular transformer ; otherwise, no pathways are enriched (see Methods). (d) Comparison of ground truth networks' overlap between cellmap, the human interactome, and genome-wide perturb-seq. (e) Benchmark over six ground truth gene networks of scPRINT-1's gene networks with its extraction method and scPRINT-2's gene networks with its extraction method, over nine different human cell types from the same dataset. (f) Comparison of the top-30 hub nodes on both gene networks. Arrows link similar genes, and colors represent similar gene groups. (g) Subset of a gene network generated by scPRINT-2 seeded at FTL1, on human macrophage cells, and on mouse macrophage cells, edge color represents the RoseTTAFold2-PPI scores for these connections, grey means no score was computed. The AlphaFold-Multimer structure and amino-acid distance map are provided for the star-marked connections. Source data are provided as a Source Data file.

extracting gene networks from scPRINT-2

Thanks to the transformer architecture, one can go beyond gene output embeddings to examine gene-gene interactions via the model's attention layers. Following the tests reported in Kalfon et al., we observed, on average, no dramatic performance gains across the methods we tested (see Table 3.2). An issue we noticed is that the problem is not well-defined. Indeed, the ground truths widely disagreed with one another (see Figure 3.6 ; see Methods). Between the genome-wide perturb-seq (gwps) ground truth and omnipath, only 800 gene-gene connections were in common over the hundreds of thousands that each contained. This suggests that diversity of ground truth will be key to showcasing the breadth of potential gene-gene connections in the cell.

We thus gathered a new set of ground truth gene networks (GN)s from recent works. Our first approach was to use protein-binding datafrom AP-MS experiments within the O2US cell line, called the *cellmap*[74] (see Methods). Additionally, thanks to protein structure models, we are now able to compute putative interactions across millions of protein pairs ; a first version of this analysis has been defined in the human *interactome* (see Methods). But here again, the disagreement was significant, with only ~1-4% of the connections in each ground truth being found in another, and no connections were reliably found across all five ground truths (see Supplementary Figure 6.4.30).

Acknowledging these disagreements, we benchmarked them against nine human cell types from the same dataset using scPRINT-1 and scPRINT-2. We use a gene network extraction method that is more computationally demanding but biases the network towards co-expressed genes (see Methods). We see that scPRINT-2's performance was often greater or similar across all benchmark networks, as indicated by the odds-ratio measures (see Figure 3.6 ; see Methods). We did not see a similar trend, however, on AUPRC (see Supplementary Figure 6.4.31). This suggests that our method is more accurate for its top-K connections. Indeed, the strongest human interactome connections were overrepresented in scPRINT-2, more so than in scPRINT-1.

cross-organism gene network analysis

To continue on our cross-organism analysis, we also aimed to further characterize some of the genes observed in our previous human/mouse datasets by interrogating the cell-specific GN identified by scPRINT-2 in *Macrophage* cells from both mammals. Looking at their hub nodes, we see that many are common and represent key conserved cell immune pathways, such as *feroptosis*, *vitamin B12*, and *Pathogen Phagocytosis Pathways* (*WikiPathway_2023_Human*), with genes like *C1Qs, RPs, ALB, and APOE*[75,76]. These mainly relate to the macrophage' s internal machinery, which is designed to eat and destroy pathogens. Other genes were clear markers of macrophages (*CD74;LYZ) and/or immune cells (HLA-DRA, B2M) or their pathways, such as interferons alpha/gamma and MHC Class II (MSigDB_Hallmark_202076–78)*. Interestingly, these networks share only 30% similarity when considering the top 20 connections for each gene. But what seemed like differences in connections and top 50 hub genes tended to disappear after thorough analysis, such as with the Ribosomal proteins, which are related in the kinds of pathways they are part of, or in their relationships

in the PPI_Hub_Proteins database[77] (see Figure 3.6).

We then extracted a subset of the macrophage networks, seeded at the *FTH1* gene, for both organisms, focusing on the top 15 connected nodes and their top 60 edges (see Figure 3.6 ; see Methods). We observed a set of hub genes in both subnetworks, with some genes being shared between human and mouse. Interestingly, these hub genes had more interactions in the human interactome ground truth than non-hub genes. We also noticed that the "hub-ness" of the subnetworks can be very variable and seems to depend on the "seed" gene (see Supplementary Figure 6.4.32).

By overlaying the human interactome ground-truth values on our subnetworks, we found that only a small subset of connections was marked as valid (i.e., score above 0.6) in the ground truth (see Figure 3.6). In the mouse *Macrophage* subnetwork, almost no connections were recovered, but this may be explained by the fact that the ground truth is the "human" interactome, computed using human proteins rather than mouse proteins. We thus wondered whether we could use scPRINT-2 to cross-validate the interactions present in this ground truth. Indeed, we know that the human interactome values are not directly computed from AlphaFold-multimer's interaction probability (ipTM) ; they come from a simpler model called "RoseTTAFold2-PPI". Testing a couple of connections predicted to be low ipTM by RoseTTAFold2-PPI but found by scPRINT-2, we readily identified two : HLA-DRA/CD74 and B2M/B2M, which, when passed to AlphaFold-Multimer, indeed formed an interaction with an ipTM of more than 0.6. This showcases the potential of scPRINT-2 in this domain and future directions for GN inference.

We have seen here how scPRINT-2's output gene embeddings and attention matrices can be used to extract meaningful biological insights and drive hypothesis generation in a cell-to-cell, state-specific manner. These outputs can also be used for fine-tuning purposes and in explainable AI-driven analysis. We also pushed our GN analysis further, defining additional benchmarks and a more powerful GN extraction mechanism. We demonstrated cross-species analysis and presented the tantalizing possibility of merging foundation models at different scales, including ESM3 fine-tuning, AlphaFold Multimer, RoseTTAFold2-PPI, and scPRINT-2. While these are just examples, they demonstrate what aggregating multiple bodies of evidence across scales can achieve for genetic interaction predictions. A first step towards using scFMs, protein Language Models, and structural models in coordination, to shed light on the cellular machinery.

3.4 Discussion

In this work, we present a gymnasium of tasks to benchmark scFMs in multiple contexts. Together with an efficient and reproducible pipeline, we test the benefits of 42 different parts of scFMs structures, encoding, and training. In this additive benchmark, 12 of these are our own contributions to scFMs, including GNN-based expression encoding, cross-foundation model fine-tuning, sub-quadratic attention mechanisms, and rich losses. This massive benchmark is the first of its kind for scFMs and assesses four different tasks. It allowed us to identify bottlenecks and limitations, issues that we solved in subsequent

analysis. Indeed, future benchmarks will benefit from using more diverse datasets, tasks, and ground truths.

We have also presented the largest pre-training database to date, encompassing more organisms, conditions, and data modalities. We have seen that, while more work is needed to obtain higher-quality, well-annotated datasets, our dataloader and preprocessing pipeline have made the most of this vast database.

Using the best feature combinations from our additive benchmarking, we build and train a next-generation cell Foundation Model, scPRINT-2. We demonstrate that, although currently 5 times smaller, scPRINT-2 outperforms scPRINT-1 across all benchmarks tested. On denoising, scPRINT-2 becomes state-of-the-art, and with our fine-tuning approach, it also outperforms every other method on the batch-correction and classification tasks of the open-problem benchmarks.

We then challenge scPRINT-2 on tasks of high relevance for cellular biology, highlighting some pitfalls in current benchmarks. We show that scPRINT-2 acquires generalizable abilities across unseen modalities and organisms, while remaining consistent in its predictions. We demonstrate it across many tasks, including cross-organism integration, unseen gene imputation, and counterfactual reasoning.

Finally, we present tools for easily extracting labels, cell-specific gene embeddings, imputing gene expression, performing gene network inference, and working with organisms unseen during pre-training. We believe our results demonstrate many domains where scFMs might confidently replace approaches that rely on heuristics, atlases, and a variety of tools and packages. However, much work remains.

Current ground-truth cell annotations are cluster-based and obfuscate the complexity of cellular states by inherent clustering biases. Batch correction metrics are similarly biased, and top scores can be easily gamed ; gene network ground-truths are not cell type specific and likely filled with false negatives. Data diversity and quality are the principal pre-training bottlenecks, and efforts will be needed to improve foundation models. Many other key modalities, such as measuring time and perturbation effects, remain scarce. They will become increasingly helpful for enriching the future comprehensive benchmarks of next-generation cell foundation models.

Our analysis and contributions highlight powerful features of scFMs and provide guidance for designing benchmarks that better highlight their strengths and weaknesses. scPRINT-2 presents a direction for future improvements, with more specialized architectures and using a combination of biological FMs working jointly across modalities and scales. This next-generation scFM is a step forward in the design of AI for cell biology.

3.5 Methods

We present an additive benchmark with over a dozen contributions to the pre-training tasks, losses, and architecture of single-cell foundation models. Along with it, **scPRINT-2** (pronounced “sprint”), a next-generation model trained on the best-performing contributions.

We analyze its out-of-distribution generalization and present methods for querying and fine-tuning it to solve various tasks. We will go through the specific techniques that made it possible.

3.5.1 Additive benchmark

We now describe in matched order with respect to Table 1, the methods behind the multiple contributions tested in our additive benchmark (see Results section 1). We bolded the ones that are further defined in the methods. In this benchmark, we are using and testing the :

1. **"base model",** every subsequent element is applied to the base model
2. "medium model", larger base model, see the base model section
3. "negative control", untrained base model

Architecture

4. "no dropout", where we remove the dropout initially applied in the base model
5. "large classifier", where the classifier sizes are increased from [input - output] in the base model to [input - 256 - output]
6. "MVC", where we replace the base model's decoder with the cell embedding's MVC approach of scGPT[1]
7. "no decoders/generation", where we removed the base model's decoder, getting a masking+classification only pre-training

Data

8. replacing our pre-training dataset with "Tahoe" 's 100M dataset
9. Chan Zuckerberg Institute ("CZI")'s cellxgene database (version 2024)
10. replacing our pretraining dataset with "CZI + Tahoe" with Tahoe's 100M database
11. replacing our pretraining dataset with "all databases", both CZI, Tahor, and Arc's scBasecount[26,27]
12. replacing our pretraining dataset with "only 200 random" human datasets
13. replacing our sampling with a "sampling without replacement"
14. **replacing our sampling with "cluster-based sampling only"**
15. **adding "meta-cell" during pre-training**

Attention

16. replacing FA3 with "softpick" attention, using the approach of Zuhri et al.[57]
17. replacing FA3 with "hyper"-attention, using the approach of Han et al.[56]
18. replacing self-attention with **"criss-cross" attention layers**
19. **adding "XPressor" layers**

Losses

20. **adding “contrastive learning”**
21. **adding “elastic cell similarity”**
22. **“no embedding independence loss”, removing the embedding independence loss**
23. replacing the ZINB loss with Mean Squared Error (“MSE”)-loss
24. **replacing the ZINB loss with “ZINB+MSE” loss**
25. **adding a “VAE compressor” loss to the Base model**

Tasks

26. **adding “variable context length” and a larger context**
27. **replacing masking with a Transcription Factor “(TF)-masking” task**
28. replacing masking with “denoising”, using the approach in scPRINT, with a random level of denoising (see below)
29. “no classification”, removing the classification pre-training task
30. **adding an “adversarial classifier”**

Input

31. replacing log1p normalization with “sum normalization” where each expression profile is normalized to sum to 10,000
32. “no random level of denoising” where we remove the random level of denoising, see the denoising section
33. **where we replace the expression encoder with a Graph Neural Network (“GNN”) encoder**
34. where we replace the continuous expression encoder with a “binning” version, following the approach of scGPT[1]
35. where we are “using only expressed genes”, as in scGPT and geneformer
36. “without using gene location”, removing the gene location information in the input tokens.
37. “learn gene embedding” where we replace the ESM3 gene embedding with learnt embeddings, as in scGPT and Geneformer.
38. **replacing the ESM3 gene encoder with a “fine-tuned ESM3” gene encoder**

The full training traces of the entire additive benchmark are available on weights and biases :

https://wandb.ai/ml4ig/scprint_ablation/reports/scPRINT-2-additive-benchmark--VmlldzoxNTIyOTYwNA

Base model and training

The additive benchmark is performed on a small model with 18.2M parameters, an embedding dimension of 256, and 8 layers and 4 heads. The model trains for 20 epochs of 20,000 batches of 64 cells per batch. Validation is performed on 10,000 minibatches. We otherwise use the same optimizer and hyperparameters as for scPRINT-2 (see **pre-training** in Methods)

Gene expression is encoded using ESM3 embedding, with gene location and MLP-based expression encoding added, as described by Kalfon et al. The output is decoded using an MLP that takes the output embeddings and depth information, then outputs a scalar expression value.

The base model is trained on CZI's cellxgene census dataset, version 2024 (compared to 2022 in Kalfon et al.). The pre-training task uses a 30% gene expression mask with an MSE loss (as is common for BERT-like encoder transformers)[1,2,7]. The Base model also uses a multi-cell-token generative loss as described in Kalfon et al.[3]. It also performs matched multi-class hierarchical classification, as defined below (see **Hierarchical classifier** in the Methods**).** Finally, it also uses a dissimilarity loss between each of our cell embeddings for a given cell (see embedding independence in Methods).

Each of these decisions is assessed within our additive study.

We pre-train the base model 6 times across multiple seeds to generate error bounds. We train using Flash-Attention-3 on 1 H100 GPU, each training of 20 epochs taking roughly 2 days. Some runs were done on A100s and V100s ; we thus had to rescale the time duration for some of these runs.

Some additive study runs use denoising as a training strategy or larger context lengths when it seemed likely that this would best highlight the abilities and shortcomings of the benchmarked element.

The **medium model** size uses an embedding dimension of 512, with 16 layers and 8 heads.

The **negative control** is a model that was not trained at all.

Weighted sampling

The goal of weighted random sampling is to de-bias regular random sampling of cells in contexts where many cells have similar profiles and expression patterns, while others are rare cell types.

We use weighted random sampling on our training data based on all the different class values we have to predict. We use a factor of S_1, meaning the rarest elements will, on average, be sampled only S_1 times less than the most common ones. The sampling factor used for each group is then $\frac{S_1}{c+S_1}$, instead of $\frac{1}{c}$, where c is the number of cells in each group.

Cluster-weighted sampling

The goal of cluster-weighted sampling is to improve weighted sampling in the condition where cell-type annotations are poor or non-existent.

For cluster-weighted sampling, we simply use the labels obtained by applying Leiden clustering to the K-NN graph of cells for each dataset during preprocessing. We used a resolution of 1 and 15 neighbors. We merge clusters if their centroid correlation exceeds a threshold (here 94%). This cluster label is then treated similarly to other labels, such as *cell_type*, *sequencer*, etc.

In this context, within datasets that lack information about tissue of origin or sequencer, or that belong to the same categories, cells from cluster 1 will be sampled with equal weight from those datasets. The sampling is not dataset-specific. This decision arises because most datasets contain some information about their tissue of origin or disease, and cluster sizes of data from the same tissue/disease often represent similar cells.

This can be applied to any dataset for training models.

Depth-weighted sampling

The goal of depth-weighted sampling is to sample cells with higher quality, in terms of the number of genes expressed, more often.

For depth-weighted sampling, we scale each cell' s sampling probability by its non-zero (nnz) gene count. Similarly, we scale this value, but this time we apply a sigmoid function beforehand to reduce the impact of extreme values.

Algorithm : scale_nnz (1)

Input :

- midpoint : 2000

- steepness : 0.003

- scale : 1000

Output : unormalized sampling probabilities

Apply sigmoid transformation

sigmoid_values = 1 / (1 + np.exp(-steepness * (nnz - midpoint)))

Then scale to [1, scale] range

return 1 + ((scale - 1) * sigmoid_values)

The values shown for Input were the ones we used across our research and were selected manually.

This can be applied to any single-cell dataset for training models.

Multi-cell sampling

For all our datasets, our preprocessing pipeline computes a K-NN graph from the PCA of the scaled, log-transformed expression data. For each sampled cell, scDataloader also retrieves its k-NN cell ID and loads them, along with their distance information. Here, we set K to 6 and the PCA components to 200.

We set the number of PCA components to 200 to retain as much information as possible, while accounting for rare cells whose expression might have only a small impact on the first PCA components.

We set K to 6 to balance the computational resources required to sample 6 times more cells per minibatch with the need for enough neighboring cells. Indeed, these computational resources are more prevalent for smaller models that perform fast iterations across many cells than for larger models. 6 neighbors per sampled cell was our limit for a small foundation model like scPRINT-2. We also note that there is likely a rapid diminishing returns beyond 6 to 15 cells for most datasets as we start sampling more often cells that are less similar to the center one.

During scPRINT-2 training, we select 0 to 6 neighbors per minibatch, so the model learns to use a variable number of cell neighbors.

GNN Expression encoder

The goal of the GNN expression encoder is to increase the information the foundation model can obtain from 1 cell to a set of neighboring cells, thereby dramatically reducing input noise.

The GNN takes multiple expression values as input, optionally along with corresponding cell-cell distances, and returns a vector encoding this information. Both continuous and GNN encodings can be configured to receive either logp1-transformed expression data, sum-normalized expression, or both. The GNN follows the DeepSet[78] implementation :

$$E_j = DeepSet(x_{ij},\ n_{ij},\ d) = \phi_1(\phi_2(x_{ij})||\phi_3(n_{ij}, d_{ij})) \quad (1)$$

Where :

- x_j is the center cell's expression for the gene j
- $n_{ij} \in \mathfrak{R}^k$ is the K nearest neighbor cell's expression for gene j and cell i
- $d_{ij} \in \mathfrak{R}^k$ is the distance of each neighboring cell to the center one
- ϕ_i are MLPs.
- $||$ is the concat operation

We selected K to be a random number between 0 and 6 during training and 6 at inference.

ESM3 fine-tuning gene-encoder

The goal of ESM3 fine-tuning is to get the best of both worlds between learning token features from the data and using learnt protein representations from a pLM as a prior.

We encode/tokenize gene IDs using ESM3[79]. The mapping process happens in the following way :

- A gene name is mapped to its canonical protein name using Ensembl114.
- We recover the protein sequence of the protein using Ensembl
- We use the protein sequence to generate an embedding using ESM3 by averaging all its amino-acid output embeddings.

For the fine-tuning part, we reuse the fine-tuning approaches presented in Kalfon et al., which place an additional adapter layer after mean-pooling and before feeding the protein representation to the model. Interestingly, using gene expression as a further signal to the adaptor layer often led to training instability.

Biased attention

The goal of biased attention is to orient our attention matrix towards genetic interaction priors to improve learning and the model's biological fidelity.

We leveraged the Rcistarget computation and ranking of the human genome for 10kb down- and upstream of each target gene[80], available at the Aerts Lab cistarget databases [1]. Using this information, we generate a weight matrix M that links each motif-defined TF to its target genes.

Given this matrix, we bias the attention matrix for all heads and layers using the attn_mask parameter of the torch.nn.functional.scaled_dot_product_attention function.

It appears in the attention computation like so : $\text{softmax}\left(\frac{QK^\top}{\sqrt{d}} + M\right)V$ where M is the attn_mask matrix and is real-valued.

Criss-Cross attention

The goal of criss-cross attention is to create an efficient attention mechanism by learning, in context, a factorisation of each attention matrix.

In criss-cross attention, we replace the self-attention mechanism with a double cross attention between the N input elements and M latent tokens (see Supplementary Figure 6.4.18). This is thus replacing a N^2 computation with a $2NM$ one, hence going below the quadratic

1. https://resources.aertslab.org/cistarget/databases/homo_sapiens/hg38/refseq_r80/mc_v10_clust/gene_based/hg38_10kbp_up_10kbp_down_full_tx_v10_clust.genes_vs_motifs.rankings.feather

bottleneck of attention. This bears resemblance to the ISAB architecture, XPressor, and perceiverIO[58,63–65,81,82]. M, in our case, is set to 10 : our 9 predicted classes plus an additional token.

Effectively, the M latent tokens are learnt at the first layer of the models. At the same time, they could also be generated from a sketching or principal components analysis (PCA) of the input tokens. They also get updated during the attention computation, so that at the second layer.

We replace the traditional attention computation $X_{l+1} = \text{Attention}(X_l, X_l, X_l) + X_l$, where Attention takes as input the Query, Key, Value elements, with :

$$\text{Attention}(X_1, X_2, X_3) = \text{softmax}\left(\frac{QK^\top}{\sqrt{d}}\right)V \tag{3.1}$$

With

— $Q = X_1 W_Q,\ K = X_2 W_K,\ V = X_3 W_V$

— $W_Q,\ W_K, W_V\ \in\ \mathfrak{R}^{dxd},\ X \in\ \mathfrak{R}^{Nxd}$

In self-attention $X_1 = X_2 = X_3$

In Criss-Cross attention, the algorithm becomes :

$V_{l+1} = Att(V_l, X_l,\ X_l) + V_l$ (3)

for the latent update and

$X_{l+1} = Att(X_l,\ V_l,\ V_l) + X_l$ (4)

for the main update

with $X_l \in \mathfrak{R}^{Nxd}$ the main embeddings and $V_l \in \mathfrak{R}^{Mxe}$the latent embeddings

XPressor model

The goal of the XPressor architecture, as presented in Kalfon et al., is to replace and generalize the class-pooling of other transformer models and the bottleneck learning of scPRINT. This makes the model more powerful at encoding cell-level features while also separating cell-level tokens from gene-level tokens. Finally, it enables a new mode of Parameter-Efficient Fine-Tuning. This bears similarities to the ideas presented in criss-cross attention above.

The **Xpressor** block uses as input a set of learned latent tokens T. It then performs cross-attention between the last layer of the gene embeddings and the latent tokens. The goal is for the **Xpressor** layers to be of smaller dimensions and context size than the main transformer layers, such that we end up with C_j a set of n tokens of dimension d_t generated from the encoded gene expression and ID matrices E_j , and G. Where G and E_j are sets of m tokens of size d_c representing the IDs of the genes and their corresponding expression in cell \$j\$, respectively, where $d_c < d_t$ and $n << m$:

$$O_j = Transformer(E_j,\ G) \quad (5)$$

$$C_j = Xpressor(O_j, T) \quad (6)$$

For a cell j, with the **Xpressor** being initialized with a learned set of input cell tokens, and C_j being the cell tokens associated with the input E_j.

The **Transformer** and **Xpressor** are both transformers with l_1 and l_2 layers, respectively. Indeed, we have designed both layers to contain a cross-attention architecture (see Figure 4A, Supplementary Figure 6.4.1) such that we can also do :

$$O_j = Transformer(C_j, G), \quad (7)$$

With O_j the output of the **Transformer** when using the **Xpressor** representation as input.

We add an optional MLP after cross-attention to transform the embeddings before the self-attention round. In our example, the decompression is performed using gene ID tokens as input only. These tokens remain the same for all cells of a given organism and thus do not depend on j. In the context of protein language models, for example, this would be replaced by positional tokens.

As shown in Supplementary Figure 6.4.1, the **Transformer** blocks are applied twice. The first application serves as an "encoder", using only self-attention, while the **Xpressor** and the second application of the **Transformer** blocks act as "decoders". We follow these definitions from the original "Attention is All You Need" paper[83]. It should be noted that, in our case, cross-attention is performed before self-attention.

Related ideas have also been explored in the NVEmbed paper, where the authors propose a cross-attention-based method to update tokens using "latent" tokens and some additional prompting tricks[66].

XPressor can be applied during pre-training or fine-tuning to replace mean-max-class pooling in Foundation models.

VAE-based compressor model

The goal of the VAE-based compressor is to reduce information sharing between output embeddings by penalizing the amount of information each embedding stores (see Figure 3.5, Supplementary Figure 6.4.1)[84].

Each VAE-based compressor is explicitly applied to a cell embedding, compressing it into a relevant latent dimension. It has a 2-layer MLP encoder and a 2-layer MLP decoder. In cases where only a small set of possible elements exists, such as in sex embeddings or cell culture, one can use the Finite Scalar Quantization (FSQ)-VAE[85].

FSQ-VAE discretizes each latent dimension **independently**. Specifically, the encoder outputs d values, each constrained to lie within a bounded range (e.g., [-1, 1]). Each dimension is then quantized into one of M discrete levels within that range (in our case 2). This dimension-wise quantization can be implemented as either a hard nearest-bin assignment

or a differentiable approximation thereof. Because FSQ enforces scalar-level discretization, it provides a simpler and more fine-grained alternative to VQ' s vector-level codebook approach, while still offering strong regularization of the latent space.

In our case, all VAEs with fewer than 8 latent dimensions used the FSQ-VAE approach.

It can be applied on top of any output embedding at pre-training or fine-tuning.

ZINB+MSE loss

The goal of the ZINB+MSE loss is to make the model' s expression-level prediction as precise as possible (thanks to the MSE) while preserving the ZINB' s expressivity and uncertainty estimation.

scPRINT-2 uses a novel expression decoder for foundation models that outputs the parameters of a zero-inflated negative binomial (ZINB) distribution for each gene i in cell j. The *ZINB* distribution is defined as

$$X \sim ZINB(\mu,\ \theta,\ \pi), \quad (8)$$

Where the parameters $\mu,\ \theta,\ \pi$ are obtained from a multi-layer perceptron (MLP) applied to the expression embeddings outputted by the transformer model at its last layer (e), which are the :

$$\mu,\ \theta,\ \pi\ =\ MLP(e\ ||\ d) \quad (9)$$

The MLP is a two-layer neural network with dimensions [*d+1, d*, 3], where || denotes the concatenation operation.

Based on the work of Jiang et al.[86], zero inflation is the best distribution for a broad range of transcriptomic measurements, as some measurements exhibit sufficiently high dropout rates and require a zero-inflation term to model them. In our case, and similarly to scVI[87], we define our *ZINB* as

$$ZINB(x \mid \mu,\ \theta,\ \pi)\ = \pi\delta_0(x)\ +\ (1\ -\pi)NB(x \mid \mu,\ \theta) \quad (10)$$

Where $\delta_0(x)$ is a point mass at zero, and $NB(x \mid \mu, \theta)$ is the negative binomial distribution with mean μ and dispersion θ.

Compared to scVI, where the overdispersion parameter θ is learned for each gene, we make scPRINT-2 output it together with $\mu,\ \pi$ (see Supplementary Figure 6.4.13)

Effectively, the model learns that dispersion may vary across genes, sequencers, cell types, and sequencing depths.

In addition, the loss adds an MSE term computed from the μ and θ output of the MLP, comparing for a gene i, $e_i\ =\ \mu_i \times (1 - \sigma(\pi_i))$ to the logp1-transform of the expression using mean-squared-error.

Where e_i is the predicted expression of gene i and σ is the sigmoid function :

$$L_{MSE} = \frac{1}{n}\sum_{i=1}^{n}(e_i - \log_2(x_i + 1))^2 \tag{3.2}$$

The zinb+mse loss is the addition of both losses with a scale parameter, here :

$L_{ZINB+MSE} = L_{ZINB} + 0.5 \times L_{MSE}$ (12)

This loss comes as a replacement for the classical MSE or ZINB in scRNA-seq models.

Embedding contrastive loss

The goal of this contrastive loss is to remove some batch effect by pushing cell embeddings obtained from the expression profile after different perturbations to be more similar to each other than they are from cell embeddings of other cell profiles, using the InfoNCE[88] loss :

Algorithm : L_contrastive (2)

Input :

- x : embeddings of cells post perturbation A [batch_size × feature_dim]

- y : embeddings of the same cells post perturbation B [batch_size × feature_dim]

- temperature : scaling parameter τ = 0.3

Output : contrastive loss value

1. // Compute similarity matrix

S ⟵ cosine_similarity_matrix(x, y) / τ

Where S[i,j] = (x[i] · y[j]) / (||x[i]|| ||y[j]|| τ)

2. // Create positive pair labels

labels ⟵ [0, 1, 2, ..., batch_size-1]

3. // Compute cross-entropy loss

loss ⟵ cross_entropy(S, labels)

Which expands to :

loss ⟵ -Σ_i log(exp(S[i,i]) / Σ exp(S[i,j]))

Return loss

This loss can be added to any scFMs at pre-training or fine-tuning (see Supplementary Figure 6.4.18).

Elastic cell similarity loss

The goal of this loss is to reduce batch effects by pushing cells that are similar to become more similar and cells that are dissimilar to become more dissimilar[1].

We implement the **cell similarity loss** of scGPT, where, given cell embeddings $e \in \mathbb{R}^{m \times d}$, where m is the number of cells and d is the embedding dimension :

$$L_{similarity} = \frac{1}{m(m-1)} \sum_{i \neq j} 1 - (\max(0, \hat{e}_i^\top \hat{e}_j) - \tau)^2 \tag{3.3}$$

Where :

$\hat{e}_i = e_i / \|e_i\|_2$ is the L2-normalized embedding of the cell i

τ is the similarity threshold (default 0.3)

$m(m-1)$ is the number of off-diagonal pairs,

This loss can be added to any scFMs.

Embedding independence loss

The goal of the embedding independence loss is to push the different class-level embeddings of a cell to encode distinct information by making them orthogonal (see Supplementary Figure 6.4.18).

Implementing a set of disentangled embeddings is not straightforward. In our case, we push the embeddings to be as different from one another as possible, with an **independence loss** defined as

$L_{independence} = \frac{1}{m^2} \sum_{i=1}^{m} \sum_{i'}^{m} 1 - cos(e_i, e_{i'})$, (14)

where e_i and $e_{i'}$ are the cell embeddings, m is the minibatch size, and cos denotes the cosine similarity. This pushes each embedding to represent different information from the others.

This loss can be added to any scFMs at pre-training or fine-tuning.

Hierarchical classifier loss

The goal of the hierarchical classifier is to enable efficient label predictions for a set of related labels defined by a known graph.

The scPRINT-1 classifier generates predictions for all possible labels in a hierarchical ontology, while producing logits only for the most fine-grained elements. To predict the other elements, it only has to aggregate their children' s logits. We improve this loss in scPRINT-2 by using the entire ontological graph : e.g., if a cell is an *olfactory neuron*, then it is also a neuron. If the classifier predicts *glutaminergic neuron*, it is wrong at this level

but correct for *neuron*, meaning we penalize it less overall than a non-neuron label, like *fibroblast* (see Figure 3.3).

In conjunction with our weighted sampler, this allows the model to learn rich gradients from a low volume of data. We also implement two additional classes for predictions in our hierarchical classifier compared to scPRINT-1 : age and tissue of origin.

During pre-training, we perform label prediction for different classes, e.g., cell type, disease, assay, age, tissue, ethnicity, sex, and organism. We created a specific relabeling of the age label that could be very fine-grained, e.g., 2 weeks, 3 weeks, 35 years old, 36 years old, into biologically relevant groups such as *embryo, fetal*, *6-month-old*, *1-year-old*, *adolescent*, young adult, and so on. We mapped both human and mouse data this way to a common age profile. These were the only two species with such labels available. The labels follow a hierarchy defined by ontologies : the Cell Ontology for cell type, MONDO for disease, EFO for assay, HANCESTRO for ethnicity, HSAPDV for age, UBERON for tissue, NCBITaxon for organism, and EFO for sex[89–92]. We do not compute the loss for cells with the unknown label.

The algorithm thus becomes :

Algorithm : L_class (Hierarchical Classification Loss) (3)

Input :

- pred : predicted logits [batch_size × n_leaf_labels]

- cl : ground truth labels [batch_size]

- labels_hierarchy : binary matrix [n_parent_labels × n_leaf_labels]

Output : hierarchical binary cross-entropy loss

1. Initialize target matrix newcl ⟵ zeros[batch_size × n_leaf_labels]

2. Initialize weight matrix weight ⟵ ones[batch_size × n_leaf_labels]

3. // Handle leaf labels (known exact labels)

For each valid leaf label cl[i] where cl[i] ∈ [0, n_leaf_labels) :

newcl[i, cl[i]] ⟵ 1

4. // Handle unknown labels

For each unknown label cl[i] where cl[i] = -1 :

weight[i, :] ⟵ 0

5. // Handle parent labels (partial knowledge)

If any cl[i] ≥ n_leaf_labels :

parent_idx ⟵ cl[i] - n_leaf_labels

// Zero out weights for unknown leaf children

weight[i, children_of_parent[parent_idx]] ⟵ 0

// Set targets for all possible children to 1

newcl[i, children_of_parent[parent_idx]] ⟵ 1

// Compute parent-level predictions and targets

For each parent p :

// Aggregate leaf predictions using logsumexp

addpred[p] ⟵ logsumexp(pred[:, children_of_parent[p]])

// Set parent target based on leaf targets

addnewcl[p] ⟵ max(newcl[:, children_of_parent[p]])

// Weight inversely proportional to the number of children

addweight[p] ⟵ addnewcl[p] / √|children_of_parent[p]|

// Concatenate parent predictions/targets with leaf ones

pred ⟵ concat(pred, addpred)

newcl ⟵ concat(newcl, addnewcl)

weight ⟵ concat(weight, addweight)

6. Return binary_cross_entropy_with_logits(pred, newcl, weight)

The hierarchical loss is available as a standalone function on GitHub Gist [2].

This loss replaces a classical pytorch classifier loss, such as binary_cross_entropy_with_logits.

Variable context length

The goal of the variable context length method is to decrease the model's bias toward a specific number of elements in context.

Indeed, we noticed that at inference time, the model's performance could be lower in variable-context situations (e.g., on gene-panel datasets or when using only expressed genes). We thus introduced a **variable-context** training scheme in which the model's context sometimes drops by a random amount (see Table 3.2 ; see Methods). This makes the model less biased toward a specific input context during inference and decreases training time (see Supplementary Materials). Again, here we see strong consistent improvement in the model's performance across our additive benchmark.

This can be applied to any transformer models where the number of elements in context can be chosen arbitrarily.

2. https://gist.github.com/jkobject/5b36bc4807edb440b86644952a49781e

Adversarial classifier loss

The goal of the Adversarial classifier is to remove batch effect[93,94].

The adversarial classifier is applied only to the *cell_type* cell embedding and is tasked to classify the organism of origin for each cell. It uses the same MLP as regular classifiers (2 layers, 256 as inner dimension). We use the reverse_gradient operation on top of a simple softmax-based binary cross-entropy classifier loss as follows :

Algorithm : L_adv (adversarial classifier) (4)

Input :

- e : input cell embedding tensor [batch_size × feature_dim]

- c : input ground truth label [batch_size]

Output : cross-entropy loss

// reverse the gradient for adversarial behavior

e = grad_reverse(e)

// compute logits from the embedding using an MLP

logits = MLP(e)

Return cross_entropy(logits, c)

with

Algorithm : grad_reverse (5)

Input :

- e : input tensor [batch_size × feature_dim]

- λ : scaling factor for gradient reversal = 1

Output : tensor with reversed gradients

If forward Pass :

1. Return e unchanged (identity function)

If backward Pass :

1. Reverse and scale the incoming gradients

e.grad_input ⟵ -λ × e.grad_output

2. Return reversed gradients

Return grad_input, None // None for λ parameter

We use it to predict both organisms and sequencers. Sequencers are mapped to a set of coarser labels, as we cannot use the hierarchical classifier in an adversarial context. Indeed,

as it is sigmoid-based, it could easily set all label logits to -inf.

This loss can be added during pre-training or finetuning of a foundation model, provided batch labels are available.

TF-masking task

The goal of the Transcription Factor (TF) masking task is to push the model to pay more attention to TFs than to other genes.

For the Transcription Factor masking task, we reuse the classic 30% masking task used in the base model (see Base Model). We then list the ENSEMBL IDs of all 13,000 TFs across our 16 organisms and sample our mask, giving increased weight to the TFs. Here, the weight is set up to be 10 for TFs and 1 for the rest.

The tool can be applied to any other set of genes as a replacement for classical masking in scFMs.

3.5.2 Additive Benchmark's datasets

The gene network analysis is performed on a test kidney single-cell dataset, using 1000 cells from the same cell type, and is compared with the omnipath ground truth (also known as the omnipath benchmark) across all cell types. It is also performed for 1000 K562 cells, comparing it to a network assembled from all genes "i" whose expression changes significantly when gene "j" is perturbed, using a genome-wide perturb-seq dataset called GWPS benchmark[95].

Knowing that perturb-seq still often implies cell-type- and patient-specific off-target effects and cannot detect many direct effects[96–99].

The cell type prediction uses accuracy, and batch correction uses scIB v2, as in Kalfon et al.[3]. Both the lung and pancreas datasets have also been used in Kalfon et al. They are test datasets, removed from the pre-training corpus, and both come from the initial scIB paper[100].

3.5.3 scPRINT-2

The model architecture is composed of :

— An **encoder/tokenizer** that takes multiple inputs, such as raw expression data, gene names, and gene locations, and embeds them in a high-dimensional space used by the transformer.
— A **trunk** with a bidirectional multi-head transformer, an XPressor bidirectional multi-head transformer, and a set of VAEs applied to each XPressor output embeddings.

— A **class decoder** that transforms the output cell embeddings of the XPressor into cell-specific label prediction logits over a range of classes.
— An **expression decoder** to transform the output embeddings into expression values

Of the above-cited additive benchmark elements, scPRINT-2 contains : **XPressor, all databases, denoising**, **cluster-based sampling, elastic cell similarity, ZINB+MSE, VAE compressor, variable context with larger context, TF masking, GNN expression encoder, and fine-tuned ESM3** (See Supplementary Figures 6.4.1, 6.4.9, 6.4.17, 6.4.18)

We now go into some more details about the model :

Encoder / Tokenizer

In scPRINT-2, each gene in a cell is converted to an embedding : It corresponds to the sum of 3 different elements :

1. An embedding representing the gene itself using ESM3 with a fine-tuning adaptor layer (see Methods)

2. An embedding of the gene location in the genome. This helps the model understand that genes with similar locations tend to be regulated by similar regulatory regions[101], a relationship well-known in cellular biology.

We encode the genes' locations using positional encoding. Every gene within 10,000 bp of the next is considered to be in the same location ; otherwise, we increment the location by 1. We do this for all genes in the Ensembl database per organism.

We then embed these locations using the Positional Encoding (PE) algorithm of Vaswani et al. [83]. We notice that adding this embedding was important to prevent divergence during training.

3. An embedding of the gene expression in the cell and its neighbor using our **GNN** (see Methods)

Finally, during pre-training, a subset of 3200 genes is used to encode a cell expression profile. If fewer than 3200 genes are expressed in both the cell and its neighbors, we pad them with randomly sampled unexpressed genes (meaning with an expression value of 0). This approach allows the model to see different patches of the same cell profile during training.

The full set of embeddings of cell i sent to the transformer is the matrix X_i where

$$X_i = [g_0 + e_{i,0} + l_0\ ,\ g_1 + e_{i,1} + l_1\ ,\ \dots\ ], \quad (15)$$

Where g_j is the gene j encoding, $e_{i,j}$ is the encoding of the expression of gene j in cell i, l_j is the gene j location encoding.

Additionally, the Xpressor layers will receive a set of learnt prototype tokens representing the different class-level cell embeddings.

Trunk

The model "trunk" is a bidirectional encoder similar to BERT[102] with n layers, h attention heads, and a dimension of d. It uses the flashattention2[103] methodology implemented in Triton to compute its attention matrix. It uses the pre-normalization technique[104], with a sped-up layer norm implemented in Triton's tutorial[105]. It uses stochastic depth with increasing dropout probability[106] (see Base for details about small and medium-sized models).

It has a 2-layer MLP with a 4x width increase in its hidden layer and a GELU activation function.

Each Layer or block is composed, in order, of a layer-norm, self-attention, layer-norm, MLP, and layer-norm, cross-attention, layer-norm, MLP, which are only used during the decoding step. It has an additional m Xpressor blocks/layers applied to its 10 latent cell tokens.

The output cell embeddings of the Xpressor layers are then compressed with VAEs with respective latent for the [cell_type, tissue, age, sex, disease, sequencer, ethnicity, organism, cell culture, additional] classes of : 64, 32, 8, 2, 16, 8, 8, 8, 2, None (no VAE)

Class Decoders

The class decoders are MLPs applied to compressed representations of their respective VAEs, with a shape of $[\mu_c,\ 256,\ n_c]$ with n_c the number of labels in the class c and μ_c the dimension of this class for the VAE.

Expression Decoder

We had noticed that scPRINT-1 initially produced embeddings that could be biased by the cell-depth token. We thus push scPRINT-2 to be depth-invariant by introducing the sequencing depth information only in the Expression Decoder, ensuring that the output gene-cell tokens contain little absolute sequencing depth information (see Figure 3.4, see Supplementary Figure 6.4.1). This debiases cell embedding to depth data and also improves denoising (see Table 1).

The expression decoder thus gets applied to the output gene embeddings and also receives the log2p1-transformed sequencing depth (also called total cell expression count) c andis of the form :

$$\mu,\ \theta,\ \pi\ =\ MLP(e\ ||\ c) \quad (16)$$

The MLP is a two-layer neural network with dimensions [d+1, d, 3], where || denotes the concatenation operation.

The parameters $\mu,\ \theta,\ \pi$ are the parameters of the ZINB and are used in the ZINB+MSE loss.

3.5.4 Pre-training

The three main tasks in the multi-task pre-training of scPRINT-2 are denoising, classification, and bottleneck learning. While the denoising loss enhances the model' s ability to find meaningful gene-gene connections, the other two try to make the model and its cell embedding representation more robust and cell-type-specific. The tasks are presented below.

Optimization method

Optimization is performed with fused ADAMW and a weight decay of 0.01. We observed a complete inability to learn when using the base ADAM algorithm, which has a similar weight decay schedule. This can be explained by a known inequivalence issue in ADAM[107].

We do not use the stochastic weight averaging[108] method during training.

During pre-training, the hyperparameters are set to a dropout of 0.1, a learning rate (LR) of 1e-4, and the precision is set to 16-mixed with residuals in fp32. We clip gradients to 10 and train over many sub-epochs of 20,000 training and 20,000 validation batches, with a warmup of 2,000 steps. Across epochs, we use a linear LR decrease of 0.6 with a patience of 2, and we stop training after 4 consecutive increases in validation loss. We initialize weights to a normal distribution around 1, biases to 0, and biases for the final layer of the Classifiers to -0.12.

Our batch size is 128, and we use a pre-norm strategy for the transformer with a linearly increasing stochastic depth dropout rate of 0.02 per layer. We use a noise parameter of 70%. We split the cells in the datasets into 98% for training and 2% for validation, and reserve at least 2% of the split datasets for testing. Our reconstruction loss is ZINB+MSE (see the ZINB+MSE section in Methods).

While many pre-training variants can be selected from contrastive learning, classification, adversarial classification, compression (with XPressor and VAE), masking, biased masking, and imputation, the choice may depend on specific biological assumptions.

scPRINT-2 is trained with denoising an input cell profile, given its nearest neighbor's expression.

Given the same information, it also performs label prediction during pre-training for : cell type, disease, sequencer, age, tissue, ethnicity, sex, cell culture, and organism. The classification task is performed jointly with the denoising task, meaning that labels are predicted from corrupted expression data and from nearest-neighbor expression information. The hierarchical classifier is applied to the VAEs' latent embeddings.

During decoding, it regenerates the expression profile for all input genes, including those dropped during variable context selection. This effectively does gene imputation.

The decoder receives only the gene location and ESM3 embedding and performs cross-attention on cell embeddings. The cell embeddings are the output of the VAEs and Xpressor layers, so the input is :

$X_i = [g_0 + l_0\ ,\ g_1 + l_1\ ,\ \ldots\ ]$, (17)

And cell-embeddings are :

$C_i = [c_{i0}, c_{i1}, \ldots] = \cup_j VAE_j(u_{ij})\ u_{ij} \in U_j$ (18)

With U_j the matrix output of Xpressor.

Finally, Embedding independence and Elastic Cell similarity losses are applied to the cell embeddings C_i for all cells i in the minibatch.

Database and sampling

The scPRINT-2 pre-training corpus is composed of all listed databases with weighted random sampling over all predicted labels, together with cluster-weighted sampling to compensate for missing cell-type labels in the Arc's scBasecount database.

Practically, during training, we apply a curriculum learning strategy whereby the S_1 factor slowly increases from 1 to 1000, letting the model initially learn across the diversity of cells and slowly retrieve the true cell state and modality distribution. We also apply depth-weighted cell sampling to each cell group (see the cluster-weighted sampling section in Methods).

Denoising pre-training task

We downsample an expression profile using a zero-inflated Poisson model of the data, following the approach in Kalfon et al. With this formulation, on average, half of the counts to be dropped are removed by randomly selecting some reads per gene, sampled from a Poisson distribution with a lambda parameter proportional to the gene' s count. The remaining half of the counts to be dropped are dropped by randomly setting some genes to 0, i.e., complete dropout of those genes. It is to be noted that, with this definition of downsampling, the exact average number of counts dropped in both parts depends slightly on the dropout *rrate.* During our pre-training, r is set to 0.7, meaning, on average, 35% of the transcript counts are dropped per cell.

Let x_i be the gene expression vector of cell i with dimensions n_{genes} ; we create a downsampled *version* by doing

$\widehat{x_i} = max((x_i - p_i) \cdot \pi_i,\ 0)$, (19)

with :

- $m \sim Uniform(0, r)$ the noise level
- $p_i \sim Poisson(x_i \times r \times 0.55)$ a vector of size n_{genes} where the Poisson is sampled for each element x_i of x
- $\pi_i = I(u \geq r \times 0.55)$ a vector of size n_{genes} , the binary mask vector indicating non-dropout genes.

- $u_i \sim Uniform(0, 1)$, a vector of size n_{genes}, of random values drawn from a uniform distribution.
- $\cdot$ denotes the element-wise multiplication.
- r being the dropout amount. We scale it by a tuning hyperparameter of 0.55 instead of 0.5 for numerical reasons.

We uniformly sample a value between 0 and 0.8 for our r, per GPU, during training of scPRINT-2 and other additive models based on denoising, except if noted otherwise.

For the GNN-encoder, we add a second "denoising" step in which we set the noise to 1 and set all expressions to 0 for the center cell. This required the model to predict its expression from the expressions of its neighbors in expression space on the same dataset.

Bottleneck learning pre-training task

During training, we predict gene expression at both the decoder output and the scPRINT-2⟶Expressor⟶scPRINT-2 pipeline outputs, following the XPressor approach in Kalfon et al.

During training, 20% of the time, scPRINT-2 drops between 0 and 2800 genes from its input context per GPU. This pushes the model to learn across a variety of context lengths, it also makes the contrastive loss more robust. Finally, at the output of the decoding step in the bottleneck learning part, the model always predicts across the full 3200 genes, effectively performing imputation during pre-training.

When cross-GPU training is performed, cell-embedding-level losses are computed across all GPUs.

Classification pre-training task

The Classification task follows the new hierarchical classifier presented in Methods and adds two novel classes : patient age and tissue of origin.

Loss aggregation

The losses are aggregated as follows :

$$L = L_{ZINB+MSE} + L_{class} + 0.2L_{similarity} + 0.3L_{independance} + 0.2L_{contrastive} + 0.001L_{KL} \quad (20)$$

The $L_{ZINB+MSE}$ is effectively added 4 times, for the reconstruction post perturbations with denoise of 0.8, 1.0, TF-masking, and post bottleneck learning.

3.5.5 Fine-tuning Task

Our fine-tuning (see Results section 2 and 4) reuses the classification, bottleneck learning, and VAE (KL) loss of our pre-training for 4 epochs with a learning rate of 0.0001. For batch correction and organism integration, we add the MMD loss between samples from batches 1 and 2 within each minibatch[67,68]. At the same time, an effective MMD loss requires minibatches that are large enough to include a good mix of both label types and cannot accommodate many labels.

With the MMD loss defined as :

$$MMD\check{s}(X,\ Y) = \frac{1}{m\check{s}} \sum_{i=1}^{m} \sum_{i'=1}^{m} k(x,\ x) + \frac{1}{n\check{s}} \sum_{j=1}^{n} \sum_{j'=1}^{n} k(y,\ y) - \frac{2}{nm} \sum_{i=1}^{m} \sum_{j=1}^{n} k(x,\ y) \quad (21)$$

For a finite set of elements from distribution source X and Y, where we use the energy distance kernel :

$$-\ k(x,\ y) = -|x - y|$$

When more than 2 domains exist, we compute MMD between each domain and the remaining domains.

All analyses are defined in the notebook : notebooks/scPRINT-2-repro-notebooks/fine_tuning_cross_species_emb_mmd.ipynb

3.5.6 Classification task

For our classifications tasks (see Results section 2), we use the F1-accuracy as our primary metric. When computing it across hierarchical classes, we consider parental relationships to ensure that even if a more precise cell type is predicted than the ground truth, it remains valid. For example, given a ground truth label of *neuron,* a predicted label of *excitatory neuron* will be considered correct.

If "unknowns" exist in the ground truth or the prediction, they are discarded from the metric.

The cross-organism generalization classification dataset was extracted from the supplementary datasets of the paper titled "Benchmarking cross-organism single-cell RNA-seq data integration methods : towards a cell type tree of life"[46] available at Figshare [3].

The context-increase classification analysis was performed on the "human multiple cortical areas"[109] Smart-seq v4 dataset available at cellxgene [4]. For each nnz gene level, we used only cells with at least that many genes expressed. We did not apply the same logic to the second version and used a smaller dataset, so the impact of zero-expressed genes in context could be more clearly seen.

3. https://figshare.com/s/6187811b6c3fae02a4d3?file=50608386
4. https://datasets.cellxgene.cziscience.com/a1d40c84-c81c-406f-bef4-e25edeb651e5.h5ad

All analyses are defined in the notebooks : notebooks/scPRINT-2-repro-notebooks/cross_species_embedding.ipynb

notebooks/scPRINT-2-repro-notebooks/smart_seq_class.ipynb

notebooks/scPRINT-2-repro-notebooks/unknown_species_classification.ipynb

notebooks/scPRINT-2-repro-notebooks/large_dataset_anallysis.ipynb

figures/nice_umap.py

notebooks/scPRINT-2-repro-notebooks/batch_corr_op ft.ipynb

notebooks/scPRINT-2-repro-notebooks/batch_corr_op v1.ipynb

notebooks/scPRINT-2-repro-notebooks/batch_corr_op.ipynb

notebooks/scPRINT-2-repro-notebooks/plot.ipynb

Logits refinement (Laplacian smoothing)

We apply logits smoothing at inference by computing the k-nearest neighbors of each cell and their distances, listed in the squared sparse matrix D, and solving for :

$\bar{P} = argmin_P ||P - P||\check{s}_F + \lambda Tr(P^T L P)$ (23)

Where P are the initial logits,

L is the graph Laplacian, and λ controls the strength of regularization and has a default value of 0.1[47]. In our case, we set K to be 6, and $L = (D + D^\top - C)$ where C is the diagonal degree matrix of $D + D^\top$.

The solution has a closed form : $\bar{P} = (I + \lambda L)\acute{z}P$

Cluster-aggregation

We compute the per-cluster logits aggregation by first clustering the test dataset and then taking the maximum logits across all cells in each cluster as the label for that cluster. Solving for :

$p_c = argmax_i(max_j(l_{i,j}))$ (24)

For $l_{i,j} \in L_c$ the j logits across all cells i in the cluster C

and p_c the prediction for cluster C

3.5.7 Denoising task

The denoising benchmark (see Results section 3) was performed on eight datasets of varying quality, assessed by the number of non-zero genes (nnz), sequencing depth, and the

distribution of gene counts.

We compute denoising as the dataset-wise percentage improvement in correlation over the 5000 most variable genes, considering only genes that are non-zero in the ground-truth.

Here is the dataset list (all cellxgene datasets available at https://datasets.cellxgene.cziscience.com/) :

- retina : 53bd4177-79c6-40c8-b84d-ff300dcf1b5b.h5ad
- kidney : 01bc7039-961f-4c24-b407-d535a2a7ba2c.h5ad
- pancreas : https://figshare.com/ndownloader/files/24539828
- intestine : d9a99b4a-3755-47c4-8eb5-09821ffbde17.h5ad
- glio_smart_highdepth : 6ec440b4-542a-4022-ac01-56f812e25593.h5ad
- lung_smart : 6ebba0e0-a159-406f-8095-451115673a2c.h5ad

human from scbasecount ID : SRX24486462 and SRX22526970

All analyses are defined in the notebook : notebooks/scPRINT-2-repro-notebooks/denoising_V2.ipynb

3.5.8 Xenium analysis

We apply the Xenium analysis on the FFPE Human Skin Primary Dermal Melanoma with 5K Human Pan Tissue and Pathways Panel found on the 10X genomics platform under :

https://www.10xgenomics.com/datasets/xenium-prime-ffpe-human-skin

Information on the dataset and its preprocessing can be found on the same webpage.

We extract a dense patch that covers 30% of the cells in the dataset, on which we perform all our analyses (see Results section 3).

3.5.9 All analyses are defined in the notebooks : notebooks/scPRINT-2-repro-notebooks/xenium_analysis.ipynb

3.5.10 Embedding task

We perform the organism-level integration task on the same two datasets listed above from the “Benchmarking cross-organism single-cell RNA-seq data integration methods : towards a cell type tree of life” paper, using the scIB metrics and the same ground truth labels (see Results section 4).

All analyses are defined in the notebooks : notebooks/scPRINT-2-repro-notebooks/cross_species_embedding.ipynb

notebooks/scPRINT-2-repro-notebooks/generative_modelling.ipynb

notebooks/scPRINT-2-repro-notebooks/batch_corr_op ft.ipynb

notebooks/scPRINT-2-repro-notebooks/batch_corr_op v1.ipynb

notebooks/scPRINT-2-repro-notebooks/batch_corr_op.ipynb

notebooks/scPRINT-2-repro-notebooks/plot.ipynb

3.5.11 Generative task

We perform the generative tasks on two human/mouse datasets extracted from the supplementary datasets of the paper titled "Benchmarking cross-organism single-cell RNA-seq data integration methods : towards a cell type tree of life" (see Results section 4).

We generate cell-embeddings for all mouse cells, giving us a matrix M of size $[10,\ n_{cell},\ d_{emb}]$. We then retrieve an average human organism embedding by using 2000 randomly selected human cells and averaging their organism cell-embedding, resulting in a vector v of size $[d_{emb}]$. We then regenerate an expression profile using the mouse cell-embeddings and the human average organism embedding by replacing it in the matrix like so : $M[:, i, :] = v$.

We then apply the decoder part of scPRINT, which performs cross-attention over the matrix M and takes the human gene embeddings as input tokens.

All analyses are defined in the notebook :

scRNA-seq datasets distances

To compute our distance metric across two scRNA-seq datasets, we first identify the 5000 most variable genes that are also orthologous between the datasets. We use human and mouse data because orthology was readily accessible and well-defined.

We then compute the W2-distance directly on the raw mouse counts, the humanized counts predicted by scPRINT-2, and the human counts. We do not expect a zero or near-zero W2 distance between the humanized mouse data and the human data, as the number of cells, the types of cell, and their composition differ between the two datasets. We perform a similar analysis of the male-to-female conversion.

Over-representation measure

For the overrepresentation analysis and plot, we work on the ordered differential expression gene lists for both human-to-mouse and humanized-mouse-to-mouse, and similarly for male-to-female conversion. We compare the overlap in genes between the two lists at all possible cutoff values from 1 to 5000 to obtain our curve and, therefore, define scores.

3.5.12 Assessment of gene output embeddings

We assess scPRINT-2's gene output embeddings by computing output gene embedding oe a random *vascular lymphangioblast* cell from the glioblastoma Smart-seq-v2 dataset using its 5000 most expressed genes in that cell type. We then cluster it using the Leiden algorithm and, for each clustered group of genes, compute the number of pathways enriched using the "KEGG_2021_Human", "GO_Molecular_Function_2025", "WikiPathways_2024_Human", and "GO_Cellular_Component_2025" gene set databases. Doing this for both XPressor and non-XPressor architectures, we then compute a t-test between the two sets of numbers.

All analyses are defined in the notebooks :

notebooks/scPRINT-2-repro-notebooks/output_embeddings.ipynb

3.5.13 Extracting meta-cell gene networks from attention matrices

in scPRINT

Transformers compute multiple attention matrices per layer, called attention heads. This is done by splitting the generated K, Q, and V embedding into m sub-embeddings, thus defining m attention heads. Each attention head computes the attention matrix via the equation :

$$\text{softmax}\left(\frac{QK^T}{\sqrt{d}}\right) \tag{3.4}$$

However, we want to aggregate those across multiple cells with similar cell states to increase the signal from a single cell. We are doing so by averaging the Keys and Queries embeddings over the set of cells U passed to the model :

$$\text{softmax}\left(\frac{\text{mean}_U(Q) \cdot \text{mean}_U(K)^T}{\sqrt{d}}\right) \tag{3.5}$$

By doing this, the attention matrix behaves as if each query vector for cell i were "looking" across the key vectors of all the cells in U. The resulting object is a row-wise normalized n^*n matrix, where n is the size of the input context (i.e., the number of genes passed to the model).

in scPRINT-2

In scPRINT-2, we found, after in-depth review, that while the solution from equation (25) allows for faster computation of much larger gene networks from attention matrices, it also decreases accuracy. We thus instead directly took :

$$\text{mean}_U\left(\text{softmax}\left(\frac{QK^T}{\sqrt{d}}\right)\right) \tag{3.6}$$

However, to prevent adding QK from genes that are not expressed in the given cell, we generate Qs and Ks from forward passes using only the expressed genes in each cell (see "using only expressed genes" in additive benchmark). This has the benefit of biasing the gene network towards genes that are co-expressed in the set of cells we are computing it on.

This means that for a list of n genes, each cell will have a subset of m Qs,Ks. We thus take the average of the set, computing the mean per gene by counting how many times each gene was expressed across the set of cells.

plotting gene sub-networks

To plot a subset of our gene networks, we choose a seed gene and get all its top-K connected nodes. We then overlay the top-N edges in this sub-network, ordered by connection strength. Here K=15 and N=50

3.5.14 Gene network task

We generated gene networks from notebooks : https://figshare.com/s/6187811b6c3fae02a4d3 ?file=50608

We used a matched cross-tissue human and mouse dataset from Zhong et al.[46]

We computed the network across all 10 cell types that were common to both human and mouse in the dataset, using the 4000 most variable genes within each cell type, with a maximum of 1024 cells (see Results section 5).

All analyses are defined in the notebooks : notebooks/scPRINT-2-repro-notebooks/gene_networks.ipynb

notebooks/scPRINT-2-repro-notebooks/gene_networks_var_2.ipynb

The Cellmap Ground truth

We used the Cellmap dataset available at https://ndexbio.org under uuid f693137a-d2d7-11ef-8e41-005056ae3c32.

It has a total of 36842 connections across 7543 genes, mainly computed from protein-binding data of AP-MS experiments in the O2US cell line[74].

The Collectri and Omnipath Ground truth

We used the Collectri ground truth from the Decoupler : https://github.com/scverse/decoupler package and the Omnipath ground truth from the Omnipath package[110,111] : https://github.com/saezlab/omnipath, both accessible with given versions within the BenGRN package : https://github.com/jkobject/benGRN.

The human interactome Ground truth

We use the RF2-PPI predicted network available at https://conglab.swmed.edu/humanPPI/. We set a cutoff of 0.4 for the benchmark and 0.7 for the high-quality (hq) network[112].

3.5.15 Gene network metrics

We use the packages benGRN and GRnnData released with this manuscript to work With Gene networks and perform our benchmarks (see Results section 5).

Our two main metrics are OR and AUPRC. They all take advantage of the fact that the predictions are generated as scores over edges between nodes :

- We have computed the diagnostic odds ratio (OR) as (TP x TN) / (FP x FN) at the cutoff score that yields K positive predictions, where K is the number of positive elements in the ground truth.
  In this context, 1 represents a random prediction, and inf represents a perfect prediction ; values below one indicate that inverting the predictor would yield better results.
- Area Under the Precision-Recall Curve (AUPRC) is the area (computed with the composite trapezoidal rule) under the curve defined by the precision ($PR = TP / (TP + FP)$) and recall ($RE = TP / (TP + FN)$), where TP is the number of true positives. FP is the number of false positives. FN is the number of false negatives. This curve is obtained by varying the cutoff from 0 predicted positives to all predicted positives. Here, we compute a version of the AUPRC where the floor of the area is not given by the Precision=0 line but by the prevalence line of the positive class. Moreover, we do not interpolate the curve between the last recall value and the perfect recall : 1. We do this to properly compare AUPRC values across benchmarks and models. Random precision values are given in the supplementary data.

3.5.16 Open Problem benchmarks

We ran all the open-problem benchmark datasets for scPRINT-2 and scPRINT-1 on a local machine, following the instructions at https://openproblems.bio/documentation. We used the same datasets and labels available at : s3://openproblems-data/resources/ (see Results sections 2 and 4). We used the non-transformed count matrices as input. We used the same metrics for classification, the same scIB package version, and the same train-test splits as in the latest run of Open Problems. All other scores displayed are directly copied from that latest run.

On Open-problems, scIB's batch correction score is equal to (avgBatch + 1.5*avgBio)/2.5, which are themselves averages over many scores. Details of each value are available in our package's notebooks[100].

- scIB avgBio is a combination of label-based and label-free metrics, using, for example,

the Adjusted Rand Index (ARI)[113] and the Normalized Mutual Information (NMI)[114] on clusters computed from the K-Nearest Neighbor graph. Other scores are used, some based on the conservation of trajectories and cell-cycle variance, others on the conservation of rare-cell populations, the overlap of highly variable genes (see scIB[100]), and more.

— scIB avgBatch is a similar combination of label-based and label-free metrics, using, for example, the average connectivity across clusters of different batches : ASW[115], the graph integration local inverse Simpson's Index : graph iLISI[116], the k-nearest-neighbor Batch Effect Test (kBET)[115], and more.

Finally, we also use two metrics in our classification task :

— Macro-F1 : also called macro-average, is the average of the F1 score across each class in a multi-class task, where the F1 score is : $2 \times \frac{PR*RE}{PR+RE}$.

— Accuracy : is computed as $\frac{TP + TN}{TP+TN +FN+FP}$

We did not run on two datasets of Open Problems : immune_cell_atlas & tabula_sapiens, as their sizes were too large for us to run scib on any of our available machines.

Moreover, while we believe it is the same for other foundation models assessed in this benchmark, most of these datasets are part of the pre-training corpus of scPRINT. Therefore, the "zero-shot" performance claims, especially classification, should be viewed in this context.

Finally, Open Problem is a living benchmark. Methods, Results, datasets, and metrics will likely change as the scores are continuously updated. We hereby present our results as they were in the 12th of November 2025.

3.6 Data availability

The model weights are publicly available on HuggingFace under : https://huggingface.co/jkobject. Pre-training logs to assess the model's training are publicly available in weights and biases [5].
The embeddings and classification results over the 350 million cells are available under the public google bucket : gs://scprint2/. The interactive viewer for a subset of these cells is available at https://cantinilab.github.io/scPRINT-2/.
The pre-training dataset is publicly available on CellxGene : https://cellxgene.cziscience.com/, under its census data release version : LTS 2024-07-01, Tahoe and ARC's scBasecount are available on https://github.com/ArcInstitute/arc-virtual-cell-atlas, commit version 68da110. All other datasets used in this work can be downloaded from their respective public databases using the helper scripts in the scPRINT, BenGRN, GRnnData, and scDataLoader packages.

5. https://wandb.ai/ml4ig/scprint_ablation/reports/scPRINT-2-additive-benchmark--VmlldzoxNTIyOTYwNA

Source data is provided with this paper to re-generate the figures. Code to download the input dataset, generate the source data, and the figures are available as a notebook in https://github.com/cantinilab/scPRINT-2. Source data are provided with this paper.

3.7 Code availability

The code and notebooks used to develop the model, perform the analyses, and generate results in this study are publicly available and have been deposited in cantinilab/scPRINT-2 at https://github.com/cantinilab/scPRINT-2 under GPLv3 license. The specific version of the code associated with this publication is archived in the same repository under the tag 1.0.0 and is accessible via https://github.com/cantinilab/scPRINT-2/tree/1.0.0/ and DOI:10.5281/zenodo.

Additional packages for this analysis are defined in the pyproject file and project submodules. Together with packages developed by us :

- GrnnData : https://github.com/cantinilab/GRnnData DOI:10.5281/zenodo.10573141
- BenGRN : https://github.com/jkobject/benGRN DOI:10.5281/zenodo.10573209
- scDataLoader : https://github.com/jkobject/scDataLoader DOI:10.5281/zenodo.10573143

3.8 References

1. Cui, H. *et al.* scGPT : toward building a foundation model for single-cell multi-omics using generative AI. *Nat. Methods* 1–11 (2024) doi:10.1038/s41592-024-02201-0.

2. Theodoris, C. V. *et al.* Transfer learning enables predictions in network biology. *Nature* **618**, 616–624 (2023).

3. Kalfon, J., Samaran, J., Peyré, G. & Cantini, L. scPRINT : pre-training on 50 million cells allows robust gene network predictions. *Nat. Commun.* **16**, 3607 (2025).

4. Wen, H. *et al.* CellPLM : Pre-training of Cell Language Model Beyond Single Cells. 2023.10.03.560734 Preprint at https://doi.org/10.1101/2023.10.03.560734 (2023).

5. Xiong, L., Chen, T. & Kellis, M. scCLIP : Multi-modal Single-cell Contrastive Learning Integration Pre-training. in (2023).

6. Zhao, S., Zhang, J., Wu, Y., Luo, Y. & Nie, Z. LangCell : language-cell pre-training for cell identity understanding. in *Proceedings of the 41st International Conference on Machine Learning* vol. 235 61159–61185 (JMLR.org, Vienna, Austria, 2024).

7. Yang, F. *et al.* scBERT as a large-scale pretrained deep language model for cell type annotation of single-cell RNA-seq data. *Nat. Mach. Intell.* **4**, 852–866 (2022).

8. De Donno, C. *et al.* Population-level integration of single-cell datasets enables multi-scale analysis across samples. *Nat. Methods* **20**, 1683–1692 (2023).

9. Yang, X. *et al.* GeneCompass : Deciphering Universal Gene Regulatory Mechanisms with Knowledge-Informed Cross-Species Foundation Model. 2023.09.26.559542 Preprint at https://doi.org/10.1101/2023.09.26.559542 (2023).

10. Bai, D. *et al.* scLong : A Billion-Parameter Foundation Model for Capturing Long-Range Gene Context in Single-Cell Transcriptomics. 2024.11.09.622759 Preprint at https://doi.org/10.1101/2024.11.09.622759 (2024).

11. Zeng, Y. *et al.* CellFM : a large-scale foundation model pre-trained on transcriptomics of 100 million human cells. *Nat. Commun.* **16**, 4679 (2025).

12. Tejada-Lapuerta, A. *et al.* Nicheformer : a foundation model for single-cell and spatial omics. *Nat. Methods* 1–14 (2025) doi:10.1038/s41592-025-02814-z.

13. Pearce, J. D. *et al.* A Cross-Species Generative Cell Atlas Across 1.5 Billion Years of Evolution : The TranscriptFormer Single-cell Model. 2025.04.25.650731 Preprint at https://doi.org/10.1101/2025.04.25.650731 (2025).

14. Ding, J. *et al.* Toward a privacy-preserving predictive foundation model of single-cell transcriptomics with federated learning and tabular modeling. 2025.01.06.631427 Preprint at https://doi.org/10.1101/2025.01.06.631427 (2025).

15. Fu, X. *et al.* A foundation model of transcription across human cell types. *Nature* **637**, 965–973 (2025).

16. Deeper evaluation of a single-cell foundation model | Nature Machine Intelligence. https://www.nature.com/articles/s42256-024-00949-w.

17. Liu, T., Li, K., Wang, Y., Li, H. & Zhao, H. Evaluating the Utilities of Foundation Models in Single-cell Data Analysis. 2023.09.08.555192 Preprint at https://doi.org/10.1101/2023.09.08.555192 (2024).

18. Reusability report : Exploring the transferability of self-supervised learning models from single-cell to spatial transcriptomics | Nature Machine Intelligence. https://www.nature.com/articles/s42256-025-01097-5.

19. Crowley, G. & Quake, S. R. Benchmarking cell type and gene set annotation by large language models with AnnDictionary. *Nat. Commun.* **16**, 9511 (2025).

20. Delineating the effective use of self-supervised learning in single-cell genomics | Nature Machine Intelligence. https://www.nature.com/articles/s42256-024-00934-3.

21. Nourisa, J. *et al.* geneRNIB : a living benchmark for gene regulatory network inference. 2025.02.25.640181 Preprint at https://doi.org/10.1101/2025.02.25.640181 (2025).

22. Bendidi, I. *et al.* Benchmarking Transcriptomics Foundation Models for Perturbation

Analysis : one PCA still rules them all. Preprint at https://doi.org/10.48550/arXiv.2410.13956 (2024).

23. Atti, S. & Subramaniam, S. Fundamental Limitations of Foundation Models in Single-Cell Transcriptomics. 2025.06.26.661767 Preprint at https://doi.org/10.1101/2025.06.26.661767 (2025).

24. Rusak, E. *et al.* InfoNCE : Identifying the Gap Between Theory and Practice. *arXiv.org* https://arxiv.org/abs/2407.00143v2 (2024).

25. Waele, G. D., Menschaert, G. & Waegeman, W. A systematic assessment of single-cell language model configurations. 2025.04.02.646825 Preprint at https://doi.org/10.1101/2025.04.02.646825 (2025).

26. Youngblut, N. D. *et al.* scBaseCount : an AI agent-curated, uniformly processed, and autonomously updated single cell data repository. 2025.02.27.640494 Preprint at https://doi.org/10.1101/2025.02.27.640494 (2025).

27. Megill, C. *et al.* cellxgene : a performant, scalable exploration platform for high dimensional sparse matrices. 2021.04.05.438318 Preprint at https://doi.org/10.1101/2021.04.05.438318 (2021).

28. Zhang, J. *et al.* Tahoe-100M : A Giga-Scale Single-Cell Perturbation Atlas for Context-Dependent Gene Function and Cellular Modeling. 2025.02.20.639398 Preprint at https://doi.org/10.1101/2025.02.20.639398 (2025).

29. Training foundation models on large collections of scRNA-seq data — Lamin Blog. https://blog.lamin.ai/arrayloader-benchmarks.

30. Malone, J. *et al.* Modeling sample variables with an Experimental Factor Ontology. *Bioinformatics* **26**, 1112–1118 (2010).

31. Wolf, F. A., Angerer, P. & Theis, F. J. SCANPY : large-scale single-cell gene expression data analysis. *Genome Biol.* **19**, 15 (2018).

32. A Comprehensive Survey on Data Augmentation. https://arxiv.org/html/2405.09591v3.

33. Kalfon, J., Cantini, L. & Peyre, G. Towards foundation models that learn across biological scales. 2025.05.16.653447 Preprint at https://doi.org/10.1101/2025.05.16.653447 (2025).

34. Lin, Z. *et al.* Language models of protein sequences at the scale of evolution enable accurate structure prediction. 2022.07.20.500902 Preprint at https://doi.org/10.1101/2022.07.20.500902 (2022).

35. Brixi, G. *et al.* Genome modeling and design across all domains of life with Evo 2. 2025.02.18.638918 Preprint at https://doi.org/10.1101/2025.02.18.638918 (2025).

36. OpenAI *et al.* GPT-4 Technical Report. Preprint at https://doi.org/10.48550/arXiv.2303.08774 (2024).

37. Kaplan, J. *et al.* Scaling Laws for Neural Language Models. Preprint at

https://doi.org/10.48550/arXiv.2001.08361 (2020).

38. Oquab, M. *et al.* DINOv2 : Learning Robust Visual Features without Supervision. Preprint at https://doi.org/10.48550/arXiv.2304.07193 (2024).

39. Chen, R. J. *et al.* Towards a general-purpose foundation model for computational pathology. *Nat. Med.* **30**, 850–862 (2024).

40. Chen, H. *et al.* Quantized multi-task learning for context-specific representations of gene network dynamics. 2024.08.16.608180 Preprint at https://doi.org/10.1101/2024.08.16.608180 (2024).

41. Predicting cellular responses to perturbation across diverse contexts with State | bioRxiv. https://www.biorxiv.org/content/10.1101/2025.06.26.661135v2.

42. Alsabbagh, A. R. *et al.* Foundation Models Meet Imbalanced Single-Cell Data When Learning Cell Type Annotations. 2023.10.24.563625 Preprint at https://doi.org/10.1101/2023.10.24.563625 (2023).

43. Luecken, M. D. *et al.* Defining and benchmarking open problems in single-cell analysis. *Nat. Biotechnol.* **43**, 1035–1040 (2025).

44. Rosen, Y. *et al.* Universal Cell Embeddings : A Foundation Model for Cell Biology. 2023.11.28.568918 Preprint at https://doi.org/10.1101/2023.11.28.568918 (2023).

45. Xu, L., Xie, H., Qin, S.-Z. J., Tao, X. & Wang, F. L. Parameter-Efficient Fine-Tuning Methods for Pretrained Language Models : A Critical Review and Assessment. Preprint at https://doi.org/10.48550/arXiv.2312.12148 (2023).

46. Zhong, H. *et al.* Benchmarking cross-species single-cell RNA-seq data integration methods : towards a cell type tree of life. *Nucleic Acids Res.* **53**, gkae1316 (2025).

47. Herrmann, L. R. Laplacian-Isoparametric Grid Generation Scheme. *J. Eng. Mech. Div.* **102**, 749–756 (1976).

48. Hu, T. *et al.* GRIT : Graph-Regularized Logit Refinement for Zero-shot Cell Type Annotation. Preprint at https://doi.org/10.48550/arXiv.2508.04747 (2025).

49. Jorstad, N. L. *et al.* Transcriptomic cytoarchitecture reveals principles of human neocortex organization. *Science* **382**, eadf6812 (2023).

50. Zaheer, M. *et al.* Deep Sets. Preprint at https://doi.org/10.48550/arXiv.1703.06114 (2018).

51. Corso, G., Stark, H., Jegelka, S., Jaakkola, T. & Barzilay, R. Graph neural networks. *Nat. Rev. Methods Primer* **4**, 17 (2024).

52. Dijk, D. van *et al.* Recovering Gene Interactions from Single-Cell Data Using Data Diffusion. *Cell* **174**, 716-729.e27 (2018).

53. Preview Data : FFPE Human Skin Primary Dermal Melanoma with 5K Human Pan Tissue and Pathways Panel. *10x Genomics* https://www.10xgenomics.com/datasets/xenium-prime-ffpe-human-skin.

54. Biancalani, T. *et al.* Deep learning and alignment of spatially resolved single-cell transcriptomes with Tangram. *Nat. Methods* **18**, 1352–1362 (2021).

55. Zhang, C. *et al.* A single-cell analysis reveals tumor heterogeneity and immune environment of acral melanoma. *Nat. Commun.* **13**, 7250 (2022).

56. Han, I. *et al.* HyperAttention : Long-context Attention in Near-Linear Time. Preprint at https://doi.org/10.48550/arXiv.2310.05869 (2023).

57. Zuhri, Z. M. K., Fuadi, E. H. & Aji, A. F. Softpick : No Attention Sink, No Massive Activations with Rectified Softmax. Preprint at https://doi.org/10.48550/arXiv.2504.20966 (2025).

58. Lee, J. *et al.* Set Transformer : A Framework for Attention-based Permutation-Invariant Neural Networks. Preprint at https://doi.org/10.48550/arXiv.1810.00825 (2019).

59. Jabri, A., Fleet, D. & Chen, T. Scalable Adaptive Computation for Iterative Generation. Preprint at https://doi.org/10.48550/arXiv.2212.11972 (2023).

60. Lopez, R., Regier, J., Cole, M. B., Jordan, M. I. & Yosef, N. Deep generative modeling for single-cell transcriptomics. *Nat. Methods* **15**, 1053–1058 (2018).

61. Moinfar, A. A. & Theis, F. J. Unsupervised Deep Disentangled Representation of Single-Cell Omics. 2024.11.06.622266 Preprint at https://doi.org/10.1101/2024.11.06.622266 (2025).

62. Xu, C. *et al.* Probabilistic harmonization and annotation of single-cell transcriptomics data with deep generative models. *Mol. Syst. Biol.* **17**, MSB20209620 (2021).

63. Jaegle, A. *et al.* Perceiver IO : A General Architecture for Structured Inputs & Outputs. Preprint at https://doi.org/10.48550/arXiv.2107.14795 (2022).

64. Jaegle, A. *et al.* Perceiver : General Perception with Iterative Attention. in *Proceedings of the 38th International Conference on Machine Learning* 4651–4664 (PMLR, 2021).

65. Carreira, J. *et al.* HiP : Hierarchical Perceiver. Preprint at https://doi.org/10.48550/arXiv.2202.10890 (2022).

66. Lee, C. *et al.* NV-Embed : Improved Techniques for Training LLMs as Generalist Embedding Models. Preprint at https://doi.org/10.48550/arXiv.2405.17428 (2025).

67. Ouyang, L. & Key, A. Maximum Mean Discrepancy for Generalization in the Presence of Distribution and Missingness Shift. Preprint at https://doi.org/10.48550/arXiv.2111.10344 (2022).

68. Zhang, C. Single-Cell Data Analysis Using MMD Variational Autoencoder for a More Informative Latent Representation. 613414 Preprint at https://doi.org/10.1101/613414 (2019).

69. McInnes, L., Healy, J. & Melville, J. UMAP : Uniform Manifold Approximation and Projection for Dimension Reduction. Preprint at https://doi.org/10.48550/arXiv.1802.03426 (2020).

70. Flamary, R. *et al.* POT : Python Optimal Transport. *J. Mach. Learn. Res.* **22**, 1–8 (2021).

71. Peyré, G. & Cuturi, M. Computational Optimal Transport. Preprint at https://doi.org/10.48550/arXiv.1803.00567 (2020).

72. Wang, M., Zhang, J., Qiao, C., Yan, S. & Wu, G. Comparative analysis of human and mouse transcriptomes during skin wound healing. *Front. Cell Dev. Biol.* **12**, (2024).

73. He, M. & Borlak, J. A genomic perspective of the aging human and mouse lung with a focus on immune response and cellular senescence. *Immun. Ageing* **20**, 58 (2023).

74. Schaffer, L. V. *et al.* Multimodal cell maps as a foundation for structural and functional genomics. *Nature* **642**, 222–231 (2025).

75. Mesquita, G. *et al.* H-Ferritin is essential for macrophages' capacity to store or detoxify exogenously added iron. *Sci. Rep.* **10**, 3061 (2020).

76. Bock, K. W. Ah receptor, vitamin B12 and itaconate : how localized decrease of vitamin B12 prevents survival of macrophage-ingested bacteria. *Front. Toxicol.* **6**, 1491184 (2024).

77. Fang, Z., Liu, X. & Peltz, G. GSEApy : a comprehensive package for performing gene set enrichment analysis in Python. *Bioinformatics* **39**, btac757 (2023).

78. Grossmann, G. *Deep Sets Are Viable Graph Learners*. (2023).

79. Hayes, T. *et al.* Simulating 500 million years of evolution with a language model. *Science* **387**, 850–858 (2025).

80. Aibar, S. *et al.* SCENIC : single-cell regulatory network inference and clustering. *Nat. Methods* **14**, 1083–1086 (2017).

81. Jabri, A., Fleet, D. & Chen, T. Scalable Adaptive Computation for Iterative Generation. Preprint at https://doi.org/10.48550/arXiv.2212.11972 (2023).

82. Hawthorne, C. *et al.* General-purpose, long-context autoregressive modeling with Perceiver AR. Preprint at https://doi.org/10.48550/arXiv.2202.07765 (2022).

83. Vaswani, A. *et al.* Attention Is All You Need. Preprint at https://doi.org/10.48550/arXiv.1706.03762 (2023).

84. Kingma, D. P. & Welling, M. An Introduction to Variational Autoencoders. *Found. Trends® Mach. Learn.* **12**, 307–392 (2019).

85. Mentzer, F., Minnen, D., Agustsson, E. & Tschannen, M. Finite Scalar Quantization : VQ-VAE Made Simple. Preprint at https://doi.org/10.48550/arXiv.2309.15505 (2023).

86. Jiang, R., Sun, T., Song, D. & Li, J. J. Statistics or biology : the zero-inflation controversy about scRNA-seq data. *Genome Biol.* **23**, 31 (2022).

87. Lopez, R., Regier, J., Cole, M. B., Jordan, M. I. & Yosef, N. Deep Generative Modeling for Single-cell Transcriptomics. *Nat. Methods* **15**, 1053–1058 (2018).

88. Rusak, E. *et al.* InfoNCE : Identifying the Gap Between Theory and Practice. Preprint at https://doi.org/10.48550/arXiv.2407.00143 (2025).

89. Diehl, A. D. *et al.* The Cell Ontology 2016 : enhanced content, modularization, and ontology interoperability. *J. Biomed. Semant.* **7**, 44 (2016).

90. Mondo : Unifying diseases for the world, by the world | medRxiv. https://www.medrxiv.org/content/10.1101/2022.04.13.22273750v3.

91. EBISPOT/efo. EBISPOT (2024).

92. Morales, J. *et al.* A standardized framework for representation of ancestry data in genomics studies, with application to the NHGRI-EBI GWAS Catalog. *Genome Biol.* **19**, 21 (2018).

93. Goodfellow, I. J. *et al.* Generative Adversarial Networks. Preprint at https://doi.org/10.48550/arXiv.1406.2661 (2014).

94. Shree, A., Pavan, M. K. & Zafar, H. scDREAMER for atlas-level integration of single-cell datasets using deep generative model paired with adversarial classifier. *Nat. Commun.* **14**, 7781 (2023).

95. Replogle, J. M. *et al.* Mapping information-rich genotype-phenotype landscapes with genome-scale Perturb-seq. *Cell* **185**, 2559-2575.e28 (2022).

96. Dalin, S. *et al.* Abstract 2710 : Associations between structural variant signatures and drug sensitivity in cell lines. *Cancer Res.* **82**, 2710 (2022).

97. Harada, T. *et al.* Rapid-kinetics degron benchmarking reveals off-target activities and mixed agonism-antagonism of MYB inhibitors. *bioRxiv* 2023.04.07.536032 (2023) doi:10.1101/2023.04.07.536032.

98. Harada, T. *et al.* Leukemia core transcriptional circuitry is a sparsely interconnected hierarchy stabilized by incoherent feed-forward loops. *bioRxiv* 2023.03.13.532438 (2023) doi:10.1101/2023.03.13.532438.

99. Misek, S. A. *et al.* Germline variation contributes to false negatives in CRISPR-based experiments with varying burden across ancestries. *Nat. Commun.* **15**, 4892 (2024).

100. Luecken, M. D. *et al.* Benchmarking atlas-level data integration in single-cell genomics. *Nat. Methods* **19**, 41–50 (2022).

101. Aguet, F. *et al.* Genetic effects on gene expression across human tissues. *Nature* **550**, 204–213 (2017).

102. [1810.04805] BERT : Pre-training of Deep Bidirectional Transformers for Language Understanding. https://arxiv.org/abs/1810.04805.

103. Dao, T. FlashAttention-2 : Faster Attention with Better Parallelism and Work Partitioning. Preprint at https://doi.org/10.48550/arXiv.2307.08691 (2023).

104. Nguyen, T. Q. & Salazar, J. Transformers without Tears : Improving the Normalization of Self-Attention. https://doi.org/10.5281/zenodo.3525484 (2019) doi:10.5281/zenodo.3525484.

105. Triton : an intermediate language and compiler for tiled neural network computations | Proceedings of the 3rd ACM SIGPLAN International Workshop on Machine Learning

and Programming Languages. https://dl.acm.org/doi/abs/10.1145/3315508.3329973.

106. Papers with Code - Deep Networks with Stochastic Depth. https://paperswithcode.com/paper/deep-networks-with-stochastic-depth.

107. Loshchilov, I. & Hutter, F. Decoupled Weight Decay Regularization. Preprint at https://doi.org/10.48550/arXiv.1711.05101 (2019).

108. Athiwaratkun, B., Finzi, M., Izmailov, P. & Wilson, A. G. There Are Many Consistent Explanations of Unlabeled Data : Why You Should Average. Preprint at https://doi.org/10.48550/arXiv.1806.05594 (2019).

109. Jorstad, N. L. *et al.* Transcriptomic cytoarchitecture reveals principles of human neocortex organization. *Science* **382**, eadf6812 (2023).

110. Müller-Dott, S. *et al.* Expanding the coverage of regulons from high-confidence prior knowledge for accurate estimation of transcription factor activities. *Nucleic Acids Res.* **51**, 10934–10949 (2023).

111. Türei, D. *et al.* OmniPath : integrated knowledgebase for multi-omics analysis. *Nucleic Acids Res.* gkaf1126 (2025) doi:10.1093/nar/gkaf1126.

112. Zhang, J. *et al.* Computing the Human Interactome. 2024.10.01.615885 Preprint at https://doi.org/10.1101/2024.10.01.615885 (2024).

113. Hubert, L. & Arabie, P. Comparing partitions. *J. Classif.* **2**, 193–218 (1985).

114. Pedregosa, F. *et al.* Scikit-learn : Machine Learning in Python. *J. Mach. Learn. Res.* **12**, 2825–2830 (2011).

115. A test metric for assessing single-cell RNA-seq batch correction | Nature Methods. https://www.nature.com/articles/s41592-018-0254-1.

116. Korsunsky, I. *et al.* Fast, sensitive and accurate integration of single-cell data with Harmony. *Nat. Methods* **16**, 1289–1296 (2019).

3.9 Acknowledgment

The project leading to this manuscript has received funding from the Inception program (Investissement d'Avenir grant ANR-16-CONV-0005) L.C., and the European Union (ERC StG, MULTIview-CELL, 101115618) L.C.. We acknowledge the help of the HPC Core Facility of the Institut Pasteur and Déborah Philipps for the administrative support. L.C..

The work of G. Peyré was supported by the French government under the management of Agence Nationale de la Recherche as part of the 'Investissements d'avenir' program, reference ANR19-P3IA-0001 (PRAIRIE 3IA Institute) G.P..

BIOART Source. bioart.niaid.nih.gov/bioart/452. DBCLS https://togotv.dbcls.jp/en/pics.html is licensed under CC-BY 4.0 International https://creativecommons.org/licenses/by/4.0/. Marcel Tisch https://twitter.com/MarcelTisch is licensed under CC-0 1.0 Universal https://creativecommons.org/publicdomain/zero/1.0/. *Library v1.1. Available via Zenodo (https://zenodo.org/records/17229908).*

3.10 Author Contribution

J.K., L.C., and G.P. designed the study. J.K. developed the tool and performed all the analysis. J.K., and L.C wrote the manuscript. G.P. revised the manuscript.

Discussion and perspectives

By the end of this thesis, we have developed a next-generation foundation models for single-cell data. In our first publication„ we examined a set of initial improvements to the previously presented tools, including novel training and encoding/decoding schemes. We focused our analysis on a set of common benchmarks and comparisons that were lacking in previous works, focusing on the internal representation of genetic interactions that these models possess. We also focused on real-world usage and accessibility with a tool competitive or state-of-the-art on many tasks orthogonal to gene network inference, such as cell type annotation, batch effect correction, and denoising.

In our second publication, we looked at an architectural change that would allow AI models to work across multiple scales of biology, from the molecules to the cells and tissues. We showed how multimodality can improve the unimodal performance of these models.

In our third publication, we reused our proposed architecture, refined our training and encodings paradigms, and scaled our model and training dataset to create a next-generation single-cell foundation model. We also separately assessed the impact of each of the model's components in an additive study across a gymnasium of tasks introduced in our first publication. We also questioned and showed how these tasks could be refined in a study of model generalization across unseen modalities and organisms.

But a lot of work remains at the crossroads of AI and biology. In the following sections, I will discuss some of the challenges and opportunities that I see in this space.

4.1 Collecting data in the wild

4.1.1 Genetic diversity

The first issue to address for a better model will be obtaining cell expression data across a much more diverse genetic background. This also means sequencing the genome of the tissues we are analyzing, which is rarely done because genomic data has strong laws

surrounding patient anonymity and public sharing.

Fortunately, we have seen projects starting around this goal, such as the 10K10K, which aims to sequence 10,000 cells from 10,000 people along with genetic data. The Sanger Institute is also doing something similar with spatial transcriptomics of 10,000s of samples in development, along with their genomes.

But these remain small-scale projects compared to the diversity of life on Earth. In genomics, scBasecamp and other for-profit companies are working on sampling life around the world from barren places to ocean depths, with the stated goal ofdeveloping higherr quality models. Single-cell models would stand to benefit just as much.

4.1.2 Interventional data

Finally, we also want interventional datasets. Currently, perturb-seq datasets with tens of thousands of perturbations exist, such as the genome-wide perturb-seq dataset and Tahoe-100M. However, here too, the scale remains too small. The Broad & Sanger Institute's PRISM and DepMap projects examined millions of perturbations, albeit without deep phenotypic readouts. Recursion assessed image-based perturbations across at least as many. Xaira has started to release a dual gene knockout dataset of unparalleled quality.

4.1.3 Data quality

Indeed, the second missing important axis is data quality. Genomics is plagued with very low-quality, noisy, or biased, poorly labeled datasets. This is due to the high cost of sequencing, the complex chemistry of the experiments, and the poor academic incentives driving the creation of these datasets.

It leads to an unstate Pareto front, where we want both more depth and more breadth : more diversity versus more quality.

It might be solved by new technologies, indeed we now have technologies like VASA-seq, 10X's Flex, and smart-seq 3 that promise unparalleled definition for a given sequencing budget. 10x's Xenium, BGI's STEREO-seq,, and expansion-based in situ method are promising for sequencing RNAs in their original 2D or even 3D context within sub-cellular locations of millions of cells at once. But we will also have to be smarter in how we select cells to sequence.

4.2 Multi modality & perturbations

Indeed,, these two modalities and their tradeoffs exist within a range of other techniques often needed to make sense of RNA biology itself.

Interventional data is also required for the model to learn causality, especially when

assessed at multiple fine-grained timescales and in higher-quality cellular models such as organoids.

But the search space is unfathomable. Tools like digital microfluidics might allow us to solve some of these problems by providing precise control over which cells receive specific perturbations and obtain particular readouts, instead of pooling experiments and sequencing budgets randomly. If paired with AI models and online active learning, we might have a shot at creating a true AI-virtual cell.

4.3 The AI virtual cell

One could view such a training modality as reinforcement learning with active feedback (RLAF) of a large pretrained AI model. It would have been pretrained on most of biology, using foundation models of single-cell multimodalities, tissues, molecules, and protein-RNA-DNA sequences, pooled together in the kind of approaches we described in Chapter 2. LLMs could allow rich reasoning across these representations, results, and the breadth of written human knowledge.

Many challenges remain in bridging fields such as data engineering, machine learning, material engineering, microelectronics, molecular biology, and cell biology, but the rewards are tremendous.

Conclusion

Single-cell Foundation Models while in their infancy, have the power to change the way we do biology and medicine.

During this Thesis, we have shown that :

- We can use the internal workings of scFMs to predict meaningful gene interactions.
- We can update their training tasks, data, losses, as well as their architectures to better capture the underlying biology of the cell.
- We can use them to perform a variety of single cell tasks in a zero-shot of few-shot manner, from cell annotations, denoising, imputation, embeddings generation, batch correction, cross-species integration and counterfactual reasoning
- We can use multiple techniques at inference and fine-tuning time to improve their performance.
- We can leverage the other foundation models pre-trained on other modalities to improve their performance.

In conclusion, the follow-up of these studies should allow to multiply the use-cases of single-cell transcriptomics in clinical applications. To integrate other modalities like sequences, epigenetics, proteomics, spatial, and imaging via multi-scale architecture and fine-tuning. But also allow these models to reason by integrating them to LLMs. Finally one will need to gather more data from novel species, patient contexts and across perturbations. To the later point especially we will want to use active learning to guide the experiments and maybe reach our goal of cellular modeling.

Bibliography

[1] Winfried S. Peters. « The Cells of Robert Hooke : Wombs, Brains and Ammonites ». In : *Notes and Records : the Royal Society Journal of the History of Science* (mai 2024). issn : 0035-9149. doi : 10.1098/rsnr.2023.0081. (Visité le 02/12/2025).

[2] Bruce Alberts et al. « Cells and Genomes ». In : *Molecular Biology of the Cell*. 6e éd. New York : Garland Science, 2015. Chap. 1.

[3] Jamie A. Davies. *Synthetic Biology : A Very Short Introduction*. Oxford University Press, juill. 2018. isbn : 978-0-19-880349-2. doi : 10.1093/actrade/9780198803492.001.0001. (Visité le 02/12/2025).

[4] Inés Zugasti et al. « CAR-T Cell Therapy for Cancer : Current Challenges and Future Directions ». In : *Signal Transduction and Targeted Therapy* 10.1 (juill. 2025), p. 210. issn : 2059-3635. doi : 10.1038/s41392-025-02269-w. (Visité le 02/12/2025).

[5] Charlotte Bunne et al. « How to Build the Virtual Cell with Artificial Intelligence : Priorities and Opportunities ». In : *Cell* 187.25 (déc. 2024), p. 7045-7063. issn : 0092-8674, 1097-4172. doi : 10.1016/j.cell.2024.11.015. (Visité le 25/02/2025).

[6] « Front Matter ». In : *Origins of Molecular Biology*. John Wiley & Sons, Ltd, 2003, p. i-xxii. isbn : 978-1-68367-216-6. doi : 10.1128/9781555817763.fmatter. (Visité le 02/12/2025).

[7] « The RNA World ». In : *Nature Structural & Molecular Biology* 31.5 (mai 2024), p. 729-729. issn : 1545-9985. doi : 10.1038/s41594-024-01327-1. (Visité le 02/12/2025).

[8] Ling-Ling Chen et V. Narry Kim. « Small and Long Non-Coding RNAs : Past, Present, and Future ». In : *Cell* 187.23 (nov. 2024), p. 6451-6485. issn : 0092-8674, 1097-4172. doi : 10.1016/j.cell.2024.10.024. (Visité le 02/12/2025).

[9] Pau Badia-i-Mompel et al. « Gene Regulatory Network Inference in the Era of Single-Cell Multi-Omics ». In : *Nature Reviews Genetics* 24.11 (nov. 2023), p. 739-754. issn : 1471-0064. doi : 10.1038/s41576-023-00618-5. (Visité le 18/04/2024).

[10] F. Sanger, S. Nicklen et A. R. Coulson. « DNA Sequencing with Chain-Terminating Inhibitors ». In : *Proceedings of the National Academy of Sciences of the United States of America* 74.12 (déc. 1977), p. 5463-5467. issn : 0027-8424. doi : 10.1073/pnas.74.12.5463.

[11] Taishan Hu et al. « Next-Generation Sequencing Technologies : An Overview ». In : *Human Immunology*. Next Generation Sequencing and Its Application to Medical Laboratory Immunology 82.11 (nov. 2021), p. 801-811. ISSN : 0198-8859. DOI : 10.1016/j.humimm.2021.02.012. (Visité le 02/12/2025).

[12] 1000 Genomes Project Consortium et al. « A Global Reference for Human Genetic Variation ». In : *Nature* 526.7571 (oct. 2015), p. 68-74. ISSN : 1476-4687. DOI : 10.1038/nature15393.

[13] Eric S. Lander et al. « Initial Sequencing and Analysis of the Human Genome ». In : *Nature* 409.6822 (fév. 2001), p. 860-921. ISSN : 1476-4687. DOI : 10.1038/35057062. (Visité le 02/12/2025).

[14] Rory Stark, Marta Grzelak et James Hadfield. « RNA Sequencing : The Teenage Years ». In : *Nature Reviews Genetics* 20.11 (nov. 2019), p. 631-656. ISSN : 1471-0064. DOI : 10.1038/s41576-019-0150-2. (Visité le 02/12/2025).

[15] Jason Buenrostro et al. « ATAC-seq : A Method for Assaying Chromatin Accessibility Genome-Wide ». In : *Current protocols in molecular biology / edited by Frederick M. Ausubel ... [et al.]* 109 (jan. 2015), p. 21.29.1-21.29.9. ISSN : 1934-3639. DOI : 10.1002/0471142727.mb2129s109. (Visité le 02/12/2025).

[16] Evan Z. Macosko et al. « Highly Parallel Genome-wide Expression Profiling of Individual Cells Using Nanoliter Droplets ». In : *Cell* 161.5 (mai 2015), p. 1202-1214. ISSN : 1097-4172. DOI : 10.1016/j.cell.2015.05.002.

[17] Aviv Regev et al. « The Human Cell Atlas ». In : *eLife* 6 (), e27041. ISSN : 2050-084X. DOI : 10.7554/eLife.27041. (Visité le 25/02/2025).

[18] Patrik L. Ståhl et al. « Visualization and Analysis of Gene Expression in Tissue Sections by Spatial Transcriptomics ». In : *Science (New York, N.Y.)* 353.6294 (juill. 2016), p. 78-82. ISSN : 1095-9203. DOI : 10.1126/science.aaf2403.

[19] Xiuer Luo et al. « Advances in Protein Sequencing : Techniques, Challenges and Prospects ». In : *TrAC Trends in Analytical Chemistry* 191 (oct. 2025), p. 118341. ISSN : 0165-9936. DOI : 10.1016/j.trac.2025.118341. (Visité le 02/12/2025).

[20] Diya B. Joseph et al. « Single Cell Analysis of Mouse and Human Prostate Reveals Novel Fibroblasts with Specialized Distribution and Microenvironment Interactions ». In : *The Journal of pathology* 255.2 (oct. 2021), p. 141-154. ISSN : 0022-3417. DOI : 10.1002/path.5751. (Visité le 23/07/2024).

[21] Lingjia Kong et al. « The Landscape of Immune Dysregulation in Crohn's Disease Revealed through Single-Cell Transcriptomic Profiling in the Ileum and Colon ». In : *Immunity* 56.2 (fév. 2023), 444-458.e5. ISSN : 1074-7613. DOI : 10.1016/j.immuni.2023.01.002. (Visité le 23/07/2024).

[22] Atray Dixit et al. « Perturb-Seq : Dissecting Molecular Circuits with Scalable Single Cell RNA Profiling of Pooled Genetic Screens ». In : *Cell* 167.7 (déc. 2016), 1853-1866.e17. ISSN : 0092-8674. DOI : 10.1016/j.cell.2016.11.038. (Visité le 19/07/2024).

[23] Britt Adamson et al. « A Multiplexed Single-Cell CRISPR Screening Platform Enables Systematic Dissection of the Unfolded Protein Response ». In : *Cell* 167.7 (déc. 2016), 1867-1882.e21. issn : 0092-8674. doi : 10.1016/j.cell.2016.11.048. (Visité le 18/04/2024).

[24] Alexander Dobin et al. « STAR : Ultrafast Universal RNA-seq Aligner ». In : *Bioinformatics* 29.1 (jan. 2013), p. 15-21. issn : 1367-4803. doi : 10.1093/bioinformatics/bts635. (Visité le 02/12/2025).

[25] Laleh Haghverdi et al. « Batch Effects in Single-Cell RNA-sequencing Data Are Corrected by Matching Mutual Nearest Neighbors ». In : *Nature Biotechnology* 36.5 (mai 2018), p. 421-427. issn : 1546-1696. doi : 10.1038/nbt.4091. (Visité le 02/12/2025).

[26] Romain Lopez et al. « Deep Generative Modeling for Single-Cell Transcriptomics ». In : *Nature Methods* 15.12 (déc. 2018), p. 1053-1058. issn : 1548-7105. doi : 10.1038/s41592-018-0229-2. (Visité le 15/07/2024).

[27] Byungjin Hwang, Ji Hyun Lee et Duhee Bang. « Single-Cell RNA Sequencing Technologies and Bioinformatics Pipelines ». In : *Experimental & Molecular Medicine* 50.8 (août 2018), p. 1-14. issn : 2092-6413. doi : 10.1038/s12276-018-0071-8. (Visité le 02/12/2025).

[28] Gökcen Eraslan et al. « Single-Cell RNA-seq Denoising Using a Deep Count Autoencoder ». In : *Nature Communications* 10.1 (jan. 2019), p. 390. issn : 2041-1723. doi : 10.1038/s41467-018-07931-2. (Visité le 15/07/2024).

[29] David van Dijk et al. « Recovering Gene Interactions from Single-Cell Data Using Data Diffusion ». In : *Cell* 174.3 (juill. 2018), 716-729.e27. issn : 0092-8674, 1097-4172. doi : 10.1016/j.cell.2018.05.061. (Visité le 15/07/2024).

[30] Huidong Chen et al. « STREAM : Single-cell Trajectories Reconstruction, Exploration And Mapping of Omics Data ». In : *bioRxiv* (18 avr. 2018). doi : 10.1101/302554. url : http://biorxiv.org/lookup/doi/10.1101/302554 (visité le 22/03/2019).

[31] Giovanni Palla et al. « Squidpy : A Scalable Framework for Spatial Omics Analysis ». In : *Nature Methods* 19.2 (fév. 2022), p. 171-178. issn : 1548-7105. doi : 10.1038/s41592-021-01358-2. (Visité le 02/12/2025).

[32] Mohammad Lotfollahi, F. Alexander Wolf et Fabian J. Theis. « scGen Predicts Single-Cell Perturbation Responses ». In : *Nature Methods* 16.8 (août 2019), p. 715-721. issn : 1548-7105. doi : 10.1038/s41592-019-0494-8.

[33] Ian Goodfellow, Yoshua Bengio et Aaron Courville. *Deep Learning*. http://www.deeplearningbook.org. MIT Press, 2016.

[34] David Ha et Jürgen Schmidhuber. « World Models ». In : (mars 2018). doi : 10.5281/zenodo.1207631. arXiv : 1803.10122 [cs]. (Visité le 02/12/2025).

[35] Remi Lam et al. « Learning Skillful Medium-Range Global Weather Forecasting ». In : *Science* 382.6677 (déc. 2023), p. 1416-1421. doi : 10.1126/science.adi2336. (Visité le 02/12/2025).

[36] Kaiming He et al. *Deep Residual Learning for Image Recognition*. Déc. 2015. DOI : 10.48550/arXiv.1512.03385. arXiv : 1512.03385 [cs]. (Visité le 07/12/2025).

[37] Karen Simonyan et Andrew Zisserman. *Very Deep Convolutional Networks for Large-Scale Image Recognition*. Avr. 2015. DOI : 10.48550/arXiv.1409.1556. arXiv : 1409.1556 [cs]. (Visité le 07/12/2025).

[38] Ashish Vaswani et al. *Attention Is All You Need*. Août 2023. DOI : 10.48550/arXiv.1706.03762. arXiv : 1706.03762 [cs]. (Visité le 10/07/2024).

[39] Hao Li et al. *Visualizing the Loss Landscape of Neural Nets*. Nov. 2018. DOI : 10.48550/arXiv.1712.09913. arXiv : 1712.09913 [cs]. (Visité le 02/12/2025).

[40] Jason Wei et al. *Emergent Abilities of Large Language Models*. Oct. 2022. DOI : 10.48550/arXiv.2206.07682. arXiv : 2206.07682 [cs]. (Visité le 02/12/2025).

[41] Rishi Bommasani et al. *On the Opportunities and Risks of Foundation Models*. Juill. 2022. DOI : 10.48550/arXiv.2108.07258. arXiv : 2108.07258 [cs]. (Visité le 02/12/2025).

[42] Yan Duan et al. « One-Shot Imitation Learning ». In : (), p. 23.

[43] Fan Yang et al. « scBERT as a Large-Scale Pretrained Deep Language Model for Cell Type Annotation of Single-Cell RNA-seq Data ». In : *Nature Machine Intelligence* 4.10 (oct. 2022), p. 852-866. ISSN : 2522-5839. DOI : 10.1038/s42256-022-00534-z. (Visité le 02/12/2025).

[44] Christina V. Theodoris et al. « Transfer Learning Enables Predictions in Network Biology ». In : *Nature* 618.7965 (juin 2023), p. 616-624. ISSN : 1476-4687. DOI : 10.1038/s41586-023-06139-9. (Visité le 18/04/2024).

[45] Haotian Cui et al. « scGPT : Toward Building a Foundation Model for Single-Cell Multi-Omics Using Generative AI ». In : *Nature Methods* (fév. 2024), p. 1-11. ISSN : 1548-7105. DOI : 10.1038/s41592-024-02201-0. (Visité le 18/04/2024).

[46] Rebecca Boiarsky et al. *A Deep Dive into Single-Cell RNA Sequencing Foundation Models*. Oct. 2023. DOI : 10.1101/2023.10.19.563100. (Visité le 19/04/2024).

[47] Abdel Rahman Alsabbagh et al. *Foundation Models Meet Imbalanced Single-Cell Data When Learning Cell Type Annotations*. Oct. 2023. DOI : 10.1101/2023.10.24.563625. (Visité le 19/04/2024).

[48] Yanay Rosen et al. *Universal Cell Embeddings : A Foundation Model for Cell Biology*. Nov. 2023. DOI : 10.1101/2023.11.28.568918. (Visité le 18/04/2024).

[49] Minsheng Hao et al. « Large-Scale Foundation Model on Single-Cell Transcriptomics ». In : *Nature Methods* (juin 2024), p. 1-11. ISSN : 1548-7105. DOI : 10.1038/s41592-024-02305-7. (Visité le 15/07/2024).

[50] Nathaniel J. Evans et al. *Graph Structured Neural Networks for Perturbation Biology*. Fév. 2024. DOI : 10.1101/2024.02.28.582164. (Visité le 19/04/2024).

[51] Gabriele Corso et al. « Graph Neural Networks ». In : *Nature Reviews Methods Primers* 4.1 (mars 2024), p. 17. ISSN : 2662-8449. DOI : 10.1038/s43586-024-00294-7. (Visité le 12/12/2025).

[52] Simon Batzner et al. « E(3)-Equivariant Graph Neural Networks for Data-Efficient and Accurate Interatomic Potentials ». In : *Nature Communications* 13.1 (mai 2022), p. 2453. ISSN : 2041-1723. DOI : 10.1038/s41467-022-29939-5. (Visité le 25/02/2025).

[53] Nicola De Cao et Thomas Kipf. « MolGAN : An Implicit Generative Model for Small Molecular Graphs ». 30 mai 2018. arXiv : 1805.11973 [cs, stat]. URL : http://arxiv.org/abs/1805.11973 (visité le 22/03/2019).

[54] Yanglan Gan et al. « Inferring Gene Regulatory Networks from Single-Cell Transcriptomics Based on Graph Embedding ». In : *Bioinformatics* 40.5 (mai 2024). DOI : 10.1093/bioinformatics/btae291. (Visité le 10/07/2024).

[55] Md Shamim Hussain, Mohammed J. Zaki et Dharmashankar Subramanian. « Global Self-Attention as a Replacement for Graph Convolution ». In : *Proceedings of the 28th ACM SIGKDD Conference on Knowledge Discovery and Data Mining*. Août 2022, p. 655-665. DOI : 10.1145/3534678.3539296. arXiv : 2108.03348 [cs]. (Visité le 19/04/2024).

[56] Guangyi Chen et Zhi-Ping Liu. « Graph Attention Network for Link Prediction of Gene Regulations from Single-Cell RNA-sequencing Data ». In : *Bioinformatics* 38.19 (sept. 2022), p. 4522-4529. ISSN : 1367-4803. DOI : 10.1093/bioinformatics/btac559. (Visité le 10/07/2024).

[57] Vijay Prakash Dwivedi et Xavier Bresson. *A Generalization of Transformer Networks to Graphs*. Jan. 2021. DOI : 10.48550/arXiv.2012.09699. arXiv : 2012.09699 [cs]. (Visité le 12/12/2025).

[58] Chaitanya K. Joshi. *Transformers Are Graph Neural Networks*. Juin 2025. DOI : 10.48550/arXiv.2506.22084. arXiv : 2506.22084 [cs]. (Visité le 12/12/2025).

[59] Eshaan Nichani, Alex Damian et Jason D. Lee. *How Transformers Learn Causal Structure with Gradient Descent*. Août 2024. DOI : 10.48550/arXiv.2402.14735. arXiv : 2402.14735 [cs]. (Visité le 12/12/2025).

[60] Peter Shaw, Jakob Uszkoreit et Ashish Vaswani. *Self-Attention with Relative Position Representations*. Avr. 2018. DOI : 10.48550/arXiv.1803.02155. arXiv : 1803.02155 [cs]. (Visité le 12/12/2025).

[61] David Lähnemann et al. « Eleven Grand Challenges in Single-Cell Data Science ». In : *Genome Biology* 21.1 (fév. 2020), p. 31. ISSN : 1474-760X. DOI : 10.1186/s13059-020-1926-6. (Visité le 19/04/2024).

[62] Yusuf Roohani, Kexin Huang et Jure Leskovec. « Predicting Transcriptional Outcomes of Novel Multigene Perturbations with GEARS ». In : *Nature Biotechnology* 42.6 (juin 2024), p. 927-935. ISSN : 1546-1696. DOI : 10.1038/s41587-023-01905-6. (Visité le 25/02/2025).

[63] Guadalupe Gonzalez et al. « Combinatorial Prediction of Therapeutic Perturbations Using Causally-Inspired Neural Networks ». In : *bioRxiv* (jan. 2024), p. 2024.01.03.573985. DOI : 10.1101/2024.01.03.573985. (Visité le 10/07/2024).

[64] Taku Harada et al. « A Distinct Core Regulatory Module Enforces Oncogene Expression in KMT2A-rearranged Leukemia ». In : *Genes & Development* 36.5-6 (mars 2022), p. 368-389. ISSN : 0890-9369, 1549-5477. DOI : 10.1101/gad.349284.121. (Visité le 25/02/2025).

[65] Taku Harada et al. « Leukemia Core Transcriptional Circuitry Is a Sparsely Interconnected Hierarchy Stabilized by Incoherent Feed-Forward Loops ». In : *bioRxiv* (mars 2023), p. 2023.03.13.532438. DOI : 10.1101/2023.03.13.532438. (Visité le 28/01/2025).

[66] Russell Littman et al. « SCING : Inference of Robust, Interpretable Gene Regulatory Networks from Single Cell and Spatial Transcriptomics ». In : *iScience* 26.7 (juill. 2023), p. 107124. ISSN : 2589-0042. DOI : 10.1016/j.isci.2023.107124. (Visité le 18/04/2024).

[67] Sara Aibar et al. « SCENIC : Single-Cell Regulatory Network Inference and Clustering ». In : *Nature Methods* 14.11 (nov. 2017), p. 1083-1086. ISSN : 1548-7105. DOI : 10.1038/nmeth.4463. (Visité le 18/04/2024).

[68] Carmen Bravo González-Blas et al. « SCENIC+ : Single-Cell Multiomic Inference of Enhancers and Gene Regulatory Networks ». In : *Nature Methods* 20.9 (sept. 2023), p. 1355-1367. ISSN : 1548-7105. DOI : 10.1038/s41592-023-01938-4. (Visité le 10/07/2024).

[69] Guangxin Su et al. *Inferring Gene Regulatory Networks by Hypergraph Variational Autoencoder*. Avr. 2024. DOI : 10.1101/2024.04.01.586509. (Visité le 10/07/2024).

[70] N. Alexia Raharinirina et al. « Inferring Gene Regulatory Networks from Single-Cell RNA-seq Temporal Snapshot Data Requires Higher-Order Moments ». In : *Patterns* 2.9 (sept. 2021), p. 100332. ISSN : 2666-3899. DOI : 10.1016/j.patter.2021.100332. (Visité le 10/07/2024).

[71] Lingfei Wang et al. « Dictys : Dynamic Gene Regulatory Network Dissects Developmental Continuum with Single-Cell Multiomics ». In : *Nature Methods* 20.9 (sept. 2023), p. 1368-1378. ISSN : 1548-7105. DOI : 10.1038/s41592-023-01971-3. (Visité le 18/04/2024).

[72] Shilu Zhang et al. « Inference of Cell Type-Specific Gene Regulatory Networks on Cell Lineages from Single Cell Omic Datasets ». In : *Nature Communications* 14.1 (mai 2023), p. 3064. ISSN : 2041-1723. DOI : 10.1038/s41467-023-38637-9. (Visité le 10/07/2024).

[73] Juexin Wang et al. « Inductive Inference of Gene Regulatory Network Using Supervised and Semi-Supervised Graph Neural Networks ». In : *Computational and Structural Biotechnology Journal* 18 (nov. 2020), p. 3335-3343. ISSN : 2001-0370. DOI : 10.1016/j.csbj.2020.10.022. (Visité le 10/07/2024).

[74] Kenji Kamimoto et al. « Dissecting Cell Identity via Network Inference and in Silico Gene Perturbation ». In : *Nature* 614.7949 (fév. 2023), p. 742-751. ISSN : 1476-4687. DOI : 10.1038/s41586-022-05688-9. (Visité le 18/04/2024).

[75] Hantao Shu et al. « Modeling Gene Regulatory Networks Using Neural Network Architectures ». In : *Nature Computational Science* 1.7 (juill. 2021), p. 491-501. ISSN : 2662-8457. DOI : 10.1038/s43588-021-00099-8. (Visité le 13/11/2024).

[76] Ann Boija et al. « Transcription Factors Activate Genes through the Phase-Separation Capacity of Their Activation Domains ». In : *Cell* 175.7 (déc. 2018), 1842-1855.e16. ISSN : 0092-8674. DOI : 10.1016/j.cell.2018.10.042. (Visité le 19/04/2024).

[77] GRETA FRIAR. *It Takes Three to Tango : Transcription Factors Bind DNA, Protein, and RNA | Whitehead Institute*. https://wi.mit.edu/news/it-takes-three-tango-transcription-factors-bind-dna-protein-and-rna. Juin 2023. (Visité le 19/04/2024).

[78] Ozgur Oksuz et al. « Transcription Factors Interact with RNA to Regulate Genes ». In : *Molecular Cell* 83.14 (juill. 2023), 2449-2463.e13. ISSN : 1097-2765. DOI : 10.1016/j.molcel.2023.06.012. (Visité le 19/04/2024).

[79] Priyanka Dey Talukdar et Urmi Chatterji. « Transcriptional Co-Activators : Emerging Roles in Signaling Pathways and Potential Therapeutic Targets for Diseases ». In : *Signal Transduction and Targeted Therapy* 8.1 (nov. 2023), p. 1-41. ISSN : 2059-3635. DOI : 10.1038/s41392-023-01651-w. (Visité le 10/07/2024).

[80] Luisa Statello et al. « Gene Regulation by Long Non-Coding RNAs and Its Biological Functions ». In : *Nature Reviews Molecular Cell Biology* 22.2 (fév. 2021), p. 96-118. ISSN : 1471-0080. DOI : 10.1038/s41580-020-00315-9. (Visité le 10/07/2024).

[81] Peizhuo Wang et al. « Deciphering Driver Regulators of Cell Fate Decisions from Single-Cell Transcriptomics Data with CEFCON ». In : *Nature Communications* 14.1 (déc. 2023), p. 8459. ISSN : 2041-1723. DOI : 10.1038/s41467-023-44103-3. (Visité le 13/11/2024).

[82] Aditya Pratapa et al. « Benchmarking Algorithms for Gene Regulatory Network Inference from Single-Cell Transcriptomic Data ». In : *Nature Methods* 17.2 (fév. 2020), p. 147-154. ISSN : 1548-7105. DOI : 10.1038/s41592-019-0690-6. (Visité le 10/07/2024).

[83] Sunnie Grace McCalla et al. « Identifying Strengths and Weaknesses of Methods for Computational Network Inference from Single-Cell RNA-seq Data ». In : *G3 Genes|Genomes|Genetics* 13.3 (mars 2023), jkad004. ISSN : 2160-1836. DOI : 10.1093/g3journal/jkad004. (Visité le 18/04/2024).

[84] Jacob Devlin et al. *BERT : Pre-training of Deep Bidirectional Transformers for Language Understanding*. Mai 2019. DOI : 10.48550/arXiv.1810.04805. arXiv : 1810.04805 [cs]. (Visité le 19/04/2024).

[85] Jeremie Kalfon. *Cantinilab/scPRINT*. Machine Learning for Integrative Genomics lab. Fév. 2025. (Visité le 17/02/2025).

[86] CZI Single-Cell Biology Program et al. *CZ CELL×GENE Discover : A Single-Cell Data Platform for Scalable Exploration, Analysis and Modeling of Aggregated Data*. Nov. 2023. DOI : 10.1101/2023.10.30.563174. (Visité le 15/07/2024).

[87] Jeremie Kalfon. *Jkobject/benGRN : Awesome Benchmark of Gene Regulatory Networks*. Jan. 2025. (Visité le 17/02/2025).

[88] Jeremie Kalfon. *Cantinilab/GRnnData*. Machine Learning for Integrative Genomics lab. Jan. 2025. (Visité le 17/02/2025).

[89] sergey ribakov jeremie kalfon. *Training Foundation Models on Large Collections of scRNA-seq Data*. https://lamin.ai/blog/arrayloader-benchmarks. (Visité le 18/04/2024).

[90] Tri Dao. *FlashAttention-2 : Faster Attention with Better Parallelism and Work Partitioning*. Juill. 2023. DOI : 10.48550/arXiv.2307.08691. arXiv : 2307.08691 [cs]. (Visité le 15/07/2024).

[91] Ana Carolina Leote, Xiaohui Wu et Andreas Beyer. « Regulatory Network-Based Imputation of Dropouts in Single-Cell RNA Sequencing Data ». In : *PLOS Computational Biology* 18.2 (fév. 2022), e1009849. ISSN : 1553-7358. DOI : 10.1371/journal.pcbi.1009849. (Visité le 15/07/2024).

[92] Zoe Piran et al. « Disentanglement of Single-Cell Data with Biolord ». In : *Nature Biotechnology* (jan. 2024), p. 1-6. ISSN : 1546-1696. DOI : 10.1038/s41587-023-02079-x. (Visité le 25/10/2024).

[93] Alexander Rives et al. « Biological Structure and Function Emerge from Scaling Unsupervised Learning to 250 Million Protein Sequences ». In : *Proceedings of the National Academy of Sciences* 118.15 (avr. 2021), e2016239118. DOI : 10.1073/pnas.2016239118. (Visité le 25/02/2025).

[94] Jun Hu et al. « Improving Protein-Protein Interaction Prediction Using Protein Language Model and Protein Network Features ». In : *Analytical Biochemistry* 693 (oct. 2024), p. 115550. ISSN : 0003-2697. DOI : 10.1016/j.ab.2024.115550. (Visité le 15/07/2024).

[95] Krzysztof Choromanski et al. *Rethinking Attention with Performers*. Nov. 2022. DOI : 10.48550/arXiv.2009.14794. arXiv : 2009.14794. (Visité le 29/10/2024).

[96] Samira Abnar et Willem Zuidema. *Quantifying Attention Flow in Transformers*. Mai 2020. DOI : 10.48550/arXiv.2005.00928. arXiv : 2005.00928 [cs]. (Visité le 15/07/2024).

[97] Kevin Clark et al. *What Does BERT Look At ? An Analysis of BERT's Attention*. Juin 2019. DOI : 10.48550/arXiv.1906.04341. arXiv : 1906.04341 [cs]. (Visité le 15/07/2024).

[98] Adrien Bibal et al. « Is Attention Explanation ? An Introduction to the Debate ». In : *Proceedings of the 60th Annual Meeting of the Association for Computational Linguistics (Volume 1 : Long Papers)*. Sous la dir. de Smaranda Muresan, Preslav Nakov et Aline Villavicencio. Dublin, Ireland : Association for Computational Linguistics, mai 2022, p. 3889-3900. doi : 10.18653/v1/2022.acl-long.269. (Visité le 15/07/2024).

[99] Vân Anh Huynh-Thu et al. « Inferring Regulatory Networks from Expression Data Using Tree-Based Methods ». In : *PLOS ONE* 5.9 (sept. 2010), e12776. issn : 1932-6203. doi : 10.1371/journal.pone.0012776. (Visité le 19/04/2024).

[100] Han Chen et al. *Quantized Multi-Task Learning for Context-Specific Representations of Gene Network Dynamics*. Août 2024. doi : 10.1101/2024.08.16.608180. (Visité le 25/10/2024).

[101] Payam Dibaeinia et Saurabh Sinha. « SERGIO : A Single-Cell Expression Simulator Guided by Gene Regulatory Networks ». In : *Cell Systems* 11.3 (sept. 2020), 252-271.e11. issn : 2405-4712. doi : 10.1016/j.cels.2020.08.003. (Visité le 25/02/2025).

[102] Zhi-Ping Liu et al. « RegNetwork : An Integrated Database of Transcriptional and Post-Transcriptional Regulatory Networks in Human and Mouse ». In : *Database : The Journal of Biological Databases and Curation* 2015 (sept. 2015), bav095. doi : 10.1093/database/bav095. (Visité le 28/10/2024).

[103] Aravind Subramanian et al. « Gene Set Enrichment Analysis : A Knowledge-Based Approach for Interpreting Genome-Wide Expression Profiles ». In : *Proceedings of the National Academy of Sciences of the United States of America* 102.43 (oct. 2005), p. 15545-15550. issn : 0027-8424. doi : 10.1073/pnas.0506580102.

[104] Dénes Türei, Tamás Korcsmáros et Julio Saez-Rodriguez. « OmniPath : Guidelines and Gateway for Literature-Curated Signaling Pathway Resources ». In : *Nature Methods* 13.12 (déc. 2016), p. 966-967. issn : 1548-7105. doi : 10.1038/nmeth.4077. (Visité le 23/07/2024).

[105] Jamie L. Marshall et al. « High-Resolution Slide-seqV2 Spatial Transcriptomics Enables Discovery of Disease-Specific Cell Neighborhoods and Pathways ». In : *iScience* 25.4 (avr. 2022). issn : 2589-0042. doi : 10.1016/j.isci.2022.104097. (Visité le 23/07/2024).

[106] Sean K. Wang et al. « Single-Cell Multiome of the Human Retina and Deep Learning Nominate Causal Variants in Complex Eye Diseases ». In : *Cell Genomics* 2.8 (août 2022), p. 100164. issn : 2666-979X. doi : 10.1016/j.xgen.2022.100164. (Visité le 06/01/2025).

[107] Eshaan Nichani, Alex Damian et Jason D. Lee. *How Transformers Learn Causal Structure with Gradient Descent*. Fév. 2024. doi : 10.48550/arXiv.2402.14735. arXiv : 2402.14735 [cs, math, stat]. (Visité le 23/07/2024).

[108] Kyuhong Shim et al. *Layer-Wise Pruning of Transformer Attention Heads for Efficient Language Modeling*. Oct. 2021. DOI : 10.48550/arXiv.2110.03252. arXiv : 2110.03252 [cs]. (Visité le 23/07/2024).

[109] William Fedus, Barret Zoph et Noam Shazeer. *Switch Transformers : Scaling to Trillion Parameter Models with Simple and Efficient Sparsity*. Juin 2022. DOI : 10.48550/arXiv.2101.03961. arXiv : 2101.03961 [cs]. (Visité le 23/07/2024).

[110] Oscar Franzén, Li-Ming Gan et Johan L M Björkegren. « PanglaoDB : A Web Server for Exploration of Mouse and Human Single-Cell RNA Sequencing Data ». In : *Database : The Journal of Biological Databases and Curation* 2019 (avr. 2019), baz046. ISSN : 1758-0463. DOI : 10.1093/database/baz046. (Visité le 23/07/2024).

[111] Arthur Liberzon et al. « The Molecular Signatures Database (MSigDB) Hallmark Gene Set Collection ». In : *Cell Systems* 1.6 (déc. 2015), p. 417-425. ISSN : 2405-4712. DOI : 10.1016/j.cels.2015.12.004.

[112] Peter J. Park. « ChIP–Seq : Advantages and Challenges of a Maturing Technology ». In : *Nature Reviews Genetics* 10.10 (oct. 2009), p. 669-680. ISSN : 1471-0064. DOI : 10.1038/nrg2641. (Visité le 19/07/2024).

[113] Liying Yan et al. « Single-Cell RNA-Seq Profiling of Human Preimplantation Embryos and Embryonic Stem Cells ». In : *Nature structural & molecular biology* 20.9 (sept. 2013), p. 1131-1139. ISSN : 1545-9985. DOI : 10.1038/nsmb.2660. (Visité le 19/07/2024).

[114] Benjamin L. Kidder, Gangqing Hu et Keji Zhao. « ChIP-Seq : Technical Considerations for Obtaining High Quality Data ». In : *Nature immunology* 12.10 (sept. 2011), p. 918-922. ISSN : 1529-2908. DOI : 10.1038/ni.2117. (Visité le 19/07/2024).

[115] Joseph M. Replogle et al. « Mapping Information-Rich Genotype-Phenotype Landscapes with Genome-Scale Perturb-seq ». In : *Cell* 185.14 (juill. 2022), 2559-2575.e28. ISSN : 1097-4172. DOI : 10.1016/j.cell.2022.05.013.

[116] Florian Wagner, Yun Yan et Itai Yanai. *K-Nearest Neighbor Smoothing for High-Throughput Single-Cell RNA-Seq Data*. Avr. 2018. DOI : 10.1101/217737. (Visité le 15/07/2024).

[117] Tavé van Zyl et al. « Cell Atlas of the Human Ocular Anterior Segment : Tissue-specific and Shared Cell Types ». In : *Proceedings of the National Academy of Sciences* 119.29 (juill. 2022), e2200914119. DOI : 10.1073/pnas.2200914119. (Visité le 19/07/2024).

[118] Joseph Burclaff et al. « A Proximal-to-Distal Survey of Healthy Adult Human Small Intestine and Colon Epithelium by Single-Cell Transcriptomics ». In : *Cellular and Molecular Gastroenterology and Hepatology* 13.5 (2022), p. 1554-1589. ISSN : 2352-345X. DOI : 10.1016/j.jcmgh.2022.02.007.

[119] Malte D. Luecken et al. « Benchmarking Atlas-Level Data Integration in Single-Cell Genomics ». In : *Nature Methods* 19.1 (jan. 2022), p. 41-50. ISSN : 1548-7105. DOI : 10.1038/s41592-021-01336-8. (Visité le 19/04/2024).

[120] *Openproblems-Bio/Openproblems-V2*. Open Problems in Single-Cell Analysis. Juill. 2024. (Visité le 15/07/2024).

[121] C. Domínguez Conde et al. « Cross-Tissue Immune Cell Analysis Reveals Tissue-Specific Features in Humans ». In : *Science (New York, N.Y.)* 376.6594 (mai 2022), eabl5197. DOI : 10.1126/science.abl5197. (Visité le 23/10/2024).

[122] Lisa Sikkema et al. « An Integrated Cell Atlas of the Lung in Health and Disease ». In : *Nature Medicine* 29.6 (juin 2023), p. 1563-1577. ISSN : 1546-170X. DOI : 10.1038/s41591-023-02327-2. (Visité le 15/07/2024).

[123] Matthew Amodio et al. « Exploring Single-Cell Data with Deep Multitasking Neural Networks ». In : *Nature Methods* 16.11 (nov. 2019), p. 1139-1145. ISSN : 1548-7105. DOI : 10.1038/s41592-019-0576-7. (Visité le 25/02/2025).

[124] Jialin Liu et al. « Jointly Defining Cell Types from Multiple Single-Cell Datasets Using LIGER ». In : *Nature Protocols* 15.11 (nov. 2020), p. 3632-3662. ISSN : 1750-2799. DOI : 10.1038/s41596-020-0391-8. (Visité le 25/02/2025).

[125] Aws Saudi et al. « Immune-Activated B Cells Are Dominant in Prostate Cancer ». In : *Cancers* 15.3 (fév. 2023), p. 920. ISSN : 2072-6694. DOI : 10.3390/cancers15030920. (Visité le 23/07/2024).

[126] *Bcl-2 Associated Athanogene 5 (Bag5) Is Overexpressed in Prostate Cancer and Inhibits ER-stress Induced Apoptosis - PMC*. https://www.ncbi.nlm.nih.gov/pmc/articles/PMC3598994/. (Visité le 25/07/2024).

[127] *Host CLIC4 Expression in the Tumor Microenvironment Is Essential for Breast Cancer Metastatic Competence | PLOS Genetics*. https://journals.plos.org/plosgenetics/article ?id=10.1371/journal.pgen.1010271. (Visité le 25/07/2024).

[128] Ru Zhu et al. « TAP1, a Potential Immune-Related Prognosis Biomarker with Functional Significance in Uveal Melanoma ». In : *BMC Cancer* 23.1 (fév. 2023), p. 146. ISSN : 1471-2407. DOI : 10.1186/s12885-023-10527-9. (Visité le 25/07/2024).

[129] *Targeting LIPA Independent of Its Lipase Activity Is a Therapeutic Strategy in Solid Tumors via Induction of Endoplasmic Reticulum Stress | Nature Cancer*. https://www.nature.com/articles/s43018-022-00389-8. (Visité le 25/07/2024).

[130] *Cancer-Associated Fibroblasts : From Basic Science to Anticancer Therapy | Experimental & Molecular Medicine*. https://www.nature.com/articles/s12276-023-01013-0. (Visité le 26/07/2024).

[131] *Fibroblast Heterogeneity in Prostate Carcinogenesis - PMC*. https://www.ncbi.nlm.nih.gov/pmc/articles/PMC8788937/. (Visité le 26/07/2024).

[132] *Epidemiology of Clinical Benign Prostatic Hyperplasia - PMC*. https://www.ncbi.nlm.nih.gov/pmc/articles/PMC5717991/. (Visité le 26/07/2024).

[133] J. Kuźnicki et al. « Calcyclin as a Marker of Human Epithelial Cells and Fibroblasts ». In : *Experimental Cell Research* 200.2 (1er juin 1992), p. 425-430. ISSN : 0014-4827. DOI : 10.1016/0014-4827(92)90191-A. URL : https://www.sciencedirect.com/science/article/pii/001448279290191A (visité le 26/07/2024).

[134] *S100A6 : Molecular Function and Biomarker Role | Biomarker Research | Full Text.* URL : https://biomarkerres.biomedcentral.com/articles/10.1186/s40364-023-00515-3 (visité le 26/07/2024).

[135] *WikiPathways 2024 : Next Generation Pathway Database | Nucleic Acids Research | Oxford Academic.* URL : https://academic.oup.com/nar/article/52/D1/D679/7369835 (visité le 26/07/2024).

[136] *THE ROLE OF BIOMARKER MACROPHAGE MIGRATION INHIBITORY FACTOR IN CARDIAC REMODELING PREDICTION IN PATIENTS WITH ST-SEGMENT ELEVATION MYOCARDIAL INFARCTION - PubMed.* URL : https://pubmed.ncbi.nlm.nih.gov/37326070/ (visité le 26/07/2024).

[137] *IGFBP7 Promotes Endothelial Cell Repair in the Recovery Phase of Acute Lung Injury - PMC.* URL : https://www.ncbi.nlm.nih.gov/pmc/articles/PMC11196208/ (visité le 26/07/2024).

[138] Yan Li et al. « The Prostate-Associated Gene 4 (PAGE4) Could Play a Role in the Development of Benign Prostatic Hyperplasia under Oxidative Stress ». In : *Oxidative Medicine and Cellular Longevity* 2022 (2022), p. 7041739. ISSN : 1942-0994. DOI : 10.1155/2022/7041739. pmid : 35633887.

[139] Chengcheng Lv et al. « PAGE4 Promotes Prostate Cancer Cells Survive under Oxidative Stress through Modulating MAPK/JNK/ERK Pathway ». In : *Journal of experimental & clinical cancer research : CR* 38.1 (18 jan. 2019), p. 24. ISSN : 1756-9966. DOI : 10.1186/s13046-019-1032-3. pmid : 30658679.

[140] Aline Marques Dias et al. « Downregulation of Metallothionein 2A Reduces Migration, Invasion and Proliferation Activities in Human Squamous Cell Carcinoma Cells ». In : *Molecular Biology Reports* 49.5 (mai 2022), p. 3665-3674. ISSN : 1573-4978. DOI : 10.1007/s11033-022-07206-6. pmid : 35107738.

[141] Jiawen Luo et al. « Mechanism of Prognostic Marker SPOCK3 Affecting Malignant Progression of Prostate Cancer and Construction of Prognostic Model ». In : *BMC Cancer* 23 (11 août 2023), p. 741. ISSN : 1471-2407. DOI : 10.1186/s12885-023-11151-3. pmid : 37563543. URL : https://www.ncbi.nlm.nih.gov/pmc/articles/PMC10416445/ (visité le 26/07/2024).

[142] Gabriela Boufelli de Freitas et al. « The Circulating 70 kDa Heat Shock Protein (HSPA1A) Level Is a Potential Biomarker for Breast Carcinoma and Its Progression ». In : *Scientific Reports* 12 (29 juill. 2022), p. 13012. ISSN : 2045-2322. DOI : 10.1038/s41598-022-17414-6. pmid : 35906272. URL : https://www.ncbi.nlm.nih.gov/pmc/articles/PMC9338230/ (visité le 26/07/2024).

[143] *CD99 at the Crossroads of Physiology and Pathology - PMC*. URL : https://www.ncbi.nlm.nih.gov/pmc/articles/PMC5842202/ (visité le 26/07/2024).

[144] Marija MILACIC et al. « The Reactome Pathway Knowledgebase 2024 ». In : *Nucleic Acids Research* 52.D1 (5 jan. 2024), p. D672-D678. ISSN : 0305-1048. DOI : 10.1093/nar/gkad1025. URL : https://doi.org/10.1093/nar/gkad1025 (visité le 26/07/2024).

[145] Mate MAUS et al. « Iron Accumulation Drives Fibrosis, Senescence and the Senescence-Associated Secretory Phenotype ». In : *Nature Metabolism* 5.12 (déc. 2023), p. 2111-2130. ISSN : 2522-5812. DOI : 10.1038/s42255-023-00928-2. URL : https://www.nature.com/articles/s42255-023-00928-2 (visité le 26/07/2024).

[146] Youliang QIAN et al. « Establishment of Cancer-Associated Fibroblasts-Related Subtypes and Prognostic Index for Prostate Cancer through Single-Cell and Bulk RNA Transcriptome ». In : *Scientific Reports* 13.1 (3 juin 2023), p. 9016. ISSN : 2045-2322. DOI : 10.1038/s41598-023-36125-0. URL : https://www.nature.com/articles/s41598-023-36125-0 (visité le 26/07/2024).

[147] Xingguo LI et al. « Accumulation of NCOA1 Dependent on HERC3 Deficiency Transactivates Matrix Metallopeptidases and Promotes Extracellular Matrix Degradation in Intervertebral Disc Degeneration ». In : *Life Sciences* 320 (1er mai 2023), p. 121555. ISSN : 0024-3205. DOI : 10.1016/j.lfs.2023.121555. URL : https://www.sciencedirect.com/science/article/pii/S0024320523001893 (visité le 26/07/2024).

[148] Athina KLADI-SKANDALI et al. « Expressional Profiling and Clinical Relevance of RNase K in Prostate Cancer : A Novel Indicator of Favorable Progression-Free Survival ». In : *Journal of Cancer Research and Clinical Oncology* 144.10 (oct. 2018), p. 2049-2057. ISSN : 1432-1335. DOI : 10.1007/s00432-018-2719-0. pmid : 30054827.

[149] *Selenoprotein T Deficiency Alters Cell Adhesion and Elevates Selenoprotein W Expression in Murine Fibroblast Cells - PMC*. URL : https://www.ncbi.nlm.nih.gov/pmc/articles/PMC3471091/ (visité le 26/07/2024).

[150] *The Effect of pH on the Extracellular Matrix and Biofilms - PubMed*. URL : https://pubmed.ncbi.nlm.nih.gov/26155386/ (visité le 26/07/2024).

[151] Francesco COLOTTA et al. « Cancer-Related Inflammation, the Seventh Hallmark of Cancer : Links to Genetic Instability ». In : *Carcinogenesis* 30.7 (1er juill. 2009), p. 1073-1081. ISSN : 0143-3334. DOI : 10.1093/carcin/bgp127. URL : https://doi.org/10.1093/carcin/bgp127 (visité le 26/07/2024).

[152] Douglas HANAHAN et Robert A. WEINBERG. « Hallmarks of Cancer : The Next Generation ». In : *Cell* 144.5 (4 mars 2011), p. 646-674. ISSN : 0092-8674, 1097-4172. DOI : 10.1016/j.cell.2011.02.013. pmid : 21376230. URL : https://www.cell.com/cell/abstract/S0092-8674(11)00127-9 (visité le 26/07/2024).

[153] Roshan RAO et al. *Transformer Protein Language Models Are Unsupervised Structure Learners*. Déc. 2020. DOI : 10.1101/2020.12.15.422761. (Visité le 25/02/2025).

[154] Jérémie Kalfon et al. *scPRINT : Pre-Training on 50 Million Cells Allows Robust Gene Network Predictions*. Juill. 2024. DOI : 10.1101/2024.07.29.605556. (Visité le 06/02/2025).

[155] Le Song, Eran Segal et Eric Xing. *Toward AI-Driven Digital Organism : Multiscale Foundation Models for Predicting, Simulating and Programming Biology at All Levels*. 9 déc. 2024. DOI : 10.48550/arXiv.2412.06993. arXiv : 2412.06993 [cs]. URL : http://arxiv.org/abs/2412.06993 (visité le 16/05/2025). Prépubl.

[156] Yunda Si et al. « Foundation Models in Molecular Biology ». In : *Biophysics Reports* 10.3 (juin 2024), p. 135-151. ISSN : 2364-3439. DOI : 10.52601/bpr.2024.240006. (Visité le 25/02/2025).

[157] Josh Abramson et al. « Accurate Structure Prediction of Biomolecular Interactions with AlphaFold 3 ». In : *Nature* 630.8016 (juin 2024), p. 493-500. ISSN : 1476-4687. DOI : 10.1038/s41586-024-07487-w. (Visité le 25/02/2025).

[158] Oscar Méndez-Lucio, Christos A. Nicolaou et Berton Earnshaw. « MolE : A Foundation Model for Molecular Graphs Using Disentangled Attention ». In : *Nature Communications* 15.1 (nov. 2024), p. 9431. ISSN : 2041-1723. DOI : 10.1038/s41467-024-53751-y. (Visité le 25/02/2025).

[159] Jerret Ross et al. « Large-Scale Chemical Language Representations Capture Molecular Structure and Properties ». In : *Nature Machine Intelligence* 4.12 (déc. 2022), p. 1256-1264. ISSN : 2522-5839. DOI : 10.1038/s42256-022-00580-7. (Visité le 25/02/2025).

[160] Boris Kozinsky et al. « Scaling the Leading Accuracy of Deep Equivariant Models to Biomolecular Simulations of Realistic Size ». In : *Proceedings of the International Conference for High Performance Computing, Networking, Storage and Analysis*. SC '23. New York, NY, USA : Association for Computing Machinery, nov. 2023, p. 1-12. ISBN : 9798400701092. DOI : 10.1145/3581784.3627041. (Visité le 25/02/2025).

[161] Anouar Benali et al. *Pushing the Accuracy Limit of Foundation Neural Network Models with Quantum Monte Carlo Forces and Path Integrals*. 2025. arXiv : 2504.07948 [physics.chem-ph]. URL : https://arxiv.org/abs/2504.07948.

[162] Benjamin Rhodes et al. *Orb-v3 : atomistic simulation at scale*. 2025. arXiv : 2504.06231 [cond-mat.mtrl-sci]. URL : https://arxiv.org/abs/2504.06231.

[163] Eric Nguyen et al. *HyenaDNA : Long-Range Genomic Sequence Modeling at Single Nucleotide Resolution*. 2023. arXiv : 2306.15794 [cs.LG]. URL : https://arxiv.org/abs/2306.15794.

[164] Hugo Dalla-Torre et al. *The Nucleotide Transformer : Building and Evaluating Robust Foundation Models for Human Genomics*. Oct. 2024. DOI : 10.1101/2023.01.11.523679. (Visité le 25/02/2025).

[165] Ning Wang et al. « Multi-Purpose RNA Language Modelling with Motif-Aware Pretraining and Type-Guided Fine-Tuning ». In : *Nature Machine Intelligence* 6.5 (mai 2024), p. 548-557. ISSN : 2522-5839. DOI : 10.1038/s42256-024-00836-4. (Visité le 25/02/2025).

[166] Philip Fradkin et al. *Orthrus : Towards Evolutionary and Functional RNA Foundation Models*. Oct. 2024. DOI : 10.1101/2024.10.10.617658. (Visité le 25/02/2025).

[167] Garyk Brixi et al. *Genome Modeling and Design across All Domains of Life with Evo 2*. Fév. 2025. DOI : 10.1101/2025.02.18.638918. (Visité le 09/03/2025).

[168] Andre Cornman et al. *The OMG Dataset : An Open MetaGenomic Corpus for Mixed-Modality Genomic Language Modeling*. Août 2024. DOI : 10.1101/2024.08.14.607850. (Visité le 09/03/2025).

[169] Yingce Xia et al. *NatureLM : Deciphering the Language of Nature for Scientific Discovery*. Fév. 2025. DOI : 10.48550/arXiv.2502.07527. arXiv : 2502.07527 [cs]. (Visité le 25/02/2025).

[170] Kasia Z. Kedzierska et al. *Assessing the Limits of Zero-Shot Foundation Models in Single-Cell Biology*. Oct. 2023. DOI : 10.1101/2023.10.16.561085. (Visité le 18/04/2024).

[171] Ihab Bendidi et al. *Benchmarking Transcriptomics Foundation Models for Perturbation Analysis : One PCA Still Rules Them All*. Nov. 2024. DOI : 10.48550/arXiv.2410.13956. arXiv : 2410.13956 [cs]. (Visité le 25/02/2025).

[172] Maxime Oquab et al. *DINOv2 : Learning Robust Visual Features without Supervision*. Fév. 2024. DOI : 10.48550/arXiv.2304.07193. arXiv : 2304.07193 [cs]. (Visité le 25/02/2025).

[173] Xiyue Wang et al. « A Pathology Foundation Model for Cancer Diagnosis and Prognosis Prediction ». In : *Nature* 634.8035 (oct. 2024), p. 970-978. ISSN : 1476-4687. DOI : 10.1038/s41586-024-07894-z. (Visité le 25/02/2025).

[174] Mark-Anthony Bray et al. « Cell Painting, a High-Content Image-Based Assay for Morphological Profiling Using Multiplexed Fluorescent Dyes ». In : *Nature Protocols* 11.9 (sept. 2016), p. 1757-1774. ISSN : 1750-2799. DOI : 10.1038/nprot.2016.105. (Visité le 25/02/2025).

[175] Johann Wenckstern et al. *AI-powered Virtual Tissues from Spatial Proteomics for Clinical Diagnostics and Biomedical Discovery*. Jan. 2025. DOI : 10.48550/arXiv.2501.06039. arXiv : 2501.06039 [q-bio]. (Visité le 27/03/2025).

[176] Shahar Alon et al. « Expansion Sequencing : Spatially Precise in Situ Transcriptomics in Intact Biological Systems ». In : *Science* 371.6528 (jan. 2021), eaax2656. DOI : 10.1126/science.aax2656. (Visité le 25/02/2025).

[177] Alexander P. Hertle, Benedikt Haberl et Ralph Bock. « Horizontal Genome Transfer by Cell-to-Cell Travel of Whole Organelles ». In : *Science Advances* 7.1 (jan. 2021), eabd8215. DOI : 10.1126/sciadv.abd8215. (Visité le 25/02/2025).

[178] Ihuan Gunawan et al. « An Introduction to Representation Learning for Single-Cell Data Analysis ». In : *Cell Reports Methods* 3.8 (août 2023), p. 100547. ISSN : 2667-2375. DOI : 10.1016/j.crmeth.2023.100547. (Visité le 27/03/2025).

[179] Yoshua Bengio, Aaron Courville et Pascal Vincent. *Representation Learning : A Review and New Perspectives*. Avr. 2014. DOI : 10.48550/arXiv.1206.5538. arXiv : 1206.5538 [cs]. (Visité le 27/03/2025).

[180] Mohammad Lotfollahi et al. « Mapping Single-Cell Data to Reference Atlases by Transfer Learning ». In : *Nature Biotechnology* 40.1 (jan. 2022), p. 121-130. ISSN : 1546-1696. DOI : 10.1038/s41587-021-01001-7. (Visité le 06/02/2025).

[181] Amy X. Lu et al. *Tokenized and Continuous Embedding Compressions of Protein Sequence and Structure*. Nov. 2024. DOI : 10.1101/2024.08.06.606920. (Visité le 06/02/2025).

[182] Fabian Mentzer et al. *Finite Scalar Quantization : VQ-VAE Made Simple*. Oct. 2023. DOI : 10.48550/arXiv.2309.15505. arXiv : 2309.15505 [cs]. (Visité le 06/02/2025).

[183] Zhihan Zhou et al. *DNABERT-S : Pioneering Species Differentiation with Species-Aware DNA Embeddings*. Oct. 2024. DOI : 10.48550/arXiv.2402.08777. arXiv : 2402.08777 [q-bio]. (Visité le 06/02/2025).

[184] Steven Schockaert. *Embeddings as Epistemic States : Limitations on the Use of Pooling Operators for Accumulating Knowledge*. Juill. 2023. DOI : 10.48550/arXiv.2210.05723. arXiv : 2210.05723 [cs]. (Visité le 27/03/2025).

[185] Chankyu Lee et al. *NV-Embed : Improved Techniques for Training LLMs as Generalist Embedding Models*. Jan. 2025. DOI : 10.48550/arXiv.2405.17428. arXiv : 2405.17428 [cs]. (Visité le 06/02/2025).

[186] Maximilian Ilse, Jakub Tomczak et Max Welling. « Attention-Based Deep Multiple Instance Learning ». In : *Proceedings of the 35th International Conference on Machine Learning*. PMLR, juill. 2018, p. 2127-2136. (Visité le 27/03/2025).

[187] Clément Christophe et al. *Med42 – Evaluating Fine-Tuning Strategies for Medical LLMs : Full-Parameter vs. Parameter-Efficient Approaches*. Avr. 2024. DOI : 10.48550/arXiv.2404.14779. arXiv : 2404.14779 [cs]. (Visité le 25/02/2025).

[188] Edward J. Hu et al. *LoRA : Low-Rank Adaptation of Large Language Models*. Oct. 2021. DOI : 10.48550/arXiv.2106.09685. arXiv : 2106.09685 [cs]. (Visité le 06/02/2025).

[189] Tim Dettmers et al. *QLoRA : Efficient Finetuning of Quantized LLMs*. Mai 2023. DOI : 10.48550/arXiv.2305.14314. arXiv : 2305.14314 [cs]. (Visité le 06/02/2025).

[190] Arijit Ray et al. *COLA : A Benchmark for Compositional Text-to-image Retrieval*. Nov. 2023. DOI : 10.48550/arXiv.2305.03689. arXiv : 2305.03689 [cs]. (Visité le 06/02/2025).

[191] Ziqi Tang et al. « Evaluating the Representational Power of Pre-Trained DNA Language Models for Regulatory Genomics ». In : *bioRxiv* (sept. 2024), p. 2024.02.29.582810. ISSN : 2692-8205. DOI : 10.1101/2024.02.29.582810. (Visité le 27/03/2025).

[192] Matthew E. Peters, Sebastian Ruder et Noah A. Smith. *To Tune or Not to Tune ? Adapting Pretrained Representations to Diverse Tasks*. Juin 2019. DOI : 10.48550/arXiv.1903.05987. arXiv : 1903.05987 [cs]. (Visité le 25/02/2025).

[193] Alexandra Chronopoulou, Christos Baziotis et Alexandros Potamianos. *An Embarrassingly Simple Approach for Transfer Learning from Pretrained Language Models*. Mai 2019. DOI : 10.48550/arXiv.1902.10547. arXiv : 1902.10547 [cs]. (Visité le 25/02/2025).

[194] Neil Houlsby et al. *Parameter-Efficient Transfer Learning for NLP*. Juin 2019. DOI : 10.48550/arXiv.1902.00751. arXiv : 1902.00751 [cs]. (Visité le 25/02/2025).

[195] Zeming Lin et al. *Language Models of Protein Sequences at the Scale of Evolution Enable Accurate Structure Prediction*. Juill. 2022. DOI : 10.1101/2022.07.20.500902. (Visité le 15/07/2024).

[196] Naftali Tishby, Fernando C Pereira et William Bialek. « The Information Bottleneck Method ». In : ().

[197] Qifei Wang et al. *Hierarchical Interpretation of Out-of-Distribution Cells Using Bottlenecked Transformer*. Déc. 2024. DOI : 10.1101/2024.12.17.628533. (Visité le 16/05/2025).

[198] Aaron van den Oord, Yazhe Li et Oriol Vinyals. *Representation Learning with Contrastive Predictive Coding*. Version 2. 22 jan. 2019. DOI : 10.48550/arXiv.1807.03748. arXiv : 1807.03748 [cs]. URL : http://arxiv.org/abs/1807.03748 (visité le 27/02/2025). Prépubl.

Supplementary Materials

6.1 Supplementary Tables for scPRINT

6.1.1 List of novelties in scPRINT and comparison to scGPT and scFoundation

features	scPRINT	scGPT	scFoundation	Geneformer v2
classification pretraining	v	x	x	x
hierarchical classification	v	x	x	x
denoising pretraining	v	x	v	x
masking pretraining	v	v	v	v
MVC pretraining	v	v	x	x
AE pretraining	v	x	x	x
large cell count GN inference	v	x	x	x
zero-shot classification	v	x	x	x
zero-shot batch correction	v	x	x	x
zero-shot denoising	v	x	x	x
genome-wide GN inference	v	x	x	x
large input context	x	x	v	x
raw count encoding	v	x	v	x
very large model	v	x	x	x
pretraining strategy and dataset	v	x	x	x
low GPU/hours implementation	v	x	x	x
weighted random sampling	v	x	x	x
protein encoding	v	x	x	x
cross-species abilities	v	x	x	x
gene location encoding	v	x	x	x
genome-wide input context	x	x	v	x
xtrimogene architecture	x	x	v	x
train / validate / test strategies	v	x	x	x
flashattention2	v	x	x	x

Comparison of the features and novelties from scPRINT compared to 2 similar published state-of-the-art methods : scGPT and scFoundation.

6.1.2 Model comparison

model name	model size	training time (hours)	training hardware	num cells	num leaf cell type	dimension (d)	layers	heads	token input size	num species	training	attention
scPRINT-small	7M	24	1xA100	41M (91M before QC)							denoising (60%) + classification + bottleneck	flashattention2
Geneformer v2	? (~50M)	72	12xV100	30M	?	256	6	4	2,048	1	masked (15%)	normal
scPRINT-medium	20M	72	1xA100	41M (91M before QC)	540	256	8	4	2,200	2	denoising (60%) + classification + bottleneck	flashattention2
scGPT	100M	?	?	33M	?	512	12	8	1,200	1	masked (15%)	flashattention1
scFoundation	100M	?	?	50M	?	768	12+12	12+8	20,000	1	masked (30%) + denoising	xtrimogene
scPRINT	90M	96	4xA100	41M (91M before QC)	540	512	16	8	2,200	2	denoising (60%) + classification + bottleneck	flashattention2
GPT2-small	117M	?	?	300B tokens (~150M cells)	x	768	12	12	1200	x	masked (15%)	normal
UCE	650M	960	24xA100	36M	(~1000 ?) likely <500	1280	33	20	1024	5	masked (20%)	normal
cellFM	700M	?	32xAscend910 NPUs	100M	?	1536	40	48	4096	1	masked (20%)	normal + LORA
scPRINT-vlarge	700M	168	24xA100	41M (91M before QC)	540	1280	20	10	2,200	2	denoising (60%) + classification + bottleneck	flashattention2

comparing different model sizes and architectures. Comparing scPRINT to other state-of-the-art methods, as well as GPT2-small and GPT3-large models

6.1.3 Ablation study and impact on performance across tasks

id	description	denoise/reco2full_vs_noisy2full	emb_lung/ct_class	emb_lung/scib	emb_panc/ct_class	emb_panc/scib	reconstruction loss	classification accuracy	denoising loss	epoch
or46096v	small	0.34	0.31	0.47	0.11	0.41	1.31	0.4	1.16	24
ghqf2hym	medium	0.12	0.58	0.55	0.52	0.51	1.25	0.33	1.125	27
7asy8qpn	large	0.18	0.69	0.56	0.52	0.50	1.23	0.76	1.109	21
24chcp2e	medium-nofreeze	0.15	0.45	0.54	0.52	0.53	1.25	0.33	1.115	23
6o76ew23	medium-2-heads	0.10	0.49	0.55	0.40	0.53	1.25	0.33	1.124	26
lsr3pvnf	medium-MSE	0.21	0.61	0.56	0.51	0.49	1.26	0.33	6.3 (diff)	29
muwj73gx	medium-MVC	0.21	0.51	0.55	0.40	0.47	1.29	0.3	1.132	37
n8jypo8z	medium-noPE	0.09	0.71	0.56	0.35	0.46	1.27	0.33	1.31	23
q0fzpj5g	medium-no-random-weighted	0.17	0.51	0.53	0.19	0.48	1.26	0.26	1.118	27
f5e4qfkr	medium-MLM	0.04	0.53	0.54	0.39	0.46	1.26	0.35	0.999	23

The table shows the results of the ablation study on denoising, embedding with batch correction, and cell-type classification tasks. Results are displayed for the medium-size scPRINT model. Top to bottom : s*mall, medium, large :* regular models of various sizes. *medium-nofreeze :* a model trained without freezing gene embedding during pre-training. *medium-2-heads :* a model trained with only two heads per layer instead of 4. *medium-MSE* : a model with Mean Squared Error instead of the ZINB loss. *medium-MVC :* a model trained with scGPT's MVC methodology for the creation of the cell embedding. medium-noPE : a model trained without positional encoding for the gene's location. medium-no-random-weighted : a model trained without weighted random sampling. *medium-MLM* : a model trained with masked language modeling instead of denoising.

6.1.4 Computational speed of various GN inference methods

model	speed for 1000 cells	speed for a dataset of 12 cell types	scale to #cells	scale to #genes
DeepSEM	10mn	2 hours	linear	quadratic
GENIE3	50mn	10 hours	quadratic	quadratic
GENIE3 (100 trees)	4mn	1 hour	quadratic	quadratic
Geneformer v2	1mn	15mn	linear	linear
scGPT	1mn	15mn	linear	linear
scPRINT	1mn	15mn	linear	linear

The computational speed of running various gene network inference methods on a set of 4000 genes and 1000 cells. It is showing that transformer-based models are far faster than previous methods, owing to their clever use of the GPU and pre-training.

6.1.5 Table S5 : Performance of GN inference methods on the Sergio simulated scRNAseq dataset

model	EPR	AUPRC	TF_targ	TF_enr
DeepSEM	0.92601	0.00101	0	FALSE
GENIE3	0.94497	0.00193	5.2	TRUE
Geneformer v2	0.699	0.00409	0	TRUE
scGPT	0.6167	0.00278	10.5	TRUE
scPRINT	1.836	0.00861	13.15	FALSE

We generate a Sergio simulated scRNAseq dataset of 1000 cells for 800 genes from the RegNetwork ground truth network. We here showcase the ability of each model to recover

the RegNetwork ground truth from this dataset. It shows how only scPRINT can recover some of RegNetwork's connections.

6.1.6 Comparison scPRINT model size on performance across tasks and GN inference abilities

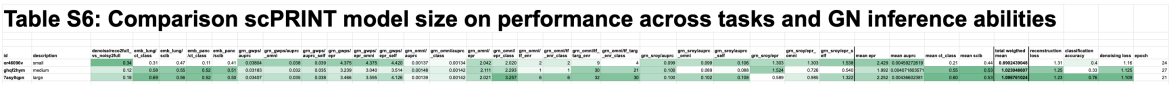
Table S6: Comparison scPRINT model size on performance across tasks and GN inference abilities

6.1.7 Overlap of different GN ground truths

comparison	precision	recall	random precision
MCalla et al. vs Omnipath	0.0520	0.0074	0.00154
MCalla et al. - T vs Omnipath	0.0155	0.0022	0.00154
gwps vs Omnipath	0.0015	0.0219	0.00129
gwps -T vs Omnipath	0.0030	0.0426	0.00129

Comparison of the overlap, expressed as precision and recall, of the three different ground truth networks used : MCalla, Omnipath, and gwps.

6.1.8 Table S8 : Omnipath benchmark results on the genome-wide perturb-seq dataset

tool	EPR	AU-PRC	TF target enr.	TF_enr	TF_only	ct_pred	RAND precision
DeepSEM	4.1	0.00192	21.4	FALSE	FALSE	FALSE	0.001633
GENIE3	4.7	0.00188	17.9	TRUE	FALSE	FALSE	0.00163
Geneformer v2	0.2	0.001796	5.9	FALSE	FALSE	FALSE	0.001528
scGPT	1.0	0.00208	14.0	TRUE	FALSE	FALSE	0.00163
scPRINT	2.8	0.00170	8.6	TRUE	FALSE	FALSE	0.00161
scPRINT (omnipath's heads)	4.7	0.00189	3.4	TRUE	FALSE	FALSE	0.00161
scPRINT (gwps' heads)	1.6	0.00190	5.0	TRUE	FALSE	FALSE	0.00161

Omnipath network overlap (EPR, AUPRC), as well as transcription factor enrichment, TF target enrichment, and cell type marker enrichment for gene networks generated by the

different tools on the genome-wide perturb seq K562 cells at steady state (no perturbations)

6.1.9 Omnipath benchmark results on the MCalla et al. datasets

tool	dataset	EPR	AUPRC	TF target enr.	TF enr.	cell type enr.
DeepSEM	**Han et. al.**	5.54	0.00029	18.9	FALSE	FALSE
DeepSEM	**Yan et. al.**	0.97	-0.00002	7.5	FALSE	FALSE
GENIE3	**Han et. al.**	1.51	0.00016	11.3	FALSE	TRUE
GENIE3	**Yan et. al.**	1.74	0.00020	0.0	FALSE	TRUE
Geneformer	**Han et. al.**	1.63	0.00010	11.3	FALSE	FALSE
Geneformer	**Yan et. al.**	1.99	0.00011	20.0	FALSE	FALSE
scGPT	**Han et. al.**	0.89	0.00016	17.0	TRUE	FALSE
scGPT	**Yan et. al.**	0.16	0.00007	20.0	FALSE	FALSE
scPRINT	**Han et. al.**	2.03	0.00019	23.6	TRUE	FALSE
scPRINT	**Yan et. al.**	1.76	0.00026	31.1	FALSE	TRUE
scPRINT (omnipath's heads)	**Han et. al.**	5.12	0.00004	3.6	TRUE	FALSE
scPRINT (omnipath's heads)	**Yan et. al.**	3.35	0.00019	13.3	FALSE	TRUE
scPRINT (Han et. al.'s heads)	**Han et. al.**	0.94	0.00030	30.9	TRUE	TRUE
scPRINT (Han et. al.'s heads)	**Yan et. al.**	0.57	-0.00004	6.7	TRUE	TRUE

Omnipath network overlap (EPR, AUPRC), as well as transcription factor enrichment, TF target enrichment, and cell type marker enrichment for gene networks generated by the different tools on the 2 human embryonic stem cell datasets used in Results Section 3 (scPRINT outperforms GENIE3 and scGPT on cell type-specific ground truths).

6.1.10 Denoising results per datasets

tools	denoising (+%) correlation. gNNpgpo6g ATjuxTE7C Cp	denoising (+%) correlation. R4ZHoQeg xXdSFNFY 5LGe	denoising (+%) correlation (RElyQZE6 OMZm1S3 W2Dxi)	denoising (+%) correlation (low cell count: 30). gNNpgpo6 gATjuxTE7 CCp	denoising (+%) correlation (low cell count: 30). R4ZHoQeg xXdSFNFY 5LGe	denoising (+%) correlation (low cell count: 30) (RElyQZE6 OMZm1S3W 2Dxi)	average denoising (+%) correlation	average denoising (+%) correlation (rare cell type)
untrained scPRINT	-16.0	X	X	-16.0	X	X	-16.0	-16.0
scPRINT	19.1	33.9	17.1	22.5	26.6	16.6	23.4	21.9
KNNsmoothing2	21.0	34.9	21.6	17.0	32.0	13.4	25.8	20.8
magic	29.3	34.6	22.7	16.8	24.4	4.6	28.9	15.3
magic (low cell dataset)	X	X	X	11.3	14.0	13.0	X	12.8

This table shows the detail of the denoising results for each of the three datasets for scPRINT-large, KNNsmoothing2, MAGIC, and MAGIC run on only the small cell type cluster. “Random scPRINT model” is the performance of an untrained scPRINT model.

6.1.11 Highlighted B-cell cluster genes in the BPH study

gene	link	in cancer	in b cell	analysis
		prostate	high expr in immune	
MBNL2	link	cancer	tissues	
MAGOH	link	cancer	high expr in immune tissues	BPH B-cell to normal B-cell diff. expr.
RANBP2	link1, link2	B-cell lymphoma	b cell validated	
		prostate	high expr in immune	
CLIC4	link	cancer	tissues	
BAG5	link	prostate cancer	b cell in cancer	
NR4A1	link1, link2	prostate cancer	b cell validated	
BAZ2A	link	prostate cancer	b cell validated	
		tumor suppressor in prostate	b cell	
ZBTB16	link1, link2	cancer	validated b cell	
TAP1	link1, link2	cancer	validated b cell	BPH B-cell to normal B-cell diff. expr. post denoising
TAS2R19	link		validated	
PRDM7	link	cancer	b cell in cancer	
TSEN54	link	cancer	b cell validated	
EHMT2	link			
ERICH6B	link	cancer	b cell in cancer	
IL10RB	link	cancer		

Table of the highlighted genes in the differential expression analysis in BPH vs normal B-cells together with their annotation on their relation to cancer and to b-cells, with sources.

6.1.12 Hub and differential hub genes in the fibroblast GN of the BPH study

TOP 15 hubs in BPH fibroblasts GN	TOP 15 hubs in normal fibroblasts GN	TOP 15 differential hubs in BPH fibroblasts vs normal	TOP 15 eigenvector_centrality differential hubs in BPH fibroblasts vs normal
HSPA1A	S100A6	HLA-A	CD99
MT2A	TGIF2-RAB5IF	MT2A	HLA-A
CREM	MIF	ATP6V0C	HSPA1A
TGIF2-RAB5IF	DNAJB9	DEFA1	LUM
HSPE1	IGFBP7	EIF4A1	ATP6V0C
CALD1	APOD	HSPA1A	CD99
SPOCK3	BRME1	LUM	EIF4A1
HLA-A	SPARCL1	SPOCK3	PAGE4
SPARCL1	TIMP1	nan-99	RYR2
RBP1	DCN	CD99	SERPINF1
C1S	C1S	CPE	C1R
BRME1-1	MGP	THBS1	COL6A2
FABP4	nan-270	LGALS1	HNRNPA0
nan-99	SLC25A6	PYDC2	SERPING1
LUM	BLOC1S5-TXNDC5	SERPING1	SERPINA3

List of the Top-15 elements in different GN analyses. Genes in yellow in the last columns are the new ones found with eigenvector centrality compared to the 3rd columns.

6.1.13 Number of elements predicted per class

ethnicity	21
sex	2
organism	2
cell type	424
disease	62
assay	26

Number of labels predicted by the model for each class. We use hierarchical classification for cell type, disease, assay, and ethnicity.

6.2 Supplementary figures for scPRINT

6.2.1 visualization of human gene embedding from ESM2

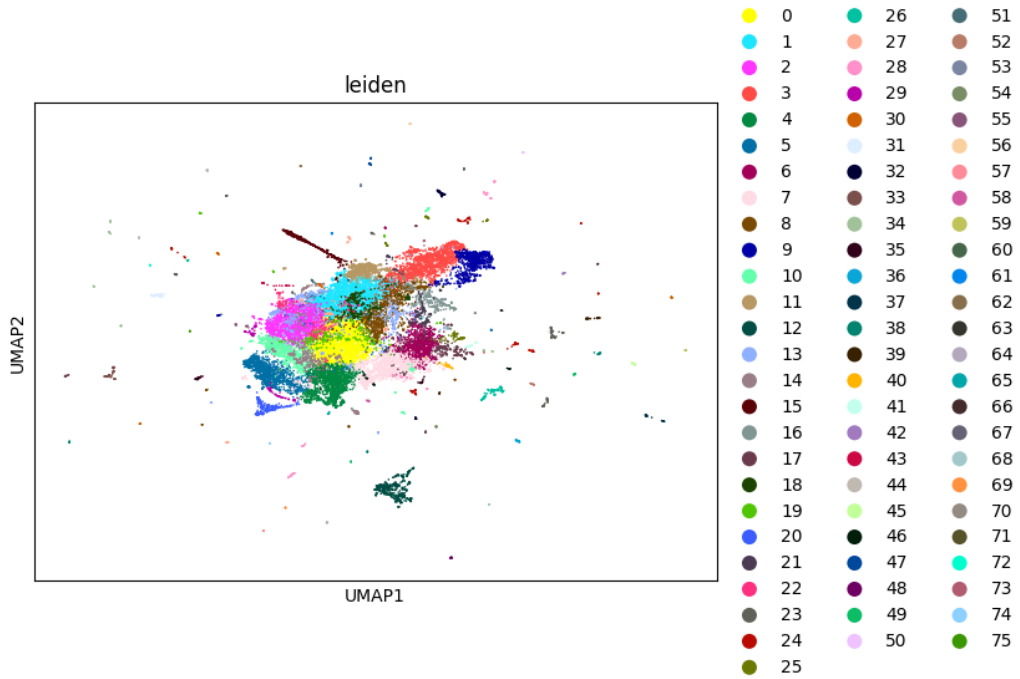

Umap of the ESM2 protein embeddings for the most common protein of all protein-coding genes in Ensembl. The PCA variance ratio is 0.856 for the top 50 principal components. We color it using the Louvain clustering of the embedding.

6.2.2 Gene network inference comparison with Omnipath per datasets

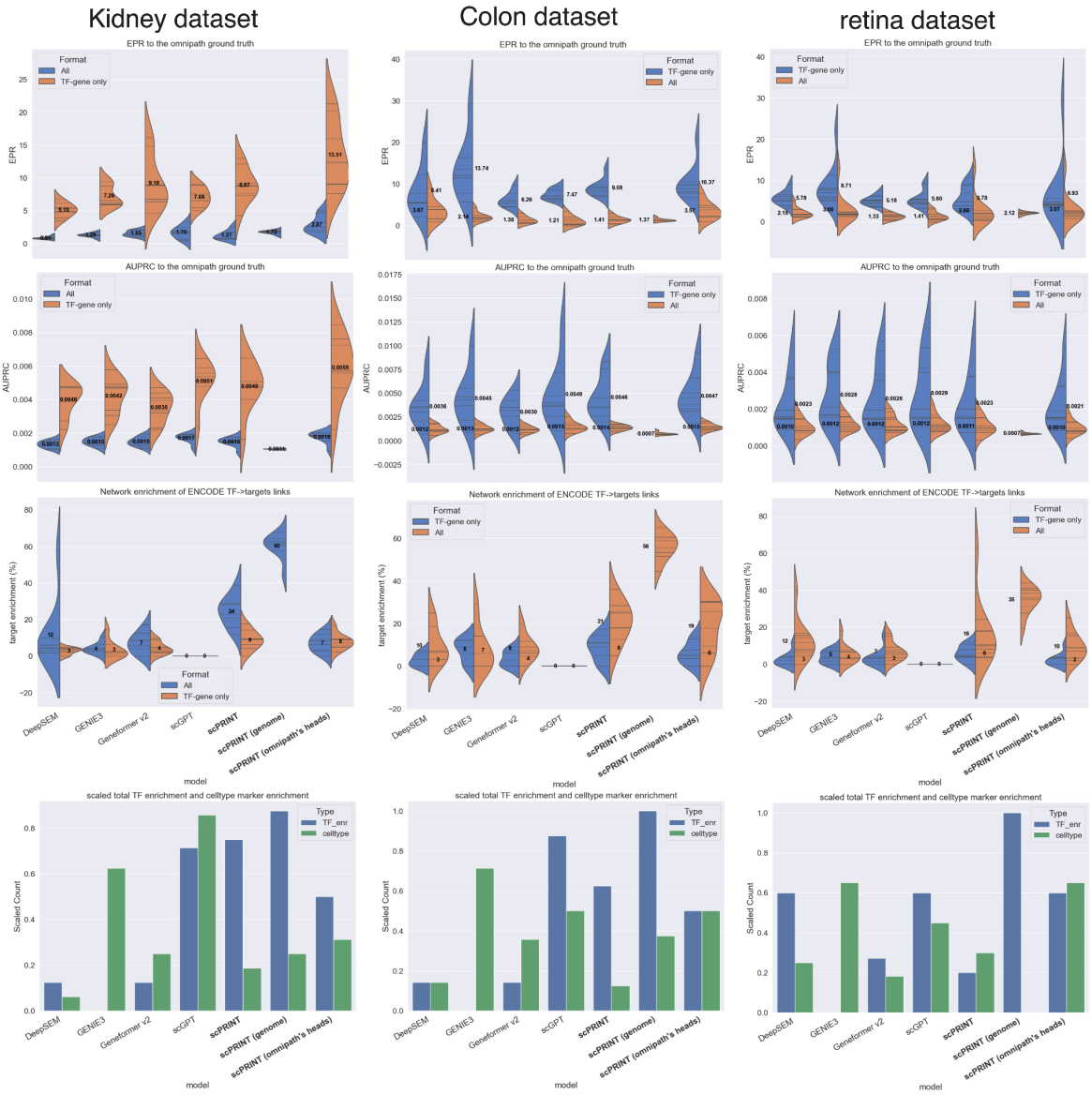

The same plots as in Figures 2B, C, and D, showing the Omnipath and enrichment results per dataset for each of the 3 datasets used. Source data are provided as a Source Data file.

6.2.3 Distribution of connection amongst the three ground truths

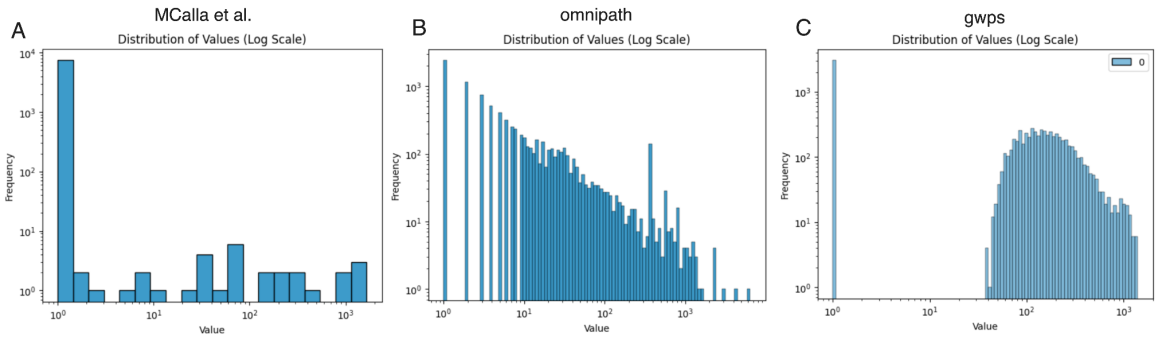

(a) Barplot of the distribution of the number of connections per edge in the MCalla human ground truth network. Most connections are 0, and there is a roughly uniform distribution of connections otherwise. This means most connections belong to the half a dozen most connected edges. (b) Barplot of the distribution of the number of connections per edge in the Omnipath ground truth network. We can see an almost linear relationship on the log-log scale, suggesting a power law distribution. (c) Barplot of the distribution of the number of connections per edge in the genome-wide perturb-seq ground truth network. We can see a very different distribution where only a few genes have little differentially expressed genes post-knock-out, and this trend increases until reaching around 200 connections. Then, it diminishes in what might be a power law. However, some of it is likely caused by the differential expression method and noise in the scRNAseq methodology.

6.2.4 Performance of each GN inference method on predicting the TF-gene only subset of the GWPS ground truth network

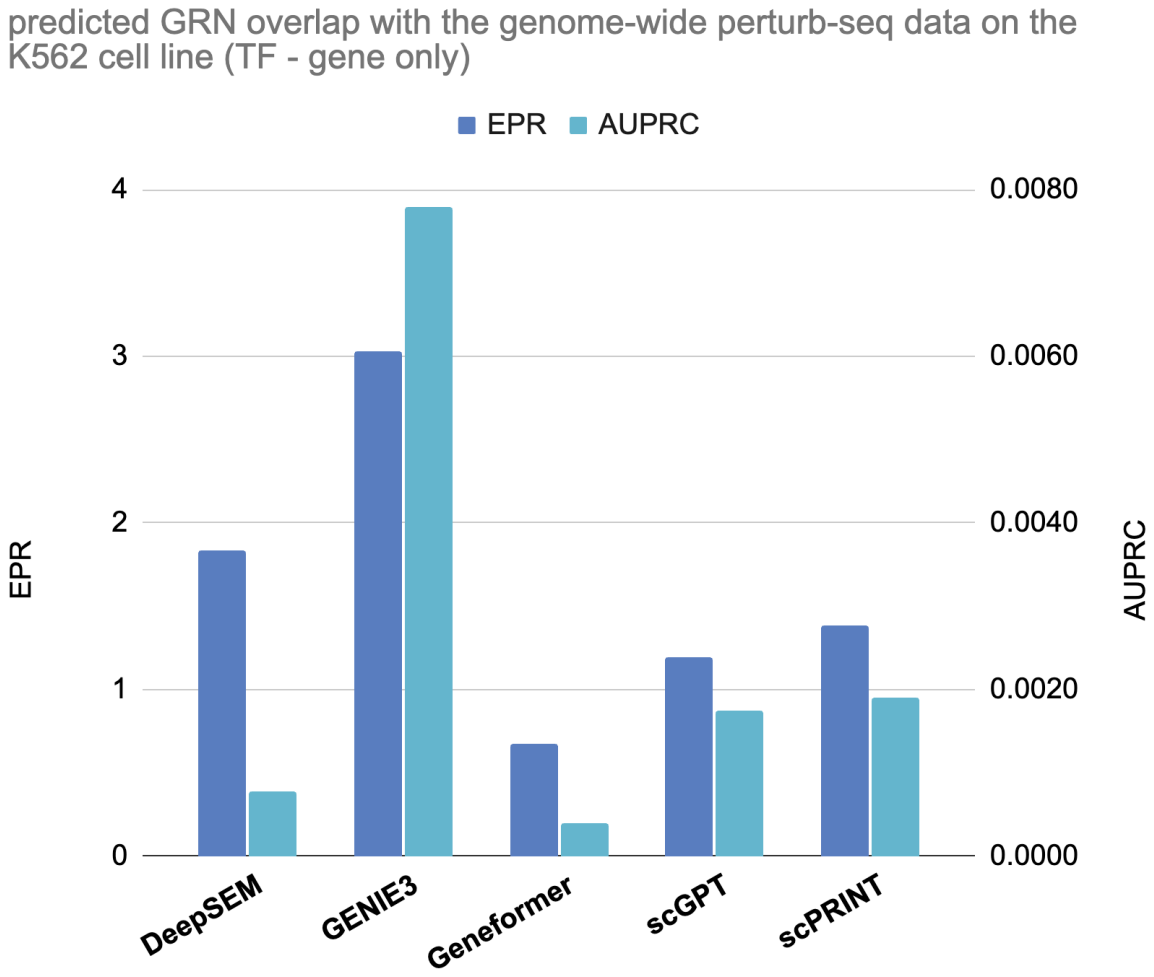

Performances of each model's networks on its overlap with the TF-gene-only subset of the genome-wide perturb seq ground truth. It shows that on this task, most foundation models do not perform well. This could be due to the way their attention matrix is normalized. Source data are provided as a Source Data file.

6.2.5 Full denoising results

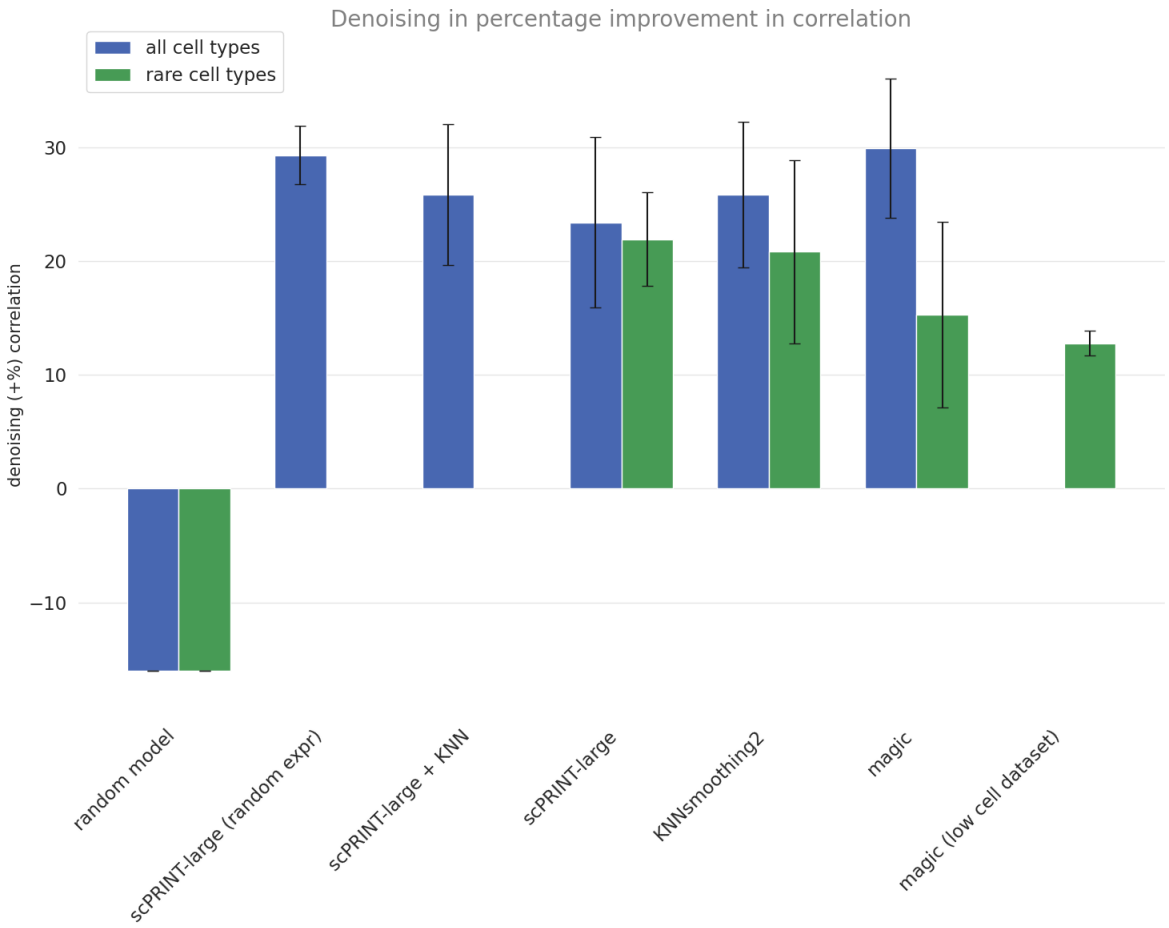

Denoising scores, similar to Figure 4A, but over more tools. “Random model” means a scPRINT model without pre-training. “Random expr” means that scPRINT was using a set of 3000 genes in a similar way as done in pre-training : Taking random expressed genes completed with random unexpressed genes if less than 3000 genes are expressed in the cell. “low cell dataset” means that MAGIC was only using the rare cell population for the dataset as presented in the methods. Source data are provided as a Source Data file.

6.2.6 Cell type classification metrics with per-batch split

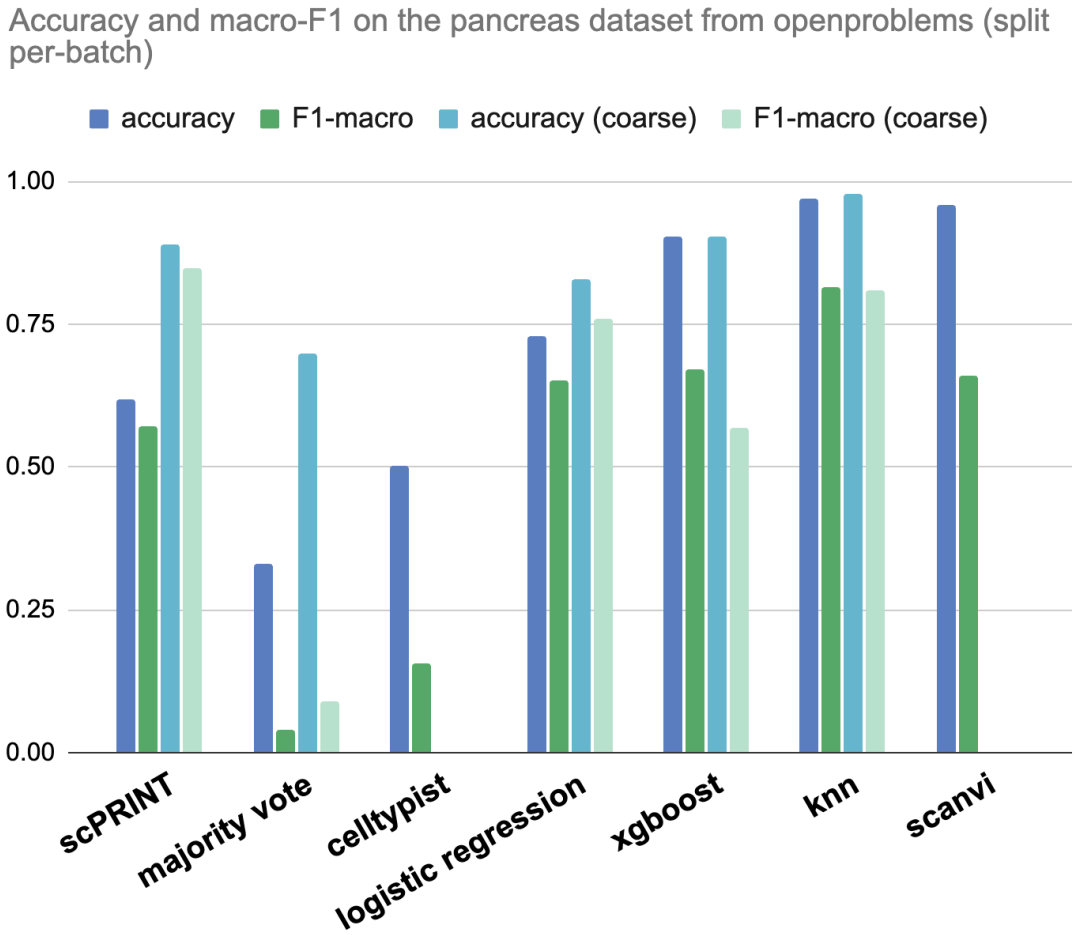

Cell type classification scores over the kidney test dataset of openproblems. Same as Figure 4B, but now the trained methods are trained on a subset of the batches representing roughly 70% of the dataset. The performance is lower in this context, and scPRINT, majority voting, and Celltypist's performance are not changing. Source data are provided as a Source Data file.

6.2.7 Full scIB batch correction scores

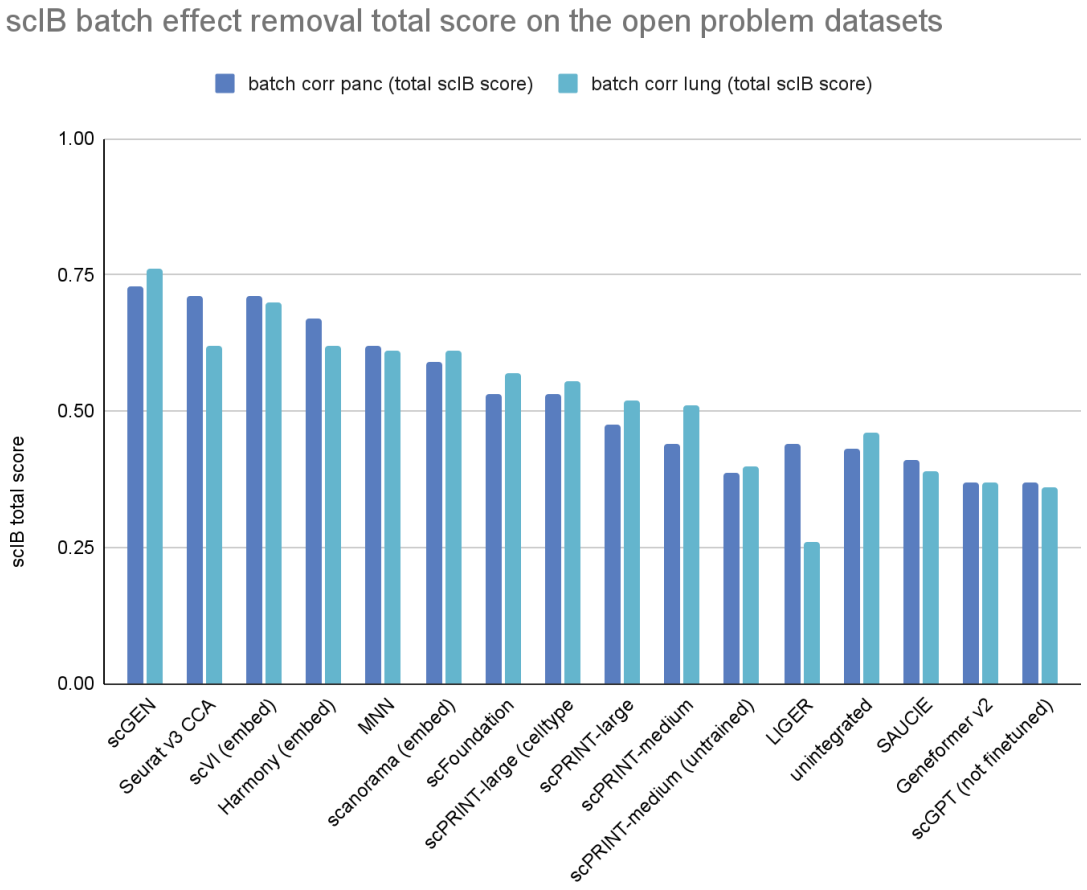

scIB benchmarking scores, averaged for the kidney and lung openproblems test datasets. Same as Figure 4C but over more tools. Cell type logits mean that the logits of the cell type classifier have been used as cell embeddings instead of the cell type embedding itself. Source data are provided as a Source Data file.

6.2.8 Full avgBio scores

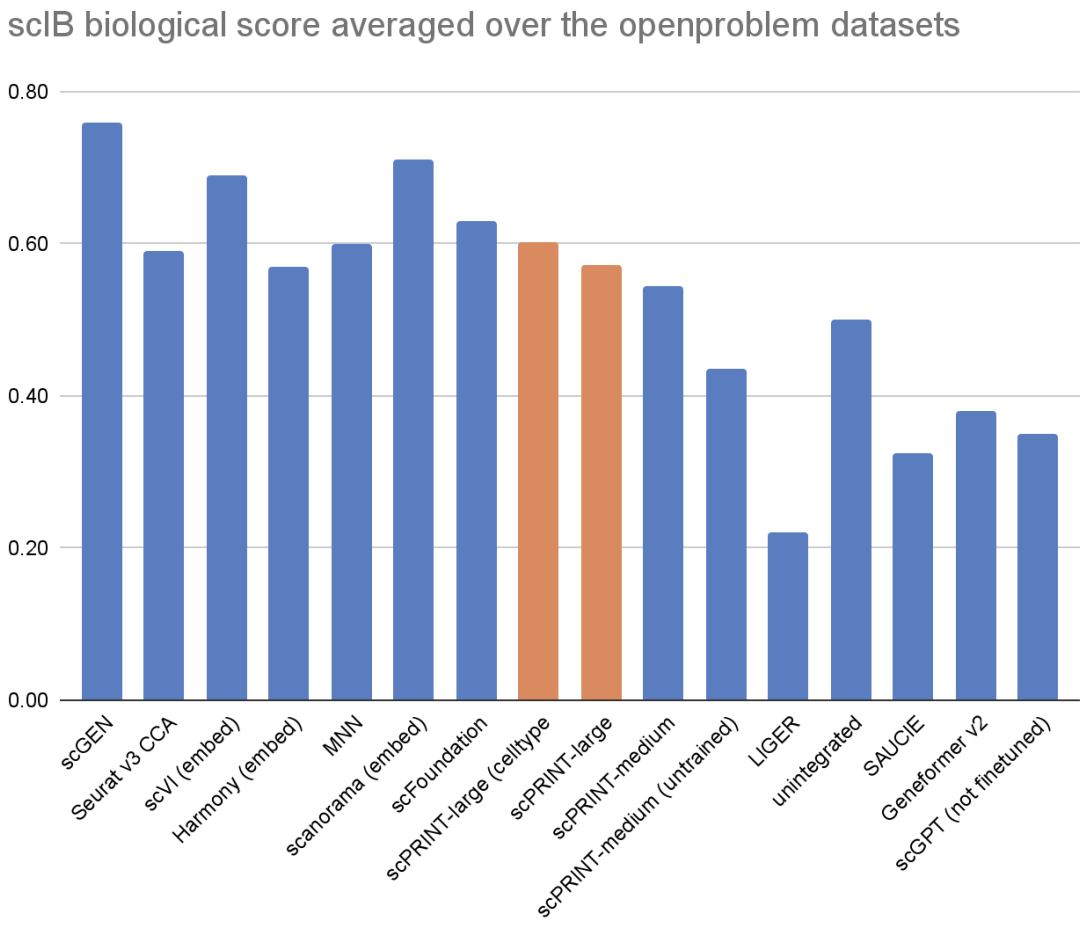

The average Biological score of the scIB benchmark averaged over the kidney and lung openproblems test datasets. Same as Figure 4D but over more tools. Cell type logits mean that the logits of the cell type classifier have been used as cell embeddings instead of the cell type embedding itself. Source data are provided as a Source Data file.

6.2.9 In-depth view of the BPH dataset and its scPRINT-predicted annotations

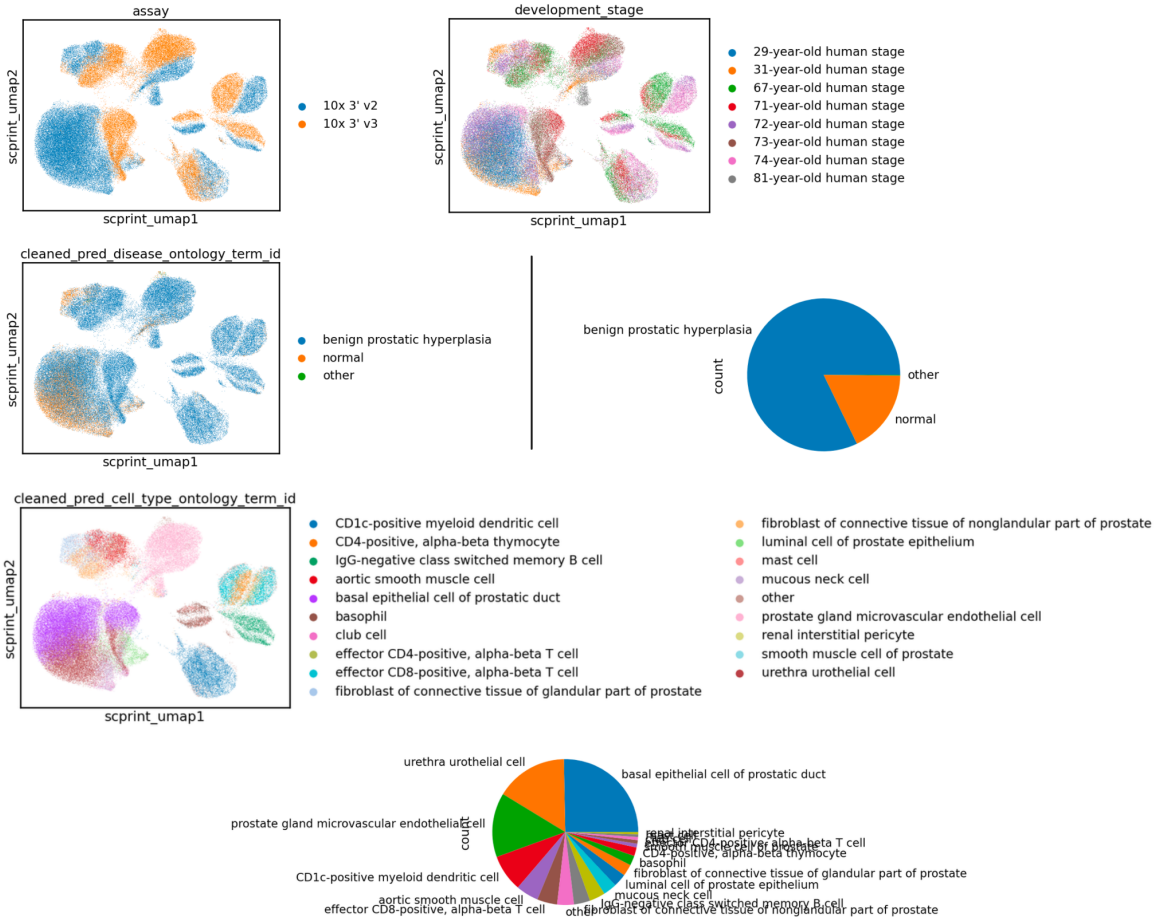

Detailed view of the assay, development stage, scPRINT-predicted diseases, and scPRINT-predicted cell types. Predicted diseases and cell types have been "cleaned" following the strategy presented in Figure 5. We also add pie charts of the relative abundance of each predicted label.

6.2.10 Differential expression analysis of the B-cell cluster vs the rest of the cells in the BPH dataset

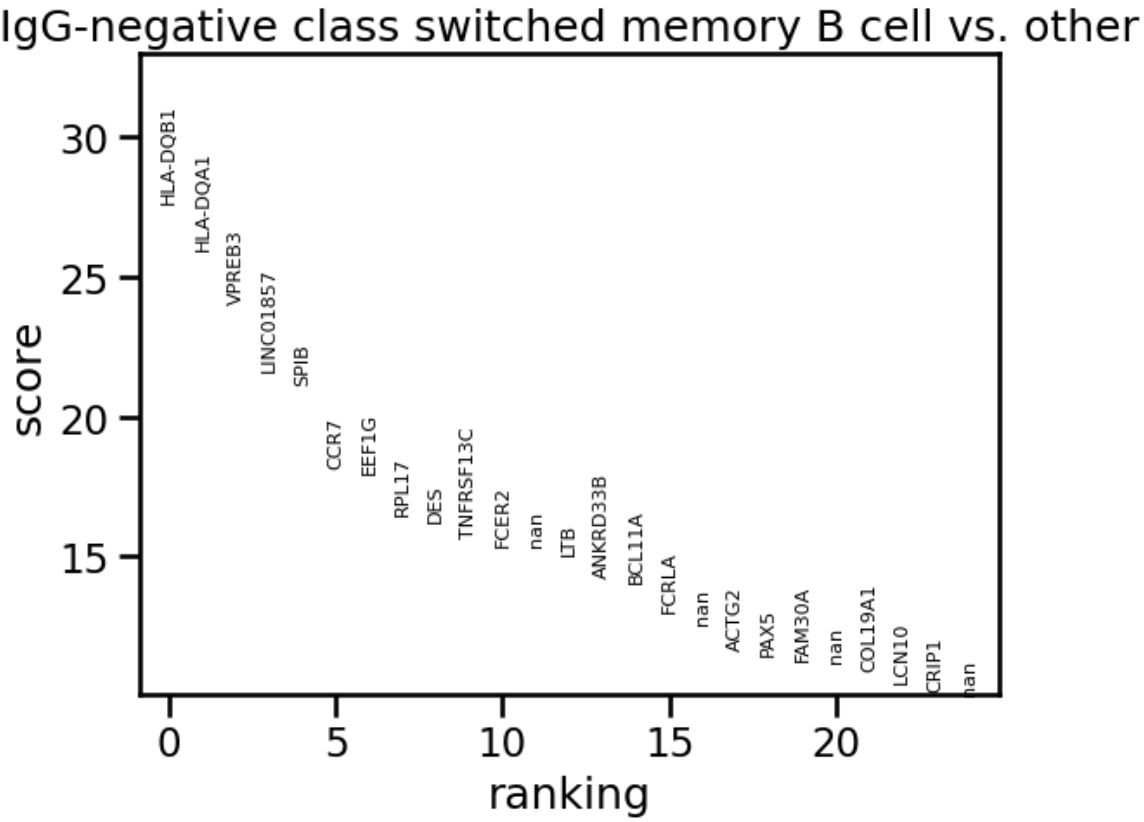

Top genes of the differential expression analysis of the scPRINT inferred B-cell cluster in vs the rest of the cells in the BPH dataset.

6.2.11 Gene enrichment comparison in the PAGE4 GN

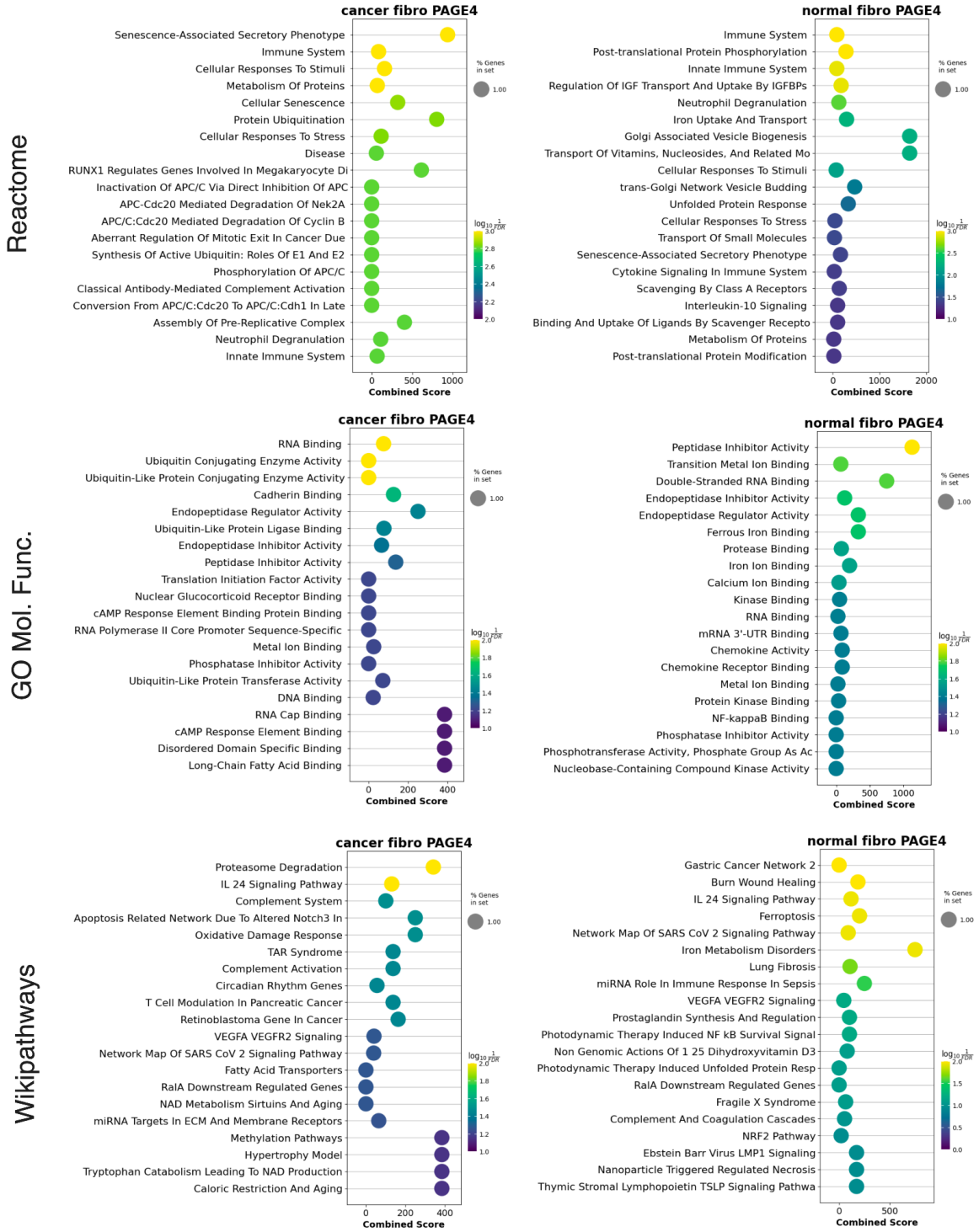

Comparison of the top 20 most enriched terms in Wikipathways, GO molecular function, and Reactome for the 40 most connected genes to PAGE4 in both BPH-associated and normal fibroblast GNs inferred by scPRINT

6.2.12 Gene Network enrichment comparison between the BPH and normal fibroblast on their Louvain communities

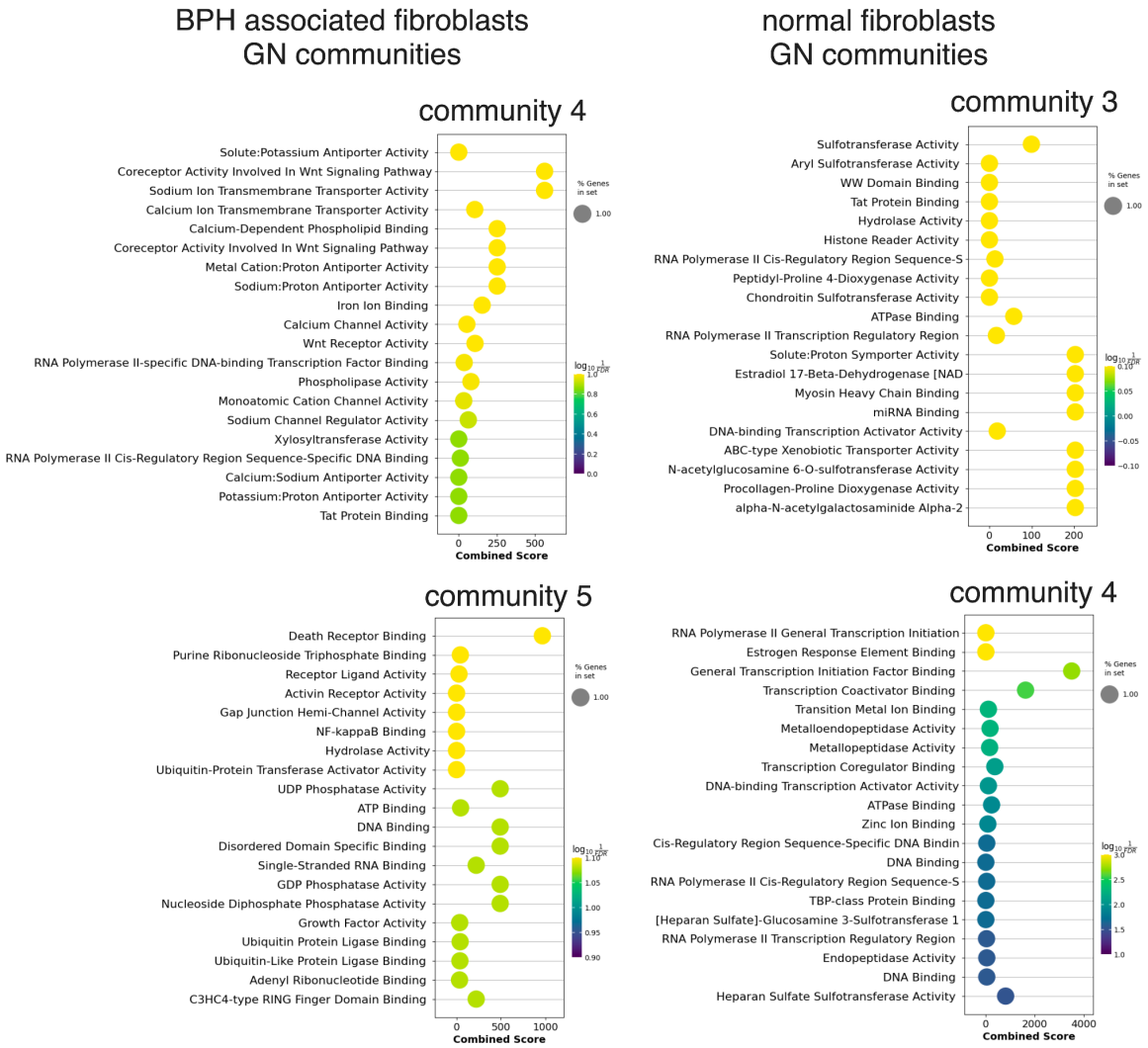

Dotplot of the top 20 GO Molecular function gene sets enriched in the Louvain communities of the BPH and normal fibroblast's Gene Networks.

6.2.13 Graphical Model

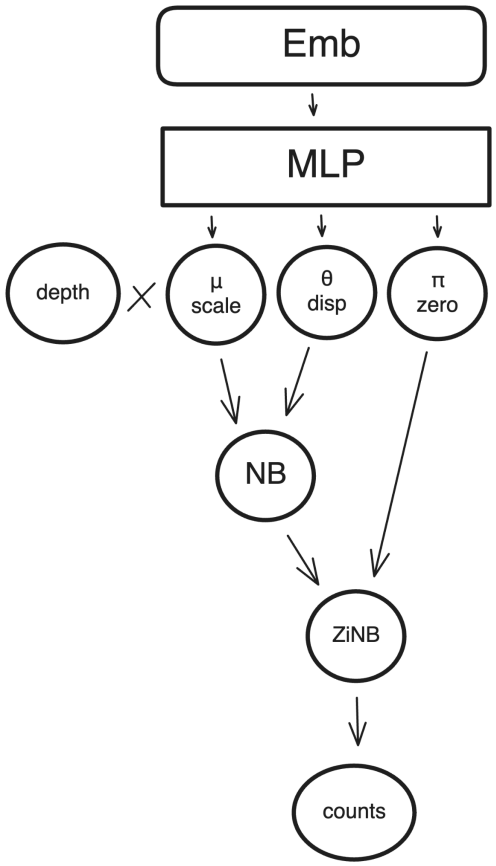

Schematic representation of the zero-inflated negative binomial graphical model of the expression decoder. We generate three values μ, θ, π which are used to model a distribution. We also multiply the μ with the depth (or total count) over the cell.

6.2.14 Hierarchical classifier

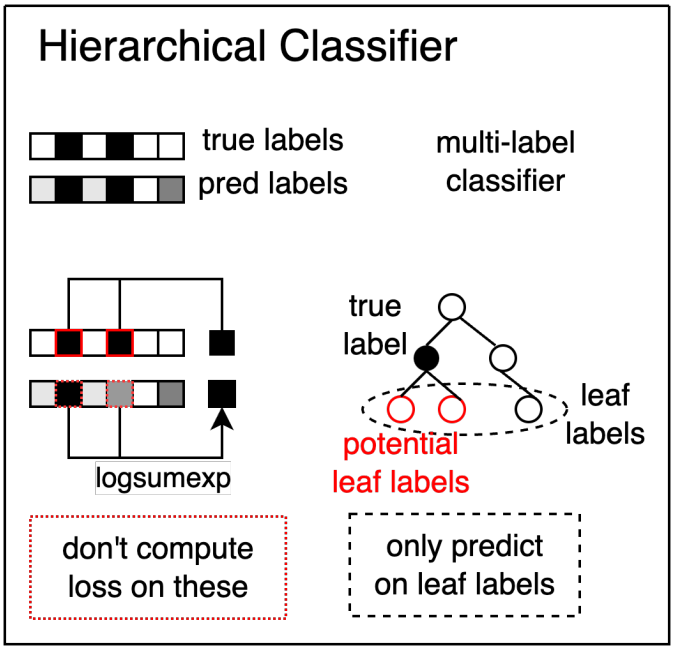

Schematic representation of the hierarchical classifier and its behavior during training. We can train on labels not predicted by the classifier as long as they are parent to one of the predicted labels in the ontological tree.

6.2.15 Detailed representation of the bottleneck learning procedure

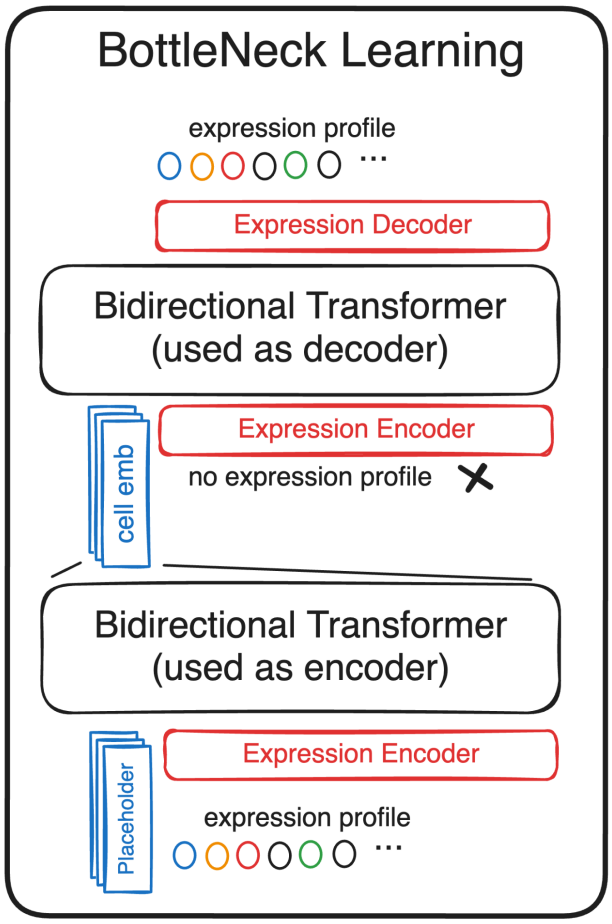

Schematic representation of the bottleneck learning procedure where scPRINT's Bidirectional Transformer Encoder is used both as the "Encoder" and "Decoder" of an auto-encoding (AE) bottleneck learning scheme.

6.2.16 Schematic representation of our dataloader

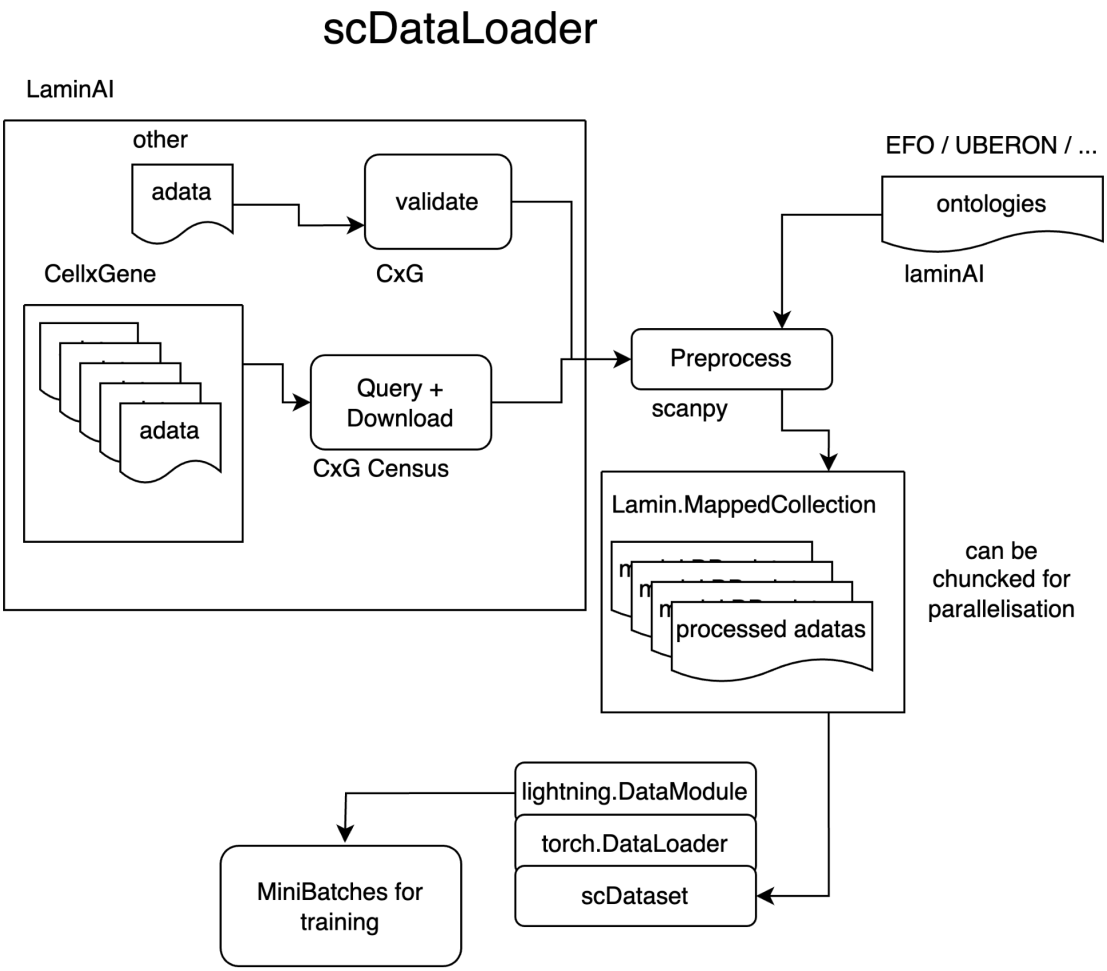

Schematic representation of scDataLoader. Using Lamin.ai, we download and preprocess all cellxgene datasets as AnnDatas. We can also add and validate other expression datasets using lamin.ai. Based on lightning's datamodule framework, torch's dataloaders, our weighted random sampler, and lamin.ai's mapped collection, we can then sample minibatches for pre-training across thousands of datasets and millions of cells with weighted random sampling.

6.3 Supplementary Tables for scPRINT-2

6.3.1 Detailed version of the additive benchmark

	names	GPU time per epoch	denoising score	embed & batch corr. lung	embed & batch corr. pancreas	cell type prediction lung	cell type prediction pancreas	gene regulatory network prediction OR gwps	OR omni.	AUPRC gwps	AUPRC omni.	run id	
Base	ross seeds (masking; ZINB loss; ? + continous expr. emb.; classif. + generative task)	130	2,5 +- 1,5	50.1 +-2.1	42.3 +-2	50 +- 8	45 +- 5	3,8. +-0.7	1,4 +- 0.3	0,044 +-0.002	0,00165 +-0.00015	efwkxesx, te0uwaz1, jsls4j6n, hobjefdj, r18nhnuz	blooming-dew-714, driven-valley-750, summer-deluge-783, silent-poltergeist-843, unraveling-pumpkin-841
	medium model	180	3	50.3	42.8	65.1	60.2	4.7	1.15	0.048	0.00188	p0znio7y	solar-durian-637
	negative control	0	-24	40.2	34.2	0	0	1	0.8	0.021	0.00123		
architecture	no dropout	130	-1	49.9	45.7	47	55.1	3.9	1.5	0.044	0.00157	dipgk9u5	expert-feather-748
	large classifier	130	0	52	43	53	49	4.4	1.8	0.046	0.00148	9q261ics	chocolate-snowball-718
	MVC	130	1	51.7	44.4	54.8	45.8	3.9	1.4	0.043	0.00143	yfvvk4cb	celestial-sun-749
	no decoders / generation	90	2	52.2	44.9	53.2	47.7	4	3.5	0.044	0.00166	z3abxa21	northern-voice-777
	XPressor	160	-4	50.4	45.6	47.3	46.8	4.2	2	0.046	0.00163	dsemm200	crimson-wildflower-791
data	only Tahoe	130	0	40	33	0	0	4.8	0.5	0.0041	0.00104	mxu0p3fs	young-bush-669
	CZI + Tahoe (denoising)	130	16.1	53.9	43.1	52.6	51.1	4.5	1.9	0.046	0.00143	nmc2l1gf	lurking-cat-846
	CZI	130	1	52.3	43.1	47.8	49.1	3.8	2	0.043	0.00162	4u5c4plu	radiant-oath-793
	all databases (denoise)	140	-4	48.6	39	44.9	40.7	3.6	1.3	0.043	0.00157	ujzjjsi3	macabre-apparition-844
	200 human datasets only	130	0	49.3	43.4	40.3	50	3.5	1.8	0.044	0.00166	c60vguww	playful-frost-804
	sampling without replacement	130	0	50	45	36	34	4.5	2.4	0.045	0.0016	lg84geoq	autumn-aardvark-702
	cluster-based sampling only	130	2.7	43.3	42	49.4	40.2	3.5	1.3	0.042	0.00157	s8wwlmxr	rosy-firefly-805
	meta-cell	130	21	52.8	47.7	53.6	51.3	3.4	1.7	0.04	0.00155	gp90j8vn	unique-dawn-806
attention	softpick (larger context)	130	3.1	50	41	53.8	44.6	3.6	1.8	0.042	0.00156	s6alkcvp	eldritch-fang-834
	criss-cross (larger context)	90	5.6	51.2	42.5	42.4	43.7	x	x	x	x	u5udxv4v	uncanny-raven-835
	hyper (denoise, larger context)	160	2	50.1	43.4	42.1	40.6	3.7	0.6	0.04	0.00115	l44og0s3	silver-grass-803
loss	contrastive learning (masking + denoising)	130	21.4	49	41.5	39.5	40.4	4	1.3	0.043	0.00149	wcg8g3hr	northern-frog-797
	elastic cell similarity	130	2.5	52.7	43.1	44.8	34.9	4.3	1.6	0.046	0.00167	qn2tyayf	hopeful-monkey-796
	no embedding ind loss	130	2.2	51.6	43	50	50	4	2.3	0.043	0.00156	4v84b9nm	devoted-wave-795
	ZINB+MSE (denoising)	130	25.5	51.3	48	49.2	42.9	3.4	1.3	0.04	0.00163	bv1r4d3h	firm-silence-747
	MSE	130	-4	54	46	62	43	3.3	1.2	0.042	0.00166	mnk73zbd	generous-dawn-666
	VAE compressor	160	3	51	42	38	27	4.2	1.7	0.044	0.0016	jwkcrxb9	wild-terrain-694
pretraining task	**var. context (larger context)**	170	29.1	53	46	52.9	52.2	3.1	1.2	0.038	0.00146	44p3fv3v	apricot-snowflake-756
	TF masking	130	2.6	49.8	42.8	49.8	42.8	3.7	2.3	0.043	0.00169	8vmjnnsb	winter-meadow-772
	denoising	130	21	52.6	45.1	50.9	54.5	3.6	1.3	0.043	0.0016	bk37305v	efficient-firebrand-753
	no classification	130	3	50	40	0	0	3.9	1.2	0.043	0.00129	oxlxtzim	copper-frost-625
	adv. classifier (+larger classif)	130	1	52	42	48	43	4.1	1.6	0.044	0.0014	2tzkv7m8	sunny-morning-629
input	sum normalization (denoise)	130	12.8	45.6	46.5	21.4	22.9	2.4	1	0.029	0.00136	ldh1fw8d	snowy-galaxy-744
	no random level of denoising	130	19	54.1	45.3	50.7	45.2	3.6	2	0.041	0.00179	0ayw97iw	divine-monkey-798
	binning	130	0	51.8	45.5	58.4	52	4.2	1.3	0.047	0.00162	op7at8xm	twilight-breeze-874
	GNN expression encoder	150	44	48	42	38	35	4	1.4	0.042	0.00128	bv6d9wpl	balmy-totem-727
	using only expressed genes	130	1.2	52.2	42.9	53.2	40.1	3.8	1.3	0.043	0.00157	xz238fyr	sage-snow-873
	without gene location	130	3.4	36.2	35	4	5.9	4.8	1.5	0.048	0.0017	r2n83z4k	youthful-snowflake-792
	learn gene emb (denoising)	130	20.9	51.7	45.1	49.7	46	3.2	1.7	0.041	0.00154	npayct6q	jumping-night-755
	fine-tuned ESM3	130	21.4	51.5	42.8	55.6	44.2	3.7	1.4	0.042	0.00181	fkcgp56s	not-snowflake-755
Main	small model (V2)	1820	44	53	49	46	47	3.5	1.6	0.041	0.0015		honest-vortex-815
	medium model (V2)	5600	x	x	x	x	x	x	x	x	x		x
	medium model (V1)	520	20.9	52.6	45.6	61.8	57.6	3.4	2.2	0.041	0.0017		bewitched-poltergeist-857
	small model (V1)	160	31.7	52.4	50	44.7	44.7	3.6	1.5	0.042	0.00138		dry-smoke-852

Detailed version of the additive benchmark, listing every value.

6.3.2 Detailed scIB biological conservation scores on the xenium dataset

Bio Metric	Isolated labels	KMeans NMI	KMeans ARI	Silhouette label	cLISI Bio conservation	**Aggregate score**
X_pca	0.446	**0.255**	**0.036**	0.382	0.955	**0.415**
scprint_emb	0.468	**0.376**	**0.125**	0.383	0.979	**0.466**

scPRINT vs PCA on expression. ScPRINT performs better, likely by denoising the expression.

6.3.3 Detailed scIB scores on the unseen species integration task

	Bio conservation					Batch correction					Aggregate score			Recomputed scores using the same elements		
	Isolated labels	KMeans NMI	KMeans ARI	Silhouette label	cLISI	BRAS	iLISI	KBET	Graph connectivity	PCR comparison	Batch correction	Bio conservation	**Total**	Batch correction	Bio conservation	**Total**
scprint_2 ft (cell_type emb)	0.64	0.81	0.75	0.69	1.00	0.69	0.00	0.01	0.91	0.00	0.32	0.78	**0.60**			
scprint_2 ft	0.55	0.72	0.63	0.56	1.00	0.58	0.00	0.00	0.65	0.00	0.25	0.69	**0.51**			
scprint_zeroshot (cell_type emb)	0.57	0.41	0.31	0.53	0.98	0.65	0.00	0.77	0.00	0.28	0.56	0.45	**0.49**			
scprint_zeroshot	0.49	0.00	0.00	0.49	0.68	1.00	0.86	0.00	0.20	1.00	0.61	0.33	**0.44**			
random	0.54	0.23	0.14	0.50	0.97	0.80	0.00	0.00	0.72	0.00	0.30	0.48	**0.41**			
no integration (pca)	0.57	0.21	0.10	0.36	0.99	0.69	0.00	0.00	0.60	0.00	0.26	0.44	**0.37**			
saturn	0.81	0.97	0.49	0.13	1.00	0.79	0.13	0.05	0.91	0.92	0.62	0.92	**0.79**	0.56	0.68	**0.63**
scGen	0.60	0.77	0.49	0.23	0.99	0.88	0.23	0.16	0.91	0.92	0.85	1.00	**0.68**	0.62	0.61	**0.62**
Seurat v4 CCA	0.58	0.57	0.48	0.23	0.97	0.84	0.23	0.13	0.90	0.89	0.73	0.92	**0.50**	0.60	0.57	**0.58**
SAMap		0.62		0.01	0.98	0.91	0.01	0.22	0.74		0.60	1.00	**0.47**	0.47	0.53	**0.51**
scVI	0.51	0.55	0.50	0.23	0.95	0.83	0.23	0.09	0.91	0.98	0.80	0.93	**0.47**	0.61	0.55	**0.57**
BBKNN		0.56		0.11	0.99	0.82	0.11	0.05	0.82		0.31	0.66	**0.41**	0.45	0.55	**0.51**
Scanorama	0.56	0.54	0.49	0.27	0.96	0.76	0.27	0.09	0.84	0.93	0.59	0.79	**0.37**	0.58	0.56	**0.57**
fastMNN	0.52	0.54	0.48	0.09	0.96	0.70	0.09	0.03	0.89	0.86	0.37	0.72	**0.36**	0.51	0.52	**0.52**
Harmony	0.51	0.54	0.44	0.06	0.96	0.70	0.06	0.03	0.86	0.70	0.15	0.70	**0.16**	0.47	0.50	**0.49**

Details of the full scIB results comparing no integration, random embeddings sampled from the multivariate Gaussian, and different versions of scPRINT zero-shot or fine-tuned, using the merged embeddings or the cell type ones

6.4 Supplementary figures for scPRINT-2

supplementary-figures-2

6.4.1 Illustration of the full scPRINT-2's architecture, input, and output

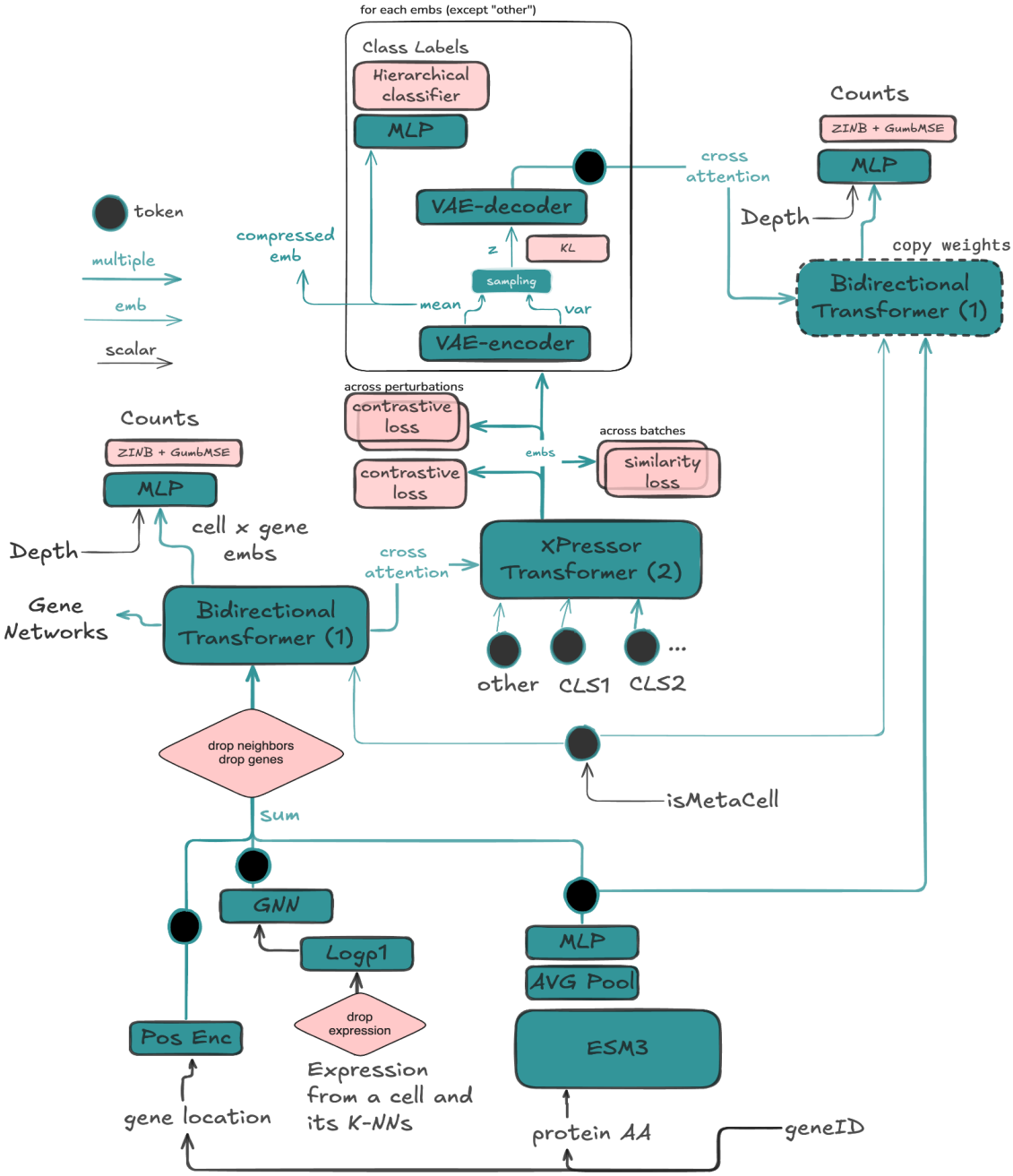

In-depth illustration of the full scPRINT-2's architecture, input, and output with all its main different components and the data flow.

6.4.2 Barplot of the F1-macro scores on the label-projection task of the Open Problem benchmark

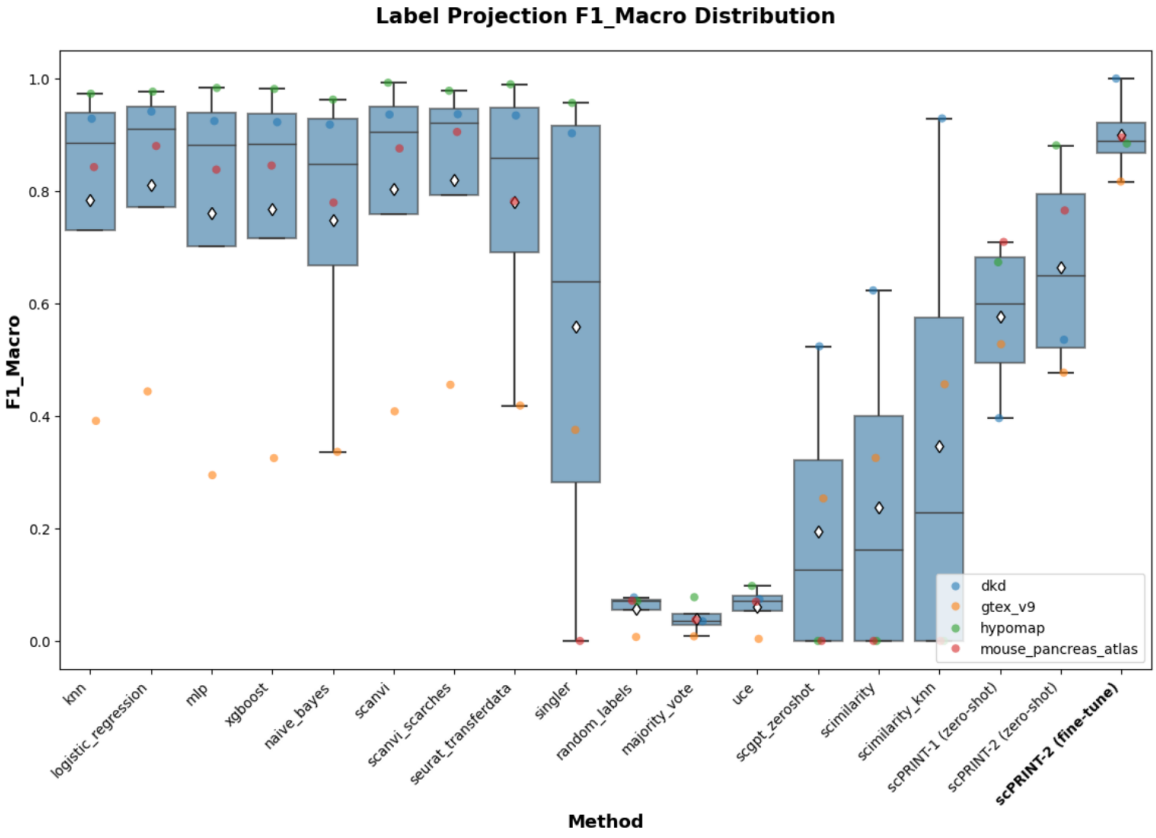

Comparison of scPRINT-1 and scPRINT-2, zero-shot and finetuned, with all other tested methods in Open Problems.

6.4.3 Heatmap of ethnicity prediction relationship across samples

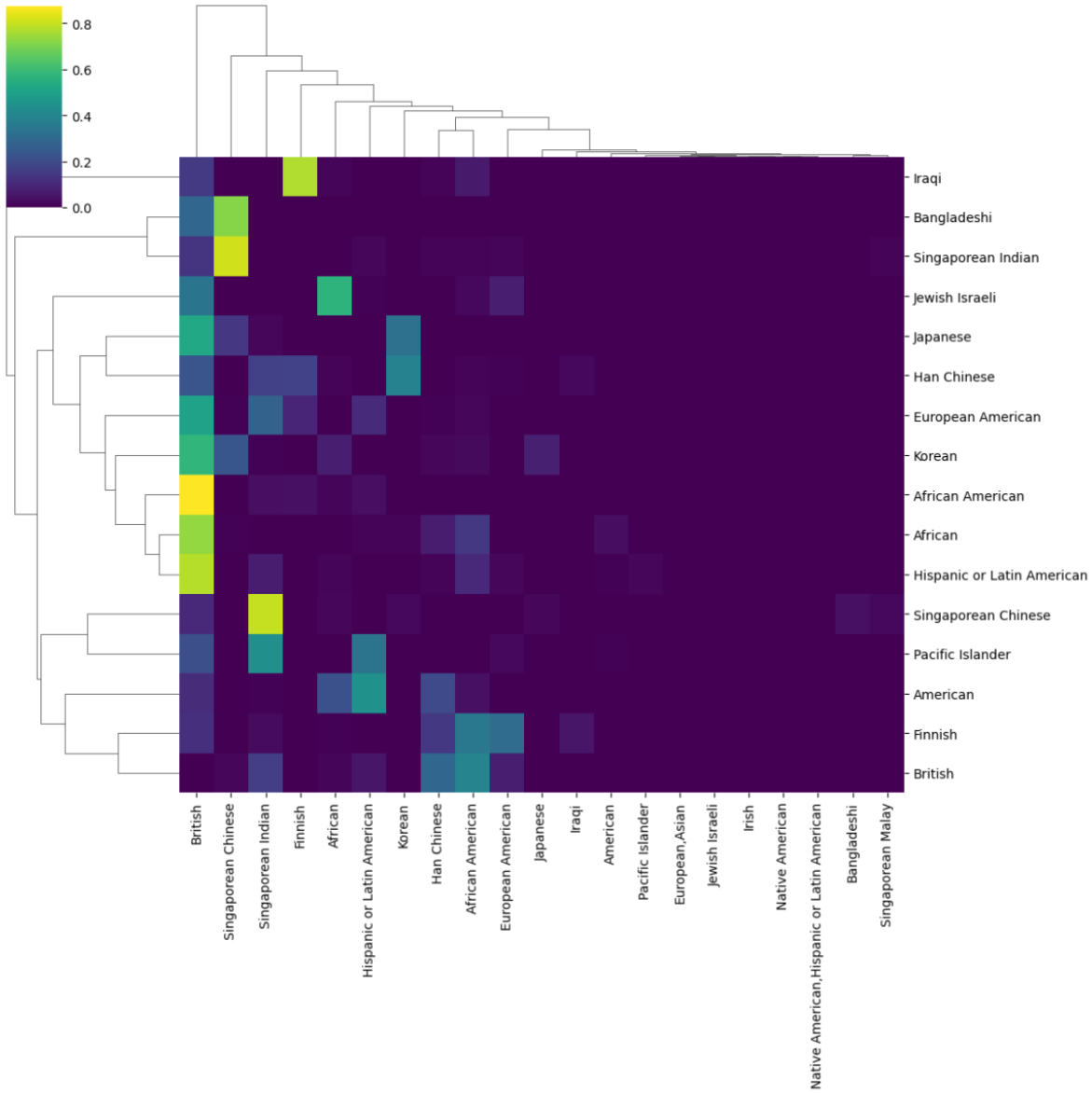

It is generated using labels predicted as top-1 (x-axis) vs second-best prediction (y-axis) across 10,000 random cells for each predicted label from the scPRINT-2 corpus.

6.4.4 Heatmap of organism prediction relationship across samples

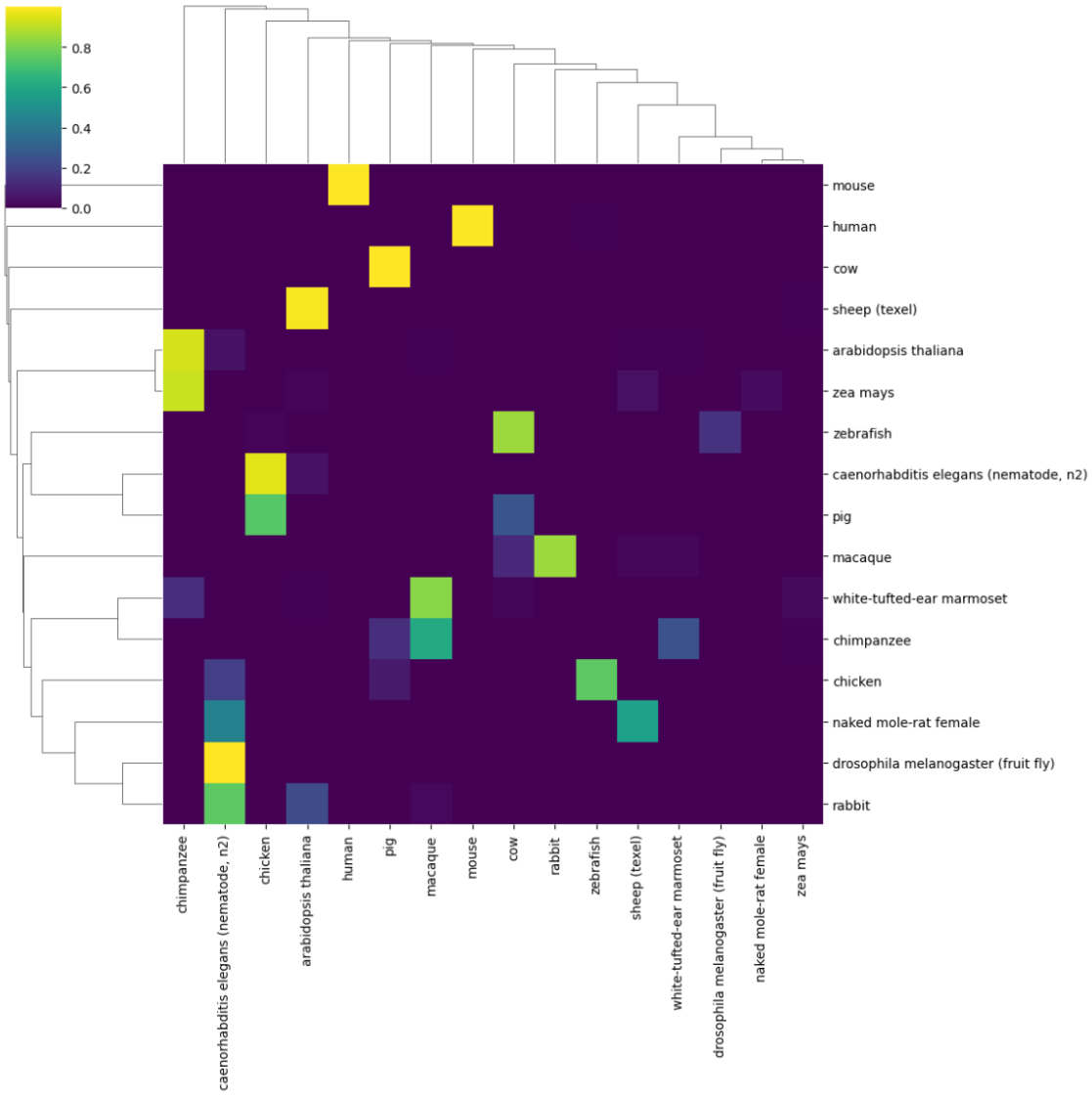

It is generated using labels predicted as top-1 (x-axis) vs second-best prediction (y-axis) across 10,000 random cells for each predicted label from the scPRINT-2 corpus.

6.4.5 Heatmap of organism prediction relationship using organism embedding similarity across samples

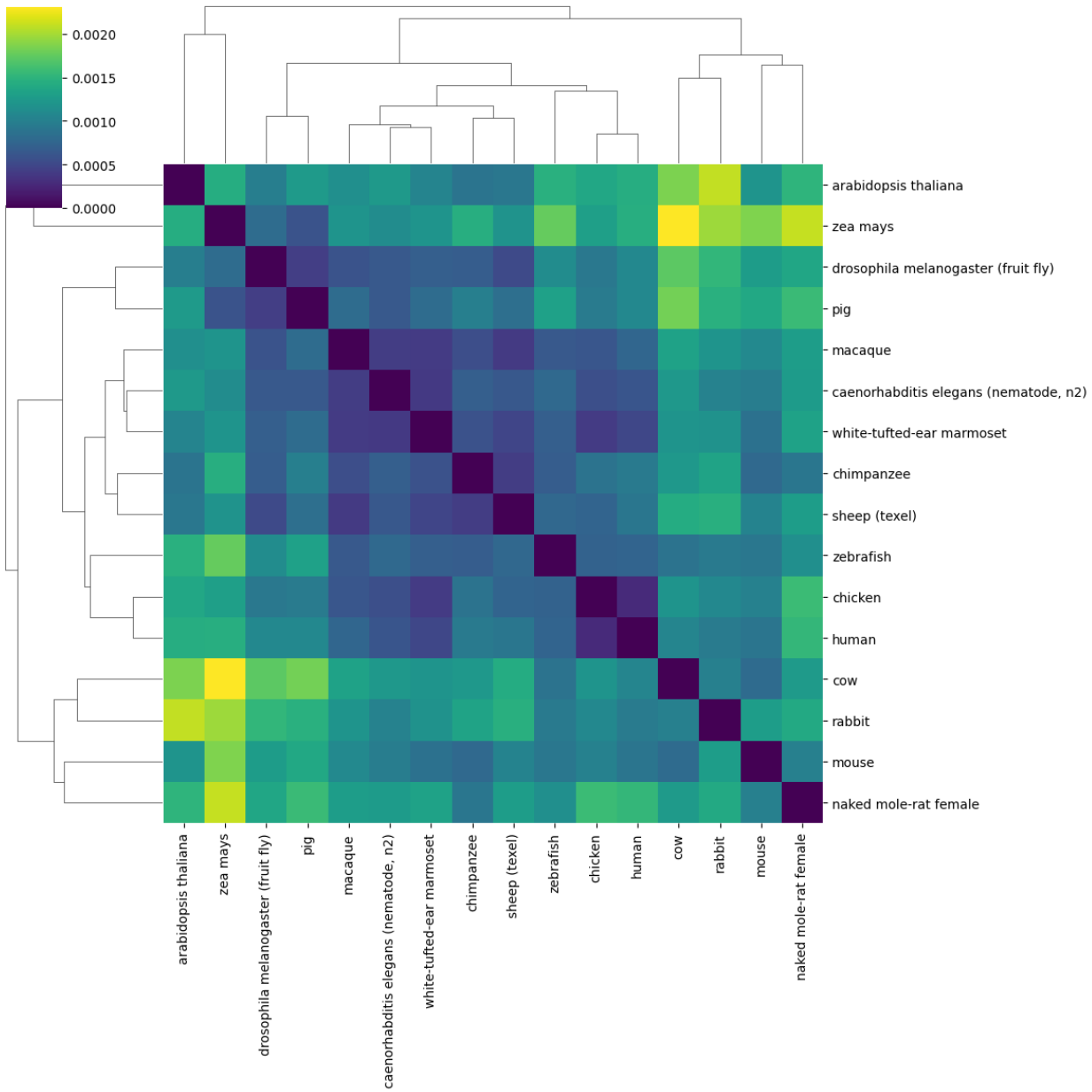

It is generated by averaging the embeddings for each predicted organism across 10,000 random cells for each predicted label in the scPRINT-2 corpus, and using the L2 distance.

6.4.6 Differential expression plots of the disagreeing cells between scPRINT-2 and ground truth

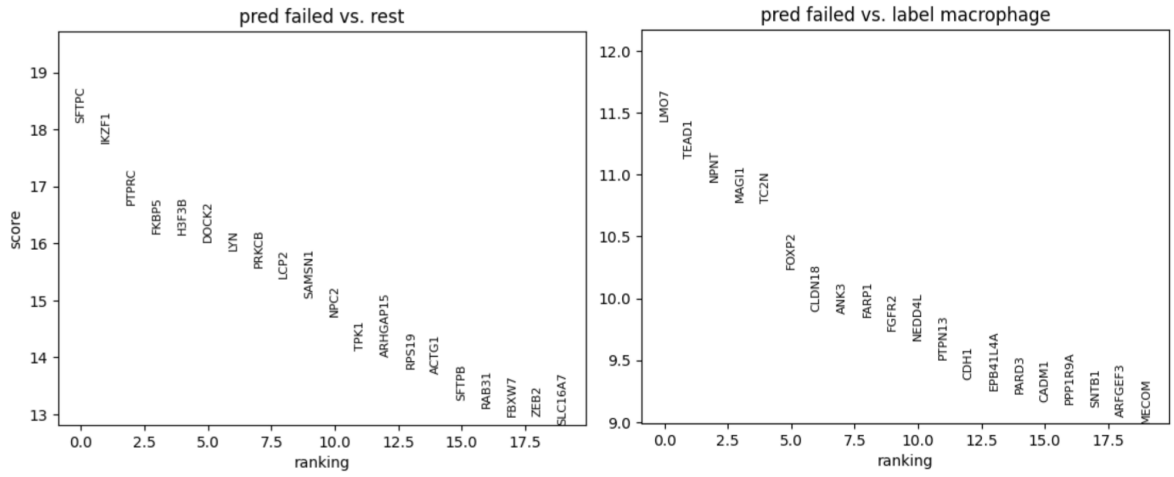

The differential expression is made on the cat/tiger cross-species dataset. “pred failed” is the macrophages labeled as type 2 pneumocytes by scPRINT-2.

6.4.7 Umap of the smart-seq dataset used in the varying context classification task

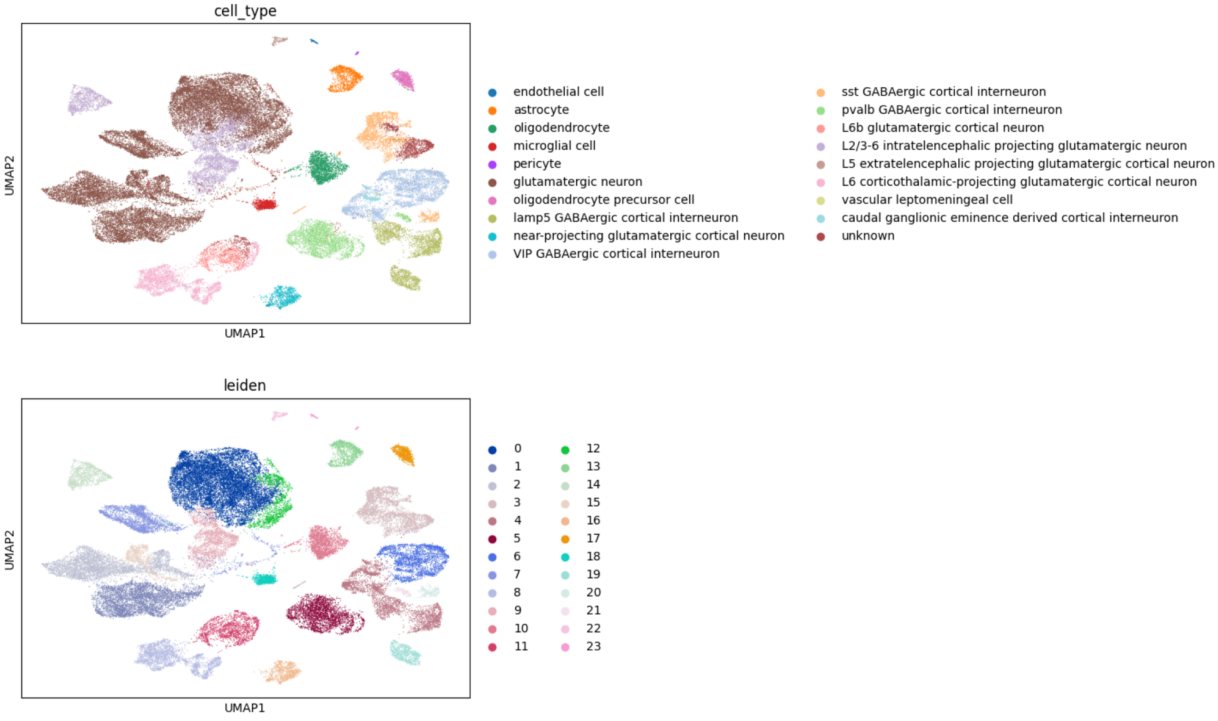

Umap of the cortical areas smart-seq v4 dataset used in the varying context classification

task in results section 2, showing Leiden clusters and ground truth cell types.

6.4.8 Line plot of the classification across varying context length, using the most expressed genes

On the same dataset, but this time using the most expressed genes. Meaning each new gene in context is 200 most expressed, then 500, 1000, etc. We can see that while cell types are often defined by their most expressed genes, and thus this doesn't change classification accuracy much, other, more complex labels continue increasing in accuracy as context length increases.

6.4.9 Illustration of the multiple perturbations applied to expression data in scPRINT-2

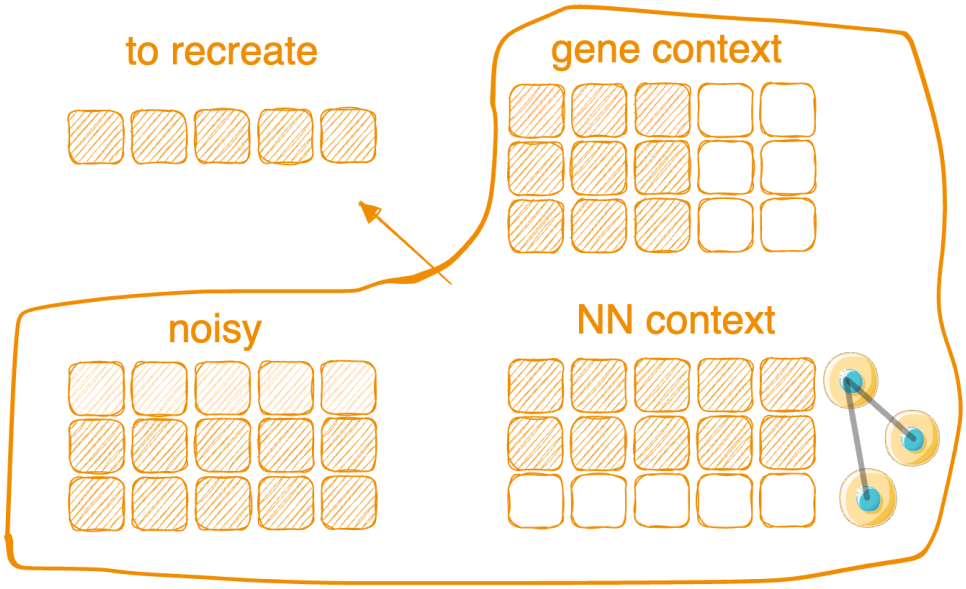

scPRINT can add noise and mask gene expression, modify the number of neighbors, and adjust context lengths.

6.4.10 Distplot of the non-zero count distribution across cells from the three dataset qualities used

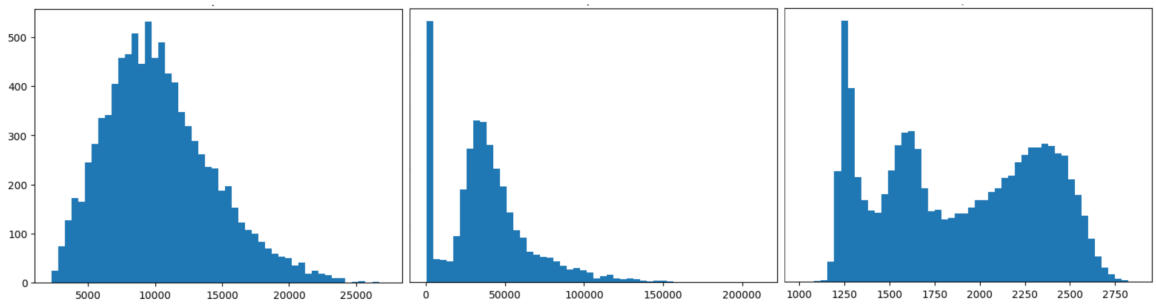

Non-zero count distributions across cells from left : good quality ; center : excellent quality ; right : poor quality datasets used in our denoising benchmark.

6.4.11 Umap over scPRINT-2 and PCA embeddings of the Xenium dataset

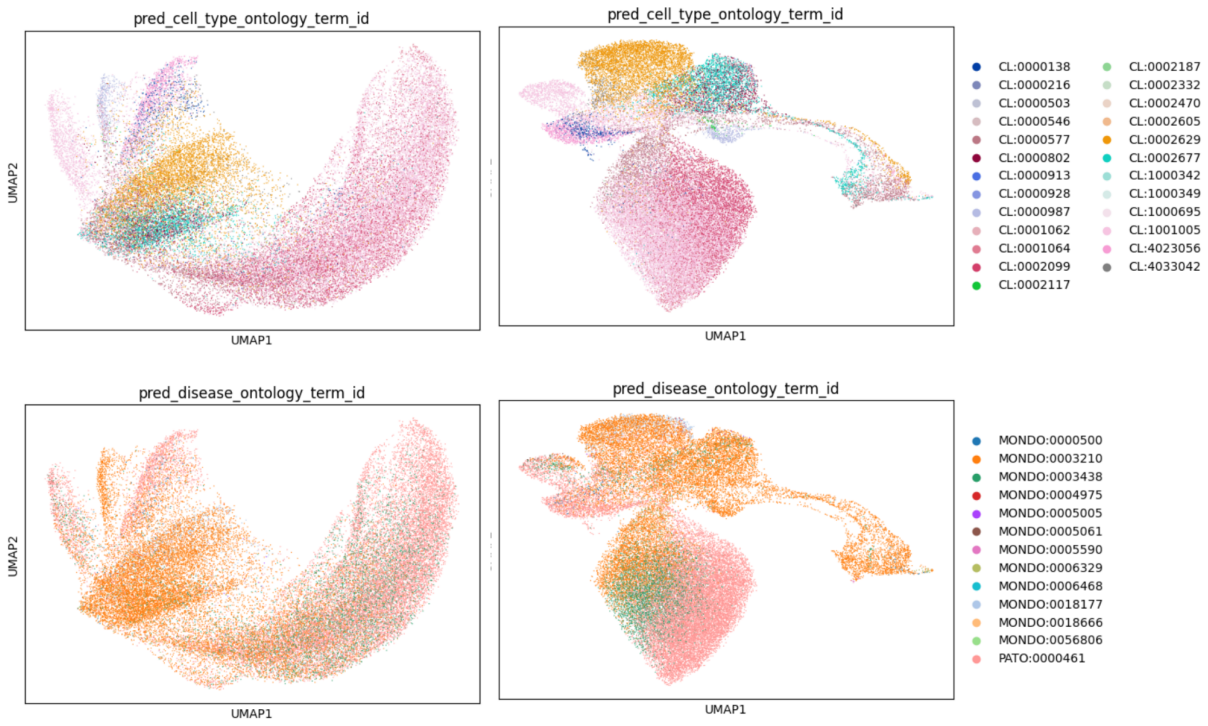

Umap of left : raw PCA expression, right : scPRINT-2 embeddings with scPRINT-2 predicted cell types and diseases.

6.4.12 Tangram mapping quality plots

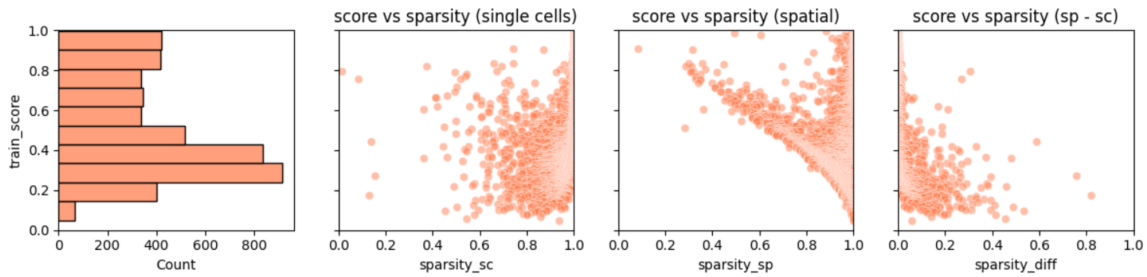

Tangram mapping quality plots on the Xenium skin melanoma datasets and 10v3 skin melanoma datasets.

6.4.13 Illustration of scPRINT-2's generative imputation mechanism

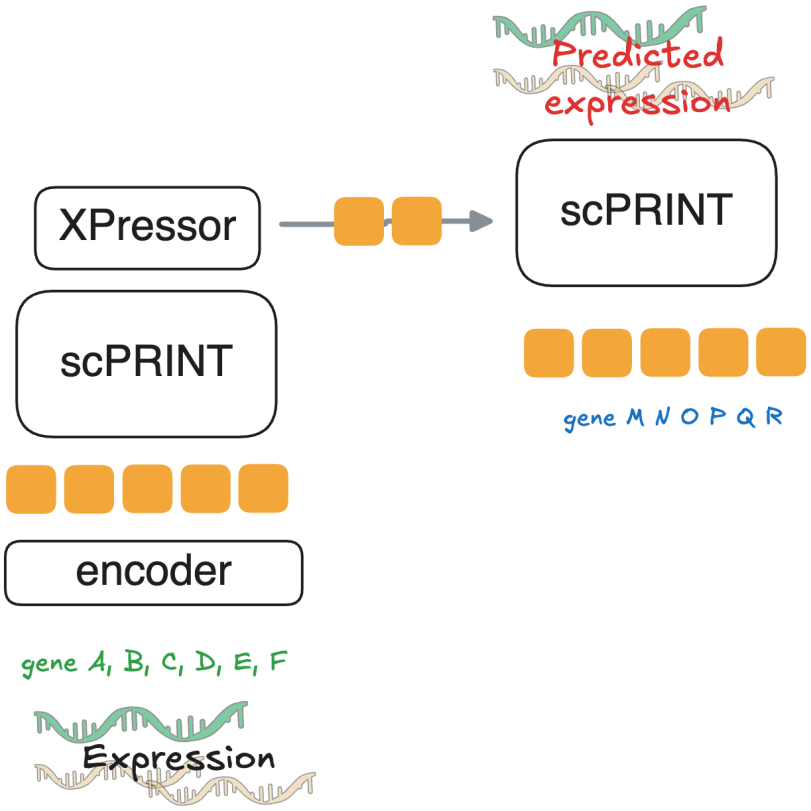

scPRINT encodes all 5000 measured genes into cell embeddings and decodes them on 5000 different unseen gene embeddings.

6.4.14 Spatial plot of the Xenium melanoma dataset with scPRINT-2 predicted cell labels

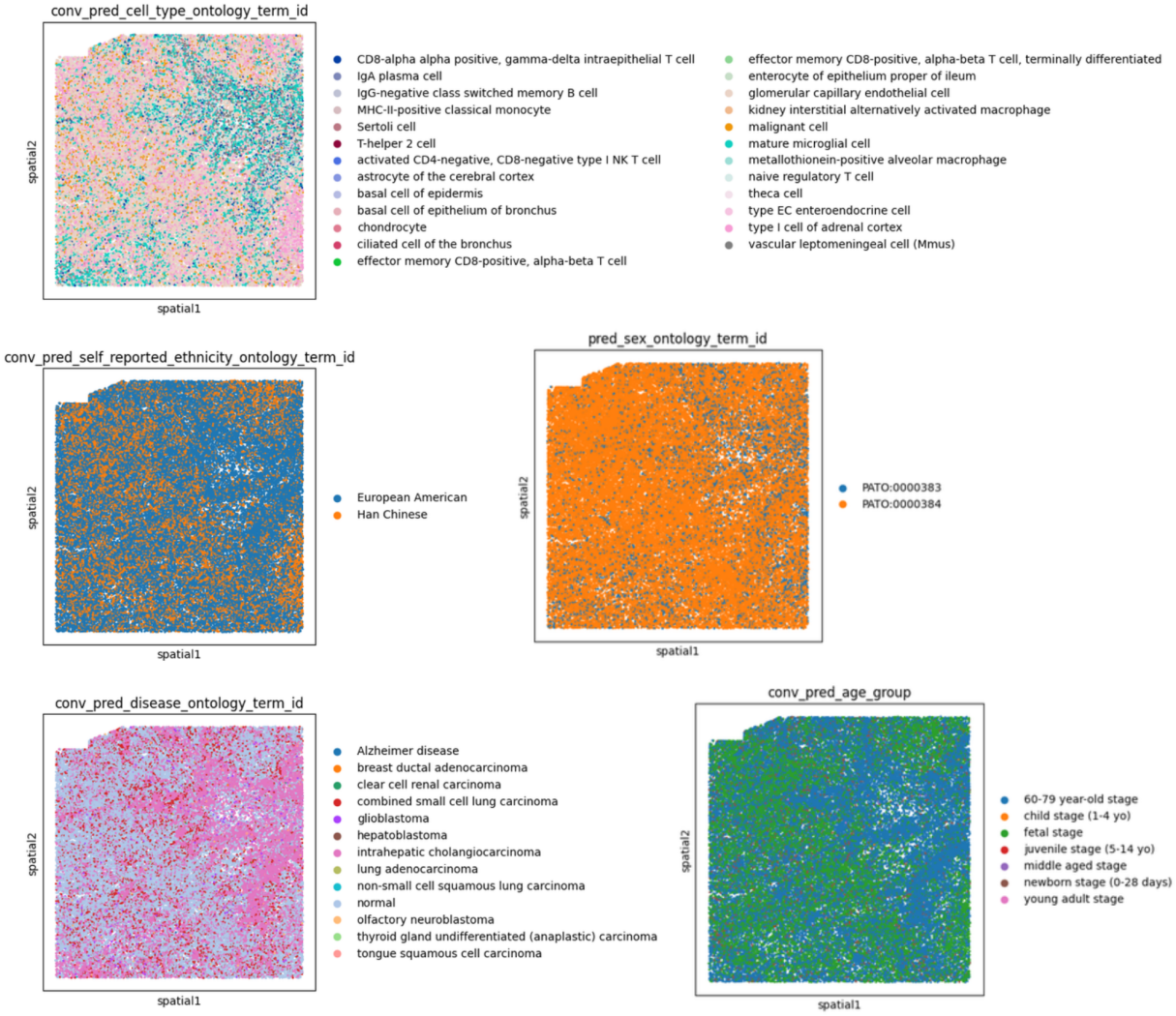

scPRINT-2 predicted cell labels for the disease, age, ethnicity, sex, and cell type labels on top of the selected Xenium skin melanoma patch.

6.4.15 Violin plot comparison of the gene's expression between predicted malignant vs the rest

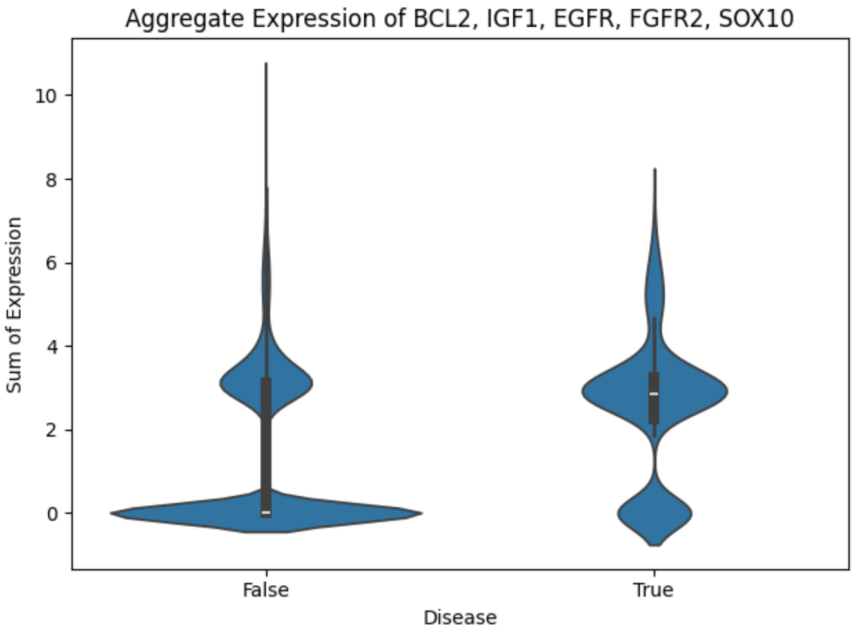

Violin plot showing that BCL2, IGF1, EGFR, FGFR2, SOX10, key melanoma markers are highly expressed in the malignant cell type label group vs the rest, with a p-value of 10^{-234}

6.4.16 Differential expression plot of “cancer” disease labelled vs rest in the xenium dataset

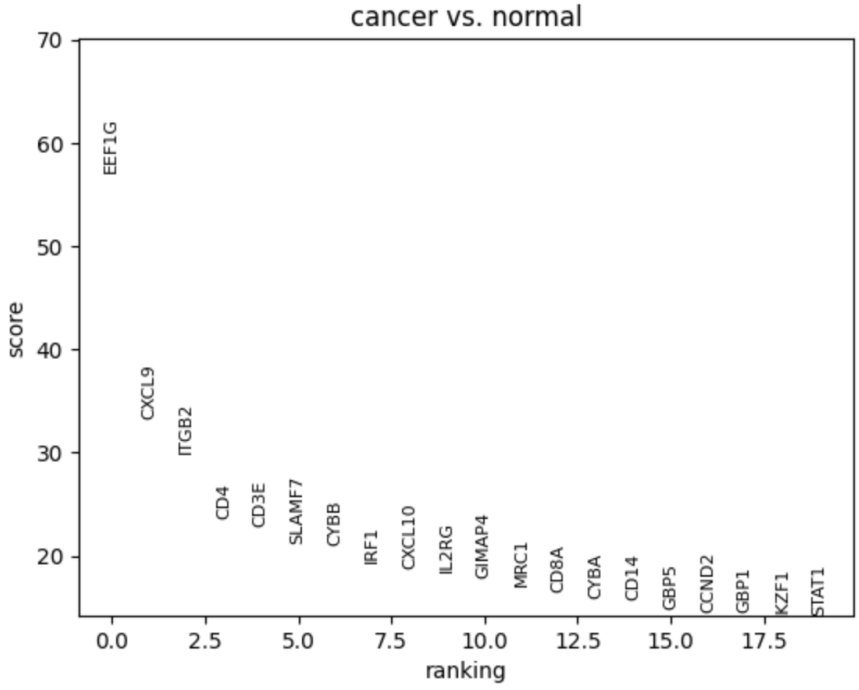

Differential expression plot of cells whose disease label is “cancer” vs the rest in the Xenium skin melanoma dataset

6.4.17 Illustration of criss-cross attention

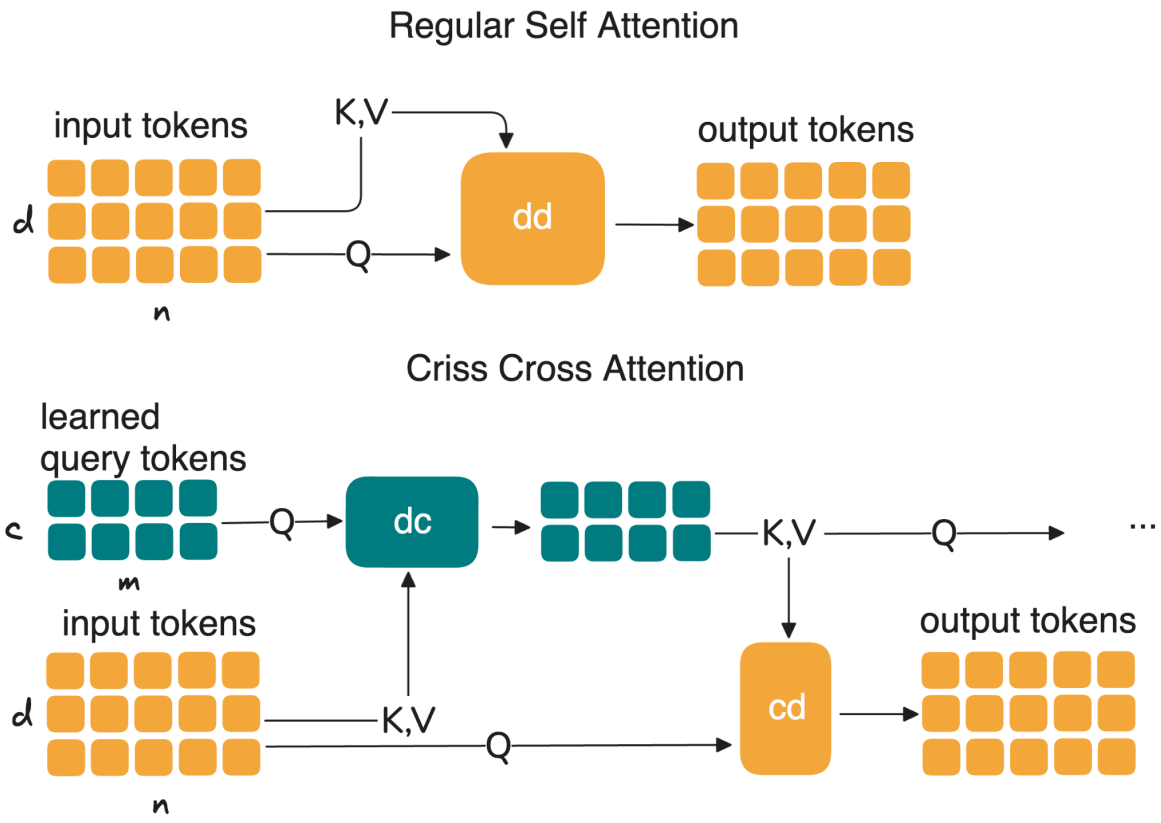

Illustration of our sub-quadratic complexity criss-cross attention mechanism

6.4.18 Illustration of the similarity and dissimilarity-based contrastive losses used in scPRINT-2

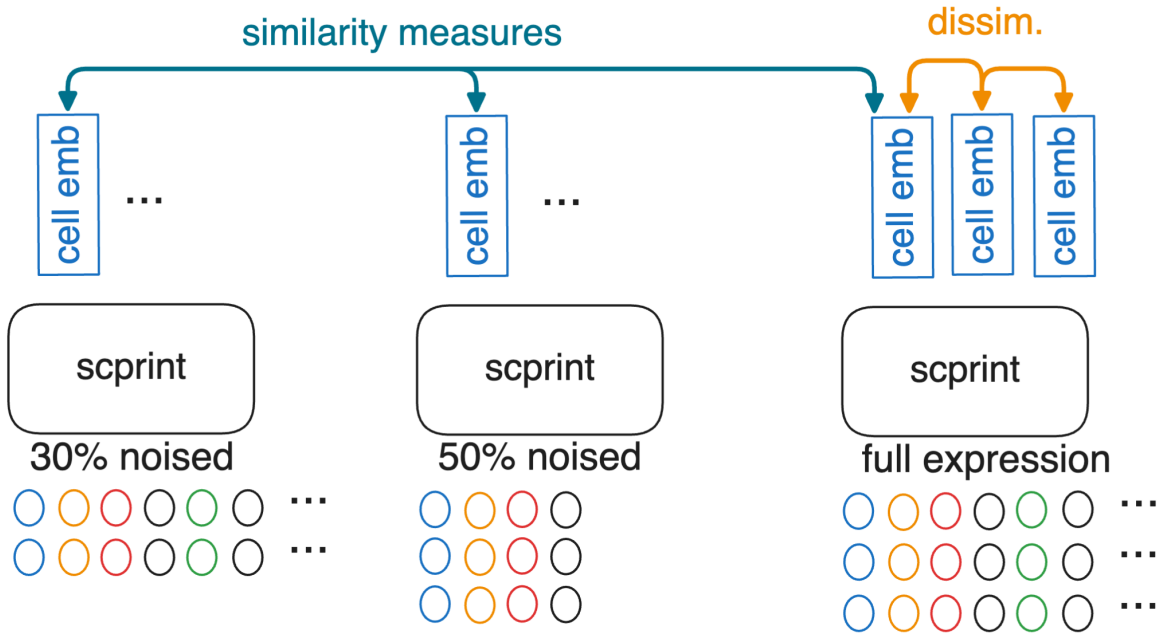

The contrastive losses push embeddings from the same cell at different noise levels to be as similar as possible.

6.4.19 Whisker plot of Open Problems' batch-integration with batch-correction-only scores

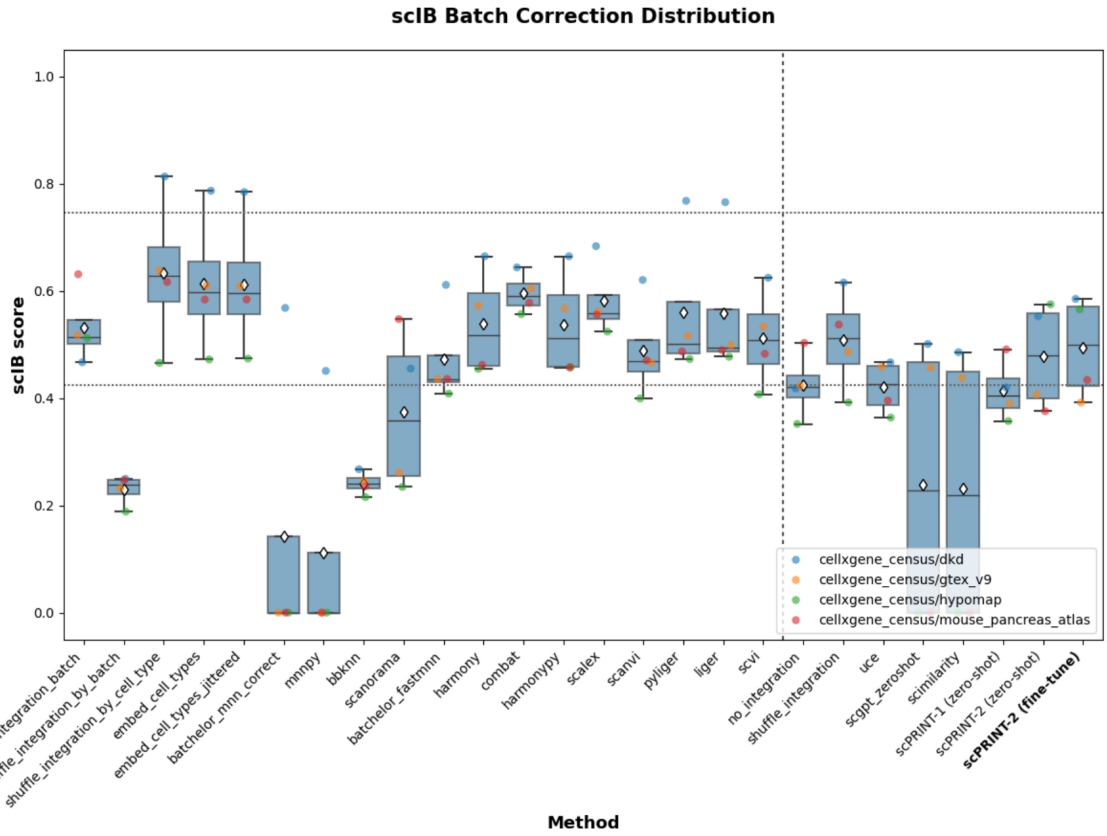

Open Problems' batch-integration with batch-correction-only scores for scPRINT-1 and scPRINT-2 zero-shot, and finetuned, and all other models assessed in open problems.

6.4.20 Whisker plot Open Problems' batch-integration with Bio-conservation-only scores

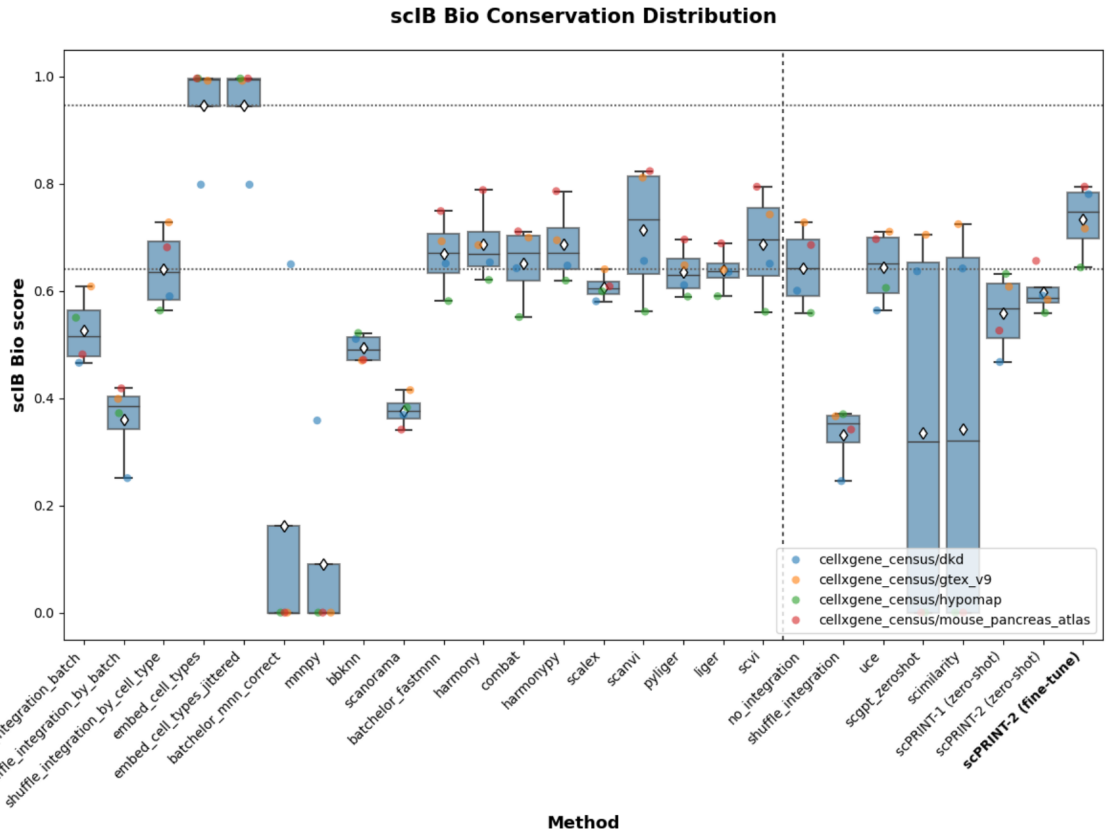

Open Problems' batch-integration with Bio-conservation-only scores for scPRINT-1 and scPRINT-2 zero-shot, and finetuned, and all other models assessed in open problems.

6.4.21 Umap of scPRINT-2's zero-shot multi-species expression embedding using the full cell-embedding

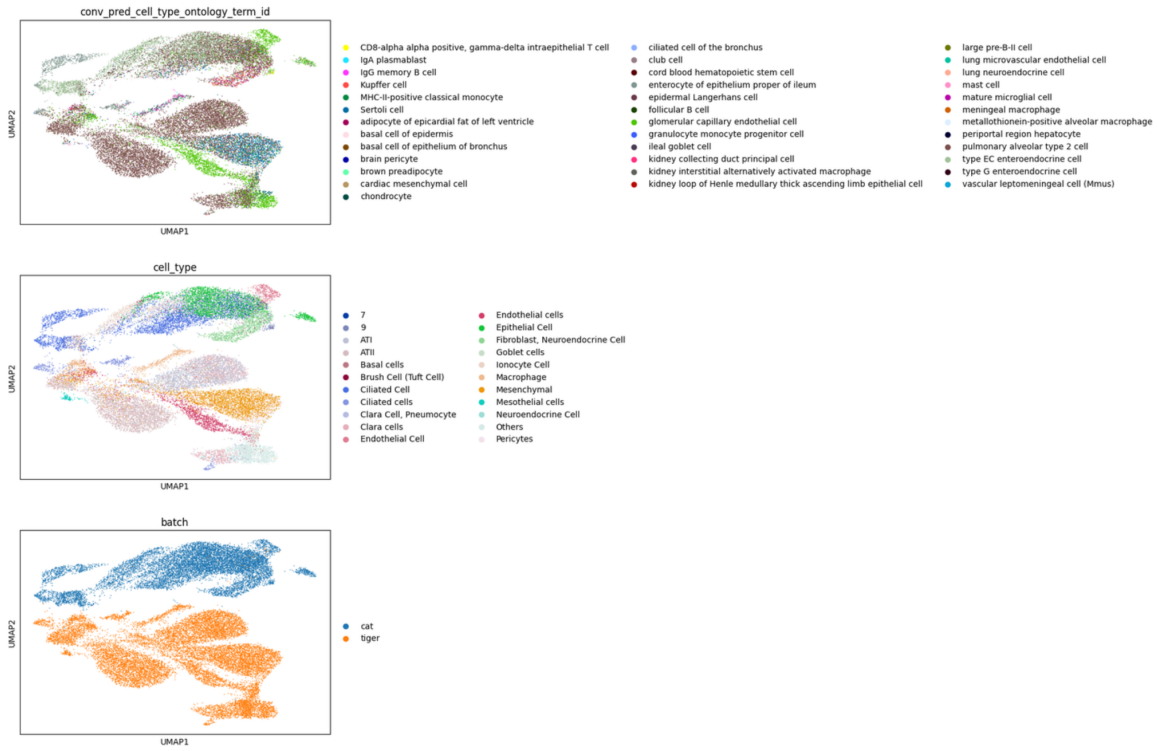

scPRINT-2's zero-shot multi-species expression embedding using the full cell-embedding from top to bottom, scPRINT-2 predicted cell type labels, ground truth cell type labels, and ground truth organism labels.

6.4.22 Barplot of scIB score on scPRINT-2's multi-species integration

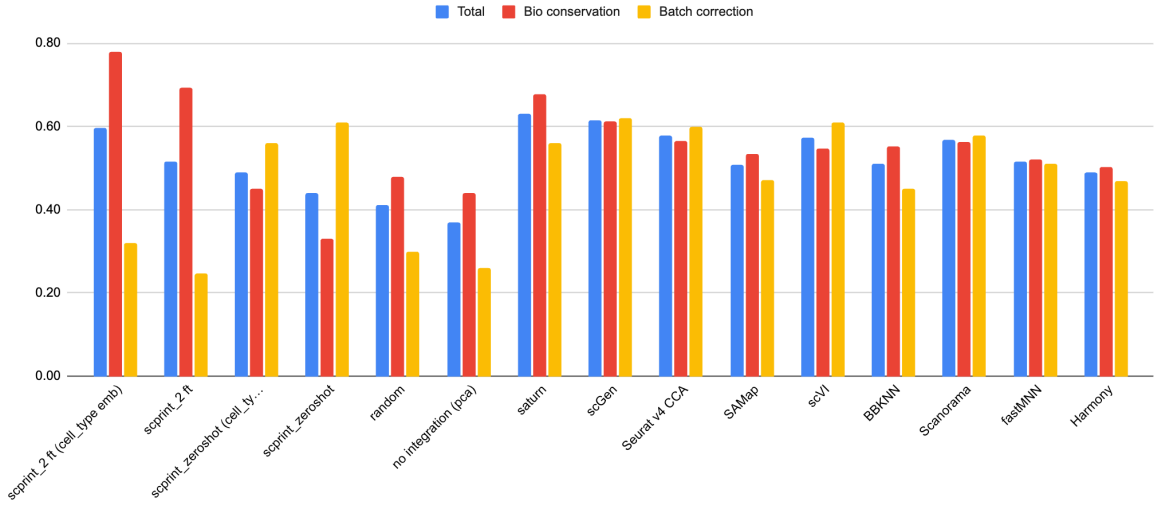

showing total, bio conservation, and batch integration across scPRINT-2 zero-shot, and fine-tuned version using both the full cell-embedding and cell-type-only cell-embedding

6.4.23 Umap of scPRINT-2's zero-shot multi-species expression embedding using the cell-type cell-embedding

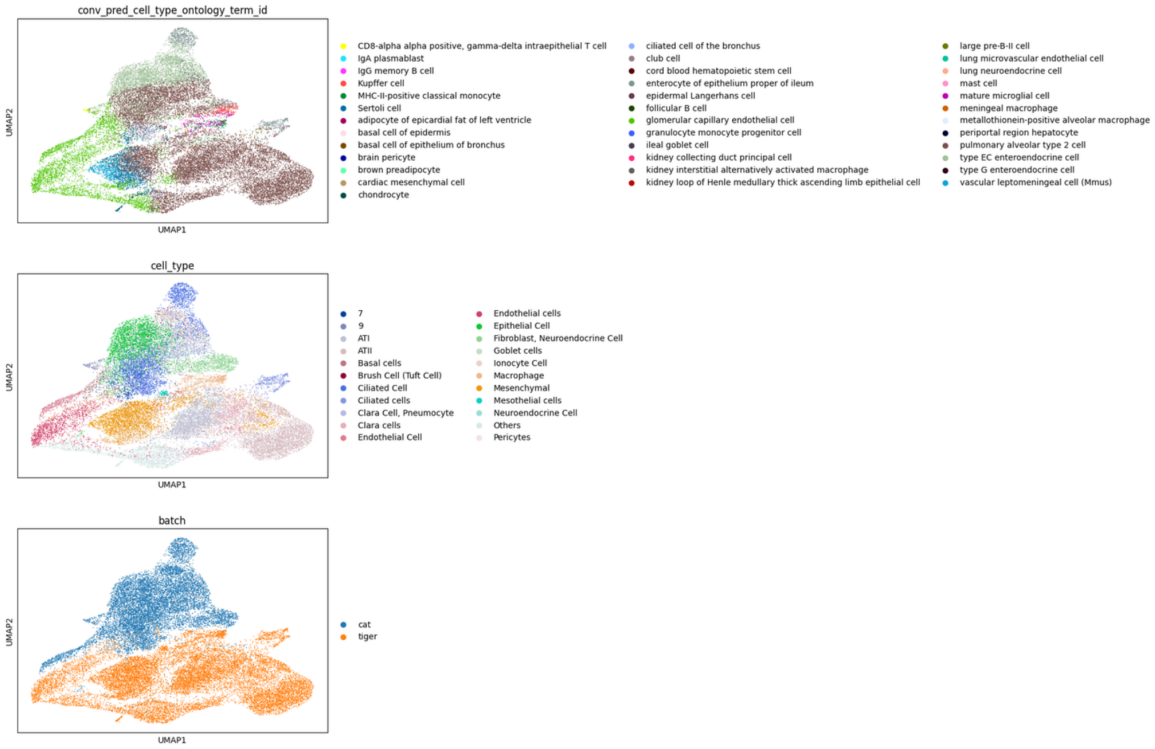

scPRINT-2's zero-shot multi-species expression embedding using the cell-type cell-embedding from top to bottom, scPRINT-2 predicted cell type labels, ground truth cell type labels, and ground truth organism labels.

6.4.24 Umap of scPRINT-2's multi-species expression embedding post-finetuning using the full cell-embedding

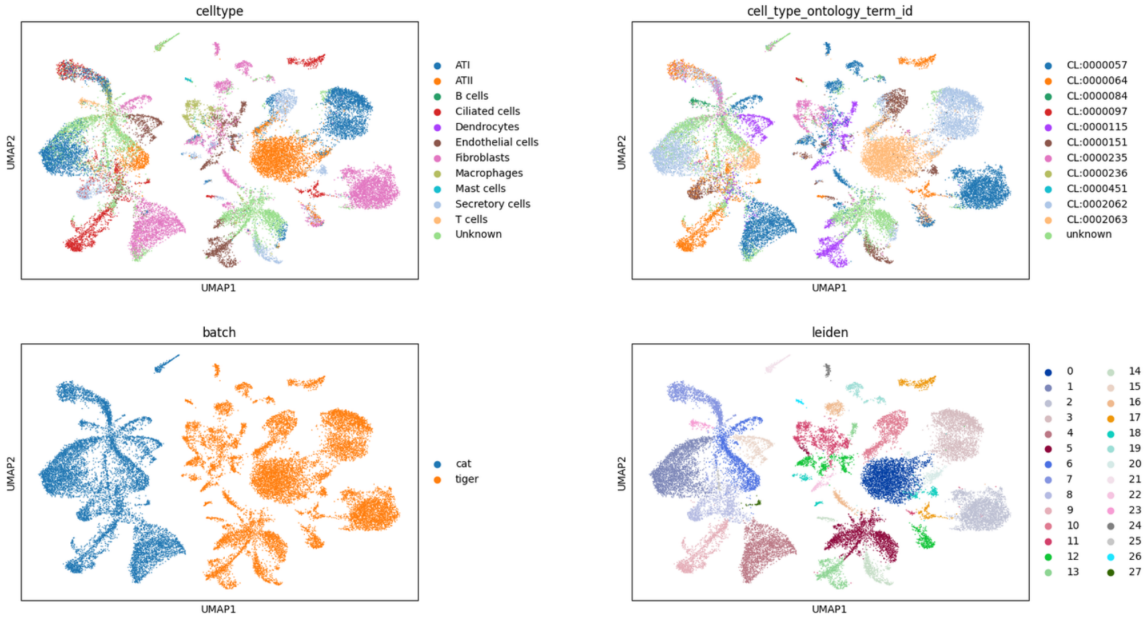

scPRINT-2's multi-species expression embedding post-finetuning using the full cell-embedding from left to right and top to bottom, ground truth cell type, scPRINT-2 predicted cell type labels, ground truth organism labels, and Leiden clusters.

6.4.25 Differential expression plot of the human vs mouse dataset from section 4

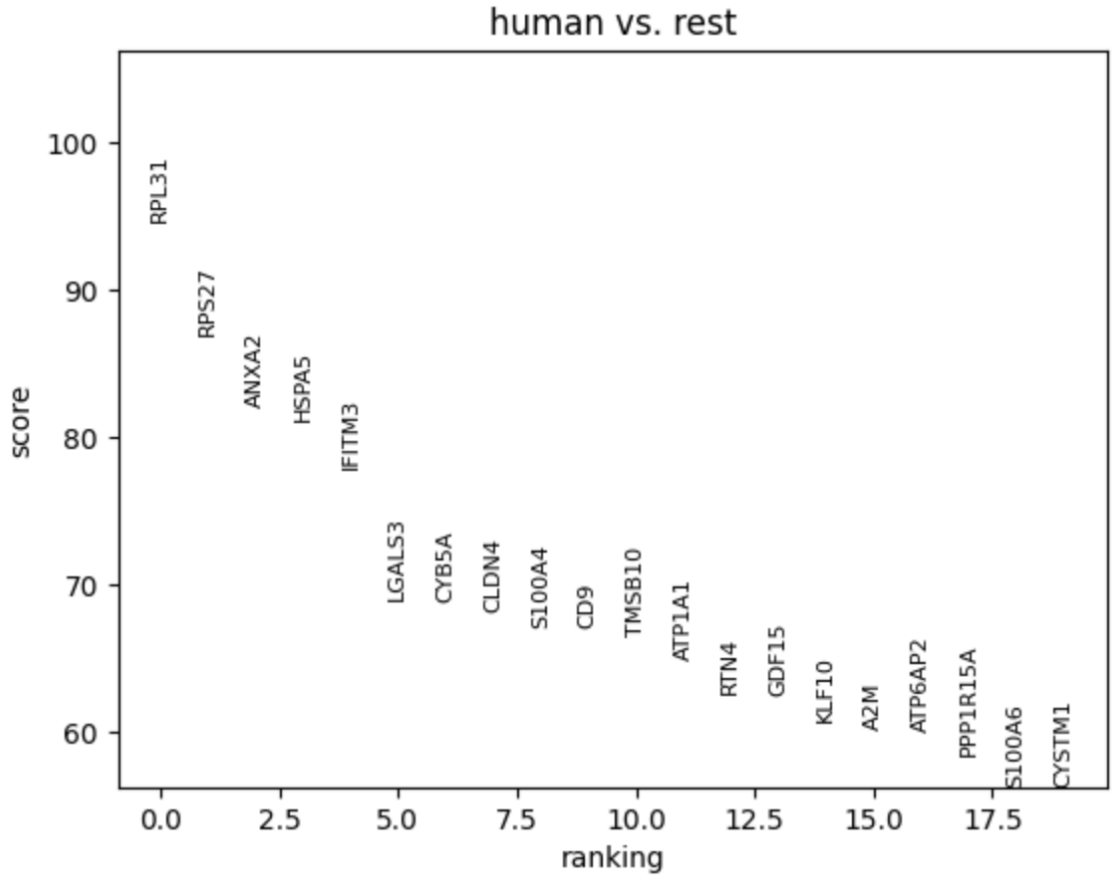

Differential expression plot of the human vs mouse dataset from section 4. Rest is mouse here.

6.4.26 Over-representation plot of humanized mouse data vs real mouse data compared to human

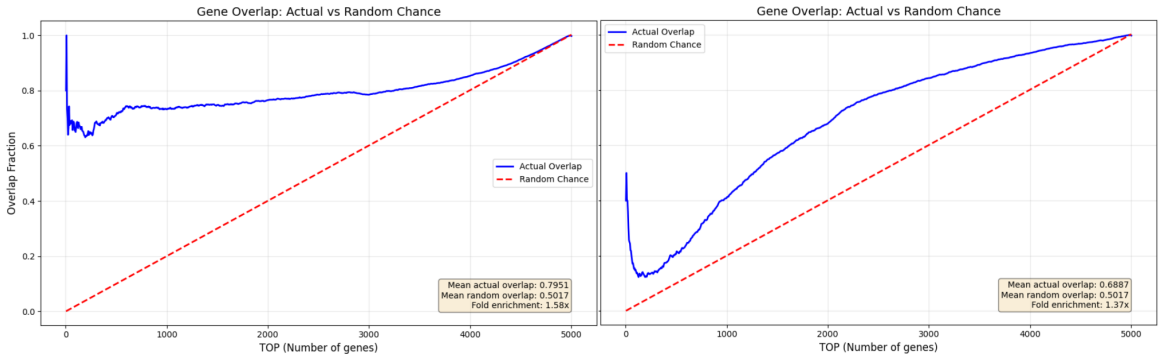

Over-representation plot of differentially expressed genes in scPRINT-2's humanized mouse data vs real mouse data compared to human.

6.4.27 Over-representation plot of female-like male data vs real female data compared to male

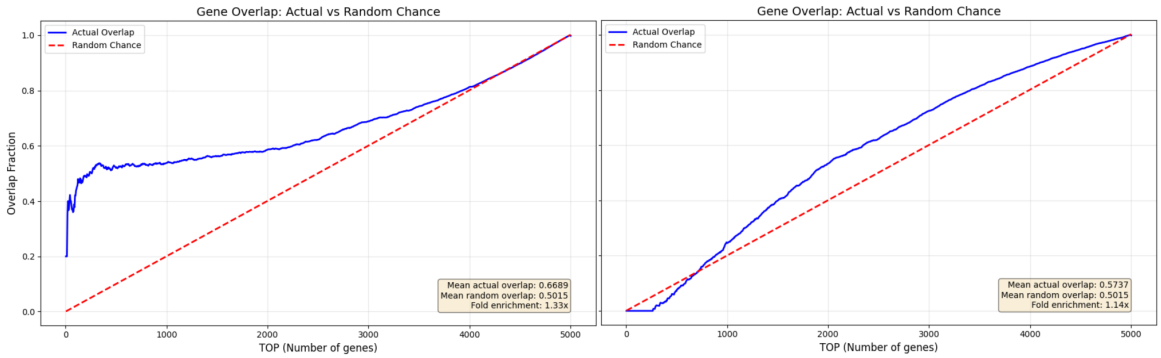

Over-representation plot of top differentially expressed genes in scPRINT-2's female-like male data vs real female data compared to male.

6.4.28 Dot Plot of Gene-set enrichment analysis over the differential expression analysis of section 4

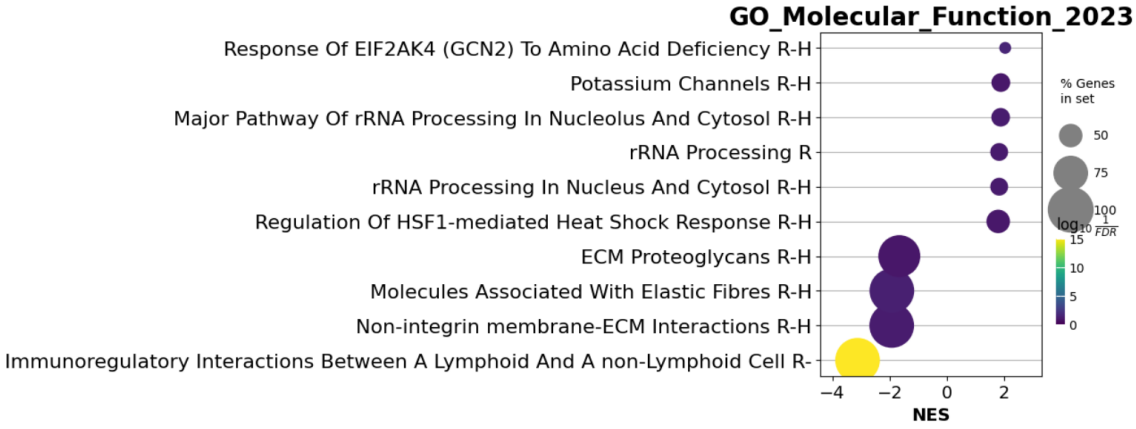

Showing the top 10 most enriched gene sets from the GO molecular function 2023 database.

6.4.29 Output gene embedding for a non-fully trained model without XPressor architecture

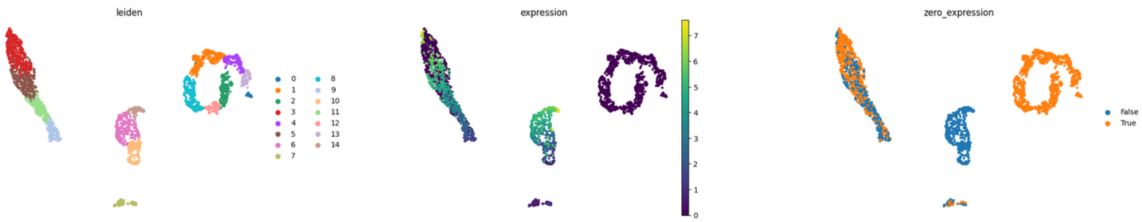

Overlaying in color, from left to right, the Leiden clusters, the expression values, and the zero vs non-zero expression. Despite displaying multiple clusters, the number of enriched pathways in each is still smaller than for a model using XPressor. (see Figure 5)

6.4.30 Venn diagram of the different ground truth gene networks

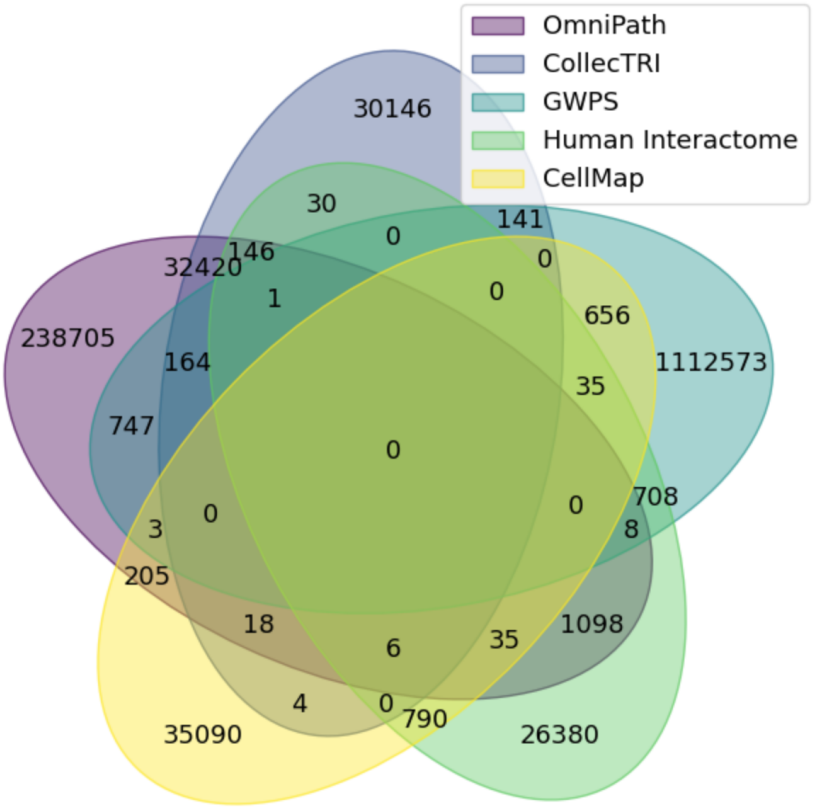

Venn diagram of the different ground truth gene networks showing overlap in the edges using gene symbols over the five ground truths used in our benchmark

6.4.31 Whisker plot of AUPRC-ratio scores for scPRINT-1 and scPRINT-2

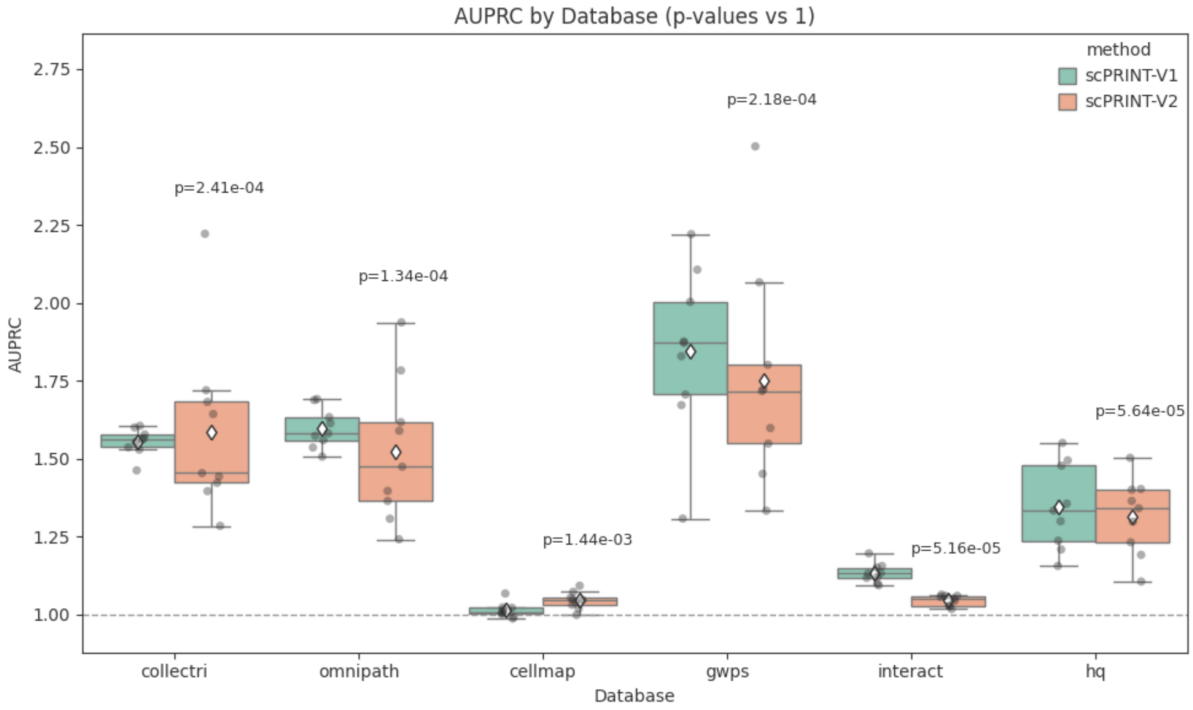

Whisker plot of AUPRC-ratio scores for the benchmark of scPRINT-1 vs scPRINT-2 using their respective GRN-extraction methods, showing that the scPRINT-2 extraction, while highlighting more relevant top connections, remains relatively similar to the scPRINT-1 version on the AUPRC-ratio scores on each of the six ground truth networks.

6.4.32 Additional scPRINT-2 generated gene network computed from CDC45

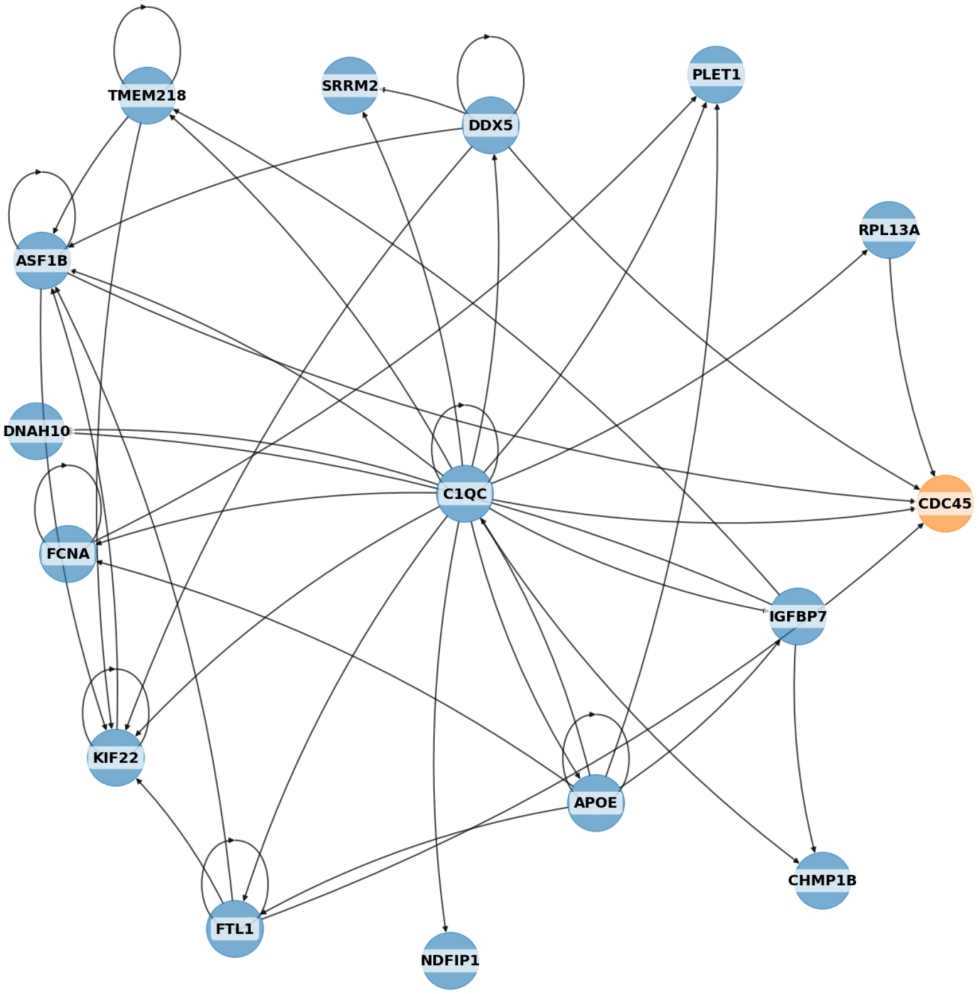

Subpart of the scPRINT-2 generated gene network using CDC45 as a seed gene and computed on 1024 mouse macrophages, showing how these networks can exhibit complex structures.